

RECEIVED

JUN 05 1998

OSTI

Advanced Separation Technology For Flue Gas Cleanup

DOE/PC/91344--99

**Final Report
February 1998**

By

**Abhoyjit S. Bhowm; Dean Alvarado
Neeraj Pakala; Troy Tagg
Tracy Riggs; Susanna Ventura
Kamalesh K. Sirkar; Sudipto Majumdar
Debabrata Bhaumick**

Work Performed Under Contract No.: DE-AC22-92PC91344

For

**U.S. Department of Energy
Office of Fossil Energy
Federal Energy Technology Center
P.O. Box 880
Morgantown, West Virginia 26507-0880**

By

**SRI International
333 Ravenswood Avenue
Menlo Park, California 94025**

MASTER

[Handwritten signature]

DISTRIBUTION OF THIS DOCUMENT IS UNLIMITED

DISCLAIMER

This report was prepared as an account of work sponsored by an agency of the United States Government. Neither the United States Government nor any agency thereof, nor any of their employees, makes any warranty, express or implied, or assumes any legal liability or responsibility for the accuracy, completeness, or usefulness of any information, apparatus, product, or process disclosed, or represents that its use would not infringe privately owned rights. Reference herein to any specific commercial product, process, or service by trade name, trademark, manufacturer, or otherwise does not necessarily constitute or imply its endorsement, recommendation, or favoring by the United States Government or any agency thereof. The views and opinions of authors expressed herein do not necessarily state or reflect those of the United States Government or any agency thereof.

DISCLAIMER

**Portions of this document may be illegible
electronic image products. Images are
produced from the best available original
document.**

CONTENTS

EXECUTIVE SUMMARY	S-1
Objectives and Approach	S-1
Summary of Tasks.....	S-3
LIST OF FIGURES	v
LIST OF TABLES	xi
TASK 1: PROJECT DEFINITION	1-1
TASK 2: CAPACITY, REVERSIBILITY, AND LIFETIME	2-1
SO _x Absorption	2-1
Early Measurements	2-1
Apparatus Modification	2-13
Understanding Discrepancies	2-22
Final Selection	2-24
NO _x Absorption	2-29
Absorption Studies	2-29
Effect of Oxygen	2-36
TASK 3: CHEMICAL SYNTHESIS	3-1
SO _x Absorbents	3-1
Synthesis of the Oligomeric Dimethylaniline (o-DMA)	3-1
Preparation of Propyleneimine and N-Phenylethyleneimine Copolymer	3-7
Synthesis of d-Siloxane and p-Siloxane	3-10
NO _x Absorbents	3-14
Tetrasodium Salt of Cobalt (II) 4,4',4'',4'''-Tetrasulfophthalocyanine 2-Hydrate	3-14
Tetrasodium Salt of Iron (II) 4,4',4'',4'''-Tetrasulfophthalocyanine 2-Hydrate	3-14
EDTA Analogs as NO _x Absorbents	3-15
Synthesis of Poly(allylamine) Functionalized EDTA Analog	3-18
Synthesis of EDTA Analog Copolymer	3-18
Synthesis of Poly(acrylate) Functionalized EDTA Analog	3-18
TASK 4: SO ₂ SCRUBBING WITH HOLLOW FIBER CONTACTORS	4-1
Experiments with Prototype HFC	4-4
Liquid Phase Mass Transfer Experiments	4-4
SO ₂ Removal Efficiency Experiments	4-8
Initial Experiments with Hoechst-Celanese HFC	4-8

Mass Transfer Tests with Pure CO ₂ and Water	4-8
Module Configuration Tests with Pure SO ₂	4-11
Mass Transfer Tests with 10% CO ₂ and Water	4-16
SO ₂ Removal Efficiency Tests	4-16
Mass Transfer Tests on 1000-Fiber Module	4-16
SO ₂ Absorption Tests with Model Flue Gas Mixture and Na ₂ SO ₃ Scrubber	4-20
Mass Transfer Control	4-31
Combined Absorption and Extraction	4-41
TASK 5: MASS TRANSFER RATE STUDIES FOR NO_x SCRUBBING IN HOLLOW FIBER CONTACTORS	5-1
CO ₂ Scrubbing	5-4
SO ₂ Scrubbing	5-7
NO _x Scrubbing	5-11
TASK 6: SO₂ LIQUOR REGENERATION	6-1
Liquid-Liquid Extraction (LLE)	6-1
Distribution Coefficient	6-9
Hollow Fiber Contained Liquid Membrane (HFCLM)	6-19
TASK 7: PARTICLE DEPOSITION	7-1
TASK 8: INTEGRATED NO LIFE TESTS	8-1
TASK 9: PERFORMANCE OF SCALABLE MODULES	9-1
Design of Rectangular Modules and Experimental Apparatus	9-1
SO ₂ Scrubbing Experiments	9-12
Combined SO ₂ Absorption/Scrubbing Liquor Regeneration	9-48
TASK 10: DEVELOPMENT OF COMPUTATIONAL MODEL	10-1
TASK 11: CONSTRUCTION OF SUBSCALE PROTOTYPE SYSTEM.....	11-1
TASK 12: OPERATION OF SUBSCALE PROTOTYPE SYSTEM	12-1
TASK 13: REFINEMENT OF COMPUTATIONAL DESIGN MODEL.....	13-1
TASK 14: ECONOMIC EVALUATION	14-1
SO ₂ Absorber	14-1
NO _x Absorber	14-4
Liquid-Liquid Extractor	14-4
TASK 15: REPORTING AND DELIVERABLES	15-1
TASK 16: CHEMICAL SYNTHESIS FOR PROCESS SCALE-UP	16-1
REFERENCES	R-1

APPENDICES

A	INITIAL PRESSURE	A-1
B	CALCULATION OF H AND H^*	B-1
C	EQUILIBRIUM CONSTANT FROM BREAKTHROUGH CURVES	C-1
D	EQUATIONS USED FOR OVERALL MASS TRANSFER COEFFICIENT CALCULATIONS	D-1
E	CALCULATION OF MINIMUM LIQUID FLOW RATE	E-1
F	SOP FOR PILOT SCALE SYNTHESIS OF 2,2'-BIS(N-METHYL-N-PHENYL)ETHYL ETHER	F-1

FIGURES

S-1	Proposed SO _x /NO _x wet scrubbing with hollow fiber contacting devices	S-2
2-1	Schematic of sorption apparatus	2-2
2-2	Algorithm for controlling absorption apparatus	2-5
2-3	SO ₂ calibration curve	2-6
2-4	SO ₂ partial pressure in the sample loop as a function of time	2-9
2-5	SO ₂ sorption using DMA	2-10
2-6	Modified absorption apparatus	2-14
2-7	Modified algorithm for controlling absorption apparatus	2-15
2-8	d-Siloxane	2-16
2-9	Equilibrium between d-siloxane and SO ₂ (GC results)	2-18
2-10	Structure of siloxane pentamer	2-19
2-11	Comparison of SO ₂ sorption capacities	2-20
2-12	Calibration curves after 10.1% SO ₂ was left standing in an initially empty absorption apparatus	2-23
2-13	SO ₂ absorption lifetime of d-DMA at 35°C and 50°C	2-27
2-14	Lifetime SO ₂ absorption/desorption run on d-DMA at 50°C	2-28
2-15	Lifetime test on d-DMA for SO ₂ absorption/desorption	2-30
2-16	NO _x absorption apparatus	2-31
2-17	Exiting NO concentration versus time for the 10-mM Fe(II)-EDTA/990-ppm NO runs	2-33
2-18	NO concentration over time for different scrubbing agents	2-34
2-19	NO _x -absorbing runs using 20 mM Fe(II)-EDTA and 100 ppm NO	2-37
2-20	Experimental flowsheet for NO _x absorption tests with on-line pH measurement	2-38
2-21	NO absorption by Co(II)-phthalocyanine in the presence of oxygen	2-39

2-22	Co(II)-phthalocyanine NO absorption capacity at 50°C	2-41
2-23	Experimental schematic for NO _x absorption at elevated temperatures	2-42
2-24	Absorption behavior of 0.1 M Co(II) phthalocyanine solution at 70°C	2-43
3-1	First route for synthesis of oligomer of DMA	3-2
3-2	Tetraethylenepentamine pentahydrochloride in the first synthesis route	3-3
3-3	Second route for synthesis of oligomer of DMA	3-4
3-4	Reaction scheme for synthesis of oligomer of DMA	3-5
3-5	Copolymerization scheme of N-phenylaziridine and propyleneimine	3-6
3-6	Silicon-containing DMA analogs	3-12
3-7	Siloxane oligomers functionalized by DMA	3-13
3-8	UV-visible spectrum of tetrasodium salt of iron 4,4',4'', 4'''-tetrasulfophthalocyanine	3-16
3-9	Comparison of UV-visible spectra for Fe(II) and Fe(III) phthalocyanine	3-17
4-1	Structure of Celgard fiber netting	4-2
4-2	Wrapping of netting around central tube	4-3
4-3	Flow pattern of gas and liquid in cross-flow module	4-5
4-4	Flow patterns in new Hoechst/Celanese cross-flow module	4-6
4-5	HFC mass transfer coefficients for pure CO ₂ absorption in water using a cross-flow module	4-7
4-6	SO ₂ removal efficiencies with a prototype HFC	4-9
4-7	Schematic of HFC test apparatus	4-10
4-8	Schematic of the cross-flow module	4-12
4-9	HFC mass transfer coefficients for pure CO ₂ absorption in water using two cross-flow modules	4-13
4-10	Schematic of HFC in the vertical configuration	4-14
4-11	HFC mass transfer coefficients with different module orientations and liquid pressures	4-15
4-12	HFC mass transfer coefficients with pure and dilute CO ₂ feed streams	4-17
4-13	SO ₂ removal efficiencies using water as the absorbent	4-18

4-14	SO ₂ removal efficiencies from simulated flue gas using water as the absorbent	4-19
4-15	HFC mass transfer coefficients for pure CO ₂ absorption in water using a 1000-fiber cross-flow module	4-21
4-16	HFC mass transfer coefficients for CO ₂ -N ₂ mixture absorption in water using a 1000-fiber cross-flow module	4-22
4-17	Sherwood number versus Reynolds number for CO ₂ absorption in water	4-23
4-18	SO ₂ removal with water at low liquid flow rates	4-24
4-19	Effect of gas flow rate on mass transfer coefficient and percent removal	4-25
4-20	SO ₂ removal efficiency at various sulfite concentrations	4-26
4-21	Effect of liquid flow rate on overall mass transfer coefficient and SO ₂ removal efficiency at low sulfite concentrations	4-28
4-22	Effect of sulfite on overall mass transfer coefficient	4-29
4-23	SO ₂ removal with water	4-34
4-24	Pure CO ₂ absorption in the 1000 fiber module	4-38
4-25	Variation of mass transfer coefficient with gas flow rates at an aqueous sulfite solution flow of 20 mL/min	4-47
5-1	Minimum liquid-to-gas flow rate ratio needed to obtain equilibrium	5-2
5-2	Schematic of HFC apparatus	5-3
5-3	Calibration using a 1.99% CO ₂ cylinder	5-5
5-4	Overall mass transfer coefficient versus water flow rate	5-6
5-5	Fiber openings for 1000 and 200 fiber modules	5-8
5-6	Overall liquid mass transfer coefficient versus liquid flow rate	5-9
5-7	Sherwood number versus Reynolds number for CO ₂ absorption in water	5-10
5-8	GC calibration with 1.46% SO ₂ in N ₂ feed	5-12
5-9	SO ₂ removal water flow rate of 25 mL/min	5-13
5-10	Calibration curve of the NO _x analyzer	5-14
5-11	Percent removal of NO versus Fe(II)-EDTA concentration	5-16
5-12	Calculated solubility of NO in 20 mM Co-phthalocyanine solution at 25°C	5-20
5-13	Effect of gas flow rate on mass transfer coefficient and percent removal	5-23

6-1	Schematic of combined absorption and liquor regeneration setup	6-2
6-2	Schematic of combined absorption and liquor regeneration setup with installation of additional valves to bypass the extraction module	6-5
6-3	Schematic of combined absorption and liquor regeneration setup with four-way valve to conduct batch mode recirculation	6-12
6-4	Schematic of batch recirculation mode of operation using a hollow fiber contactor	6-14
6-5	Modified absorption and liquor regeneration setup for distribution coefficient measurement	6-15
6-6	Schematic of combined absorption and liquor regeneration setup modified for HFCLM runs	6-22
7-1	Schematic of Wright nebulizer	7-3
7-2	Size distribution of dispersed silica particles	7-5
7-3	Log-normal distribution of dispersed silica particles	7-6
7-4	Inspiron (400 cm ³) nebulizer performance characteristics	7-8
7-5	Particle size distribution for the sampling time of 1 s	7-9
7-6	Particle size distribution for the sampling time of 40 s	7-10
7-7	Particle capture efficiency in an HFC	7-12
7-8	Variation of gas-side overall mass transfer coefficient with gas flow rate	7-13
7-9	Effect of gas flow on the pressure drop across the HFC	7-15
7-10	Experimental setup for particle generation	7-17
7-11	Variation of ΔP_g across HFC	7-18
7-12	Pictures of HFC end caps and gas inlet and outlets ends of fibers	7-19
7-13	Enlarged view of a portion of particle cake formed at the gas inlet end of HFC	7-20
7-14	Pressure drop across the HFC during an 80-h period	7-22
7-15	Influence of particle deposition on the MTC	7-23
8-1	NO _x absorption/desorption experimental schematic	8-2
8-2	Modified NO _x absorption and desorption experimental arrangement	8-4
8-3	Simultaneous NO _x absorption and desorption tests using Co(II)-phthalocyanine ...	8-5

8-4	Simultaneous NO _x absorption and desorption tests using Co(II)-phthalocyanine (30 hours of operation)	8-7
8-5	Simultaneous absorption and desorption tests using Co(II)-phthalocyanine (40 hours of operation)	8-8
8-6	Modified NO _x absorption and desorption experimental arrangement	8-9
8-7	Flow calibration curve	8-11
8-8	Co(II) pthalocyanine - standard curves.	8-12
8-9	Absorption and desorption processes exiting gas NO concentrations as a function of time	8-14
8-10	NO _x scrubbing solution lifetime data	8-16
8-11	NO _x absorption/desorption experimental setup (enhanced desorption operation) ...	8-17
8-12	NO _x scrubbing lifetime studies (Aug. 1995)	8-19
8-13	NO _x scrubbing solution lifetime data.....	8-20
9-1	Cross-flow pattern of gas and liquid flow in a rectangular hollow fiber cassette (module)	9-2
9-2	Apparatus for scalable module testing	9-7
9-3	Drawing of rectangular housing. (Dimensions in inches)	9-9
9-4	Design features of a submodule. (Dimensions in inches)	9-10
9-5	Top-view of the gas-side and plates of housing. (Dimensions in inches)	9-11
9-6	SO ₂ Analyzer for continuous monitoring of gas streams	9-13
9-7	Percent SO ₂ removal versus water flow rate	9-15
9-8	Percent SO ₂ removal versus gas flow rate	9-16
9-9	SO ₂ -water equilibrium curve	9-17
9-10	Mass transfer coefficient versus water flow rate	9-19
9-11	Mass transfer coefficient versus gas flow rate	9-20
9-12	Percent SO ₂ removal versus liquid flow rate. Gas flowrate = 100 SLPM	9-21
9-13	Percent SO ₂ removal versus gas flow rate. Liquid flowrate = 1 L/min.	9-22
9-14	SO ₂ equilibrium curves in various sodium sulfite solutions	9-23
9-15	Overall mass transfer coefficient versus liquid flowrate. Gas flowrate = 100 SLPM	9-24

9-16	Overall mass transfer coefficient versus gas flowrate. Liquid flowrate = 1 L/min	9-25
9-17	Percent removal versus water flow rate	9-27
9-18	Mass transfer coefficient versus water flow rate	9-28
9-19	Apparatus for scalable module testing	9-29
9-20	Sherwood number vs. Reynolds number (liquid)	9-36
9-21	Sherwood number vs. Reynolds number (liquid)	9-37
9-22	Sherwood number vs. Reynolds number (gas)	9-38
9-23	Sherwood number vs. Reynolds number (gas)	9-39
9-24	Sherwood number vs. Reynolds number (liquid)	9-40
9-25	Sherwood Number vs. Reynolds Number	9-43
9-26	Sherwood Number vs. Reynolds Number (water). Re (gas) = 70	9-44
9-27	Sherwood Number vs. Reynolds Number (0.2M Na_2SO_3). Re (gas) = 70	9-45
9-28	Sherwood Number vs Reynolds Number (water)	9-48
14-1	Proposed SO_x/NO_x wet scrubbing with hollow fiber contacting devices	14-2

TABLES

S-1	Project Tasks and Schedule	S-3
S-2	Milestone Log for Contract DE-AC22-92PC91344 at the End of Task 7	S-5
2-1	Absorption Measurement Procedure	2-3
2-2	Chromatography Columns Tested for O ₂ /N ₂ /SO ₂ Separation Ability	2-4
2-3	Compounds Synthesized and Tested in SO ₂ Sorption Runs	2-8
2-4	Parameters for SO ₂ Sorption Runs with DMA	2-12
2-5	Results for SO ₂ Sorption Runs	2-12
2-6	SO ₂ Sorption by d-Siloxane	2-13
2-7	SO ₂ Sorption by Siloxane Pentamer	2-21
2-8	Comparison of H* for d-Siloxane and d-DMA	2-21
2-9	SO ₂ Sorption by Dimer DMA	2-25
2-10	Equilibrium Constants (K) Using 100 ppm NO in N ₂ and 0.02 M Aqueous NO _x -Absorbing Solutions at 25°C	2-35
4-1	Results of SO ₂ Absorption in 0.2 M Na ₂ SO ₃	4-30
4-2	Summary of Results on CO ₂ Absorption in the 1000 Fiber Unit	4-37
4-3	Summary of Absorption Data in Simultaneous Absorption-Extraction Runs	4-40
4-4	Results of SO ₂ Absorption Runs Using 0.2 M Na ₂ SO ₃ at 20 mL/min	4-42
4-5	Summary of Absorption Data in Simultaneous Absorption-Extraction Runs	4-43
4-6	Results of SO ₂ Absorption Runs Using 0.2 M Na ₂ SO ₃ at 20 mL/min	4-46
4-7	Absorption Data in Absorption-Extraction Runs Using High and Low Flow Rates of DMA	4-49
4-8	Absorption Data to Determine Distribution Constant (m) Using HFCs for Absorption-Extraction	4-51

5-1	Experimental Results on NO _x Absorption Using HFCs	5-18
5-2	Experimental Results on the NO _x Scrubbing with 300-Fiber HFC	5-21
6-1	Summary of Extraction Data in Simultaneous Absorption-Extraction Runs	6-6
6-2	Summary of Extraction Data in Simultaneous Absorption-Extraction Runs	6-7
6-3	Absorption Data in Absorption-Extraction Runs Using High and Low Flow Rates of DMA	6-10
6-4	Determination of Distribution Coefficient	6-18
6-5	Results of Run AE-12 and Other Runs with Higher Recovery of SO ₂ by LLE	6-20
6-6	Geometric Characteristics of the Coated Fiber Module for HFCLM	6-24
7-1	Particle Generation Using Nebulizers	7-4
8-1	Mass Flow Controllers (MFC) and Settings	8-10
9-1	Discussions With Membrane Manufacturers	9-5
9-2	Results of SO ₂ Absorption in water	9-31
9-3	Results of SO ₂ Absorption in 0.01M Na ₂ SO ₃ Solution	9-32
9-4	Results of SO ₂ Absorption in 0.05M Na ₂ SO ₃ Solution	9-33
9-5	Results of SO ₂ Absorption in 0.02M Na ₂ SO ₃ Solution	9-34
9-6	Results of SO ₂ Absorption in 0.2M Na ₂ SO ₃	9-41
9-7	Gas Flow Distribution in Four-Unit Welded Module	9-42
9-8	Flow Rate Distribution in Four-Unit Welded Module	9-47
9-9	Physical Properties of d-DMA	9-49
14-1	Basic for Example Design of 500 MW(e) SO _x /NO _x Plant	14-3
14-2	Cost of Major Equipment and Utility Items in Option A for a 500-MW(e) Power Plant	14-6
14-3	Cost of Major Equipment and Utility Items in Option A for a 500-MW(e) Power Plant (<u>CORRECTION</u>).....	14-7

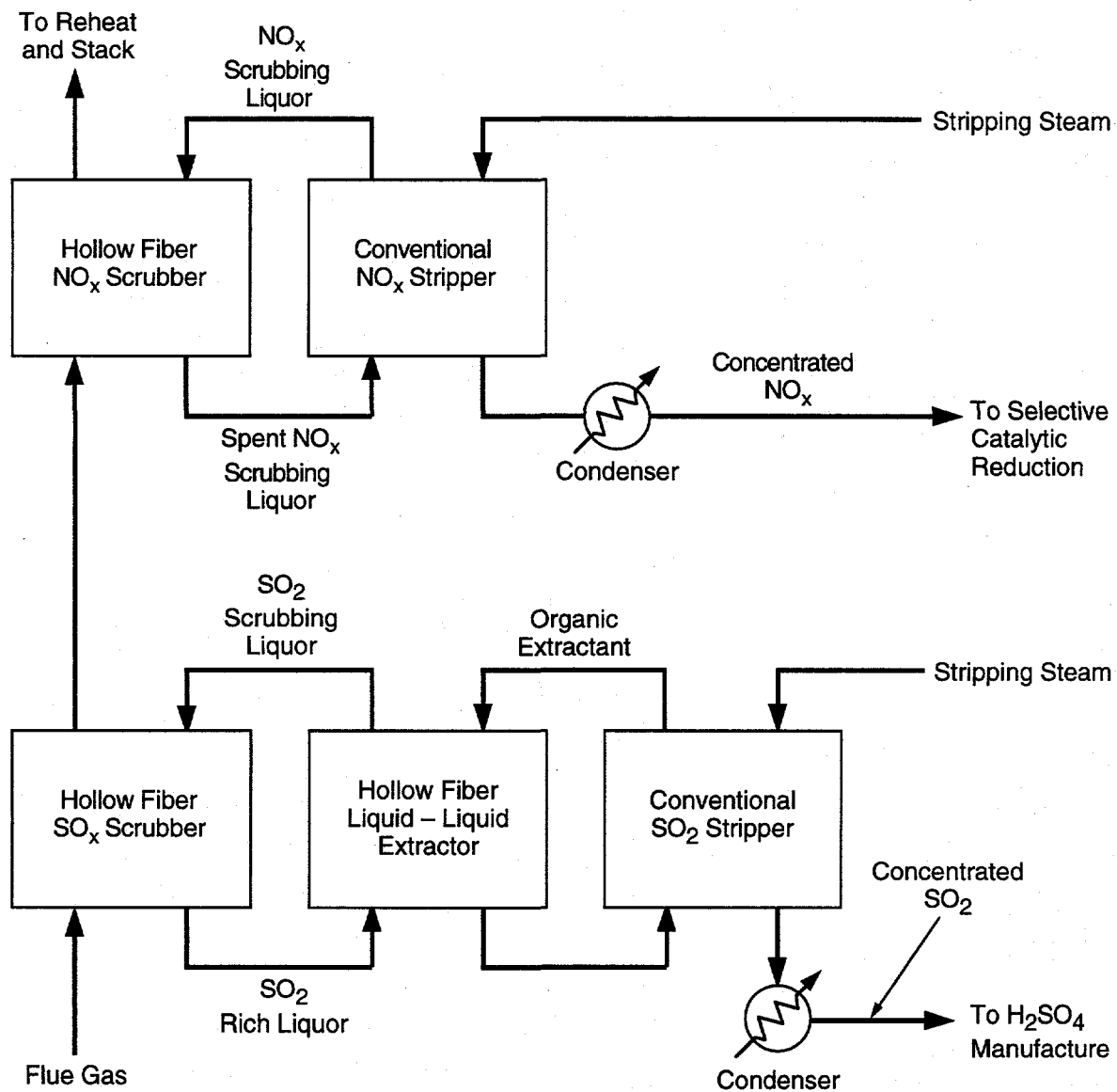
EXECUTIVE SUMMARY

OBJECTIVES AND APPROACH

The objective of this work by SRI International was to develop a novel system for regenerable SO₂ and NO_x scrubbing of flue gas that focuses on (1) a novel method for regenerating spent SO₂ scrubbing liquor and (2) novel chemistry for reversible absorption of NO_x. High efficiency, hollow fiber contactors (HFCs) were proposed as the devices for scrubbing the SO₂ and NO_x from the flue gas. Figure S-1 is a schematic of the process. The system would be designed to remove more than 95% of the SO₂ and more than 75% of the NO_x from flue gases typical of pulverized coal-fired power plants at a cost that is at least 20% less than combined wet limestone scrubbing of SO_x and selective catalytic reduction of NO_x. In addition, the process would generate only marketable by-products, if any (no waste streams are anticipated).

The major cost item in existing technology is capital investment. Therefore, our approach was to reduce the capital cost by using high-efficiency, hollow fiber devices for absorbing and desorbing the SO₂ and NO_x. We also introduced new process chemistry to minimize traditionally well-known problems with SO₂ and NO_x absorption and desorption. For example, we extracted the SO₂ from the aqueous scrubbing liquor into an oligomer of dimethylaniline to avoid the problem of organic liquid losses in the regeneration of the organic liquid. Our novel chemistry for scrubbing NO_x consisted of water-soluble phthalocyanine compounds invented by SRI as well as polymeric forms of Fe⁺⁺ complexes similar to traditional NO_x scrubbing media described in the open literature. Our past work with the phthalocyanine compounds, used as sensors for NO and NO₂ in flue gases, shows that these compounds bind NO and NO₂ reversibly and with no interference from O₂, CO₂, SO₂, or other components of flue gas.

The final novelty of our approach was the arrangement of the absorbers in cassette (stackable) form so that the NO_x absorber can be on top of the SO_x absorber. This arrangement is possible only because of the high efficiency of the hollow fiber scrubbing devices, as indicated by our preliminary laboratory data. This cassette (stacked) arrangement makes it possible for the SO₂ and NO_x scrubbing chambers to be separate without incurring the large ducting costs and the large gas pressure drop necessary if a second conventional absorber vessel were used. Because we have separate scrubbers, we will have separate liquor loops and simplify the chemical complexity of simultaneous SO₂/NO_x scrubbing.



CM-360583-49

Figure S-1. Proposed SO_x/NO_x wet scrubbing with hollow fiber contacting devices.
SO₂ liquor regeneration occurs in hollow fiber, liquid-liquid extraction (LLE) device.

Work was planned to be conducted over a 60-month period (May 1992 through April 1997), encompassing 16 tasks, as shown in Table S-1, beginning with studies of the fundamental chemistry and the mass transfer characteristics of small HFC modules in the laboratory. We would then examine the most favorable method of SO₂ liquor regeneration, determine the ability of the HFC devices to withstand particulate matter, and examine the behavior of scalable modules. The project was terminated by DOE without completion of Tasks 9 and 10 and without executing Tasks 11,12, and 13. This final report therefore presents an anthology of data, rather than a summary, because the project is largely unfinished. We hope that this anthology will prove useful if the project is re-initiated in the future.

**Table S-1
PROJECT TASKS AND SCHEDULE**

Task Number	Title	Status
1	Project Definition	Complete
2	Capacity, Reversibility and Lifetime	Complete
3	Chemical Synthesis	Complete
4	SO ₂ Scrubbing with HFCs	Complete
5	NO _x Scrubbing with HFCs	Complete
6	SO ₂ Liquor Regeneration	Complete
7	Particle Deposition	Complete
8	Integrated NO _x Life Tests	Complete
9	Scalable Modules	Incomplete
10	Computational Model	Incomplete
11	Construction of Subscale Prototype	Not executed
12	Operation of Subscale Prototype	Not executed
13	Refinement of Computational Model	Not executed
14	Economic Evaluation	Complete for work done to date
15	Reporting	Complete for work done to date
16	Chemical Synthesis for Process Scaleup	Complete for work done to date

SUMMARY OF TASKS

In Task 1, an overall management plan was submitted to the DOE and approved. The management plan was submitted each subsequent year for approval.

In Task 2, we tested several SO₂ and NO_x absorbing compounds for reversibility, capacity, and lifetime. For SO₂, d-DMA was selected as the best choice, while for NO_x, Co(II)-phthalocyanine was selected as the best choice.

In Task 3, we synthesized several of the compounds tested in Tasks 2 and 5.

In Task 4, we demonstrated 99% SO₂ removal efficiency with laboratory modules and extensively characterized the mass transfer properties of HFCs.

In Task 5, we used Co(II)-phthalocyanine solutions to demonstrate 85% NO removal efficiency with laboratory modules.

In Task 6, we achieved 99% SO₂ liquor regeneration efficiency with laboratory modules.

In Task 7, we completed an 80-hour particle deposition experiment. Unexpected results stopped further deposition tests.

For Task 8, we conducted a 300 h test to test the life of the Co(II)-phthalocyanine, the NO_x absorbing compound. No degradation of the compound was observed.

In Task 9, steady state conditions were not obtained using the scalable modules before the project was terminated.

In Task 10, we developed correlations based on mass transfer data obtained in the previous tasks.

Tasks 11 through 13 were not executed.

In Task 14, we completed economic estimations on the process. The results indicate some savings in capital investments.

In Task 15, we prepared and submitted the required documents to the DoE.

In Task 16, we scaled-up synthesis of the SO₂-absorbing compound (d-DMA) and the NO_x-absorbing compound (Co(II)-phthalocyanine) that were tested in Tasks 8 and 9.

Table S-2
MILESTONE LOG FOR CONTRACT DE-AC22-92PC91344 AT THE END OF TASK 7

Element Code	Description	Planned Completion Date	Actual Completion Date	Comments
1	Development of Management Plan	6/92	8/92	
2A	Test First DMA Oligomer	2/93	4/93	Difficult to obtain quality data.
2B	Test First NO _x Scrubbing Compound	6/93	10/93	Two major oil contaminations.
3A	Synthesize 10 g of DMA Oligomer	1/93	1/93	
3B	Synthesize 40 g Phthalocyanine	5/93	6/93	
4	Achieve 99% SO ₂ Removal Efficiency with Laboratory Modules	1/93	1/93	
5	Achieve 85% NO _x Removal Efficiency with Laboratory Modules	5/93	9/93	NO _x analyzer received 8/93 from another DOE contractor. Blocked fibers discovered in one module.
6	Achieve 99% SO ₂ Liquor Regeneration Efficiency with Laboratory Modules	11/93	3/94	Delay in obtaining HFCs from manufacturer.
7	Complete One-Month Particle Deposition Test	2/94	-	Unexpected results after 80 h deposition. SRI's proposal for further investigation was not funded by DOE.
8A	Operate Integrated Absorption/Desorption System with Water	10/94	12/94	
8B	Complete One-Month Life Test of NO _x Chemistry	3/95	3/95	
9	Achieve 97% SO ₂ Absorption and Liquor Regeneration with Scalable Modules	3/95	-	Steady-state not achieved.
10	Develop Computational Model	8/95	-	Insufficient data to complete model.
11	Operate Subscale Prototype with Water	1/96	-	Task not executed.
12	Achieve 95% SO ₂ and 75% NO _x Removal Efficiency with Subscale Prototype	1/97	-	Task not executed.
13	Refine Computational Model	3/97	-	Task not executed.
14	Prepare Detailed Evaluation of Process Economics	8/96	8/96	
15	Submit Required Reports	1/97	1/97	
16	Synthesize Chemicals for Process Scale-up	3/96	3/96	Only scale-up for Phase II was executed.

TASK 1: PROJECT DEFINITION

The first task (project definition) began in early May 1992 shortly after the contract was signed by the Department of Energy and SRI International. Specific activities associated with Task 1 included preparation of the Management Plan, the Milestone Schedule Plan (F1332.3), the Cost Plan (F1332.7), the Notice of Energy RD&D Project (F1430.22), and a Hazardous Substance Plan.

TASK 2: CAPACITY, REVERSIBILITY, AND LIFETIME

The purpose of this task was to establish the reversible absorption capacity of the chemistries we intend to use for SO₂-liquor regeneration and for NO_x scrubbing. Any commercially successful SO₂ and NO_x chemistry must be essentially fully reversible and lose less than 10% of its activity in one year. The real issues are the economics of replacement chemicals and the disposal of spent chemicals. The maximum allowable cost for replacement and renewal of spent chemicals was anticipated to be about 0.1 mil/kWh in an actual power plant operating environment.

SO_x ABSORPTION

To determine the reversible adsorption capacity, we measured the equilibrium absorption behavior of SO₂ in an automated apparatus designed for this purpose and shown in Figure 2-1. We placed samples of the SO₂ regeneration liquid into the sample cell and repeatedly exposed the liquid to various partial pressures of SO₂ (partial pressures characteristic of flue gas).

Early Measurements

The apparatus used for this study was designed so that dead volume in our system would be minimized. Also, a gas cabinet was installed into the system to contain cylinder leaks and to provide inert purging of gas lines and automatic shut-off in case of a power failure.

The reversible absorption apparatus uses a combination of volumetric and chromatographic techniques to measure absorption. The absorption measurement procedure, summarized in Table 2-1, was designed to reduce the time required for each measurement. The time-limiting step for a measurement is the diffusion time required to ensure that all the gas is in equilibrium with the liquid.*

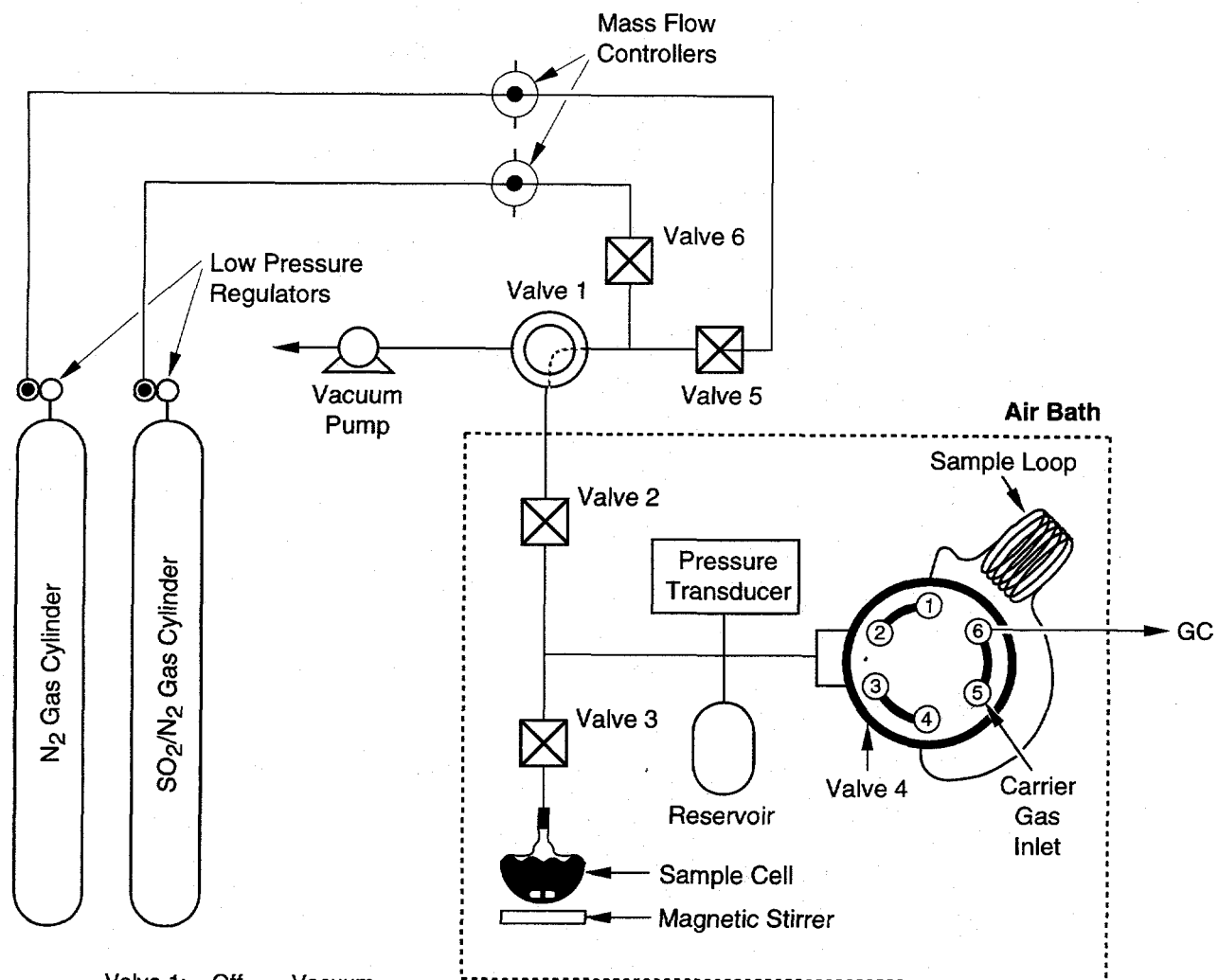
An indication of the time required for diffusion to occur is given by the characteristic diffusion time:

$$\tau = \frac{L^2}{d} \quad (2-1)$$

where

- τ = Characteristic diffusion time
- L = Length of diffusion path
- d = Diffusivity of gas

* It is not practical to force circulation of gas through the GC sample loop, because any mechanism forcing circulation would add uncertainties to the internal volume of the apparatus or introduce incompatible materials.



Valve 1: Off = Vacuum
 On = Gas

Valve 4: Off = Inject
 On = Load

CM-3501-11

Figure 2-1. Schematic of sorption apparatus.

Table 2-1
ABSORPTION MEASUREMENT PROCEDURE

(Refer to Figure 2-1)

1. The region below Valve 2 is evacuated.
 2. Valve 3 is closed, the region between Valves 2 and 3 is charged with a known quantity of gas (SO_2), and 2 is closed. (Knowing the temperature, pressure, and volume of this region, we can determine the moles of gas charged.)
 3. Valve 3 is opened, allowing the gas to contact the absorbent sample.
 4. The apparatus is given time to allow equilibration between the gas (including that contained in the reservoir, sample cell, GC sample loop, and connections) and the liquid.
 5. The total moles remaining in the gas phase after absorption are determined.
 6. The composition of the gas is determined by sending a gas sample to the GC.
 7. The moles of SO_2 absorbed by the liquid are determined by mass balance.
-

The largest contributor to diffusion time in our apparatus is the sample loop. To reduce the diffusion time, we connected both ends of the GC sample loop to the reservoir region and shortened the sample loop by using larger diameter tubing. With these modifications, the characteristic diffusion time is about 10 min. We expected the equilibration step in our procedure to be at least ten times the characteristic diffusion time. Before beginning absorption measurements, we experimentally determined the actual time required for the entire gas volume to equilibrate with the absorbent.

We began evaluating chromatography columns for SO_2 analysis by GC. Our goal was to identify a column that will separate SO_2 , N_2 , and O_2 . The ability to separate O_2 would allow us to check for leaks on each run. If there was an O_2 peak, we would know there was a leak and could correct it (because N_2 was used as the diluent for SO_2 , a N_2 peak would not indicate a leak). Many columns can separate SO_2 from O_2/N_2 and O_2 from N_2 , but few can separate all three simultaneously. Table 2-2 lists the columns we tested and the results.

Table 2-2
CHROMATOGRAPHY COLUMNS TESTED FOR
O₂/N₂/SO₂ SEPARATION ABILITY

<u>Column</u>	<u>Result</u>
Porapak Q	Does not separate O ₂ from N ₂
Molecular sieve 5a	Irreversibly adsorbs SO ₂
Molecular sieve 13x	Irreversibly adsorbs SO ₂
Chromosorb 102	Does not separate O ₂ from N ₂

To help us evaluate the results from absorption experiments, we developed a computer spread sheet that calculates the solubility coefficient from a set of experimental results. The spread sheet can also be used to determine the optimum experimental conditions (the pressure, volume, and composition of the initial gas charge) for the absorption measurements.

To fully automate the absorption procedure, we connected all six valves and the pressure transducer to a Macintosh computer. We programmed the computer according to the algorithm shown in Figure 2-2. The algorithm will check for leaks, desorb gases from the sample liquid, pressurize the apparatus with SO₂, monitor the pressure over time, and determine the equilibrium SO₂ concentration in the apparatus by GC.

We focused on obtaining three important characteristics of the absorption apparatus: the gas chromatograph calibration curve, sample cell and head space volumes, and the time required for SO₂ to diffuse from the sample cell to the sample loop.

We calibrated the gas chromatograph using a 0.91% SO₂ in N₂ mixture at various pressures. Figure 2-3 shows results for SO₂. We also measured the leak rate of the apparatus as approximately 3 torr/day. This value is lower than the expected operating pressures of 400-800 torr. Thus, the apparatus is essentially leak-free.

In preparation for the experiments, we measured the sample cell and head space volumes by filling the sample cell to a known pressure with N₂ and expanding it into the head space volume. Knowing the initial pressures in the two volumes and the final equilibrium pressure, we can compute the ratio of the two volumes. Next, ball bearings of a known volume were placed in the sample cell and the entire exercise was repeated; this yielded a different ratio of volumes. From the two ratios

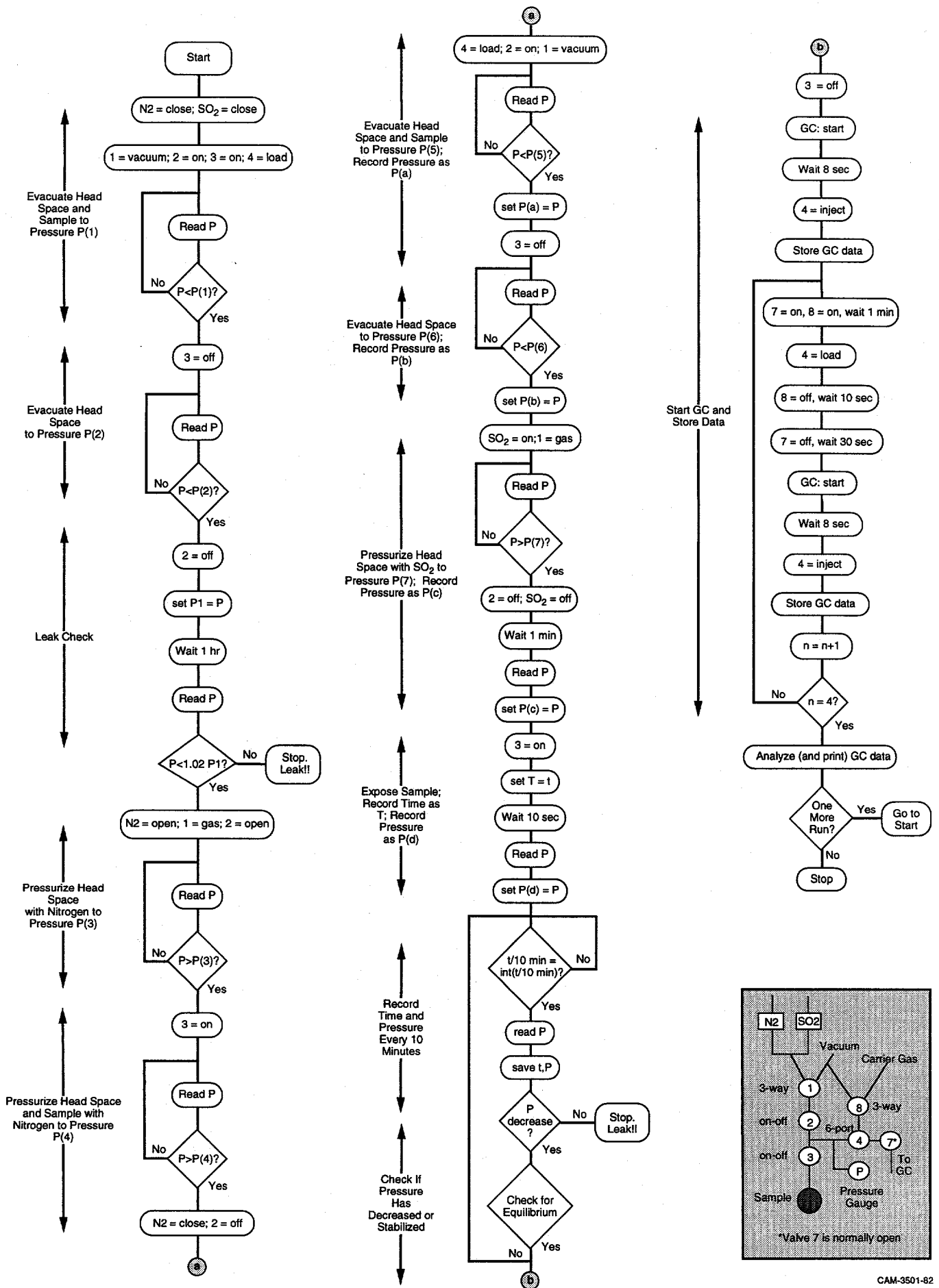
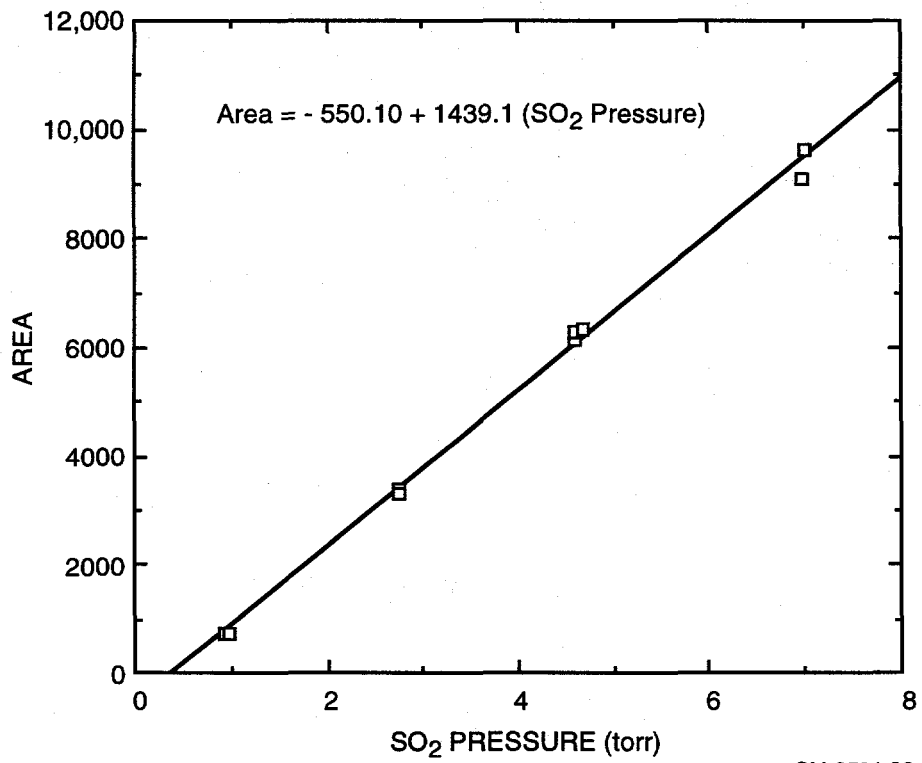


Figure 2-2. Algorithm for controlling absorption apparatus.



CM-3501-86

Figure 2-3. SO₂ calibration curve.

the actual volumes can be calculated: we calculated the sample cell volume as 17.01 cm³ and the head space volume as 19.81 cm³.

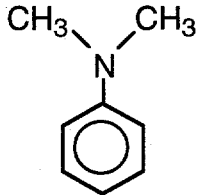
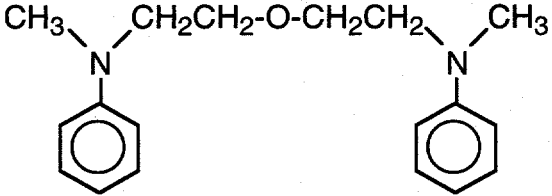
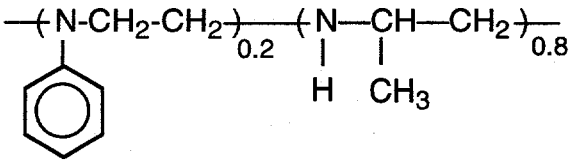
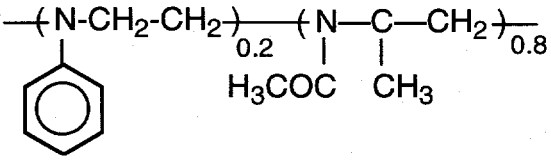
We measured the time required for SO₂ to diffuse from the sample cell to the sample loop by charging the sample cell with 0.91% SO₂ in N₂ and the head space with 100% N₂ to approximately 760 torr. In some cases, the head space was initially evacuated. After a fixed time, the sample loop was checked for SO₂ content. We expect the equilibrium SO₂ partial pressure to be the same as if the head space was initially evacuated. Figure 2-4 shows SO₂ partial pressures in the sample loop from experiments that lasted between 0.5 and 17.2 h. (The data at 25 h are for measurements with the head space initially evacuated.) The solid line is the expected value based on the initial SO₂ charge and the sample cell and head space volumes described above. Hence, we predict the diffusion time at 760 torr to be between 20 and 24 h. At lower pressures, the diffusion time should be proportionately smaller.

The procedure for the sorption runs is as follows: a known amount of liquid is placed in the sample cell and the remaining sample cell and headspace volumes are evacuated. The headspace is then charged with gaseous 10.1% SO₂ in N₂ to a known pressure. At time 0, Valve 3 is opened. The total pressure is recorded over time by a pressure transducer, and after equilibrium, the headspace partial pressures are measured by a gas chromatograph. The entire apparatus is computer controlled.

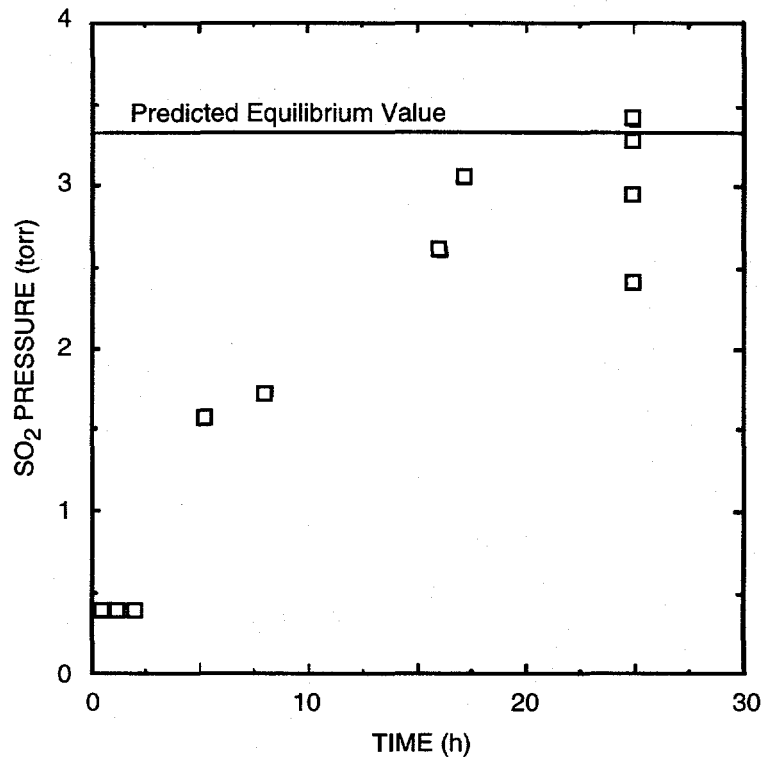
To quantify the sorption capacity of liquids, the scientific literature often reports the partition coefficient, H , defined as the equilibrium partial pressure of SO₂ in the vapor divided by the equilibrium mole fraction SO₂ in the liquid. A comparison of the sorption capacity of two liquids based on such a definition, however, is difficult because the two liquids may have different molecular weights. To circumvent this problem, we introduce H^* , a quantity similar to H but a more useful engineering parameter. H^* is defined as the volume of liquid needed to treat a unit volume of SO₂ at STP. H is more common in the scientific literature, while H^* is more useful in engineering design calculations. Details of calculations are given in Appendices A and B.

Initially, we conducted SO₂ sorption runs with four compounds: DMA, d-DMA, MAPA, and AMAPA, whose structures and complete names are shown in Table 2-3. Figure 2-5 shows the pressure changes over time for 10.1% SO₂ in N₂ over DMA for four runs. These curves are typical of all other sorption runs. To partially account for slight differences in the initial pressure $P(0)$ between runs, the plots are shown as $P/P(0)$ versus time. By doing so, we do not imply that $P/P(0)$ should collapse the curves into a single line; rather, we simply give the starting point for all curves.

Table 2-3.
COMPOUNDS SYNTHESIZED AND TESTED IN SO₂ SORPTION RUNS

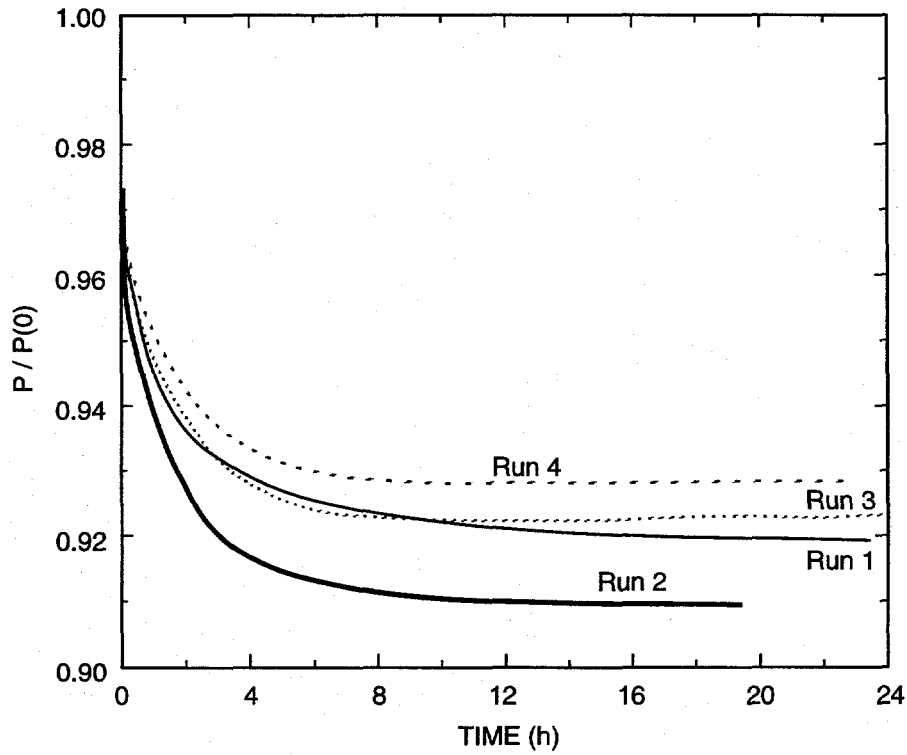
Structure	Name	Abbreviation
	N,N'-Dimethylaniline	DMA
	2,2'-Bis(N-methyl-N-phenylamino)ethyl ether	d-DMA
	Poly(2-methylaziridine-co-N-phenylaziridine)	MAPA
	Poly(N-acetyl-2-methylaziridine-co-N-phenylaziridine)	AMAPA

CM-3501-12D



CAM-3501-85

Figure 2-4. SO₂ partial pressure in the sample loop as a function of time.



CAM-3501-13B

Figure 2-5. SO_2 sorption using DMA.

Because the initial change pressures in the headspace and sample cell were slightly different, a direct comparison of these numbers is difficult. Table 2-4 details the experimental conditions.

If we assume that N₂ does not absorb in the liquid, we can attribute the entire pressure change solely to SO₂ absorption. This gives us the amount of SO₂ absorbed from pressure transducer measurements. From GC measurements, we also obtain the amount of SO₂ absorbed at equilibrium. Thus, we have two independent measurements of the amount of SO₂ absorbed, from which we can calculate two independent values for H*, shown in Table 2-5. For each run, the H* values calculated from the GC data and from the pressure transducer data are not the same. Moreover, the H* values calculated from the GC data increase with run number, whereas those calculated from the pressure transducer data fluctuate with run number.

One important reason for the discrepancy and fluctuation is that errors in measuring the final SO₂ partial pressure, P_{SO₂(f)}, are propagated through the calculations. The most important quantity measured in the experiments is the final SO₂ partial pressure. From this quantity, we calculate the amount of SO₂ absorbed by the liquids by subtracting the final SO₂ partial pressure from the initial SO₂ partial pressure. The GC measures the final SO₂ partial pressure, whereas the pressure transducer infers it by assuming that the pressure change over time is due solely to the amount of SO₂ absorbed. Thus, the GC results are more reliable than the pressure transducer results.

The increasing value of H* for DMA and d-DMA indicates that the sorption capacity decreases with each run, assuming the GC data are more reliable. Thus, desorption steps between runs are incomplete or there may be irreversible changes to the liquid with exposure to SO₂. We subsequently modified the apparatus so that it made multiple injections of the headspace. This gave us a more reliable analysis of the gas composition. In addition, we account for factors such as partial pressure of the liquid and leak rates in our calculations. These modifications have helped close the gap between the GC and transducer results, but not completely. Details of these calculations are given in Appendices A and B.

From either the GC or transducer measurements, we reach the favorable conclusion that the sorption capacities of the test liquids were higher than or equal to DMA, but with lower vapor pressure.

$$H_{\text{DMA}}^* \approx H_{\text{d-DMA}}^* > H_{\text{AMAPA}}^*$$

The value for H_{MAPA}^{*} is not compared because SO₂ showed complete, irreversible absorption into MAPA. The boiling points of these compounds are

$$T_{\text{DMA}} \approx 194^\circ\text{C}, \quad T_{\text{d-DMA}} \gg 300^\circ\text{C}, \quad T_{\text{AMAPA}} \gg T_{\text{d-DMA}}$$

Hence, the vapor pressures of d-DMA and AMAPA are much lower than that for DMA.

Table 2-4
PARAMETERS FOR SO₂ SORPTION RUNS WITH DMA

Parameter	Symbol	Units	Value
SO ₂ mole fraction in charge gas	y^0	—	0.101
Temperature	T	K	308.15
Headspace volume	VHS	cm ³	19.81
Sample cell volume	VSC	cm ³	17.01
Liquid volume	VL	cm ³	0.67
Liquid vapor pressure	VP	torr	1.5224
Liquid molar concentration	CL	mol/cm ³	0.00789

Table 2-5
RESULTS FOR SO₂ SORPTION RUNS

Liquid	Run	H*, cm ³ liq/cm ³ SO ₂ (STP)		
		Predict ^a	GC	Transducer
DMA, 35°C	1	0.3611	0.3518	0.4203
DMA	2	0.3623	0.3544	0.3792
DMA	3	0.3625	0.3649	0.4504
DMA	4	0.3623	0.3671	0.4751
Average		0.3620	0.3596	0.4312
d-DMA, 35°C	1		0.3471	0.4677
d-DMA	2		0.3560	0.4200
d-DMA	3		0.3639	0.4207
Average			0.3557	0.4361
MAPA, 80°C	1,2	Complete, Irreversible Absorption		
AMAPA, 80°C	1		0.2434	0.3569
AMAPA	2		0.2202	0.2973
Average			0.2318	0.3271

^a From Demyanovich and Lynn, 1987.

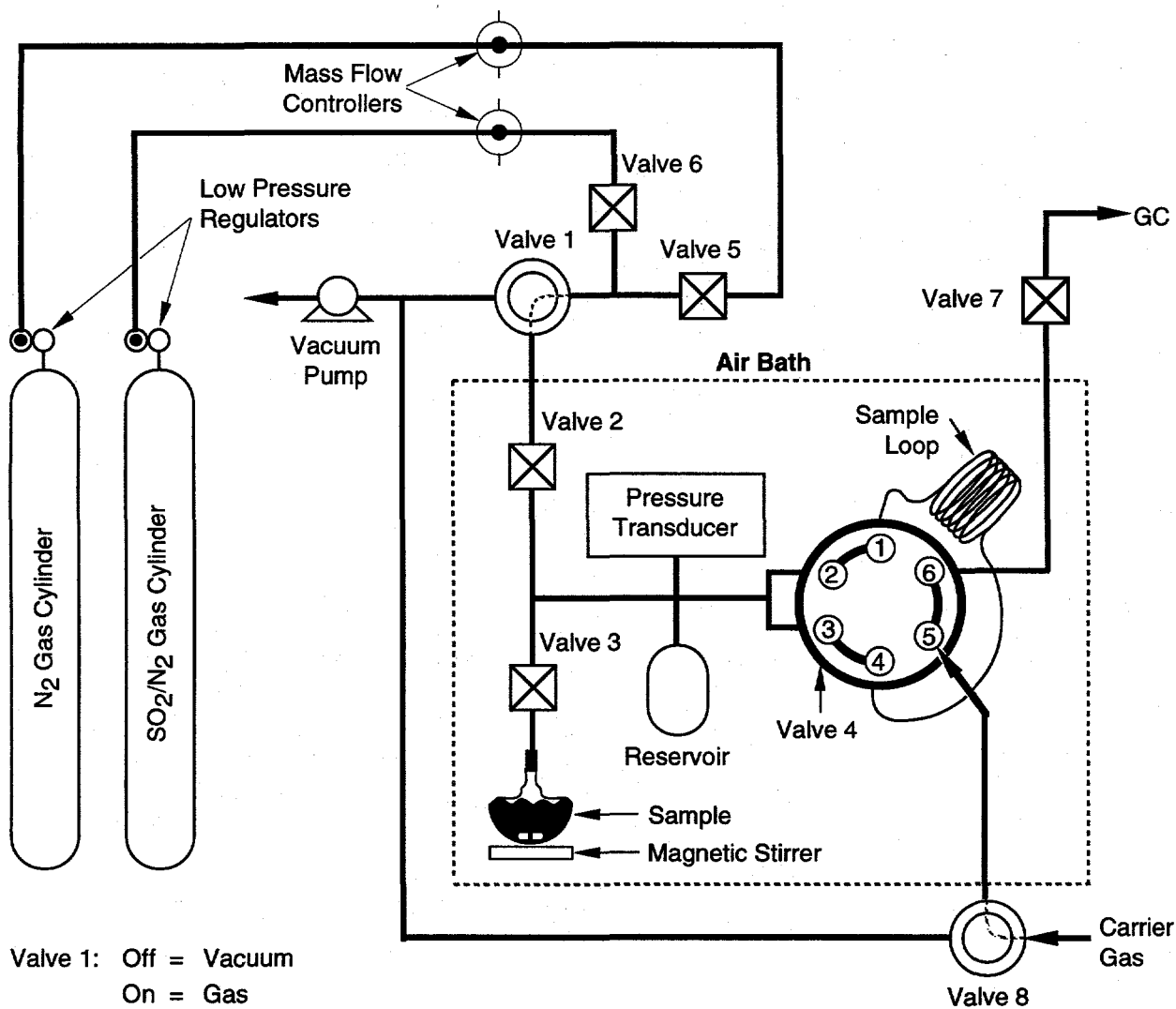
Apparatus Modification

Before performing more sorption runs, we modified the absorption apparatus such that it injects multiple samples of the headspace when the system reaches equilibrium. With this modification, an average SO₂ concentration can be calculated from several injections rather than from a single injection. This modification essentially added Valves 7 and 8 (see Figure 2-6). These valves, along with the remaining six valves, are connected to a computer to control the apparatus. Figure 2-7 shows the new algorithm for the computer program.

With the modifications complete, we measured the sorption capacity of a siloxane dimer, d-siloxane, whose structure is shown in Figure 2-8. Its synthesis is described in Task 3. We tested the compound to various atmospheres of 10.1% SO₂ in N₂ at 35°C. Four runs were made: two with an initial total pressure of 520 torr, one with 416 torr, and another with 274 torr. The final pressures for each run, along with the value of H* calculated from the pressure transducer and GC measurements, are shown in Table 2-6. Recall that H* is defined as the volume of liquid needed to absorb 1 cm³ of SO₂ at STP and has the units of cm³ liq/cm³ (STP) SO₂. The key observation here is that H* for the d-siloxane is inversely related to the final pressure. That is, the lower the final pressure, the more liquid is needed to absorb 1 cm³ SO₂ at STP.

Table 2-6
SO₂ SORPTION BY d-SILOXANE

Run No.	P _{tot} , init. (torr)	P(F), SO ₂ (torr)	H*, Transducer	H*, GC
1	520.14	8.95	0.406	0.294
2	520.16	8.80	0.457	0.293
3	416.14	6.17	0.470	0.358
4	274.14	2.68	1.056	0.513



Valve 1: Off = Vacuum
On = Gas

Valve 4: Off = Inject
On = Load

Valve 8: Off = Connect to Valve 4
On = Connect to Vacuum

Sample Cell = Volume below Valve 3, including liquid

Head Space = Volume between Valve 2, Valve 3, pressure transducer, reservoir, and Valve 4 in the load position (includes sample loop).

CM-3501-11E

Figure 2-6. Modified absorption apparatus.

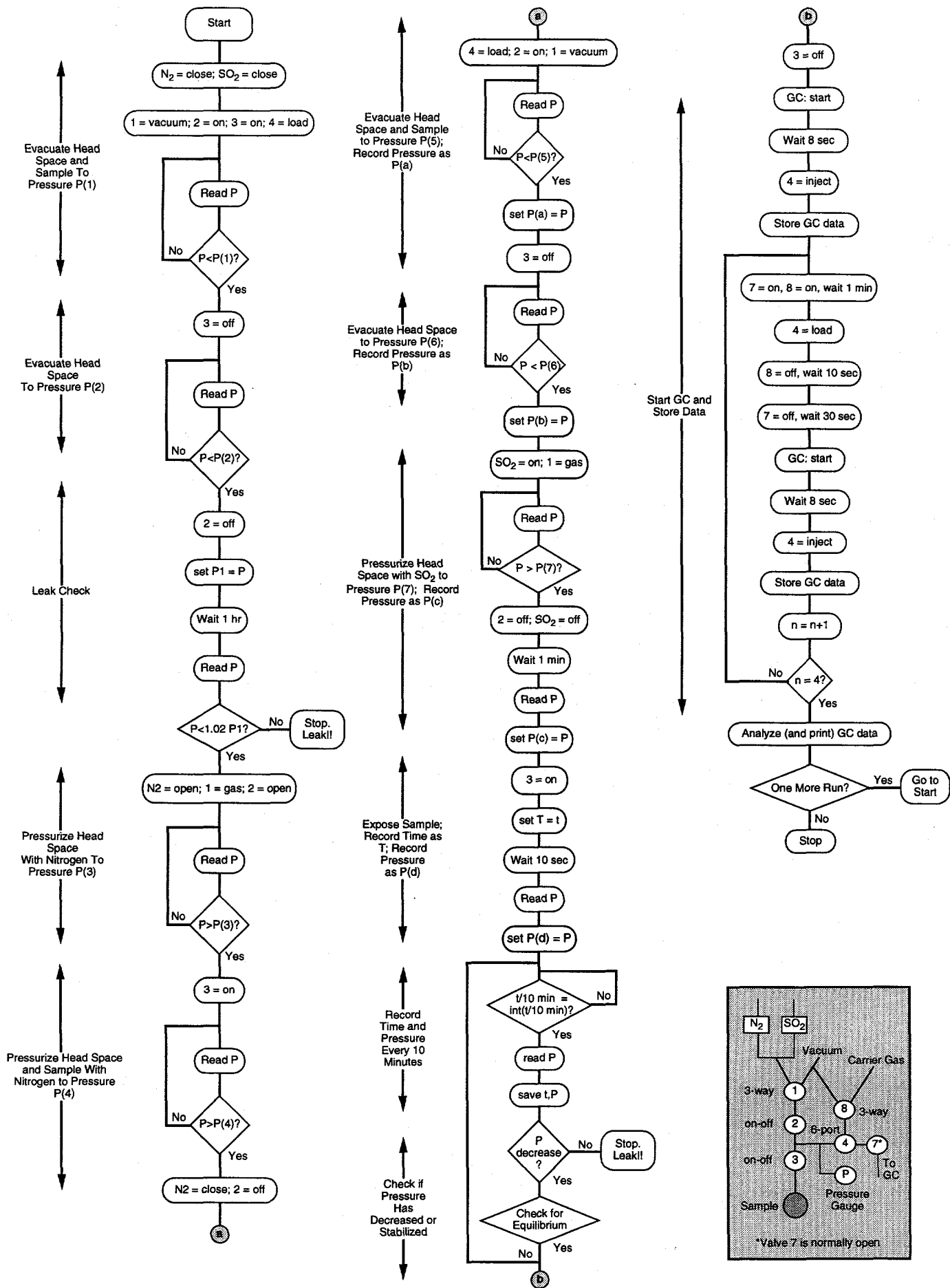
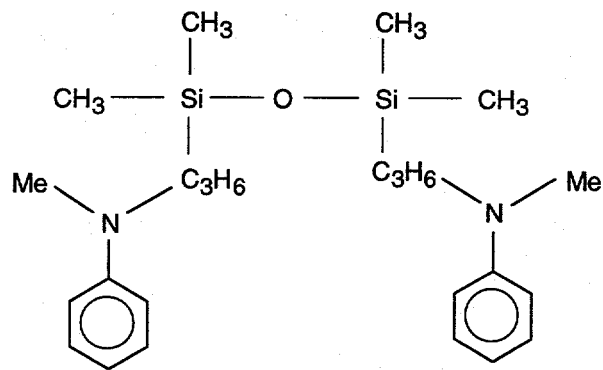


Figure 2-7. Modified algorithm for controlling absorption apparatus.

CAM-3501-53



CAM-3501-36A

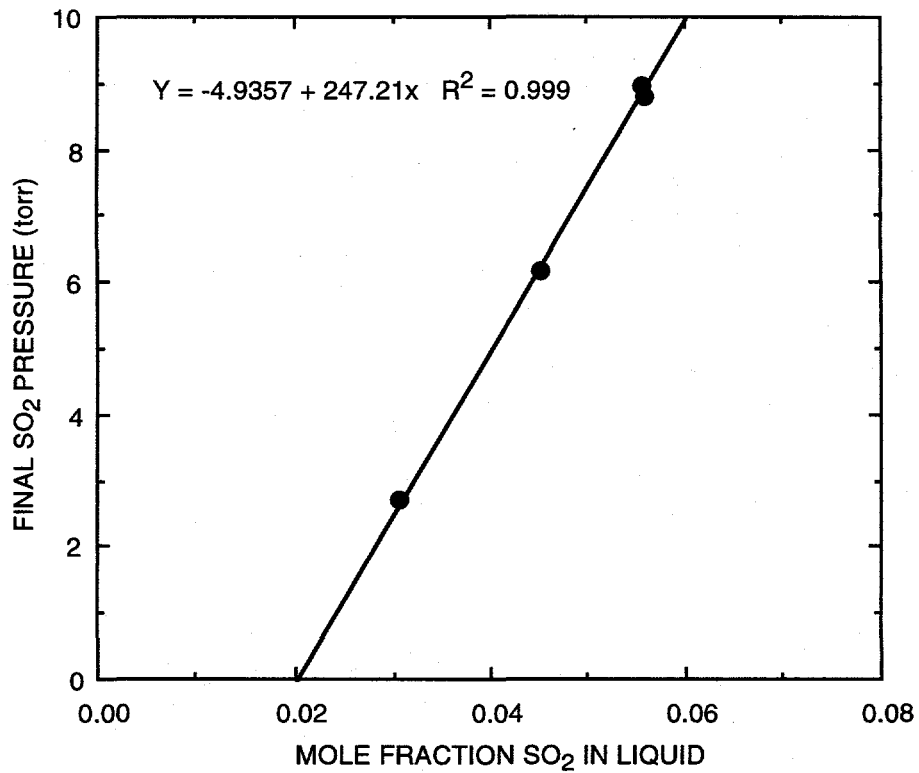
Figure 2-8. d-Siloxane.

We also computed the partition coefficient H for the four siloxane runs. Recall that H is defined as the final partial pressure of SO_2 divided by the mole fraction of SO_2 in the liquid at equilibrium. Thus, H has the units of torr/mole-fraction. A plot of the final SO_2 partial pressure versus the mole fraction SO_2 in the liquid should be linear. Figure 2-9 shows such a plot for the four d-siloxane runs. The curve through the four points is linear, but it fails to go through the origin. We suspect that, at such high mole-fractions, the SO_2 -siloxane system may be nonideal and thus Henry's law would fail. Indeed, other researchers have reported nonideal behavior with SO_2 -DMA systems at comparable concentrations (Demyanovich and Lynn, 1987).

The d-siloxane compound we tested seems more reversible than the d-DMA (the SO_2 sorption capacity of d-DMA decreased with each run). However, as shown in Table 2-6 for the d-siloxane results, the first and second runs gave identical sorption capacity. We further tested the reversibility and capacity of the d-siloxane.

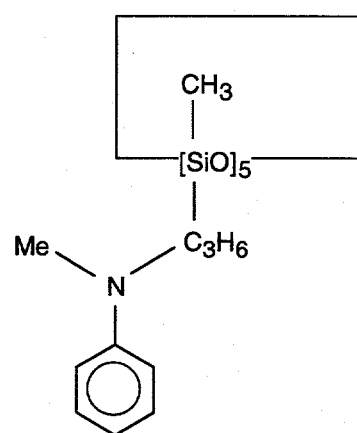
Next, we studied the sorption capacity of a siloxane pentamer similar to the dimer siloxane described above. The capacity of the siloxane pentamer, whose structure is shown in Figure 2-10, is comparable to that of the siloxane dimer. However, since the pentamer was more viscous than the dimer, it might be less adaptable to industrial applications. Table 2-7 summarizes the H^* values calculated for the siloxane pentamer.

We next compared the sorption capabilities for some of the compounds tested in this study. Figure 2-11 shows several trends in this comparison. In all cases, the H^* values calculated from



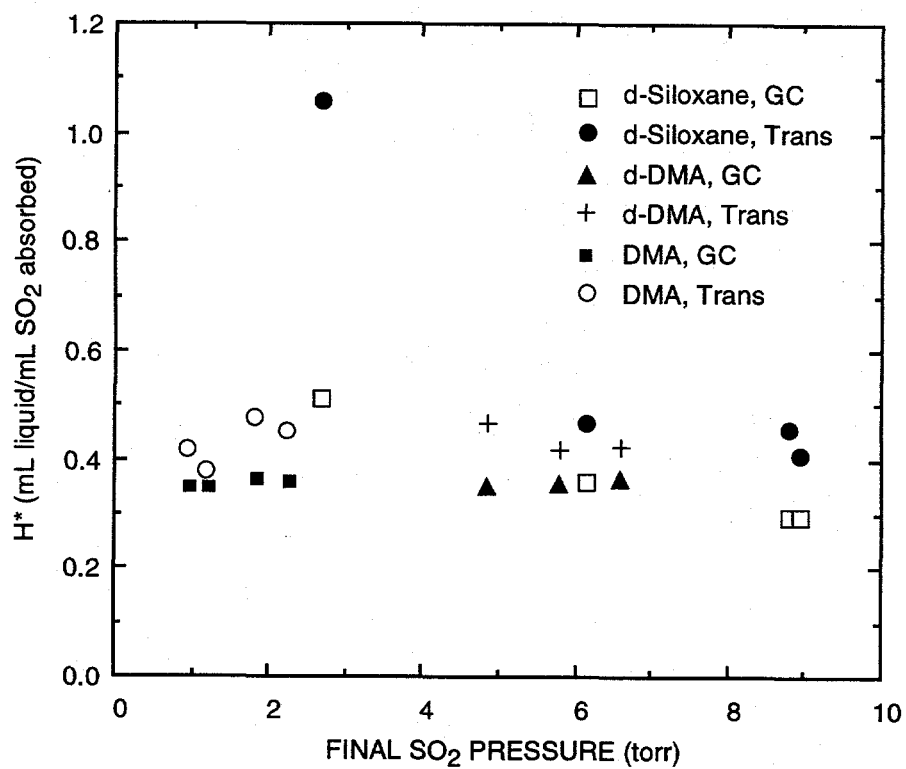
CAM-3501-41

Figure 2-9. Equilibrium between d-siloxane and SO₂ (GC results).



CAM-3501-36B

Figure 2-10. Structure of Siloxane pentamer.



CAM-3501-44

Figure 2-11. Comparison of SO₂ sorption capacities.

Table 2-7
SO₂ SORPTION BY SILOXANE PENTAMER

<u>Run No.</u>	<u>Initial Total Pressure</u>	<u>Final SO₂ Pressure (torr)</u>	<u>H*, Transducer</u>	<u>H*, GC</u>
1	596.62	6.75	0.370	0.288
2	596.90	5.30	0.555	0.280

transducer-measured pressures are higher than those calculated from GC values. This issue has been previously addressed. Also, for some of the compounds, even though the initial total pressure was the same for each run, the final SO₂ pressure was not always the same. In the case of d-DMA, the final SO₂ pressure increased slightly with each run, indicating that d-DMA is slowly losing its sorption capacity. Finally, all the GC H* values for the compounds listed fell between 0.3 and 0.5.

We determined that the DMA monomer is to be too volatile for further study and the DMA oligomers (except d-DMA) are too viscous for industrial application. The only two remaining choices were the d-DMA and d-siloxane. The characteristics of these two compounds are very similar, as shown in Table 2-8.

Table 2-8
COMPARISON OF H* FOR d-SILOXANE AND d-DMA

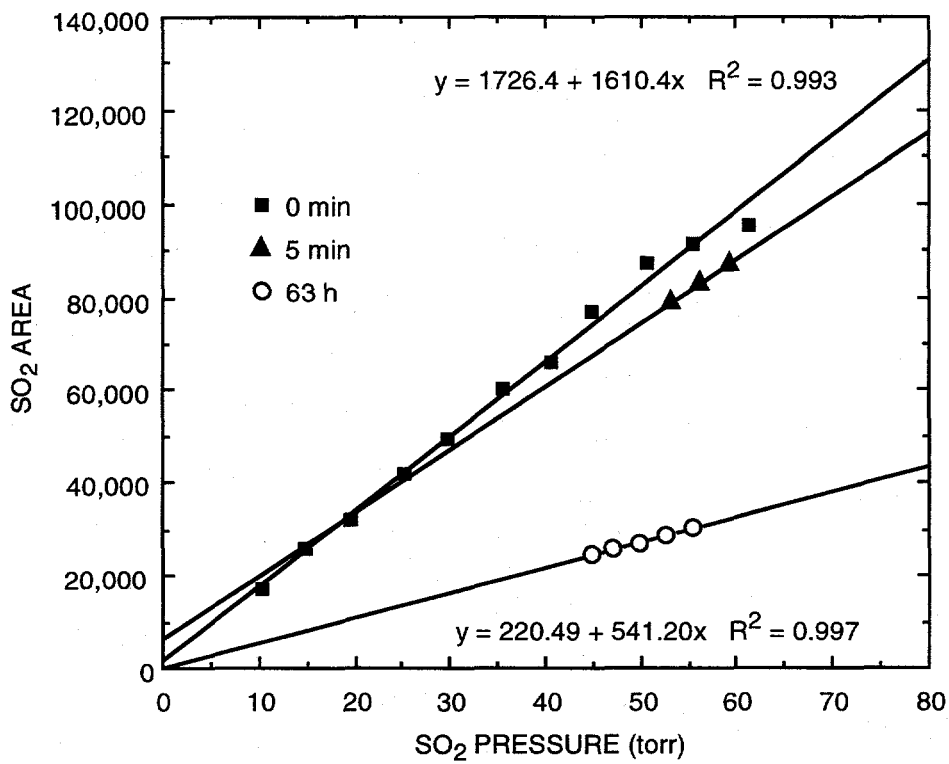
<u>Liquid</u>	<u>Run No.</u>	<u>Initial Total Pressure</u>	<u>Final SO₂ Pressure (torr)</u>	<u>H*, Transducer</u>	<u>H*, GC</u>
d-Siloxane	1	520.14	8.95	0.406	0.294
	2	520.16	8.80	0.457	0.293
	3	416.14	6.17	0.470	0.358
	4	274.14	2.68	1.056	0.513
d-DMA	1	418.95	4.86	0.468	0.347
	2	416.78	5.79	0.420	0.356
	3	417.13	6.62	0.421	0.364

For the same initial charge pressure, the siloxane and the d-DMA have similar H^* values. However, because the d-DMA seemed to slightly lose some capacity with each run (increasing H^*), the d-siloxane compound was initially thought to be more efficient. However, as discussed later, this loss in d-DMA's capacity is an artifact.

Understanding Discrepancies

We performed several tests to examine the difference between GC and transducer-measured H^* values.

In the first test, a blank run was made using an empty vial as the sample cell. The empty sample cell and head space were charged with 10.1% SO_2 gas and the system was left to stand for 63 h. During this time, the pressure transducer measured no significant change in overall pressure. After this length of time, part of the gas was injected into the GC and the area of the SO_2 peak was measured. Next, a calibration of the GC was immediately performed using the same gas as that with which the system had been charged. Finally, another 10.1% SO_2 sample was charged into the system and allowed to stand just 5 min. This sample was then injected into the GC. Figure 2-12 plots the results from these three sets of injections. Because no liquid absorbent was present,



CAM-3501-54

Figure 2-12. Calibration curves after 10.1% SO₂ was left standing in an initially empty absorption apparatus.

the three lines should collapse onto each other. Because this is not the case, it appears that SO₂ is being lost over time.

Because this loss of SO₂ seemed to be interfering with test results, tests similar to the one described above were performed to isolate sections of the apparatus responsible for the loss of SO₂. Also, a similar test was run using CO₂ instead of SO₂ to ensure that the problem was SO₂-specific; and it was. The SO₂ loss was occurring in the valve just above the sample cell in the apparatus (Valve 3). When the valve was taken apart, some residual matter was found, presumably the remnants of one or more previous experiments. Perhaps the residue had been splattered into and collected by the valve during a run. Since the valve was contaminated, a new valve was ordered and put in place.

To prevent splattering in the future, the sample vial design was modified by partially blocking off the neck of the vial. This modification allowed gases to flow through easily, and minimized liquids being splashed directly onto the valve. We decided to retest some of our samples with the new valve.

The first few retests were made to ensure that the contamination problem had been corrected. These tests consisted of charging the head space and sample cell (with no absorbent present) with 10.1% SO₂ gas and allowing the system to stand for approximately 42 h. After this period of time, the gas in the apparatus was analyzed with the gas chromatograph and compared with a calibration curve that had been made using the 10.1% SO₂ gas. These tests showed that the contamination problem had been solved, within the error limits of our experiments.

Final Selection

Because the tests performed previously on the dimer DMA (d-DMA) were not necessarily valid (it was not known whether the contamination occurred before or after the tests), four d-DMA tests were repeated. Table 2-9 shows the results of these tests. In reading this table, recall that H* is defined as the volume of liquid needed to absorb an unit volume of SO₂ at STP and has the units of cm³ liq/cm³ (STP) SO₂.

Table 2-9
SO₂ SORPTION BY DIMER DMA

Run No.	Initial Total Pressure (torr)	Final SO₂ Pressure (torr)	H*, Transducer	H*, GC
1	764.51	4.96	0.538	0.442
2	762.81	4.853	0.552	0.442
3	953.23	3.60	0.794	0.339
4*	502.85	2.98	0.663	0.995

* A large leak occurred during Run 4, making the data for Run 4 questionable.

Runs 1 and 2 were with one batch of d-DMA, while Runs 3 and 4 were with another batch. Runs 1 and 2 gave the same H*, a result we did not observe in our previous set of runs. In the earlier runs, we observed a decrease in sorption capacity with each run. Runs 3 and 4 may involve leaks. These data are more suspect.

Moreover, the values of H* for these tests are slightly higher than the values found in earlier tests on d-DMA. The earlier H* values were closer to 0.35 in the GC calculations (see Table 2-5). This difference is most likely the result of contamination, which made the initial capacity seem better. We now believe d-DMA may be a good candidate for SO₂ absorption and planned reversibility tests with it.

After the last dimer DMA run was made, some oil from the vacuum pump leaked into the system, contaminating the lines and valves. Contaminated parts were either cleaned or replaced.

After the repairs to the apparatus were completed, we decided to use pure SO₂ for the remaining SO_x absorption experiments. This enabled us to run the experiments with a smaller head space in the apparatus, which resulted in quicker run times and less gas leaks. We installed the pure SO₂ gas cylinder into the gas cabinet.

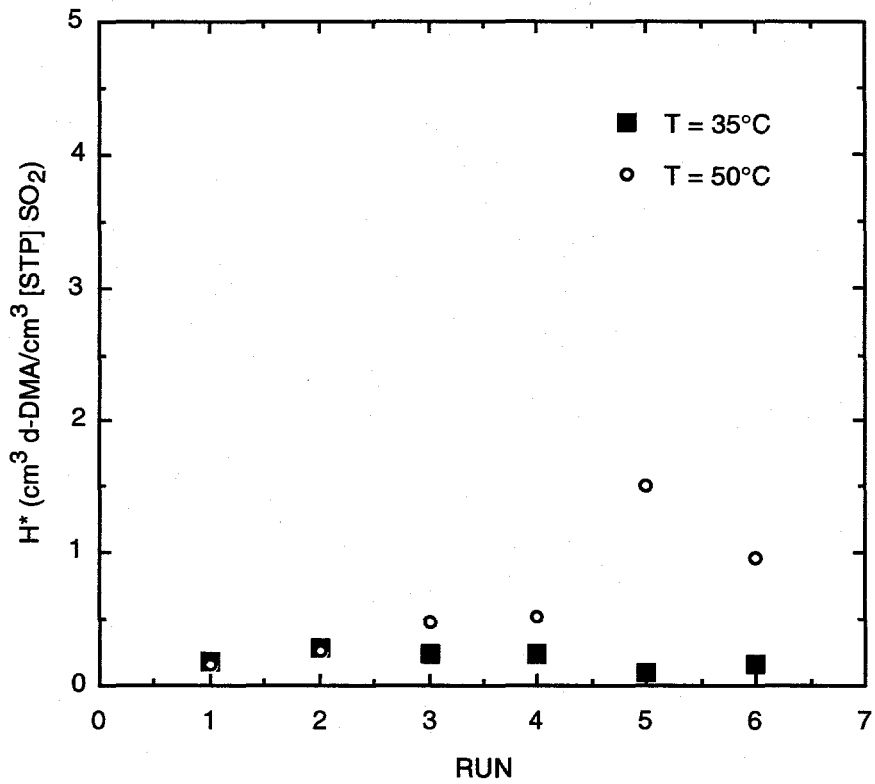
The concentration of this cylinder is 99.98% SO₂ (Liquid Carbonic; San Carlos, CA). We ran two new sets of experiments on the d-DMA to determine its reversibility for SO₂ absorption. The first set had a temperature of 35°C, and the second set had a temperature of 50°C. In each experiment, we placed approximately 0.5 mL of d-DMA into the sample cell of the SO₂ absorption apparatus. During the 35°C run, we pressurized the apparatus to 900 torr with 99.98% SO₂. Then we exposed the sample to the gas and recorded the final equilibrium pressure above the sample

cell. After the SO₂ pressure reached a steady state, we evacuated the space above the sample cell with a vacuum pump to remove the SO₂ absorbed into the d-DMA. After the d-DMA was free of SO₂, we repeated the run with the same sample at the same temperature. This absorption run was performed five more times. For the 50°C experiments, we used a fresh 0.5 mL sample of d-DMA in the absorption apparatus. Then, we repeated the absorption and desorption runs as was done with the 35°C sample.

The data from both the 35°C and the 50°C experiments were used to calculate d-DMA's capacity for SO₂ absorption in each run. As stated earlier, the absorption capacity is defined as H*, having units of cm³ d-DMA/cm³ (STP) SO₂. These values are shown as a function of their experimental run number in Figure 2-13. For the first few experiments, the H* values of d-DMA at 35°C and 50°C are similar, indicating that, initially, d-DMA's SO₂ absorption capacity is independent of flue gas temperature. During later runs of the experiments, d-DMA at 50°C shows an increase in H*, leading to lower absorption capacity. Also in Figure 2-13, the H* for the 50°C d-DMA still appears to be increasing. Therefore, we conducted additional experiments with the same sample and temperature to determine the final value of H* for d-DMA at 50°C.

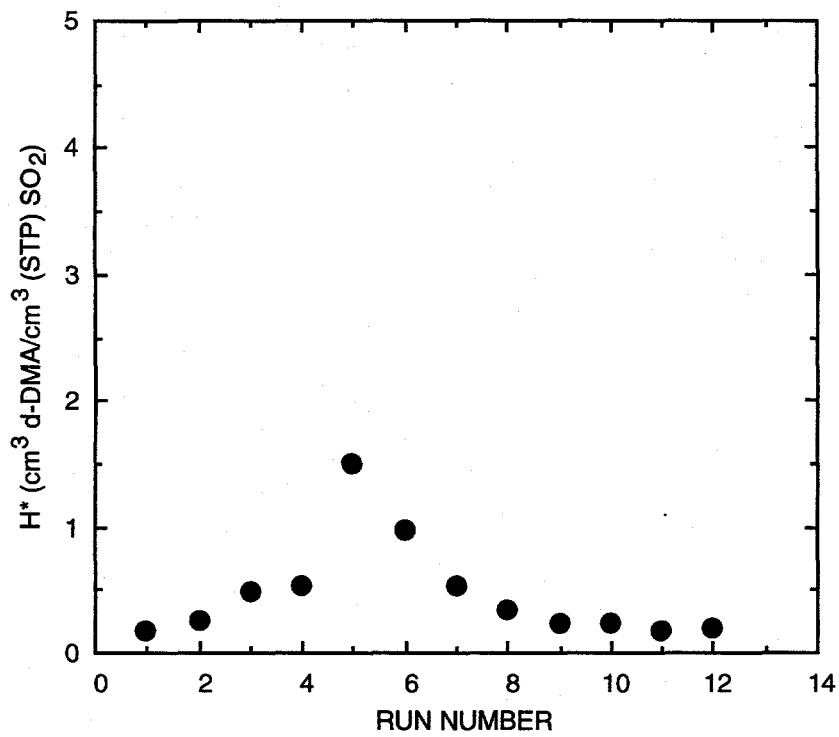
The absorption capacity for SO₂ is characterized by H*, which has units of cm³ d-DMA/cm³ (STP) SO₂. For a constant volume of d-DMA, a large H* would denote a small SO₂ absorption capacity, and a small H* would signify a large absorption capacity. As stated above, we observed that H* at 50°C increased significantly on the fifth run (Figure 2-13), and again decreased on the sixth run. Therefore, not much SO₂ was absorbed on the fifth run, but more of it was absorbed on the sixth run.

We followed the same procedure as before for measuring d-DMA's SO₂ absorption capacity. Six more runs were performed with the same 0.5 mL sample of d-DMA at 50°C. The H* values for these runs were then calculated and are plotted in Figure 2-14. In this figure, the first six runs are the ones reported in Figure 2-13. Runs 7 through 12 show a higher absorption for SO₂ than Runs 5 and 6. Also, the H* values of Runs 9 through 12 are similar to the values observed in the earliest runs of this d-DMA sample. A probable reason for the higher values of H* in Runs 5 and 6 could be that the d-DMA was not sufficiently desorbed of its SO₂ from the previous run. This would cause its lower absorption capacity during Runs 5 and 6. Therefore, d-DMA's ability for absorbing SO₂ does not degrade upon repeated exposure to SO₂ at 50°C. Upon completion of the SO₂ absorption/desorption runs with d-DMA at 35°C and 50°C, we performed additional runs at 100°C. We desorbed SO₂ from the sample after completing the last 50°C test. The SO₂ stripping operation was conducted using vacuum at 50°C. Then the same sample was heated to 100°C in the



CAM-3501-76

Figure 2-13. SO₂ absorption lifetime of d-DMA at 35° and 50°C



CM-3501-79

Figure 2-14. Lifetime SO₂ absorption/desorption run on d-DMA at 50°C.

absorption apparatus. The temperature was allowed to equilibrate to prevent any erroneous pressure readings by the pressure transducer.

The result of the 100°C run is shown along with the 35° and 50°C results in Figure 2-15. In the figure are two data points for 100°C. During the run, we experienced some difficulty with the pressure transducer. The pressure above the sample at time zero of SO₂ exposure was 393.37 torr. Initially, when we calibrated the pressure transducer at 100°C, we noticed some fluctuations in the pressure reading. This fluctuation stopped before we performed the absorption run. These two equilibrium pressures could be due to the drift in the pressure transducer sensitivity. Also, the pressure transducer may not have been able to handle 100°C temperatures. We calculated H* for both of the final pressures, as given in Figure 2-15. These H* values appear to be slightly higher than the H* values at the lower temperatures. This is expected, because usually the solubility of a gas in a liquid decreases with increasing temperature. However, their values are within 75% of the other H* values. This shows that the d-DMA does have significant absorption capacity for SO₂ at the elevated temperatures. This is the same sample that was used for the 50°C tests. This would make the 100°C test its thirteenth run. Thus, after thirteen runs, d-DMA exhibits its continued performance as a good candidate for SO₂ absorption. This concluded our lifetime studies for the d-DMA.

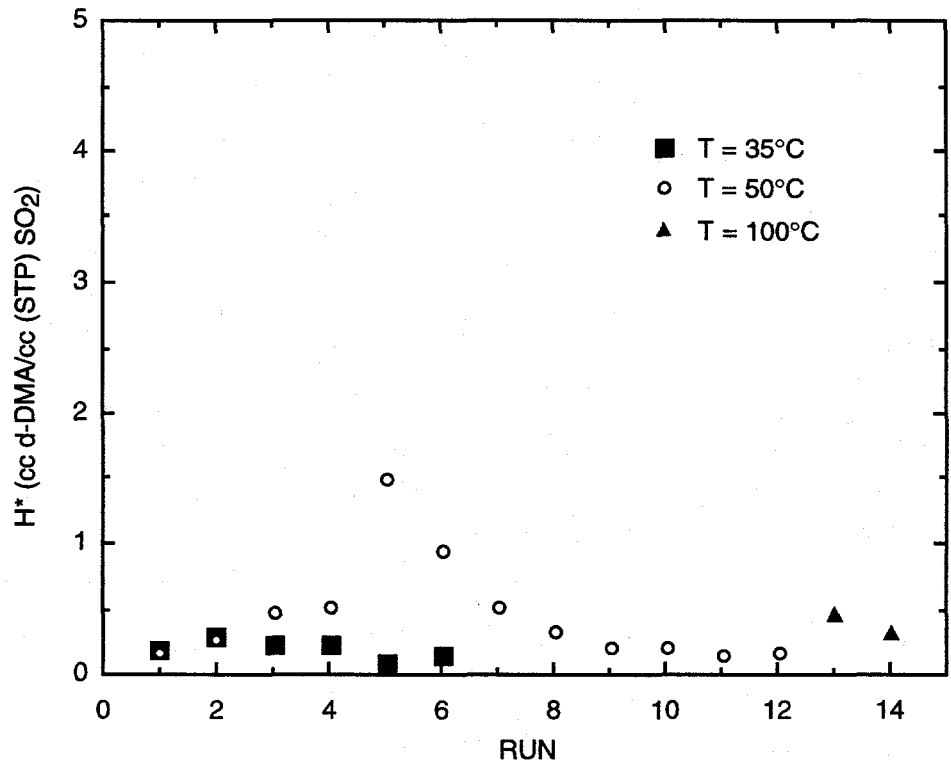
NO_x ABSORPTION

Absorption Studies

Figure 2-16 shows the completed assembly of the NO_x-absorption apparatus. A mixture of NO_x/N₂ is blended with N₂ and humidified by passing it through a bubbler containing deionized water (Millipore Milli-Q Water Purification System) and then scrubbed by passing it through another bubbler containing a NO_x-absorbing solution. The NO_x depleted gas emerging from the second bubbler is sent to the NO_x analyzer. By monitoring the flow rates and the inlet and outlet NO_x concentrations at the bubblers over time, we can calculate the amount of NO_x absorbed by the solution.

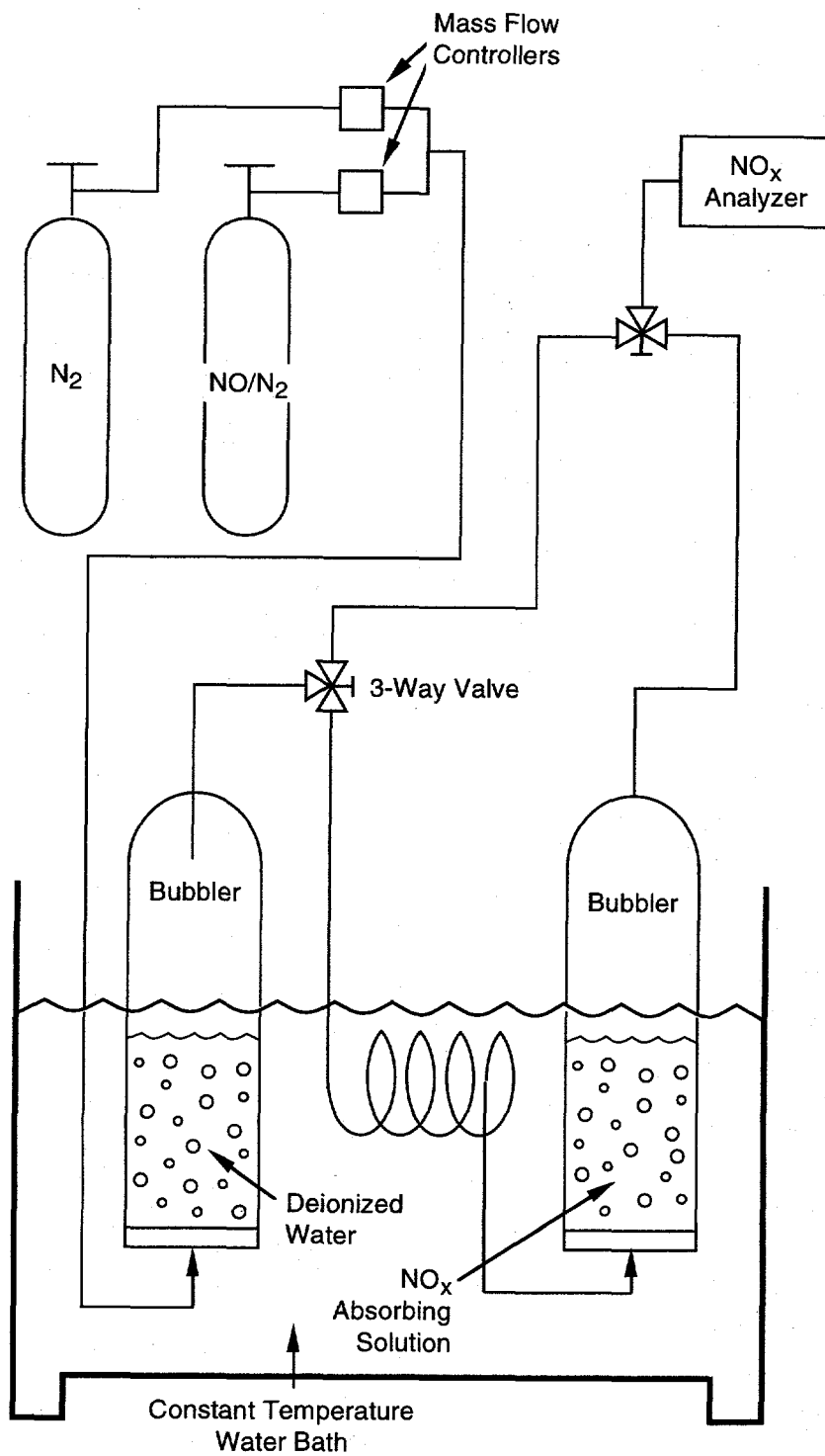
Initially, we tested our apparatus by duplicating experiments reported in the literature (Sada et al., 1984). Sada et al. report the equilibrium constant K at 35°C for the reaction to be





CM-3501-80

Figure 2-15. Lifetime tests on d-DMA for SO₂ absorption/desorption.



CM-4334-21A

Figure 2-16. NO_x absorption apparatus.

9.9×10^5 L/mol. Our first goal was to duplicate this result using the NO_x absorption apparatus. A 900 sccm, 990 ppm NO/balance N_2 gas stream was used as the simulated flue gas. The NO_x -absorbing solution for this experiment was a 450-mL, 0.01-M solution of $\text{Fe}^{\text{II}}(\text{EDTA})^{2-}$ prepared by adding equimolar amounts of ethylenediaminetetraacetic acid disodium salt-dihydrate and ferrous sulfate-heptahydrate (both from Sigma Chemical Co., St. Louis, MO). The scrubbing solution was kept at 35°C , and the gas was humidified and preheated to 35°C before entering the bubbler. The exiting gas stream was sent to the NO_x analyzer where its NO concentration was recorded over time. The experimental run was stopped once the exiting gas stream's NO concentration reached the inlet concentration.

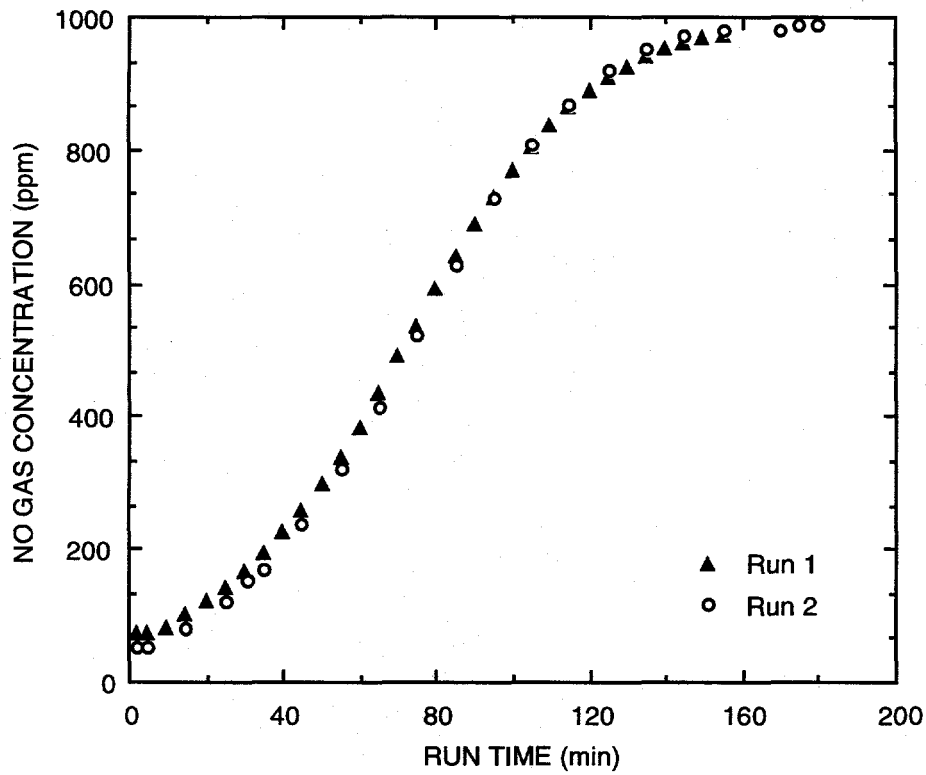
This experiment was performed twice to test the reproducibility of the apparatus. Figure 2-17 shows the results of the two experiments. These data were then used to calculate the equilibrium constant (K) for the reaction shown in Eq. (2-2). Details of this calculation are given in Appendix C. The values of K from both experiments were calculated to be 9.41×10^5 L/mol and 1.03×10^6 L/mol, respectively. They are close to one another, indicating reproducibility, and are within 5% of that reported by Sada et al.

In our next series of experiments, we performed additional NO_x -absorption runs with solutions of Fe(II)-EDTA, Fe(III)-phthalocyanine, Fe(II)-phthalocyanine, Co(II)-phthalocyanine, Ni-phthalocyanine, and Cu-phthalocyanine-3,4',4'',4'''-tetrasulfonic acid, tetrasodium salt, 85% pure (Aldrich Chemical Company, Inc., Milwaukee, Wisconsin). (Refer to Task 3 of this report for synthesis procedures.) These experiments were conducted with a 0.02 M NO_x -absorbing solution, a flue gas concentration of 100 ppm NO, and a gas/liquid temperature of 25°C , similar to the NO_x scrubbing experiments with the hollow fiber contactor (HFC) (Task 5). In all the absorption runs, a 50-mL volume of a NO_x -absorbing solution was used; other conditions were similar to the two previous NO_x -absorption runs.

Figure 2-18 shows the results from these experiments. We have plotted the axes in dimensionless quantities: C/C_0 versus Qt/V , where C is the measured exiting NO concentration, C_0 is the inlet NO concentration, Q is the gas flow rate, t is the run time, and V is the liquid volume. As outlined in Appendix C, these results may be used to calculate the reaction equilibrium constant K of the reaction

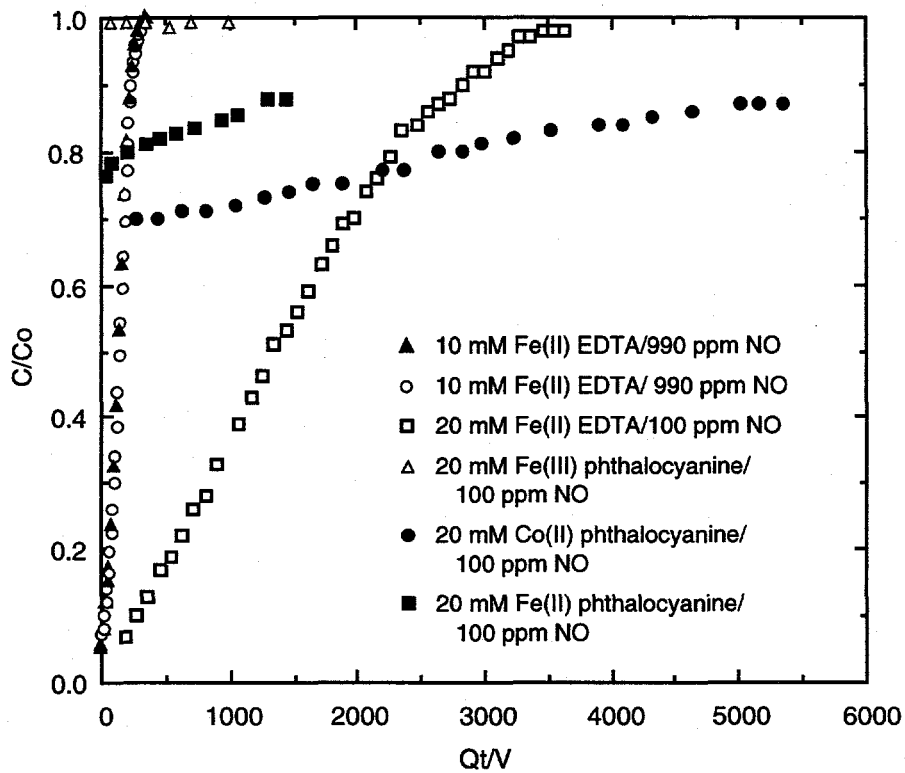


where M represents the NO-binding compound. Table 2-10 gives the results of this exercise. As shown in the table, the K value for the 0.02 M Fe(II)-EDTA solution is higher than the one for the 0.01 M solution (reported above). We believe that this is due to the lower temperature.



CAM-3501-56

Figure 2-17. Exiting NO concentration versus time for the 10-mM Fe(II)-EDTA/990-ppm NO runs.



CAM-3501-57A

Figure 2-18. NO concentration over time for different scrubbing agents.

Table 2-10
EQUILIBRIUM CONSTANTS (K) USING 100 ppm NO IN N₂ AND
0.02 M AQUEOUS NO_x-ABSORBING SOLUTIONS AT 25°C

<u>Compound</u>	<u>Equilibrium Constant, K (L/mol)</u>
Fe(II)-EDTA	2.89 x 10 ⁶
Fe(III)-phthalocyanine	0
Fe(II)-phthalocyanine	3.41 x 10 ⁵
Co(II)-phthalocyanine	2.03 x 10 ⁶
Ni-phthalocyanine	0
Cu-phthalocyanine	0

Also in Table 2-10 are the K values found for the phthalocyanine solutions. K could not be calculated for Fe(III) phthalocyanine, Ni-phthalocyanine, or Cu-phthalocyanine solutions because NO_x removal was not observed. Overall, the Fe(II)-EDTA solution is the best NO_x-absorbing compound, followed by Co(II)-phthalocyanine and by Fe(II)-phthalocyanine. The Co(II)-phthalocyanine did absorb almost as much NO_x as the Fe(II)-EDTA, but the kinetics to do so appear to be much slower. However, this may not be an issue, because kinetics do not usually dominate absorption in a HFC; mass transfer does.

We also repeated the experiment of determining the NO absorption capacity of Fe(II)-EDTA (described above) to see if our results would be reproducible at 100 ppm NO. A 50-mL, 0.02-M Fe(II)-EDTA solution was made by mixing equimolar amounts of FeSO₄ • 7 H₂O and Na₂-EDTA. As before, gas from a 1.04% NO/balance N₂ cylinder was diluted by adding N₂ to form a 900-sccm, 100-ppm NO feed stream. The feed was sent through the NO_x-absorbing apparatus where it was heated, humidified, and contacted with the Fe(II)-EDTA solution. The temperature of the gas and of the Fe(II)-EDTA was set at 25°C. The exiting NO concentration was monitored over time by the NO_x analyzer until it reached the feed's concentration of 100 ppm NO.

The results of this experiment are very close to those of the original Fe(II)-EDTA experiment. As shown in Figure 2-19, the breakthrough curves from both experiments are similar. Also, the calculated equilibrium constants, K , for the reaction listed in Eq. (2-2) from both experiments agree closely. In the first experiments reported in Table 2-10 was K 2.89×10^6 L/mol. In this experiment, K was calculated to be 2.7×10^6 L/mol. These values differ only by 6.5%. Therefore, we confirmed the NO absorption capacity for Fe(II)-EDTA for 990 ppm and 100 ppm NO feeds.

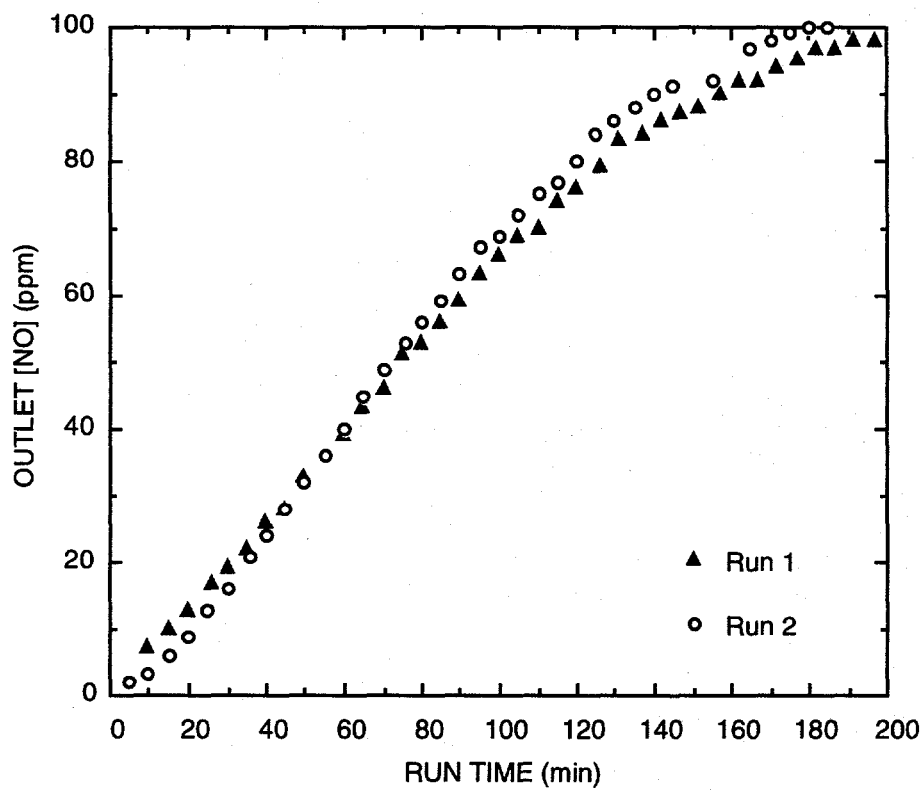
We also tested a series of new NO_x -absorbing compounds, and we modified the NO_x -absorbing apparatus to fit the characteristics of these new scrubbing compounds.

We continued the research work in two directions. To better understand the NO_x absorption chemistry, we modified our original NO_x absorption apparatus to continuously monitor the pH of the absorbing solution, as shown in Figure 2-20. The pH variation of the solution with NO loading would provide us with more insight into the chemical interactions of the species present in the solution. Also, we conducted several experiments using the modified apparatus after its testing with the base case of Fe(II)EDTA solution. The objective of these experiments was to test new chemicals as well as to reexamine already tested chemicals with feed gas streams containing representative compositions of coal-burning power plant flue gases.

Effect of Oxygen

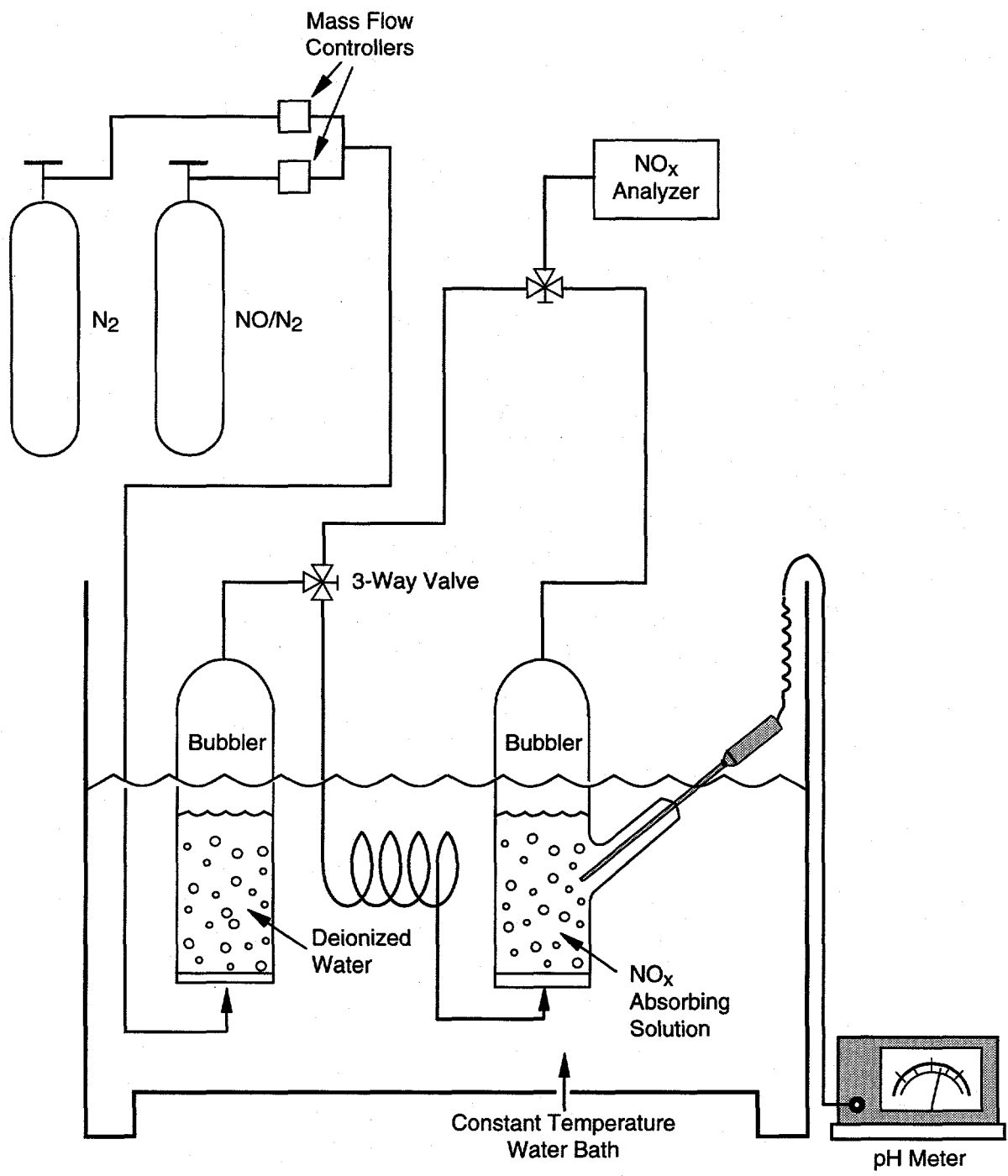
Flue gases from coal-burning utility stations often consist of several hundred ppm of NO and 3% to 4.5% of O_2 . We incorporated these compositions into our experimental runs to simulate realistic conditions. Approximately 50 mL of the polymeric analogue to Fe(II) EDTA (synthesis at pH 6 and pH 4.2, as described in Task 3) was tested for NO absorption capacity. The feed gas flow rate for these experimental runs was 900 sccm (500 ppm NO with balance N_2). The newly synthesized chemicals did not exhibit any NO absorption and hence were not considered in further work.

The literature has long established that iron chelates oxidize in the presence of O_2 , which deactivates their activity toward absorption of NO. From our past experimental data on nonferrous chelates (Table 2-10), it is evident that Co-phthalocyanine is another promising candidate agent. Therefore, we conducted an experimental run using 50 mL of 0.02 M Co-phthalocyanine solution with 4.5% O_2 in the feed gas stream. Figure 2-21 shows the variation of outlet NO concentration



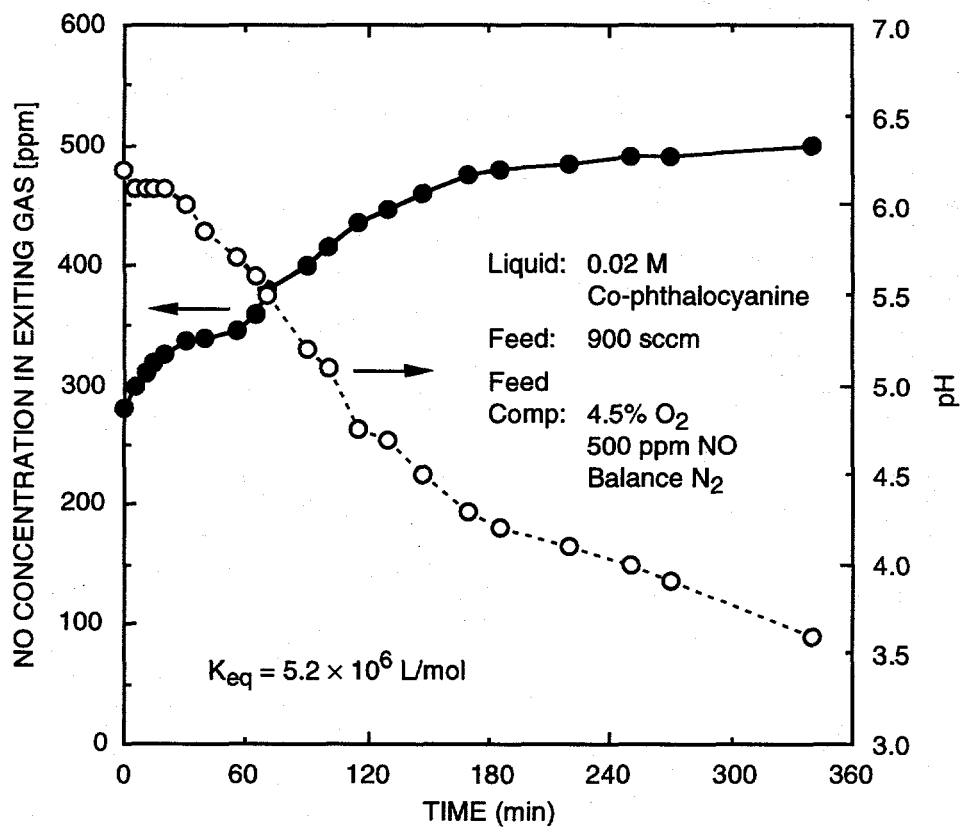
CAM-3501-58

Figure 2-19. NO_x-absorbing runs using 20 mM Fe(II)-EDTA and 100 ppm NO.



CM-4334-21B

Figure 2-20. Experimental flowsheet for NO_x absorption tests with on-line pH measurement.



CM-3501-62

Figure 2-21. NO absorption by Co(II)-phthalocyanine in the presence of oxygen.

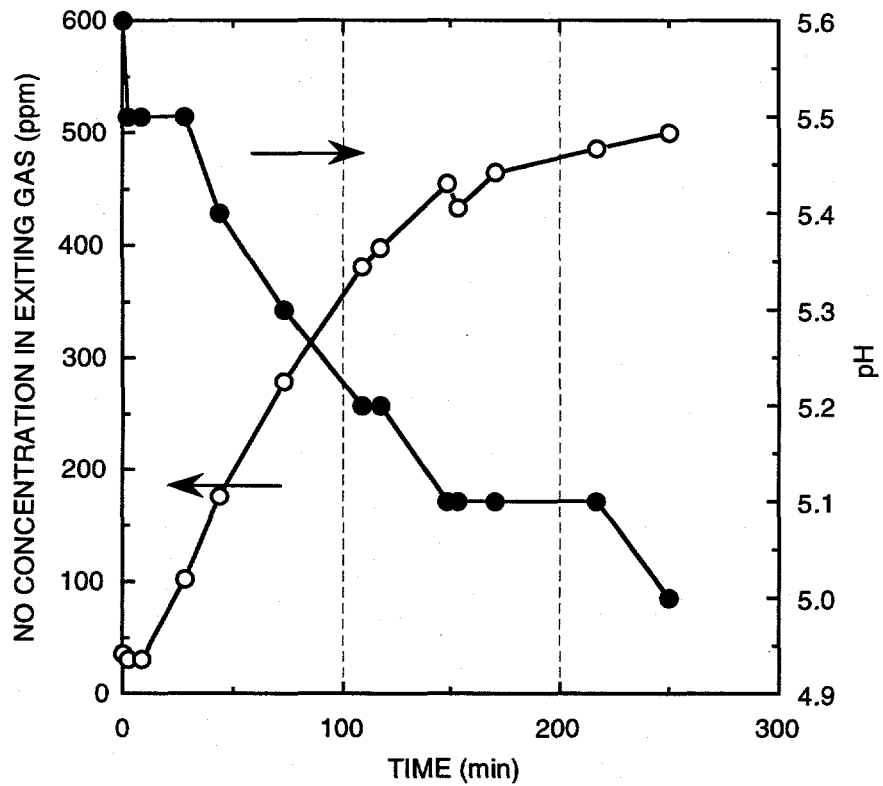
and pH of the solution with time. The equilibrium constant (K) is calculated to be 5.2×10^6 L/mol. This encouraging high K value in the presence of oxygen prompted us to take this absorption chemistry further in Task 5, where we studied the NO-absorption behavior in an HFC.

Next, we performed two new NO_x absorption experiments with two absorbing solutions: Co(II)-phthalocyanine and Co(II)-EDTA. The gas composition for both experiments was 500 ppm NO, 4.5% O_2 , and balance N_2 . From our previous NO_x absorption experiments with Co(II)-phthalocyanine, we noticed that this solution had a NO_x capacity comparable to Fe(II)-EDTA. However, the kinetics of the NO complexation reaction in the cobalt solution were slower than that of the Fe(II)-EDTA. This behavior is shown in Figure 2-21, where the slope of NO concentration of the gas leaving the absorption bubbler tends to be flat (slope ~ 0) with time. In all the earlier Fe(II)-EDTA runs, the slopes of NO concentrations were steeper than the one shown in the figure. To overcome the slow kinetics of this solution, we conducted another 500 ppm NO absorption run using a 50-mL, 100-mM Co(II)-phthalocyanine solution at elevated temperatures.

The temperature of the aqueous liquid was heated to 50°C using a water bath. Figure 2-22 shows the results of this experiment. As expected, increasing the concentration and the temperature of the cobalt solution increased the rate of the NO complexing reaction. The initial concentration of NO in the gas coming out of the bubbler reached nearly 30 ppm as opposed to 300 ppm in Figure 2-21. This shows that increasing the Co solution concentration and temperature increased the rate at which NO was bound. The equilibrium constant, K , for this experiment was calculated to be 7.04×10^5 L/mol. As a result, we used this 100-mM Co(II)-phthalocyanine solution heated to 50°C in the NO_x scrubbing experiments for Task 5. These results are presented under Task 5.

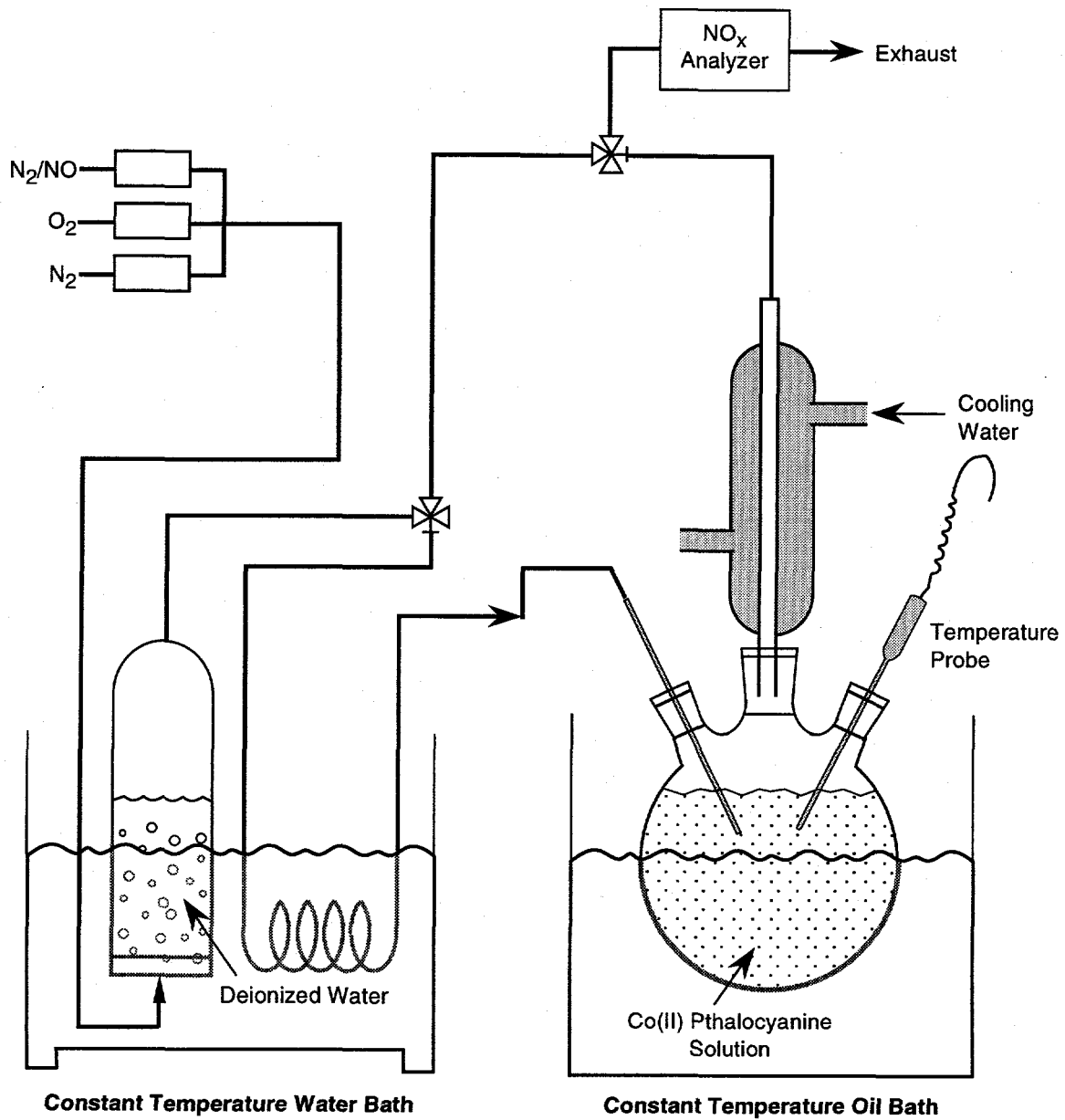
From chemical synthesis work (Task 3), we received a 20-mM solution of Co(II)-EDTA, prepared by mixing equimolar amounts of Co(II) sulfate hydrate (Aldrich Chemical Co; Milwaukee, WI) and EDTA (Sigma Chemical Co., St. Louis, MO). We performed a NO_x -absorbing experiment with 50 mL of the 20-mM Co(II)-EDTA solution. The temperature of the gas and the solution were maintained at 50°C . We ran this experiment to determine Co(II)-EDTA's ability to bind NO. However, at the beginning of the run, we observed only 4% removal of NO using this compound. This implies that Co(II)-EDTA would not be a good candidate scrubbing solution for NO.

The Co(II)phthalocyanine appears to be the best candidate for NO_x absorption. However, the desorption characteristics of the Co(II)-phthalocyanine solution at higher temperatures have not been examined. Therefore, we conducted an experiment at $70 \pm 3^\circ\text{C}$ to study the binding/releasing properties of Co(II)-phthalocyanine with dissolved NO.



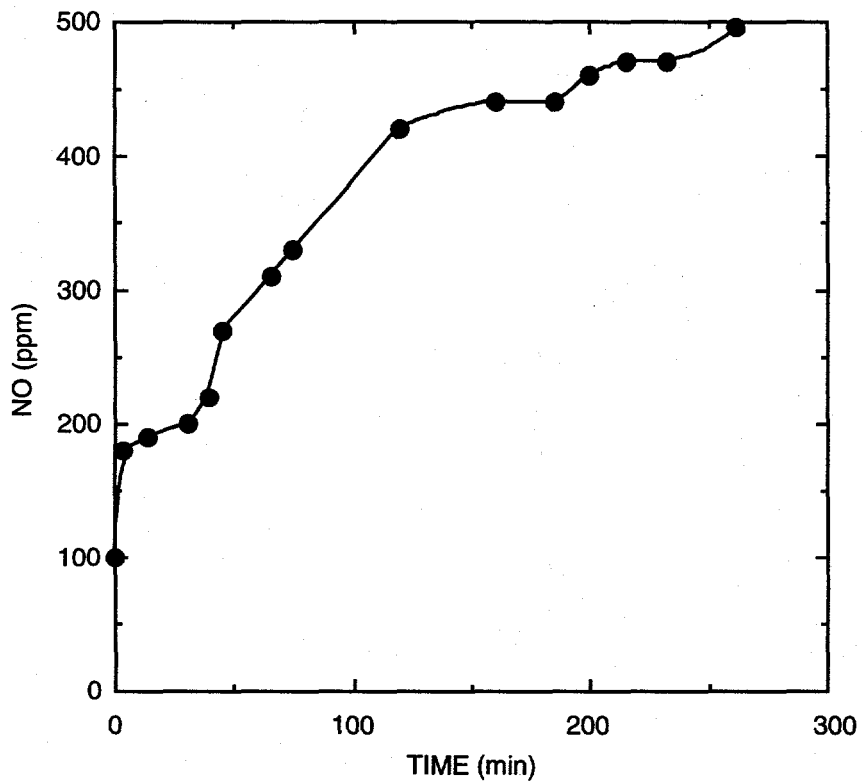
CM-3501-71

Figure 2-22. Co(II)-phthalocyanine NO absorption capacity at 50°C.



CM-4334-21D

Figure 2-23. Experimental schematic for NO_x absorption at elevated temperatures.



CM-3501-92

Figure 2-24. Absorption behavior of 0.1 M Co(II) phthalocyanine solution at 70°C.

TASK 3: CHEMICAL SYNTHESIS

The objectives of this task were to synthesize an oligomer of dimethylaniline (DMA) for our study of SO₂ liquor regeneration and to synthesize compounds suitable for reversible absorption of NO_x in aqueous solutions. We chose to make an oligomer of DMA for SO₂ liquor regeneration to reduce the vapor pressure of the SO₂ regeneration media, thereby minimizing any losses of the SO₂ regeneration chemical.

SO_x ABSORBENTS

We identified two routes for synthesizing oligomers of DMA. In the first, as described in the original management plan, we convert low molecular weight poly(ethyleneimine) to the corresponding chloroamine polymer, followed by benzylation, as shown in Figure 3-1. To standardize the chemistry of this approach, we use tetraethylenepentamine pentahydrochloride, shown in Figure 3-2. Chlorination and benzylation reactions are optimized on this model reagent before proceeding with the reaction on the polyethyleneimine oligomer.

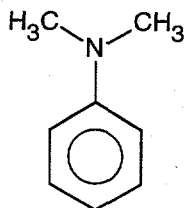
In the second route, we synthesize 1-phenylaziridine from the commercially available 2-anilinoethanol, as shown in Figure 3-3. 2-Anilinoethanol is treated with sulfuric acid to afford the desired 2-anilinoethyl sulfate. Cyclization to yield 1-phenylaziridine is then accomplished by treatment with aqueous sodium hydroxide. Conventional ring-opening polymerization is then carried out.

To date, we have synthesized several polymers of DMA, all via the second synthesis route. The first, an oligomer of DMA, resulted in an insoluble (to most solvents) solid unsuitable for use as an absorbent. Second, to produce a liquid material, we synthesized DMA copolymers. A 50:50 (mole ratio) copolymer of N-phenylaziridine and propyleneimine also resulted in a solid. Third, reducing the ratio of N-phenylaziridine to propyleneimine (to 30:70) produced a viscous liquid at room temperature. We prepared fourteen grams of the 30:70 copolymer to study its absorption properties. The reaction scheme for the DMA oligomer is shown in Figure 3-4, and for the copolymer in Figure 3-5. Details of the synthesis procedure follow.

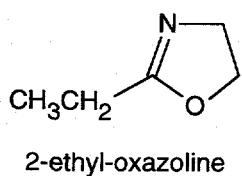
Synthesis of the Oligomeric Dimethylaniline (o-DMA)

We prepared o-DMA by polymerization of N-phenylaziridine according to the four-step scheme shown in Figure 3-4.

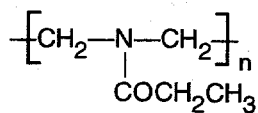
Dimethylaniline (DMA):



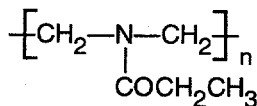
Synthesis of Oligomer of DMA:



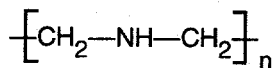
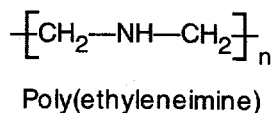
Methylsilylate
(Catalyst)



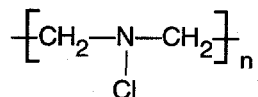
Poly[N-(carboxyethyl)-ethyleneimine]



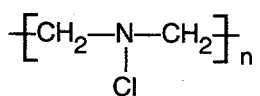
8 N HCl



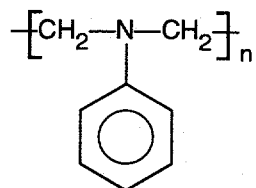
NaOCl



Poly(N-chloroethyleneimine)



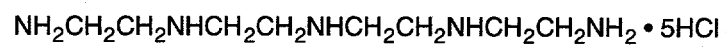
Benzene
96% H₂SO₄/Fe(II)



Oligomer of DMA

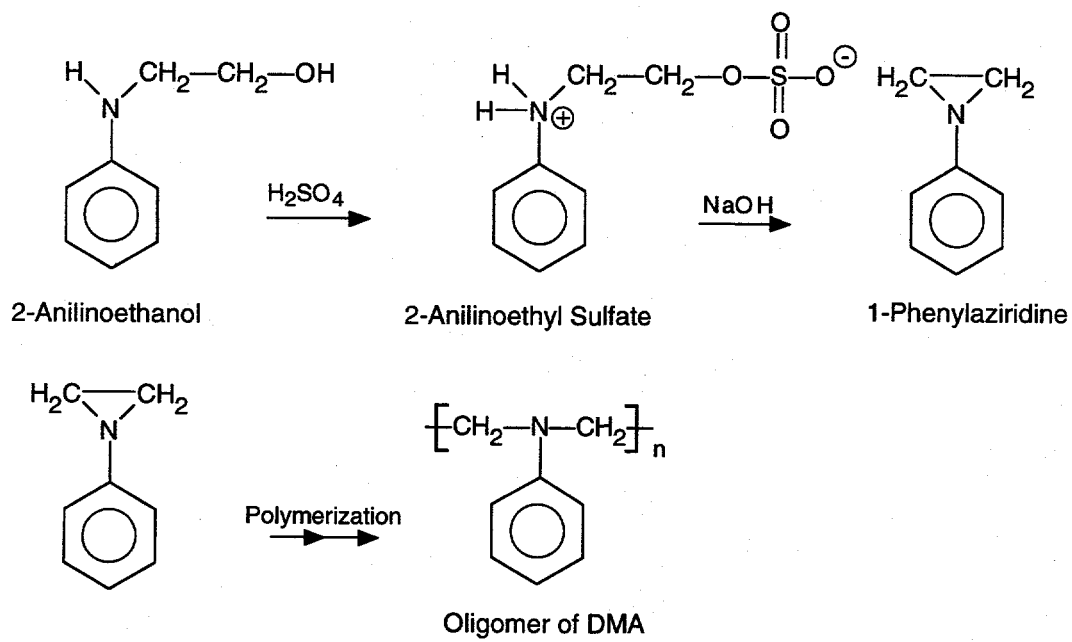
CAM-360583-47A

Figure 3-1. Reaction scheme "A" for synthesis of oligomer of DMA.



CM-3501-1

Figure 3-2. Tetraethylenepentamine pentahydrochloride in the first synthesis route.



CM-3501-2

Figure 3-3. Second route for synthesis of oligomer of DMA.

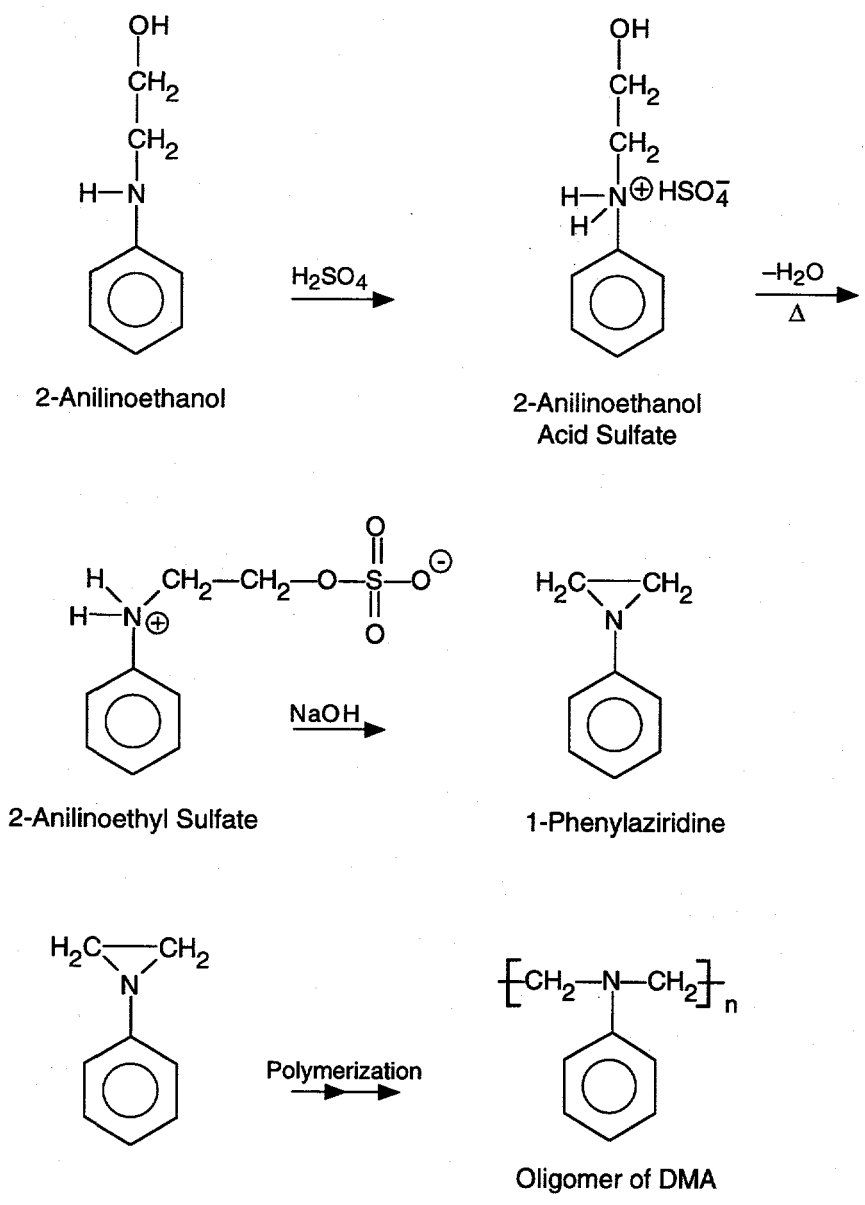
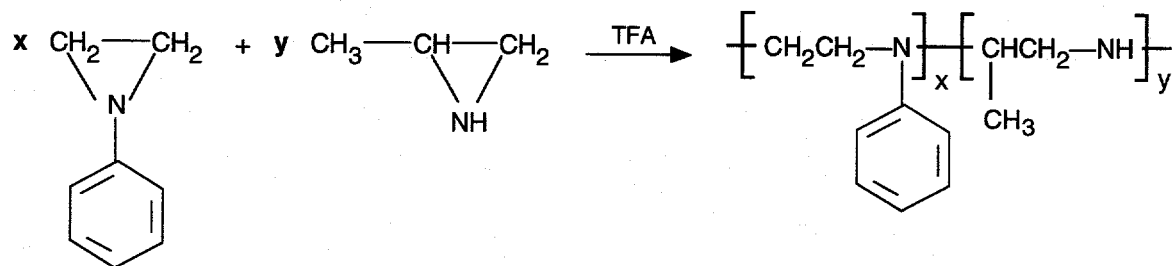


Figure 3-4. Reaction scheme for synthesis of oligomer of DMA.



CM-3501-5

Figure 3-5. Copolymerization scheme of N-phenylaziridine and propyleneimine.

Step 1: Synthesis of 2-Anilinoethanol Acid Sulfate. 2-Anilinoethanol (13.7 g, 0.1 mol) was diluted with water (13.7 g) and cooled to 0°C. This solution was added to 96.4% H₂SO₄ (10.1 g, 0.1 mol) diluted with 10.1 g of water. After mixing, the water was removed by rotary evaporation, and the product was precipitated out by the addition of acetone. The mixture was thoroughly stirred, and the solid product was filtered and dried to give a white solid (yield: 22 g, 93%). The product was characterized by ¹H NMR: (δ, D₂O): 3.3 - 3.8 (m, 4 H), 7.5 (s, 5 H).

The thermal gravimetric analysis of the product showed three steps of decomposition on heating from 40° to 550°C. The first step begins at 125°C and ends at 150°C due to the loss of water, the reaction desired for Step 2 of the synthesis.

Step 2: Synthesis of 2-Anilinoethyl Sulfate. 2-Anilinoethanol acid sulfate (4.7 g, 0.02 mol) was heated at 130°C under a vacuum of 5 mmHg for 1 h to yield the desired product (2-anilinoethanol sulfate). Upon heating, the starting material melted and water condensed out to yield a pale brown viscous liquid that turned into a glassy solid after cooling to room temperature. The solid was stirred with methanol, filtered, and dried to yield the product (4.2 g, 96.7% yield).

Step 3: Synthesis of 1-Phenylaziridine. A solution of 2-anilinoethylsulfate (136 g, 0.63 mol) and sodium hydroxide (100 g, 2.5 mol) in water (800 mL) was stirred at 110°C for 90 min, during which the color changed from clear gray to dark brown and finally to yellow. This solution was then steam-distilled at 160°C; we separated the product from the condensate by extraction with ether, forming a turbid aqueous layer and a pale yellow organic layer. More product was extracted into the organic layer (the aqueous layer turned clear) by the addition of potassium hydroxide (20 g) to the aqueous phase. The ether solution was dried over anhydrous sodium sulfate, the ether was evaporated off, and the remaining yellow liquid was distilled at 64.4°C and 10.1 mmHg, resulting in a 65% yield of 1-phenylaziridine. The product was characterized by FT-NMR: ¹H-NMR (δ/CDCl₃): 2.15 (s, 4 H, CH₂), 7.2 (m, 5 H, aromatic H).

Step 4: Polymerization of 1-Phenylaziridine. The polymerization procedure is the same as that described below for the propyleneimine/N-phenylethyleneimine copolymer except that only freshly distilled N-phenylaziridine was used.

Preparation of Propyleneimine and N-Phenylethyleneimine Copolymer (70:30)

Because the homopolymer of N-phenylaziridine was a solid that was insoluble in most organic solvents, we decided to copolymerize N-phenylaziridine with commercially available

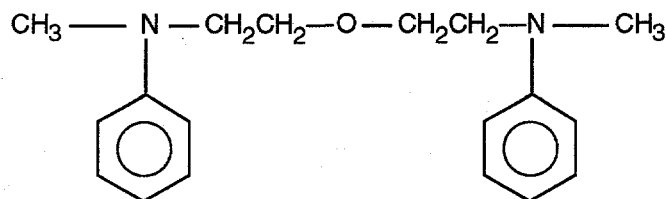
propyleneimine to optimize solubility and produce an amorphous or liquid polymer at room temperature.

The copolymerization was conducted in acetonitrile in the presence of trifluoroacetic acid (TFA) as catalyst. A strong acid catalyst was selected to favor the formation of an oligomer with low molecular weight. We found that the polymerization should be quenched after about 30 min to preferably yield an oligomer. Initially, we copolymerized N-phenylaziridine and propyleneimine in the relative molar ratio of 1:1. The resulting polymer was a waxy solid at room temperature. In an attempt to synthesize a liquid polymer, we reduced the relative ratio of N-phenylaziridine and propyleneimine to 30:70. In this case, the resulting copolymer was a viscous liquid at room temperature. This polymer was insoluble in water, while soluble in chloroform and only partially soluble in tetrahydrofuran. The polymerization scheme is shown in Figure 3-5 and the experimental procedure is described below.

Procedure for Preparing the Propyleneimine and N-Phenylethyleneimine

Copolymer. Freshly distilled propyleneimine (6.4 g, 70 mole%, b.p. = 66°C) and N-phenylaziridine (5.73 g, 30 mole%, b.p. = 64°C/10.1 mm) were dissolved in acetonitrile (20 mL) in a 50-mL round-bottomed flask fitted with a stirring bar and a septum cap. The solution was stirred and cooled to -78°C in an acetone/dry ice bath. Trifluoroacetic acid (3.66 g or 2.47 mL, 20 mole%) was then added through a syringe under stirring, and the acetone/dry ice bath was removed. The whole reaction mixture was brought to room temperature and stirred for 30 min. Benzylamine (3.37 g or 3.43 mL, 20 mole%) was added to quench the reaction, and the solution was stirred for 30 min. Acetonitrile was distilled off, and the residue was repeatedly washed with hexane (3 x 30 mL). After drying, a pale yellow viscous liquid was obtained (yield = 14 g). The product was characterized by FT-NMR: ¹H NMR (δ/CDCl₃): 1.1 (broad singlet), 2.0-3.0 (broad singlet), 4.0 (broad singlet), 6.4-7.4 (multiplet).

Synthesis of d-DMA. The structure of 2,2'-bis(N-methyl-N-phenyl)ethylether is shown below.



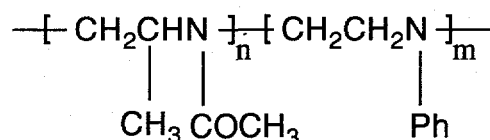
2,2'-bis(N-methyl-N-phenyl)ethylether

This compound consists of two DMA-analog functional groups linked by oxyethylene. Although we previously observed that even low molecular weight DMA oligomers are highly insoluble, this

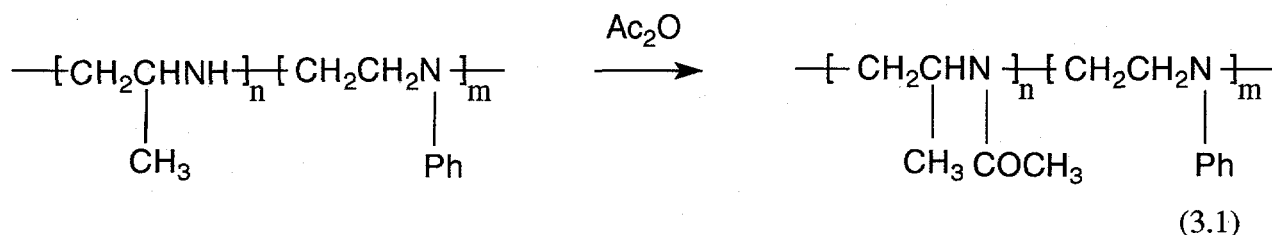
compound has good solubility in organic solvents because of the oxyethylene group. 2,2'-Bis(N-methyl-N-phenyl)ethylether represents a functionalized dimer of DMA (referred to as d-DMA) and has been studied for its SO₂ liquor regeneration properties: its performance has been compared with that of DMA. Because of its higher molecular weight, d-DMA has a lower vapor pressure than DMA. The synthesis of 2,2'-bis(N-methyl-N-phenyl)ethylether is described next.

We added n-butyl lithium (1.28 g, 10 mL of 2 M n-butyl lithium in cyclohexane) dropwise to a stirred solution of N-methylaniline (2.14 g, 0.02 mol) in dry THF (20 mL) at -10°C under argon atmosphere. The reaction mixture was allowed to attain room temperature and was stirred for 1/2 h. Bischloroethyl ether (1.43 g, 0.01 mol) was added and the reaction mixture was refluxed overnight. The mixture was cooled and filtered to remove precipitated LiCl. Cyclohexane and THF were removed from the filtrate by rotary evaporation. The residue was dissolved in chloroform, washed with water and saturated NaCl solution, and dried over anhydrous Na₂SO₄. A brownish yellow liquid remained after rotary evaporation to remove chloroform. This liquid was distilled under vacuum to remove any unreacted starting materials. Thin layer chromatography showed the product to be pure. The procedure yielded 2.5 g of 2,2'-bis(N-methyl-N-phenyl)ethylether (88% yield). The product was characterized by NMR: ¹H-NMR (S/CDCl₃): 2.98 (s, 6 H, N-Me), 3.51 (t, 4 H, CH₂O), 3.58 (t, 4 H, CH₂-N); 6.7-7.3 (m, 10 H, aromatic CH). ¹³C-NMR (ppm/CDCl₃): 38.98 (N-Me); 52.60 (CH₂O); 68.86 (CH₂N); 112.14, 116.27, 129.21 (o, m, p-phenyl CH); and 221.0 (aromatic >C<).

Synthesis of MAPA and AMAPA. Another compound synthesized for SO₂ liquor regeneration, acetylated poly(1-methylaziridine-N-phenylaziridine) is shown below.



This oligomer, abbreviated MAPA, was prepared by acetylation of the correspondent copolymer of 1-methylaziridine and N-phenylaziridine (described earlier). By acetylation of poly(1-methylaziridine-N-phenylaziridine), abbreviated AMAPA, we converted the basic secondary amine to the correspondent amide with markedly lower basicity. This is expected to minimize possible irreversible adsorption of SO₂ at basic sites other than the DMA analog -CH₂(NPh)CH₂ functional group. The reaction scheme is illustrated below.



The starting copolymer (whose synthesis was described earlier) was dissolved in benzene and treated with anhydrous acetic anhydride at reflux for a few hours. The solvent was then evaporated off, and the functionalized polymer was isolated. The acetylation reaction was confirmed by FT-IR spectroscopy.

Synthesis of d-Siloxane and p-Siloxane

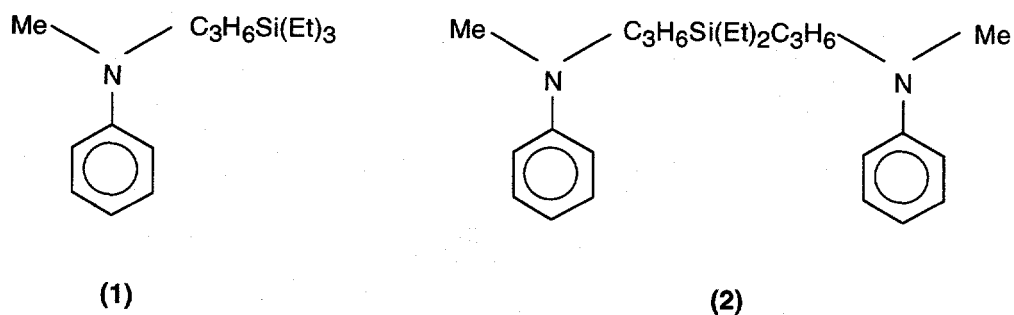
We also synthesized silicon-containing DMA analogs (their structures are shown in Figure 3-6) and siloxane oligomers functionalized by DMA moieties (their structures are shown in Figure 3-7). The low vapor pressure and viscosity of low molecular weight siloxane oligomers are very desirable properties of the newly developed SO₂ absorbent material.

The synthesis of (1) and (2) in Figure 3-6 is a two-step reaction: first N-methyl N-allylaniline is formed, followed by the hydrosilylation reaction of trimethylsilane and dimethylsilane, respectively. The synthesis of (3) and (4) in Figure 3-7 is by hydrosilylation of tetramethyldisiloxane and pentamethylcyclopenta-siloxane with N-methyl N-allylaniline. The synthesis of (1) and (2) is presented next. The synthesis of (3) and (4) is similar.

Preparation of N-methyl N-allylaniline. To a solution of N-methylaniline (924.9 g, 0.23 mol) in dry THF (75 mL) at 0°C under argon atmosphere, n-BuLi in cyclohexane (116 mL, 2 M solution) was added dropwise under stirring. The reaction was stirred for 30 min at 0°C, and allylbromide (28 g, 0.23 mol) in dry THF (50 mL) was added dropwise to this yellow reaction mixture. Upon addition of allylbromide, the reaction mixture turned clear pale yellow. The reaction was stirred at room temperature for 30 min and then refluxed overnight. The reaction was cooled, and all the volatile materials were allowed to evaporate completely. The residue was taken in ethylether, washed with water (3 x 50 mL), and dried over anhydrous MgSO₄. The solvent was evaporated using a rotary evaporator. The residual pale yellow liquid was vacuum distilled, and the product was obtained in 88% yield (b.p. 66° - 68°C at 5 mmHg). The product was characterized by ¹H and ¹³C NMR.

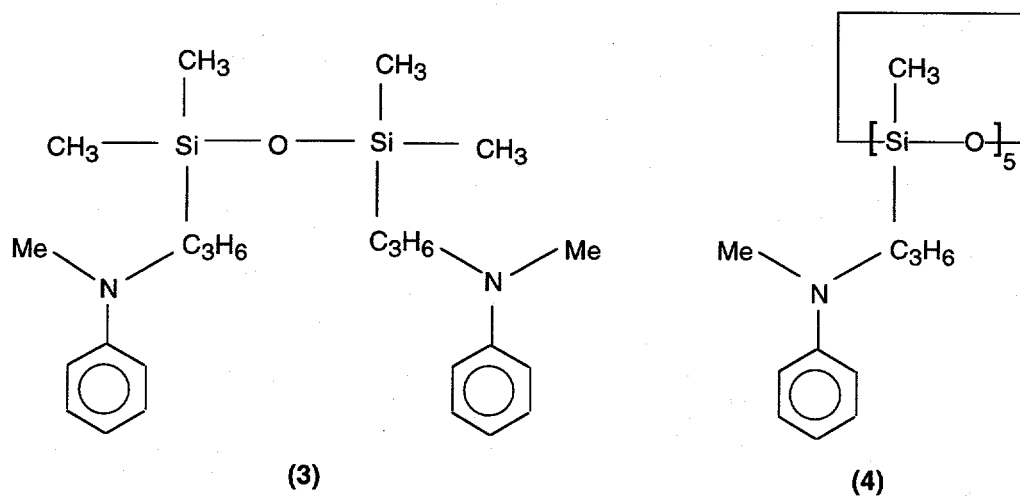
Hydrosilylation of N-methyl N-allylaniline. Hydrosilylation reactions were conducted in toluene at 80°C in the presence of chloroplatinic acid as a catalyst. The typical reaction time was 18 h.

Compound (1) (Figure 3-6) distilled at 115°C at 0.38 mmHg, and compound (2) did not distill even at 130°C at 0.5 mmHg. The vapor pressure of these compounds is therefore significantly lower than that of DMA, which has a boiling point of 194°C at atmospheric pressure.



CAM-3501-35

Figure 3-6. Silicon-containing DMA analogs.



CAM-3501-36

Figure 3-7. Siloxane oligomers functionalized by DMA.

We also synthesized about 20 g of the dimer siloxane by hydrosilylation of tetramethyl-disiloxane with N-methyl N-allylaniline, as described earlier. Low viscosity, high boiling point, low vapor pressure, and good reversibility make these promising materials for SO_x absorption.

NO_x ABSORBENTS

Our major focus in synthesizing an NO_x absorbent with a high capacity lifetime and reversibility has been water-soluble phthalocyanine. Tetrasodium salts of cobalt (II) and iron (II) 4, 4', 4'', 4'''-tetrasulfophthalocyanine were synthesized as follows.

Tetrasodium Salt of Cobalt(II) 4, 4', 4'', 4'''-Tetrasulfophthalocyanine 2-Hydrate

The monosodium salt of 4-sulfophthalic acid (30 g, 111.9 mmol), ammonium chloride (3.3 g, 61.6 mmol), urea (40.8 g, 673.3 mmol), ammonium molybdate (0.5 g, 0.4 mmol), and cobalt(II) sulfate hydrate (5.1 g, 32.9 mmol) were ground together until homogeneous. (The monosodium salt of 4-sulfophthalic acid was obtained by neutralization of a 50% aqueous solution of 4-sulfophthalic acid with 15 N NaOH and was purified by washing with 95% ethanol). The solid mixture was transferred to a 500-mL three-necked flask fitted with a condenser and a mechanical stirrer. After nitrobenzene (40 mL) was added to the flask, the reaction mixture was heated to 180°C for 10 h and then allowed to cool to room temperature. The crude product was filtered, ground, and washed with methanol several times. Then, the dark black powder was stirred with 400 mL methanol for 24 h, filtered, stirred with 400 mL methanol for another 24 h, and filtered. The resulting blue solid was dissolved in water (350 mL) and filtered. The filtrate was concentrated with a rotary evaporator and dried under vacuum at 60°C for 16 h to get 26.0 g dark blue solid. (95%, λ_{\max} , 656 nm, $\epsilon = 37000 \text{ M}^{-1} \text{ cm}^{-1}$).

Tetrasodium Salt of Iron (II) 4, 4', 4'', 4'''-Tetrasulfophthalocyanine 2-Hydrate

The monosodium salt of 4-sulfophthalic acid (30 g, 111.9 mmol), ammonium chloride (3.3 g, 61.6 mmol), urea (40.8 g, 673.3 mmol), ammonium molybdate (0.5 g, 0.4 mmol) and iron(II) sulfate heptahydrate (9.0 g, 32.4 mmol) were ground together until homogeneous. The solid mixture was transferred to a 500-mL three-necked flask fitted with a condenser and a mechanical stirrer. After nitrobenzene (40 mL) was added to the flask, the reaction mixture was heated to 180°C for 20 h and then allowed to cool to room temperature. The crude product was filtered, ground, and washed with methanol several times. Then the dark black powder was stirred with 400 mL methanol for 24 h, filtered, stirred with 400 mL methanol for another 24 h, and filtered. The resulting blue solid was dissolved in water (400 mL) and filtered. The filtrate

was concentrated with a rotary evaporator and dried under vacuum at 60°C for 16 h to get 22.5 g of a dark blue solid. (82%, λ_{\max} , 630 nm, $\epsilon = 30900 \text{ M}^{-1} \text{ cm}^{-1}$, $\lambda_{\max}(\text{sh})$, 664 nm, $\epsilon = 18000 \text{ M}^{-1} \text{ cm}^{-1}$).

One more metal phthalocyanine, the tetrasodium salt of copper 4,4',4'',4'''-tetrasulfo-phthalocyanine, was purchased from Aldrich. Because the purity of this compound is 85%, we attempted to purify it by precipitation.

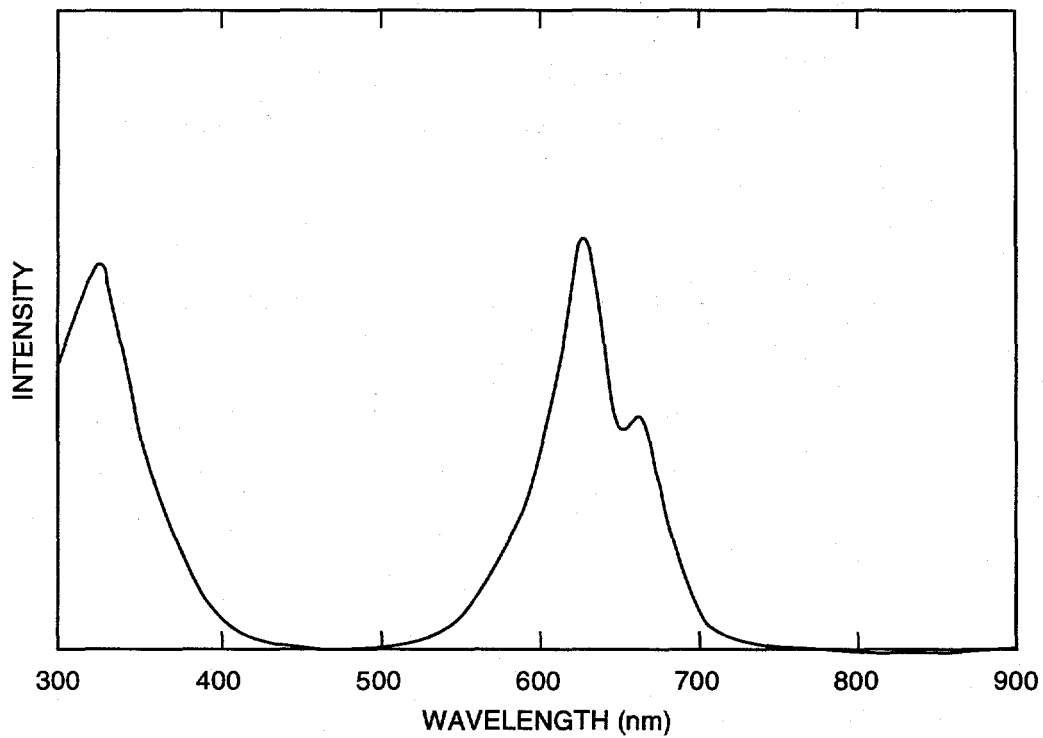
Also, an additional tetrasodium salt of iron 4,4',4'',4'''-tetrasulfo-phthalocyanine (about 160 g) was synthesized as previously described. A detailed analysis of the UV-visible spectrum of this phthalocyanine compound in water showed that the phthalocyanine compound is constituted by a mixture of Fe(II) and Fe(III) phthalocyanines. As shown in Figure 3-8, the absorption maximum at 630 nm corresponds to the Fe(III) compound, while the shoulder at 664 nm is attributed to the Fe(II) compound.

We electrochemically converted the Fe(III) phthalocyanine to the corresponding Fe(II) compound as follows. (We chose this method over chemical reduction because of the high reversibility of the Fe(II)/Fe(III) transformations). Electrolysis was performed on an aqueous solution of Fe(III) phthalocyanine (8 g in 100 mL) using a lead cathode and a platinum wire anode. The electrolysis was conducted under nitrogen using a current of 50 mA. We did not have to add any supporting electrolyte because of the ionic nature of the phthalocyanine compound. Therefore, after reduction, no further purification was necessary and the solution was directly used for NO_x absorbing tests. The reduction of Fe(III) phthalocyanine to Fe(II) phthalocyanine was monitored by VIS spectroscopy. Figure 3-9 compares the VIS spectra of Fe(II) and Fe(III) phthalocyanine. We also prepared the tetrasodium salt of Ni(II) 4,4',4'',4'''-tetrasulfo-phthalocyanine.

EDTA ANALOGS AS NO_x ABSORBENTS

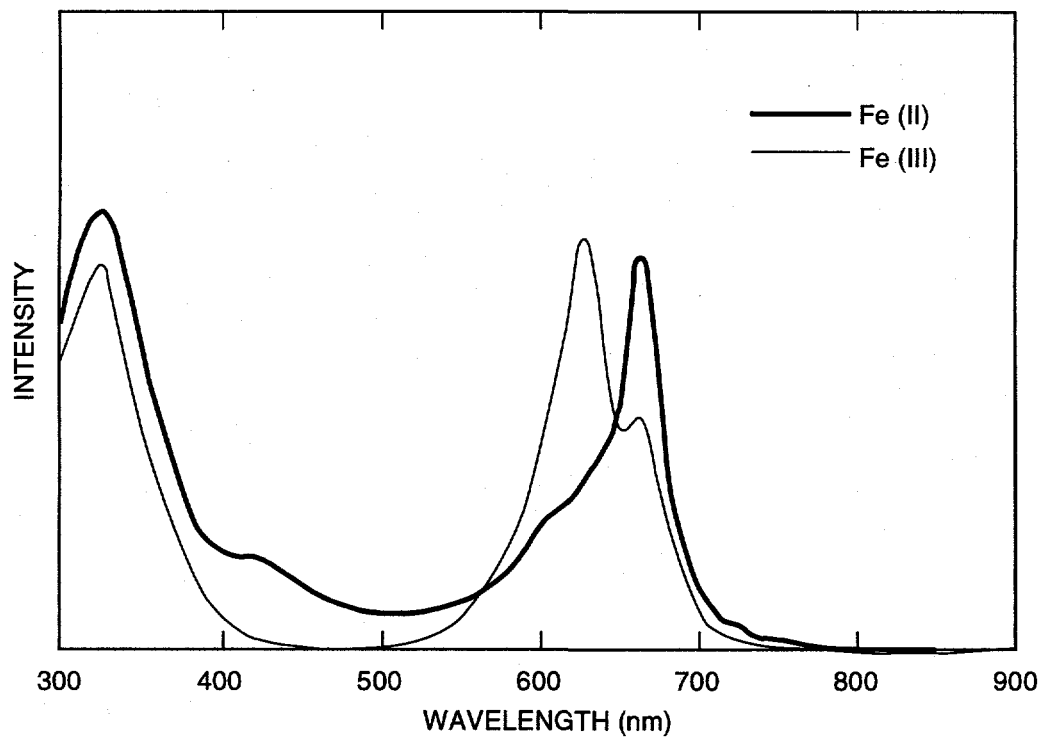
Nitric oxide is known to form a coordination complex with Fe^{2+} -EDTA whose reaction rates are very fast. The drawback of this chemistry is that the regeneration process is expensive, because the Fe^{2+} species is oxidized readily to the ineffective Fe^{3+} species.

To overcome the limitations of the Fe^{2+} -EDTA NO_x removal process, we developed polymeric analogs to EDTA. This approach was pursued in parallel with the development of phthalocyanine-based sorbents. To date no information has been reported on the lifetime of polymeric analogs to EDTA, but we expect that their lifetime will vary with the nature of the polymer backbone and that the reversible absorption capacity for NO will vary with structural changes.



CM-3501-51

Figure 3-8. UV-visible spectrum of tetrasodium salt of iron 4,4',4'',4''' — tetrasulfophthalocyanine.

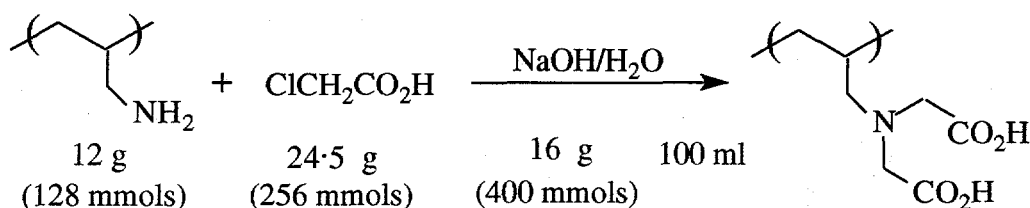


CM-3501-51A

Figure 3-9. UV-visible spectrum of tetrasodium salt of iron 4,4',4'',4''' tetrasulfophthalocyanine.

To investigate these differences, we studied the synthesis of polymeric analogs to EDTA. To be of practical use, these polymers should be soluble in water. Accordingly, we initially focused on the functionalization of polyethyleneimine, a water-soluble polymer. In one approach, we functionalized poly(ethyleneimine) by alkylation with chloroacetic acid. The resulting polymer was soluble in water. However, upon addition of Fe^{2+} , a crosslinked gel was formed. We believe that gelation is taking place because of the intermolecular formation of the Fe^{2+} complex. To minimize intermolecular complexation and instead favor the intramolecular process, it is desirable to functionalize the polymer with iminodiacetic acid. Accordingly, we attempted to functionalize polyethyleneimine with ethylenediaminetetracetic dianhydride. However, the resulting polymer was partially cross-linked.

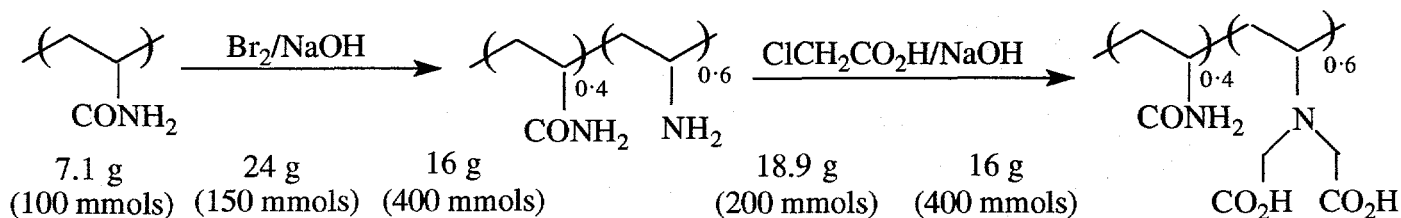
Synthesis of Poly(allylamine) Functionalized EDTA Analog



The reaction mixture was heated at 90°C for 4 h. NMR indicated small amounts of unreacted $\text{ClCH}_2\text{CO}_2\text{H}$. An additional 8 g of $\text{ClCH}_2\text{CO}_2\text{H}$ and 8 g of NaOH were added, and the reaction was heated for an additional 4 h.

After cooling to room temperature, the reaction mixture was acidified to pH 1.5 by concentrated HCl. A white precipitate was obtained. The product was filtered, washed with acetone, and dried. A solution of 20 mM of this polymer with FeSO_4 was prepared at pH 4.2 and pH 6 for further testing on NO_x absorption.

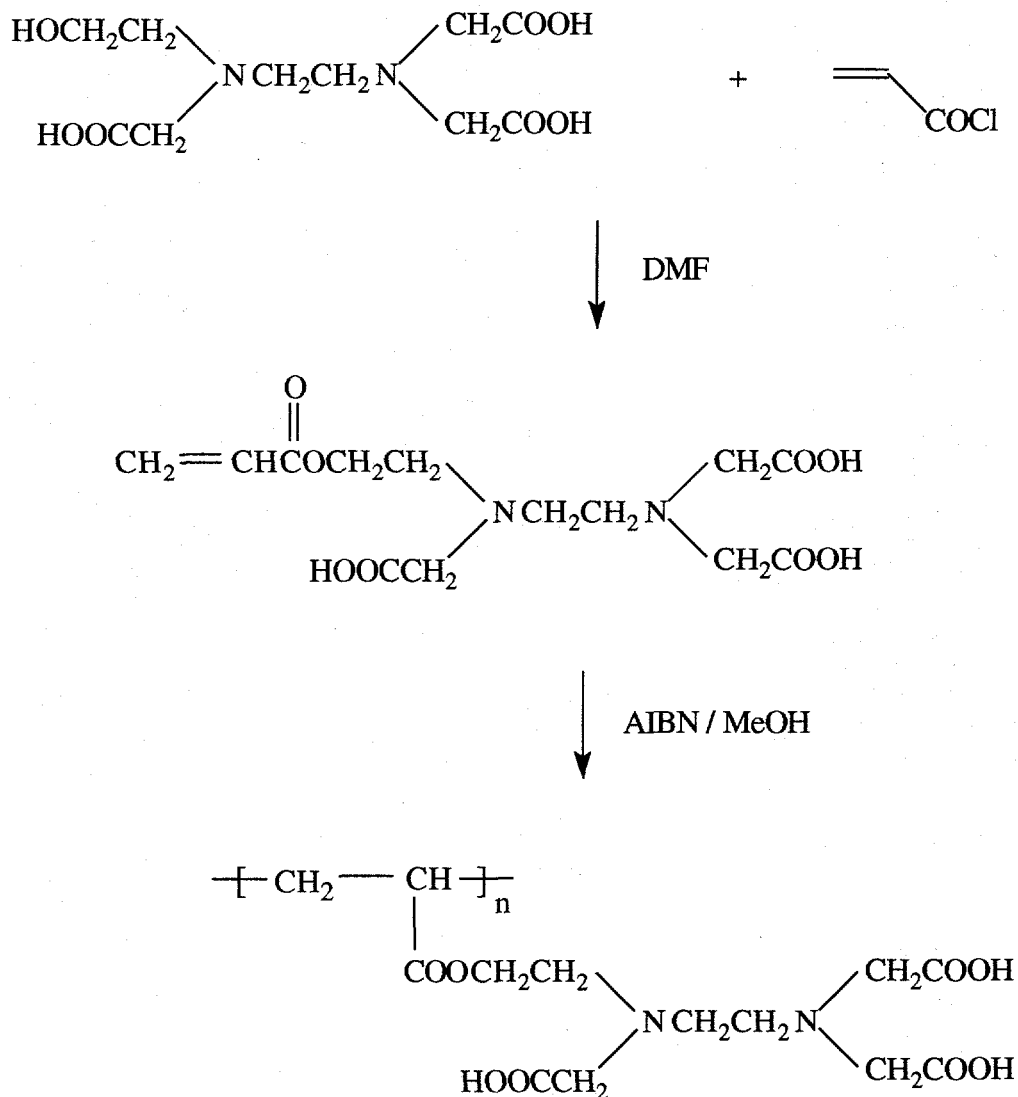
Synthesis of EDTA Analog Copolymer



Br₂ was added dropwise to the cooled solution of polyacrylamide (MW 10⁶) and NaOH in water at -5°C. The reaction mixture was stirred at room temperature for 3 h and at 90°C for 2 h. Next, ClCH₂CO₂H and NaOH were added and the reaction was heated at 90°C for 4 h. After it cooled to room temperature, the reaction mixture was adjusted to pH 1.5 by adding concentrated HCl. The precipitated product was washed with diluted HCl and then with acetone and was dried in a vacuum oven.

Attempts to prepare 20 mM solution of the polymer with FeSO₄ resulted in precipitation. This may be due to the high molecular weight of the polymer, which makes the complete alkylation of the -NH₂ group very difficult.

Synthesis of Poly(acrylate) Functionalized EDTA Analog



A solution of hydroxyethyl ethylenediaminetriacetic acid (EDTA) and acryloyl chloride was stirred at 0°C for 2 h and at room temperature for 1 h. The excess of acryloylchloride and DMF was evaporated, yielding a syrupy product. The NMR spectrum of the material was consistent with the desired product.

Polymerization of the product was sluggish. Three portions of 100 mg of AIBN were necessarily added. The mixture was heated at 70°C for 3 days to bring the polymerization to completion.

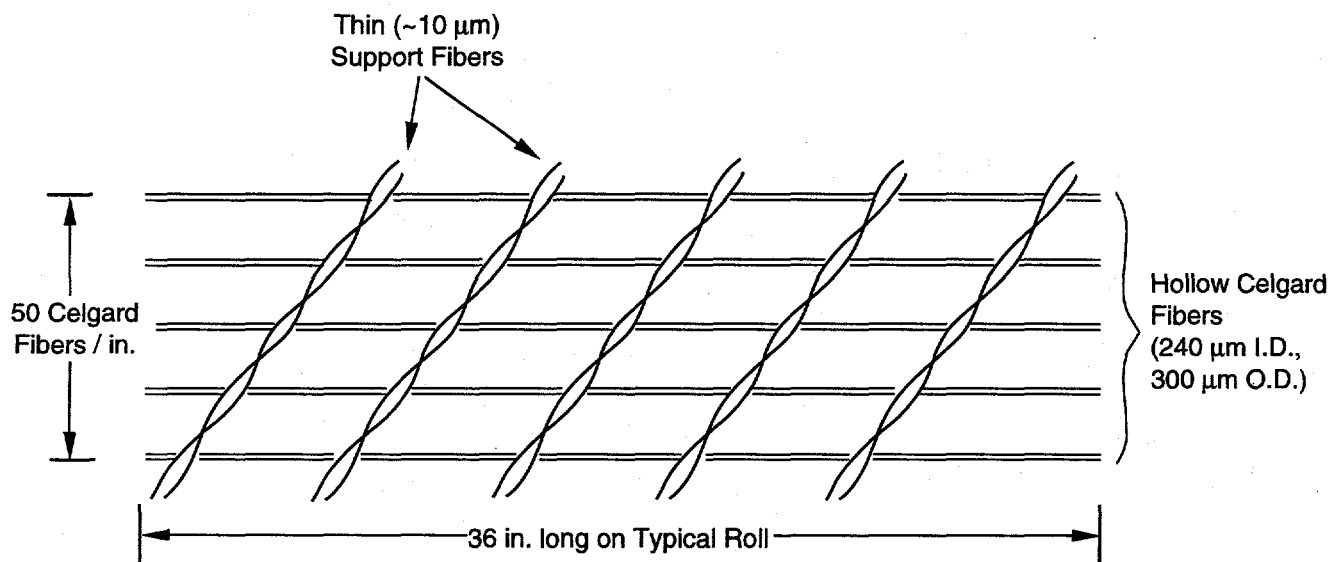
TASK 4: SO₂ SCRUBBING WITH HOLLOW FIBER CONTACTORS

The objective of this task was to determine the fundamental mass transfer characteristics of hollow fiber contactors (HFCs) for scrubbing SO₂ from a simulated flue gas. These devices can remove more than 99% of the SO₂ from a simulated flue gas. However, the principles of mass transfer in HFCs are not firmly established, especially for a system with a liquid-phase chemical reaction.

Under subcontract to SRI, Dr. K. Sirkar at the New Jersey Institute of Technology (NJIT) was responsible for Task 4. The goal was to gather a series of steady mass transport data under various conditions by systematically varying the gas flow rate, the liquid flow rate, the liquid composition, and the HFC module properties (such as the length and diameter of the hollow fibers and the fiber packing fraction of the module). Experiments were performed both at room temperature and at 70°C. This work was done with small modules in cylindrical form to achieve a well-defined flow distribution in the module. Along with the mass transport rate data, we compiled gas-side and liquid-side pressure drop data.

During the early stages of the project, SRI established the NJIT subcontract and reached an agreement with Hoechst/Celanese (HC) on exactly what modules would be tested in the first two years of the project. HC agreed to supply modules that had a "cross-flow" geometry and contained enough fibers so that feed gas flows could be kept below 10 L/min (a practical laboratory upper limit) and so that we could achieve a wide range of SO₂ and NO_x scrubbing efficiencies. The term "cross-flow" refers to the fact that the feed gas will flow at 90° to the scrubbing liquor in the module. Because this geometry will be the geometry of the large scale modules, our lab results should be scalable.

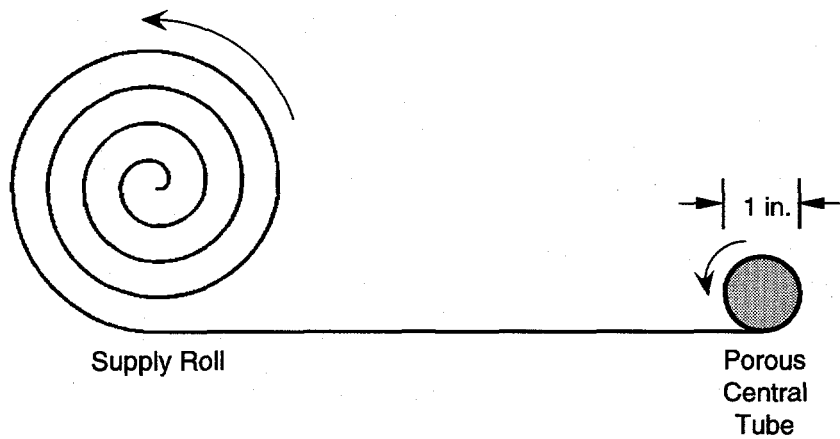
To understand the flow geometry of the HC module, it is helpful to envision how the module is made. First, the hollow fibers (300- μ m-O.D. Celgard fibers) are woven with a netting made of very narrow polyester fibers (about 10 μ m diameter) as shown in Figure 4-1. This netting comes on a roll like a roll of carpet. The roll is typically 36 inches long (along the axis of the roll; this is the length of the hollow Celgard fibers). Transverse to the axis are 50 Celgard fibers per inch. To make a module, HC starts with a porous central tube. Netting is wrapped around this central tube continually, adding layer upon layer until the netting reaches a suitable thickness (e.g., 4 inches), as shown in Figure 4-2. This module roll is glued and cut to a desired length (currently HC prefers 11- and 27-inch lengths). The ends of the module are potted with



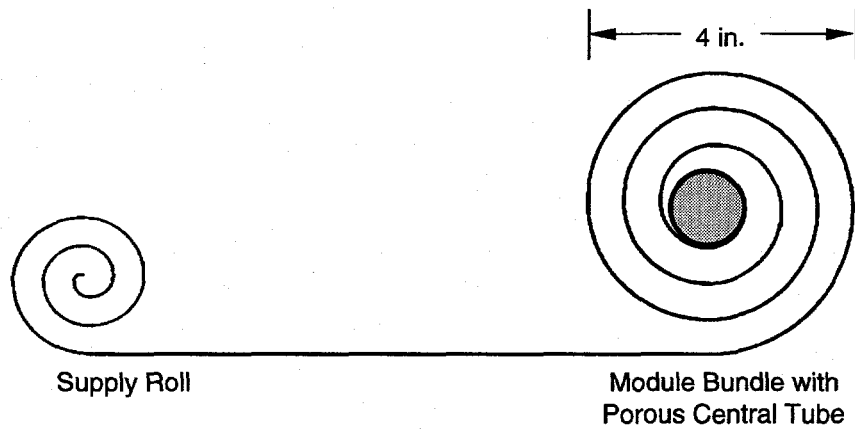
CM-340525-40

Figure 4-1. Structure of Celgard fiber netting.

The support fibers are interwoven transverse to the Celgard hollow fibers.



(a) Beginning of wrapping process



(b) End of wrapping process

CM-340525-41

Figure 4-2. Wrapping of netting around central tube.

epoxy and cut, and end caps are attached. In a finished module, a liquid passes into the central tube and then flows radially outward over the hollow fibers. The gas is passed down the lumen of each fiber, as shown in Figure 4-3.

The HFC modules were not received from HC until late December 1992, limiting us to prototype modules for the initial efforts.

EXPERIMENTS WITH PROTOTYPE HFC

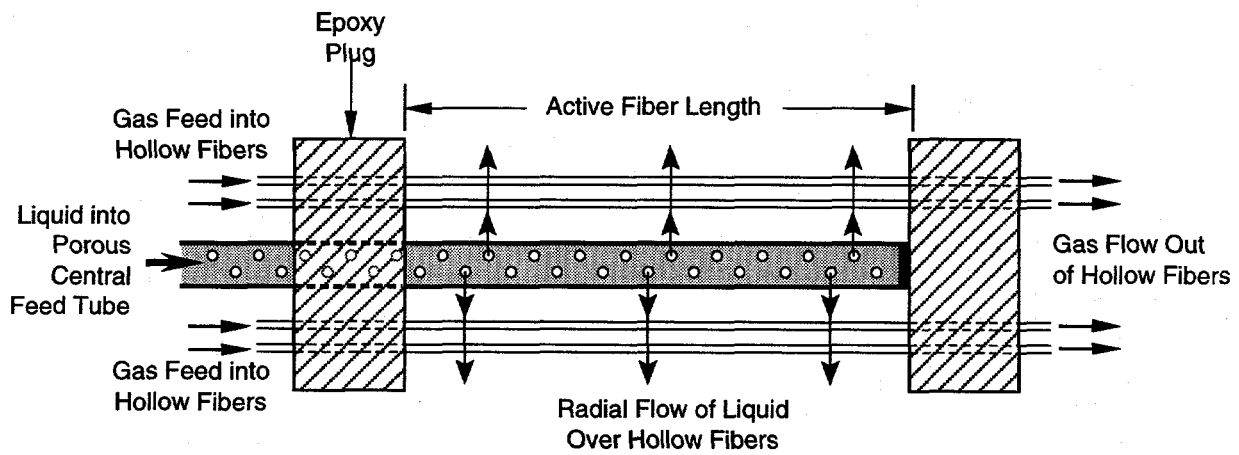
Liquid Phase Mass Transfer Experiments

Two sets of liquid phase mass transfer experiments were performed using pure CO₂ as the gas and water as the scrubbing liquid. In the first set of experiments pure gas was used to eliminate the gas phase mass transfer resistance. The second set of experiments, differed from the first in that the HFC module was dried under vacuum between experiments to prevent water from condensing in the fiber pores between experiments. When water fills the pores, a dissolved gas molecule must travel the pore length through the liquid. Because diffusion rates are lower in liquids than in gases, this results in a higher mass transfer resistance. The second set of experiments (where the module was dried under vacuum) resulted in MTCs (MTCs) three times greater than those in the first set (where the module was not dried).

These experiments were performed using a prototype HC HFC with the flow geometry (cross-flow) similar to the new HC product shown in Figure 4-4. The prototype module had an outside diameter (OD) of 2 inches and contained 6084 fibers, each with an inside diameter (ID) of 240 μm and an OD of 300 μm . The active length of each fiber was 24.1 cm (13,800 cm² of active contact area based on the OD of the fiber).

Figure 4-5 shows the results from the first set of experiments (not dried). We found that the overall MTC had very little dependence on the liquid flow rate in contrast to the earlier HC counter-current module design (Karoor, 1992). This result indicates a greater efficiency of mass transfer in the liquid phase. The quantitative significance of the result must await further data, but it was a favorable and unexpected result. The MTC shown in Figure 4-5 is defined in Appendix D.

The results from the second set of experiments (vacuum dried) are also shown in Figure 4-5. The overall MTC was three times higher than that obtained during the first set of experiments. Again, the overall MTC had very little dependence on the liquid flow rate, indicating that the liquid phase resistance is negligible under these operating conditions.



CM-340525-42

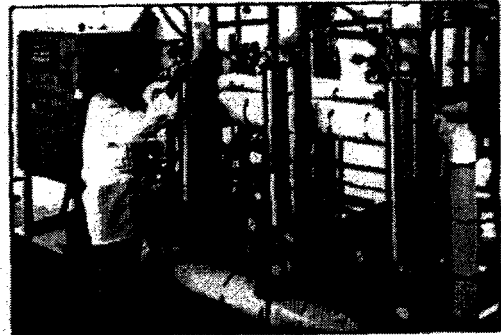
Figure 4-3. Flow pattern of gas and liquid in cross-flow module.

The fluid passed into the central tube flows radially across the hollow fibers.

What Flavor Extraction Looks Like Without Emulsion Formation:

You're looking at the new Liqui-Cel® Extra-Flow Membrane Contactor. The new generation of award-winning, proprietary membrane technology from Hoechst Celanese designed to improve the flavor and productivity of all your citrus essential oil extractions – without emulsion formation. Now Liqui-Cel Extra-Flow Membrane Contactor brings all the benefits of non-dispersive liquid/liquid extraction membrane technology to process scale. Each contactor contains thousands of Celgard® microporous hollow fiber membranes around a central Distribution Tube. As Fluid One's essential oils flow through the Distribution Tube, Liqui-Cel Contactor's unique patent-pending Baffled design forces them out and around the Baffle, then back into the Collection Tube. By-passing of available contact area is eliminated. This enhanced "radial flow" dynamics

brings the essential oils into direct contact with Fluid Two's aqueous/organic stream flowing countercurrent through the Celgard® hollow fiber membranes, thereby achieving better fluid distribution – for increased flow capacity and efficiency. Because heat is not required, you never vaporize the desirable "high notes" of the flavorful product, without the subsequent addition flavor enhancers. Right now, Liqui-Cel Extra-Flow Membrane Contactors are available in a range of process stream configurations. Liqui-Cel Systems are modular and skid-mounted for easy expansion. For cost-effective customization to your exact flavor extraction needs, call Hoechst Celanese at 1-800 235-4273 today!



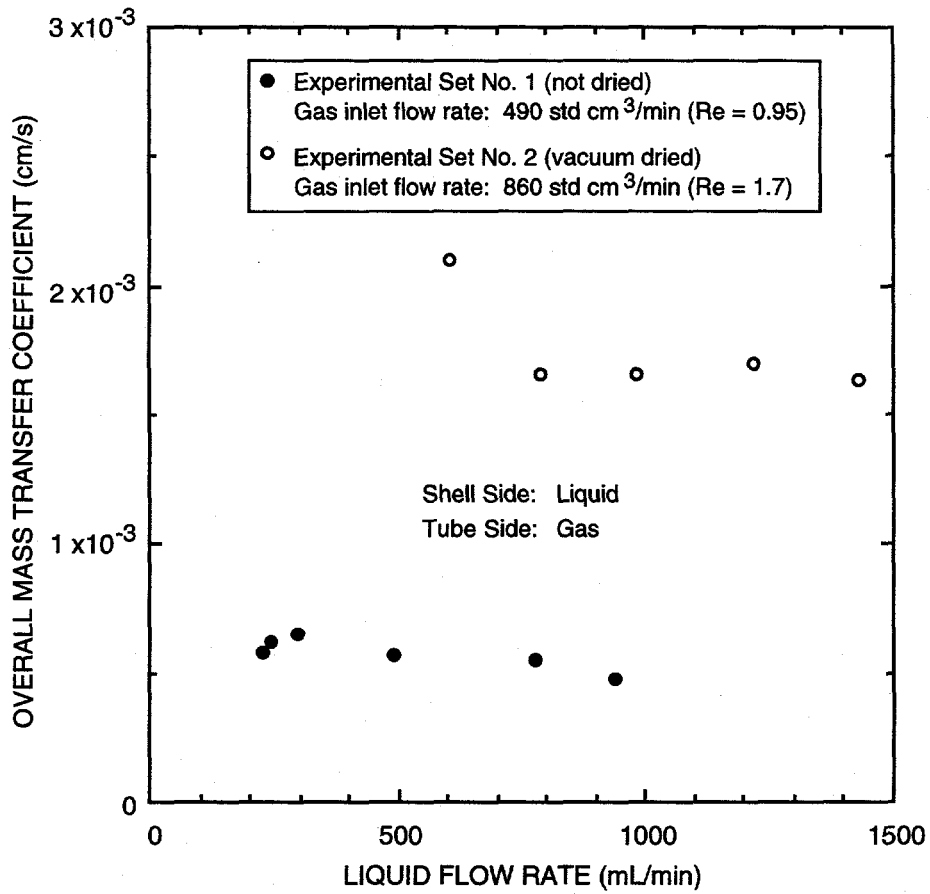
Separation Products Division
Hoechst Celanese Corporation

Hoechst Celanese

Hoechst 

CPM-3501-135

Figure 4-4. Flow pattern in new Hoechst/Celanese crossflow module.



CM-3501-4A

Figure 4-5. HFC mass transfer coefficients for pure CO₂ absorption in water using a cross-flow module.

The mass transfer coefficient is relatively insensitive to liquid flow rate.

SO₂ Removal Efficiency Experiments

For the very first few experiments, we used a small module available from earlier projects (the modules described above were too large for these tests). The module had an OD of 0.25 inch and contained 75 fibers, each with an ID of 240 μm and an OD of 300 μm . The active length of each fiber was 18 cm (127 cm^2 of active contact area based on the OD of the fiber). A gas mixture containing 1.61% SO₂ in N₂ was fed to the fiber lumen at 92.9 std cm^3/min at a pressure slightly above atmospheric. Pure water was pumped through the shell side at 2 to 3 psi higher than the gas stream pressure.

During the experiments, water leaked into the fiber lumen (because this module had been used extensively for an earlier project). However, these experiments generated preliminary results before we used the new HC modules. Figure 4-6 shows the results for experiments with liquid flow rates between 50 and 200 mL/min. The SO₂ removal rate was about 70% at low water flow rates and over 96% at increased water flow rates.

INITIAL EXPERIMENTS WITH HOECHST-CELANESE HFC

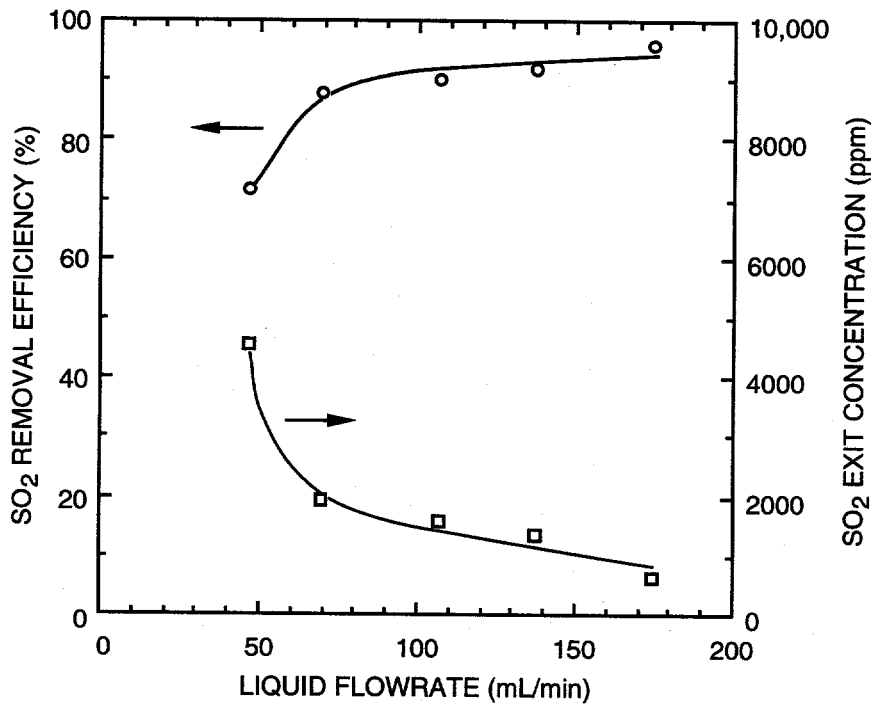
During the first quarter of 1993, we began experiments with the new cross-flow modules received from HC. We conducted four sets of experiments:

- Mass transfer tests with pure CO₂ and water to determine the liquid phase resistance.
- Module configuration tests with pure SO₂.
- Mass transfer tests with 10% CO₂ and water to determine the significance of the gas phase (including membrane pore) resistance.
- SO₂ removal efficiency tests to demonstrate the effectiveness of the proposed technology.

Later in the year, we used a CO₂/water system to perform mass transfer tests on a larger HFC module containing 1000 fibers. We also performed SO₂ absorption tests that used a model flue gas mixture and aqueous solutions of Na₂SO₃ as the scrubbing medium. All these tests were performed on the apparatus illustrated in Figure 4-7.

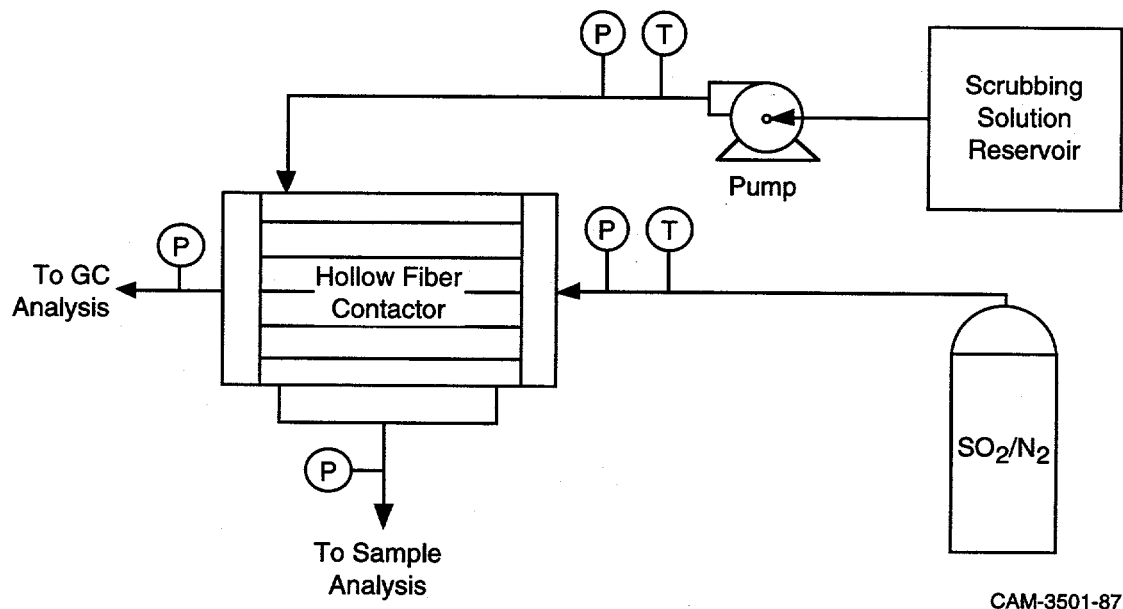
Mass Transfer Tests with Pure CO₂ and Water

The rate of mass transfer is a function of liquid-side film resistance, gas-side film resistance, and pore resistance (a stagnant gas phase in the flue gas application). To determine the liquid-side film resistance, we performed mass transfer tests with pure CO₂ and water. When a



CAM-3501-6

Figure 4-6. SO₂ removal efficiencies with a prototype HFC.
Water was used as the scrubbing medium.



CAM-3501-87

Figure 4-7. Schematic of HFC test apparatus.

pure gas is absorbed into a liquid, there is no resistance in the gas phase; thus a measured resistance is due only to the liquid-side film resistance. The new HC cross-flow module used in these experiments contained 200 fibers, each with an ID of 240 μm and an OD of 300 μm . The active length was 23 cm and the contact area (based on the OD) was 433 cm^2 . Figure 4-8 shows a schematic of the module. The results of these tests are shown in Figure 4-9 for two versions of HC's HFC module. The new module has an overall MTC as high as the prototype module, but at much lower liquid flow rates. At higher flow rates, the new module has the potential for even greater mass transfer rates.

Module Configuration Tests with Pure SO_2

Our second set of experiments was aimed at determining the effect of module orientation and liquid pressure on the rate of mass transfer. In Figure 4-10 the module is mounted vertically with water exiting from only one port. The flow in this case is a combination of countercurrent and cross-flow. MTCs resulting from this configuration were lower than those from the horizontally mounted module (Figure 4-11).

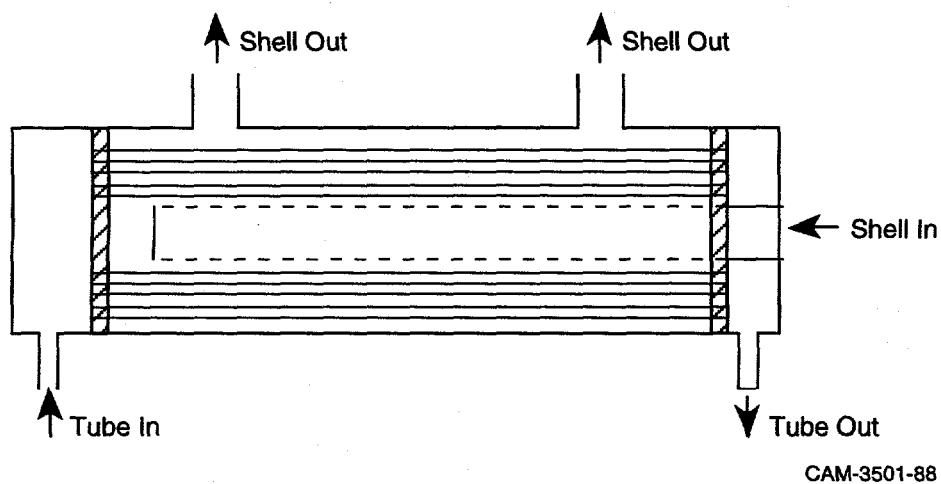
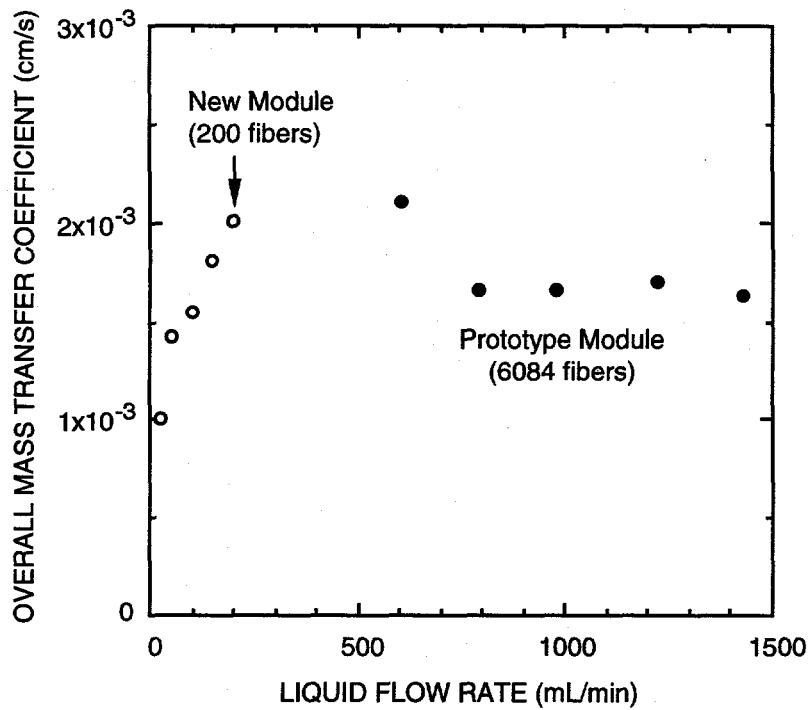


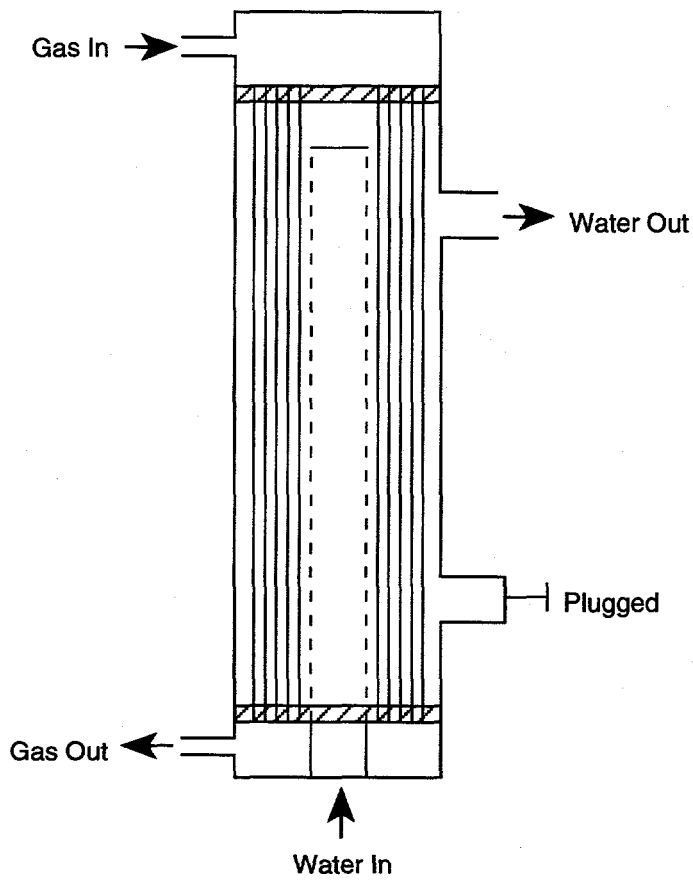
Figure 4-8. Schematic of the cross-flow module.
Liquid flow through the shell-side and gas through to the tube side.



CM-3501-8

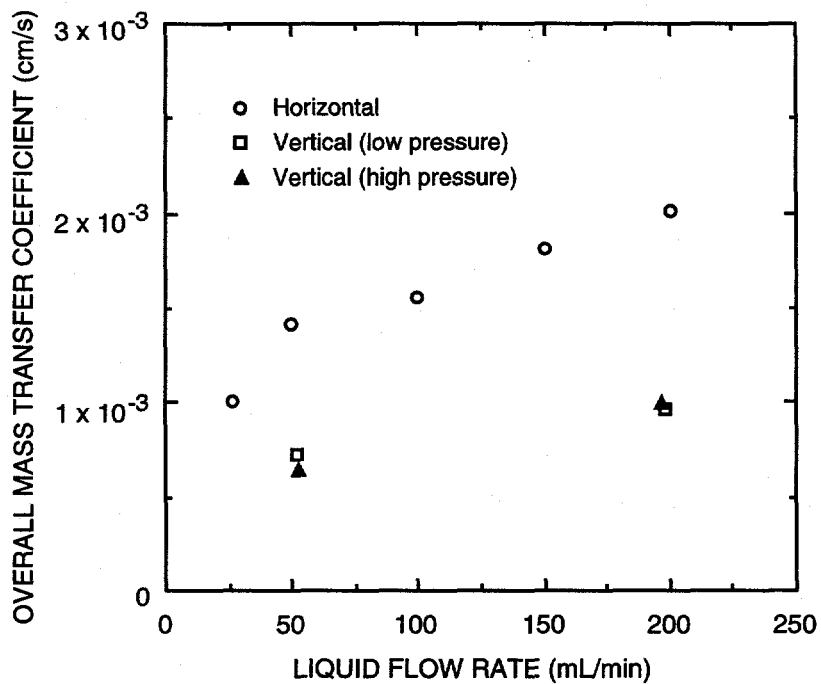
Figure 4-9. HFC mass transfer coefficients for pure CO_2 absorption in water using two cross-flow modules.

The new module has an overall mass transfer coefficient as high as the prototype module, but at much lower liquid flow rates. Higher mass transfer coefficients are probably achievable with higher liquid flow rates.



CM-3501-9

Figure 4-10. Schematic of HFC in the vertical configuration.
Liquid exits the module only through the top port.



CM-3501-10

Figure 4-11. HFC mass transfer coefficients with different module orientations and liquid pressures (pure CO₂ absorption in water).

Mounting the module horizontally resulted in higher mass transfer coefficients; liquid pressure had no effect on the mass transfer coefficient.

In the experiments described so far, the liquid was maintained at a pressure of 1-3 psig. In two additional experiments (using the vertical configuration), we increased the pressure to 10 psig, maintaining the same gas flow rate. The results in Figure 4-11 show that the liquid pressure does not affect the overall MTC.

Mass Transfer Tests with 10% CO₂ and Water

The third set of tests, with 10% CO₂, was performed to determine if the gas phase resistance is significant in the HFC module. The overall MTC was determined using 10% CO₂ under the same conditions as with pure CO₂. The results of these tests are shown in Figure 4-12 and compared with the pure CO₂. The MTCs with 10% CO₂ are indistinguishable from those with pure CO₂, which indicates that the gas-phase resistances (gas-side film and pore resistances) are negligible compared to the liquid resistances.*

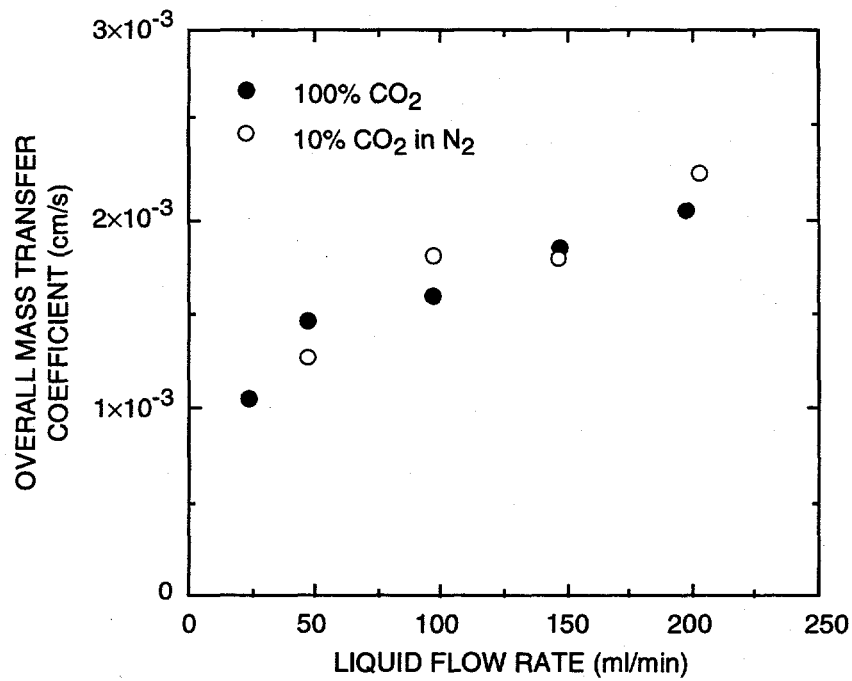
SO₂ Removal Efficiency Tests

The fourth set of experiments was performed to demonstrate the effectiveness of the HFC scrubbing technology for removing SO₂ from flue gas. We scrubbed SO₂ (1.6% SO₂ in nitrogen) with water at various liquid flow rates. Figure 4-13 shows that, for all but the lowest flow rate, there was no detectable SO₂ remaining in the gas after scrubbing. Further, we used a simulated flue gas mixture with water at different gas flow rates in the same module. Even at high gas flow rates (~500 std cm³/min), no SO₂ was detected in the purified gas stream (Figure 4-14). These high SO₂ removal efficiencies demonstrate the high mass transfer rates that can be achieved with HFCs.

Mass Transfer Tests on the 1000-Fiber Module

Next, we evaluated the mass transfer characteristics of a larger module containing 1000 fibers, using the CO₂/water system. We also conducted SO₂ removal efficiency experiments at low water flow rates and SO₂ removal efficiency experiments with aqueous Na₂SO₃ as the scrubbing medium.

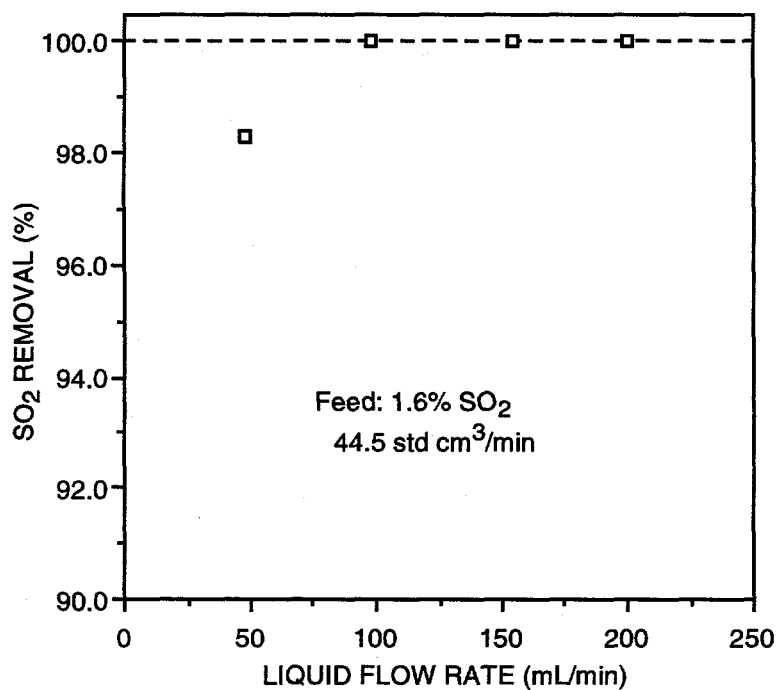
* These experiments show that the gas phase resistance is negligible for the case of CO₂ absorption from a 10% mixture into pure water only. However, it is reasonable to infer that the gas phase resistance for SO₂ would also be small.



➔ NEGLIGIBLE GAS PHASE RESISTANCE

CAM-3501-22

Figure 4-12. HFC mass transfer coefficients with pure and dilute CO₂ feed streams (liquid absorbent is water).



CAM-3501-89

Figure 4-13. SO₂ removal efficiencies using water as the absorbent.

For liquid flow rates above 100 mL/min, no SO₂ could be detected in the gas outlet.

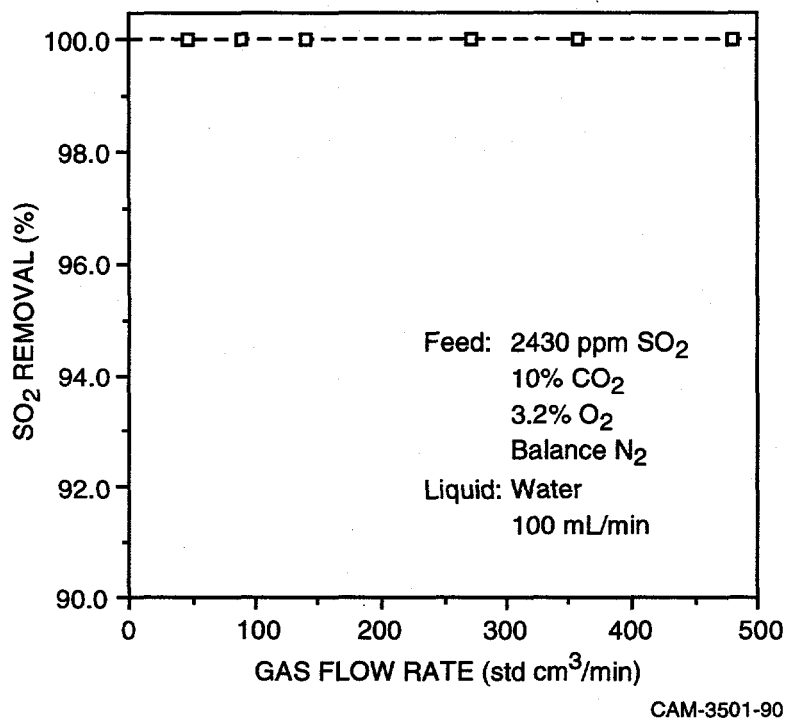


Figure 4-14. SO₂ removal efficiencies from simulated flue gas using water as the absorbent.

No SO₂ could be detected in the outlet over the range of gas flow rates studied.

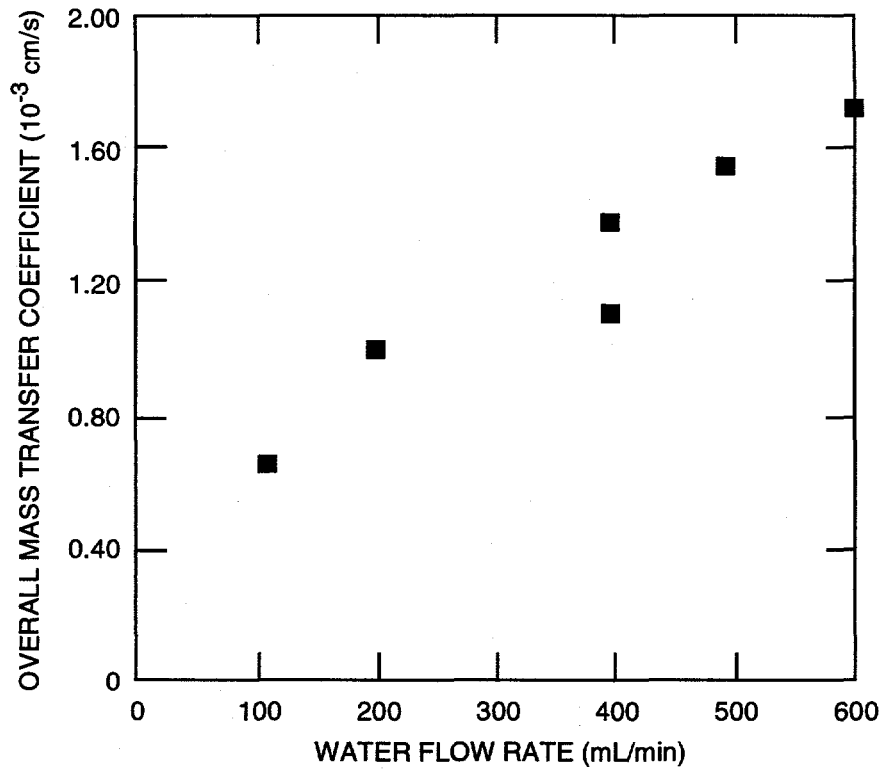
Mass transfer experiments were performed with a 1000-fiber HC cross-flow module using both pure and dilute (10%) CO₂ as the feed gas. The module contained 1000 hollow fibers, each with an active length of 23 cm. The ID and OD of the hollow fibers were 240 and 300 μm, respectively. The active contact area is 2170 cm² based on the OD. The module is unbaffled. The overall MTCs, shown in Figures 4-15 and 4-16, are similar to those obtained with the smaller (200-fiber) module. These and previous MTC data were reduced to show a correlation between the Sherwood number, the Reynolds number, and the Schmidt number (Figure 4-17). The MTCs resulting from our experiments with the HC cross-flow module were significantly higher than those obtained by other researchers.

SO₂ Absorption Tests with the Model Flue Gas Mixture and the Na₂SO₃ Scrubber

We focus next on SO₂ absorption experiments that used a model flue gas mixture and aqueous solutions of Na₂SO₃ as the scrubbing medium. The tests were conducted in a HC cross-flow module (unbaffled) containing 200 fibers, each with an active length of 23 cm. The ID and OD of the hollow fibers were 240 μm and 300 μm, respectively. The active contact area was 433.5 cm² based on the OD. The module achieved very high removal of SO₂, often 100% from the same model flue gas using deionized water. These experiments with deionized water used gas flow rates of 0-500 sccm and water flow rates of 50-100 mL/min. The model flue gas contained 2430 ppm SO₂, 3.17% O₂, 10% CO₂, and the balance N₂. The gas was supplied to the tube side of the module from a certified, standard, gas mixture cylinder (Matheson, East Rutherford, NJ). For aqueous Na₂SO₃ solutions, the gas flow rate was varied from 0-1000 sccm, whereas the flow rate of aqueous Na₂SO₃ solution through the shell side was maintained between 5 and 30 mL/min. The sulfite concentrations studied were 0.01 and 0.05 M.

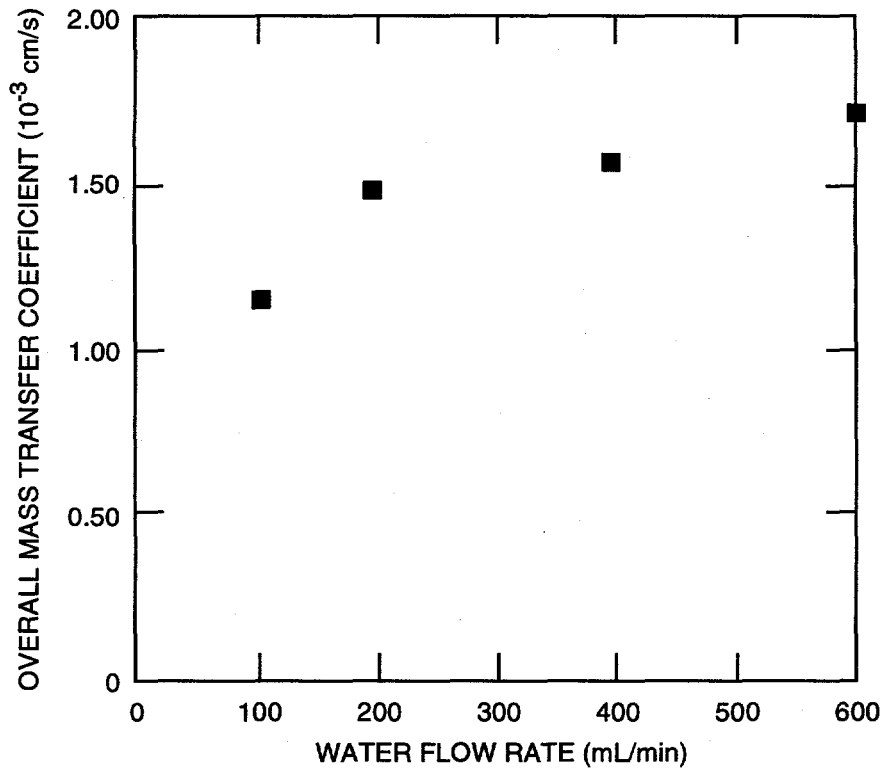
Earlier, we reported virtually 100% SO₂ removal efficiencies at a water flow rate of 100 mL/min. To obtain the operational characteristics of the HFC module when the SO₂ removal efficiency is less than 100%, we used a lower water flow rate, 50 mL/min. Figure 4-18 shows these results. We also conducted SO₂ removal efficiency experiments using Na₂SO₃ as the scrubbing medium. We achieved high removal efficiencies (>90%) with liquid flow rates about 10 times lower than were used when water was the scrubbing medium, as shown in Figure 4-19.

The percentage removal of SO₂ at different sulfite concentrations and flow rates are also plotted in Figure 4-20. For a given liquid flow rate and sulfite concentration, the percentage



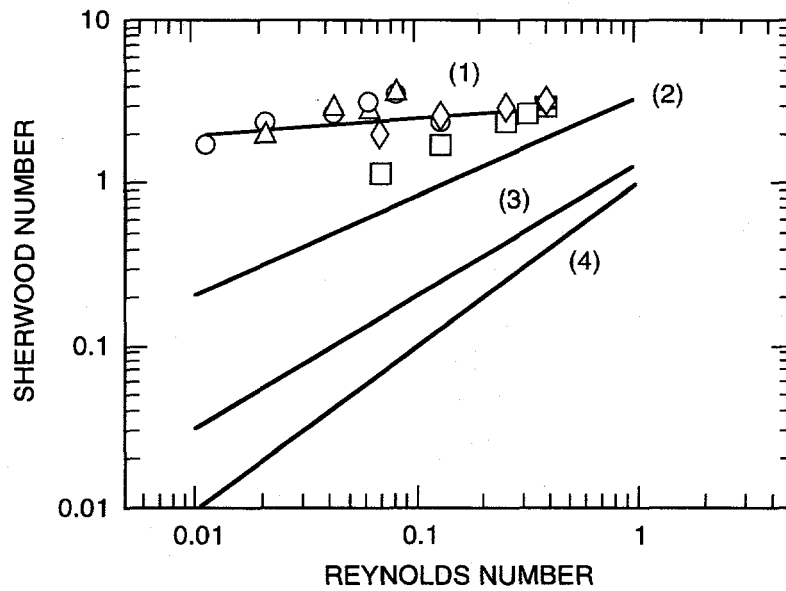
CM-3501-15

Figure 4-15. HFC mass transfer coefficients for pure CO_2 absorption in water using a 1000-fiber cross-flow module.



CM-3501-16

Figure 4-16. HFC mass transfer coefficients for CO₂-N₂ mixture absorption in water using a 1000-fiber cross-flow module.

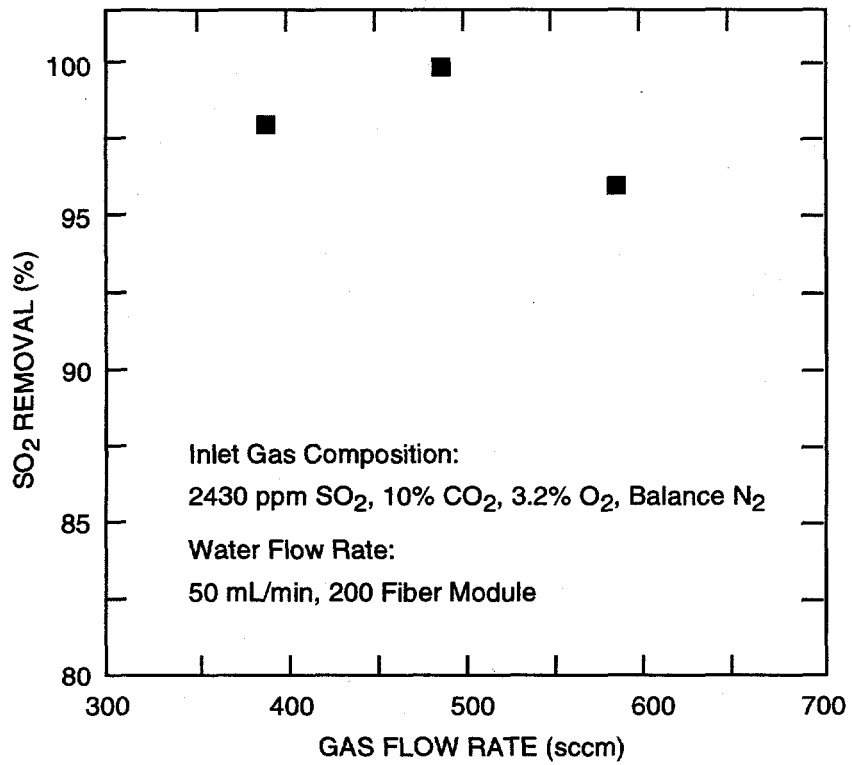


Module	Pure CO ₂	CO ₂ -N ₂
200 Fibers	○	△
1000 Fibers	□	◇

- (1) This work
 $Sh = 0.38 Re^{0.08} Sc^{0.33}$
- (2) Kreith and Black, 1986
 $Sh = 0.39 Re^{0.59} Sc^{0.33}$
- (3) Wickramasinghe et al., 1992
 $Sh = 0.15 Re^{0.8} Sc^{0.33}$ for $Re > 2.5$
- (4) Literature correlation (Yang and Cussler, 1986)
 $Sh = 0.39 Re^{1.0} Sc^{0.33}$ for $Re > 2.5$

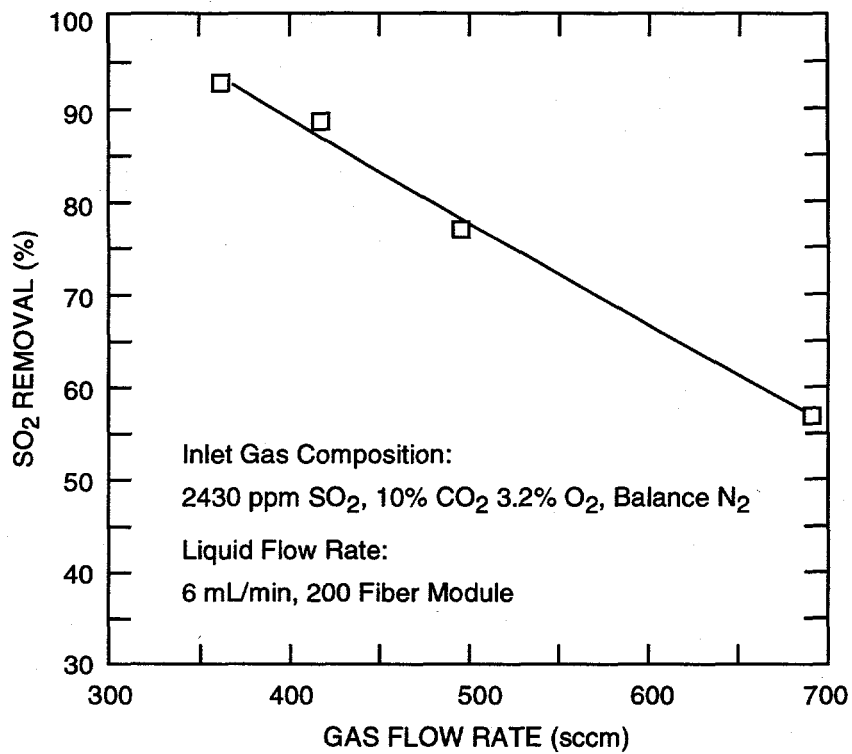
CM-3501-17

Figure 4-17. Sherwood number versus Reynolds number for CO₂ absorption in water.



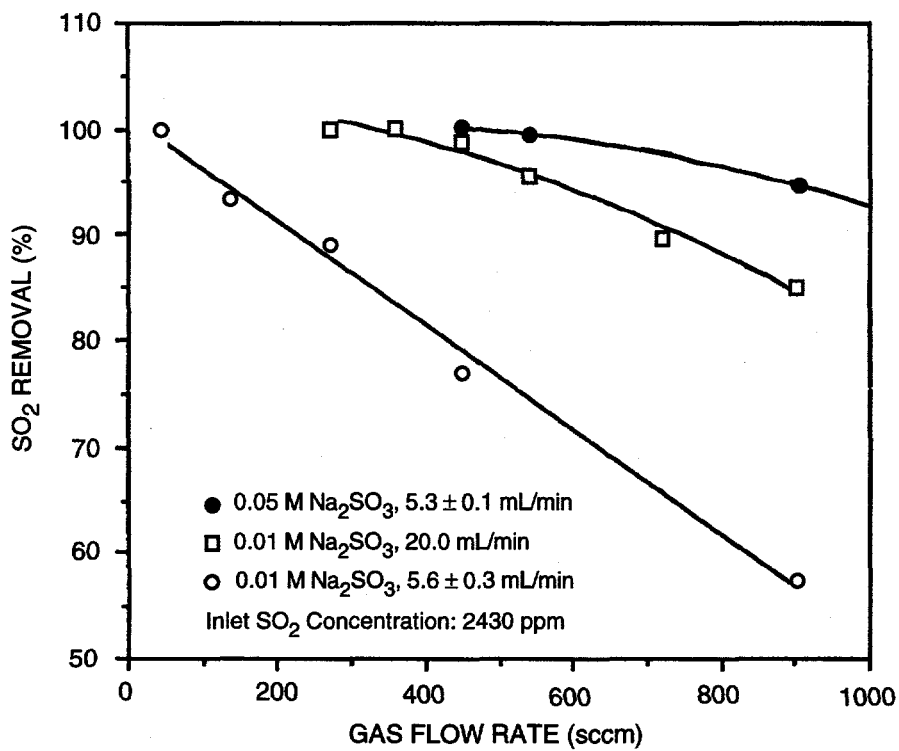
CM-3501-18

Figure 4-18. SO₂ removal with water at low liquid flow rates.



CM-3501-19

Figure 4-19. SO₂ removal with 0.01 M Na₂SO₃ solution.



CAM-3501-32

Figure 4-20. SO₂ removal efficiency at various sulfite concentrations.

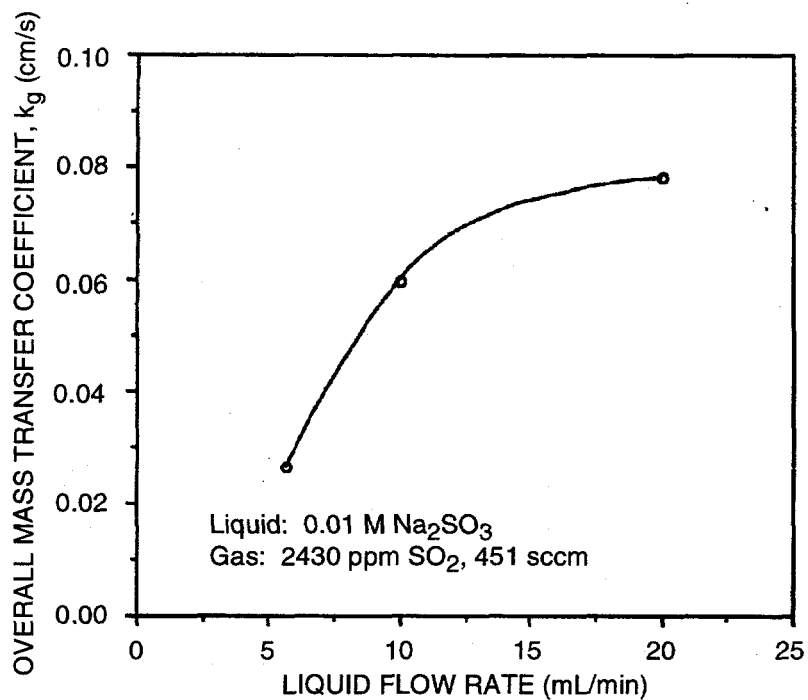
removal decreases with increasing gas flow rate. When the concentration of the sulfite solution is raised from 0.01 to 0.05 M, a considerably higher SO₂ removal rate is obtained because of the increase in the absorption capacity of the liquid. For 0.01 M Na₂SO₃ solution, more SO₂ is absorbed as the liquid rate is increased from 5 to 20 mL/min. Such a behavior suggests that the liquid phase might offer considerable resistance to mass transfer at low sulfite concentrations.

Figure 4-21(a) shows the effect of liquid flow rate on the overall gas phase based MTC for SO₂. The data were taken at a constant gas flow rate of 451 sccm. The overall MTC (K_g) increases with higher liquid flow rates. The SO₂ removal efficiency as a function of liquid flow rate is plotted in Figure 4-21(b). SO₂ is completely removed when the liquid flow rate is 30 mL/min. The overall MTC cannot be calculated when the outlet gas stream does not contain SO₂, because a logarithmic-mean driving force is used in its calculation.

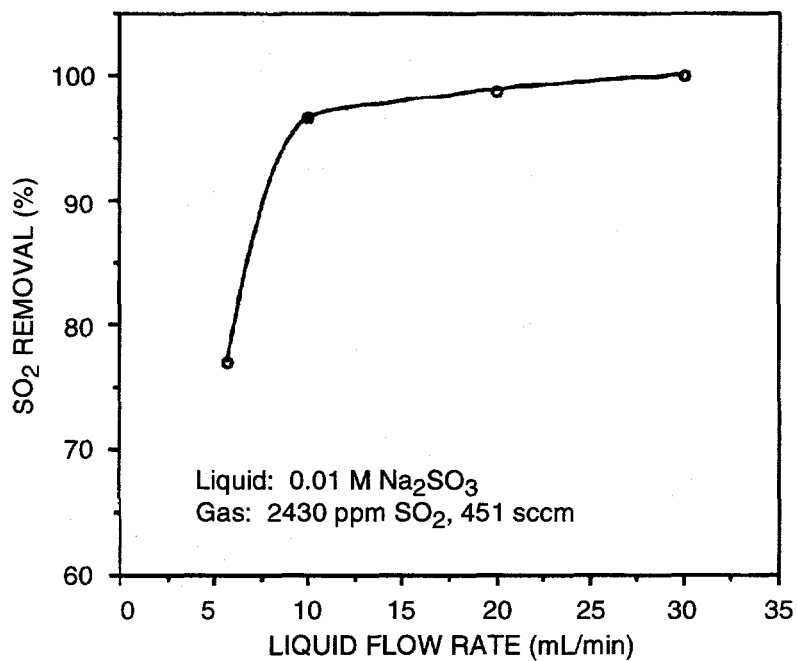
Figure 4-22 shows the effect of gas flow rate variations (from 0 to 1000) sccm on K_g at two sulfite concentrations. The liquid flow rate was maintained around 5.6 mL/min in this set of experiments. (Only two data points are shown for 0.05 M Na₂SO₃ solution because the SO₂ removal was 100% for lower gas flow rates.) In both cases, K_g is nearly independent of the gas flow rate, indicating that the liquid film resistance is controlling at low sulfite concentrations. At higher sulfite concentrations, the controlling resistance is expected to shift from liquid to gas phase.

Next, we present the results of raising the concentration of Na₂SO₃ in the liquid to determine the critical concentration where the gas phase resistance controls the absorption. To obtain gas-phase-controlled transfer, a series of runs were conducted using 0.2 M aqueous Na₂SO₃. The SO₂ absorption capacity of 0.2 M Na₂SO₃ solution is high; so we opted for a lower liquid flow rate of 5 mL/min and a relatively high gas flow rate range of 1800-2750 sccm in the first set of runs. Such a combination was expected to bring out gas-phase-controlled absorption and still have some SO₂ in the outlet gas stream. An experiment yielding complete removal of SO₂ is not useful because the MTC cannot be determined. Obtaining a steady residual concentration of SO₂ at the outlet gas stream was the experimental goal; gas and liquid flow rates were varied at a specified sulfite level in the liquid. Certified mixtures of model flue gases from different cylinders were used. The average composition was 2250 ± 350 ppm SO₂, 3% O₂, 10% CO₂, and the balance N₂.

Table 4-1 shows the results. Two out of five runs having a liquid flow rate of 5 mL/min reached steady state (i.e., the effluent gas stream attained a constant SO₂ composition with time). Three other runs yielded a continually increasing SO₂ level at the outlet. Initially, we concluded that the pores remained wet from the previous run and became more so in the course of a given



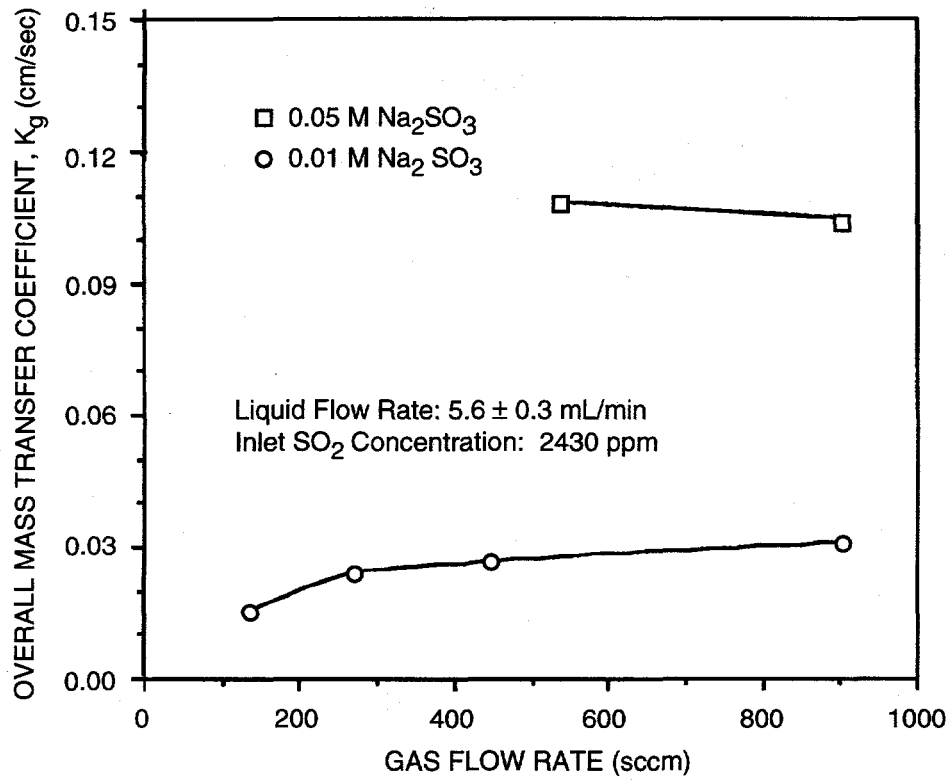
(a) Overall mass transfer coefficient



(b) SO₂ removal efficiency

CAM-3501-33

Figure 4-21. Effect of liquid flow rate on overall mass transfer coefficient and SO₂ removal efficiency at low sulfite concentrations.



CAM-3501-34

Figure 4-22. Effect of sulfite on overall mass transfer coefficient.

Table 4-1
RESULTS OF SO₂ ABSORPTION IN 0.2 M Na₂SO₃

Run No.	Temp. (°C)	Liquid Flow (mL/min)	Gas Flow (sccm)	Inlet SO ₂ Composition (ppm)		Steady State	Outlet SO ₂ (ppm)	SO ₂ Removal (%)	Kg (cm/s)
				Dry	Humid				
1	21.5	5.3	1809	2430	----	Yes	115	95	0.207
2	21.0	5.0	2713	2430	----	Yes	205	91	0.249
3	22.0	5.1	2261	2610	----	No	----	----	----
4	23.0	4.9	1809	2610	----	No	----	----	----
5	22.0	5.0	1809	2610	----	No	----	----	----
6	22.0	9.9	1809	2610	----	Yes	55	98	0.267
7	21.5	10.0	2261	2610	----	Yes	90	97	0.288
8	22.0	10.0	2713	2610	----	No	----	----	----
9	25.5	9.9	2713	2020	----	No	----	----	----
10	29.0	10.0	2713	----	1927	Yes	53	97	0.367
11	27.0	10.1	2713	----	2082	Yes	290	86	0.201
12	28	20	2713	2210	2050	Y	65	97	0.349
13	23	20	2713	2210	2082	Y	71	96	0.337

run, resulting in poor performance. After each run, therefore, the module was cleaned and dried thoroughly. Both the shell and tube sides were simultaneously washed with running deionized (DI) water, first with water warmed to 45°C and then with water at room temperature. Then the module was vacuum dried overnight. This was followed by runs having 5 mL/min of liquid flow rate and a gas flow rate of 1800-2260 sccm; however, we could not reproduce the steady state results.

The liquid flow rate was increased to 10 mL/min in later runs. Steady state conditions were observed for 1809 and 2261 sccm gas flow rates. Again, runs with a gas flow rate of 2713 sccm did not attain steady state. The HFC module was carefully dried, but repeated runs failed to yield a constant level of SO₂ at the exit gas. We concluded that salt deposition was taking place from 0.2 M sulfite solution within or near the pores, since the high gas flow rate must have been drying up the liquid layer at the gas membrane interface.

We realized that proper humidification of the feed gas entering the HFC was necessary to prevent the sulfite solution from drying near the pores inside the module. The model flue gas was humidified by using two separate HFCs connected in series at the inlet gas line. The shell sides of these modules had stagnant water maintained at 5 psi. Trials with N₂ gas flowing at about 2700 sccm showed that the stream attained 96% humidity within 2 h. In such humidifying modules, a part of the flue gas SO₂ will be absorbed into the water in the shell side, and there will be an equilibrium between the water and the inflowing gas.

We decided to measure the SO₂ content of such incoming flue gas by GC only after the experimental run reached steady state. The first run with humidified flue gas attained a steady state within 5 h. The effluent SO₂ concentration was about 50 ppm, indicating SO₂ removal to be 97%. In the next run, the inlet SO₂ concentration was higher. This run achieved steady state after 7 h. The effluent had 86% of SO₂ removed. Some salt deposition and pore wetting probably occurred, giving rise to poor performance in the contactor. To minimize the possible drying of liquid inside the module at these high gas flow rates, we later increased the liquid flow rate to 20 mL/min.

MASS TRANSFER CONTROL

Thus, we reported results of SO₂ absorption experiments using 0.2 M aqueous Na₂SO₃ solution in a cross-flow module containing 200 hollow fibers. At higher sulfite concentrations, the controlling resistance to mass transfer should shift to the gas phase, since there is little or no resistance in the liquid phase. The process becomes efficient because higher absorption can be achieved by increasing the gas flow rate. Experiments to obtain such gas-phase-controlled transfer

are useful for determining the optimum concentration of aqueous Na_2SO_3 to be used in the flue gas desulfurization. We considered 0.2 M sulfite concentration as high and fashioned our experiments in the following manner. At a certain gas flow rate, if there is no increase in mass transfer due to variation in the liquid flow rate, the transfer is not controlled by the liquid phase. In that liquid flow rate range, where the mass transfer increases with increased gas flow rates, gas phase control is achieved.

We started with low liquid flow rates and high gas flow rates. Several of our runs did not attain steady state at liquid flow rates of 5 and 10 mL/min and a gas flow rate of 2713 sccm. We concluded that drying of the liquid solution was occurring and that salt deposition was taking place from 0.2 M sulfite solution within or near the pores, since the high gas flow rate must have been drying up the liquid layer at the gas-membrane interface. The model flue gas was humidified to prevent the sulfite solution from drying near the pores inside the module. Two runs with humidified incoming flue gas attained steady state after 5 and 7 h. The second run yielded a lower MTC. Some salt deposition and pore wetting probably occurred, giving rise to poorer performance in the contactor.

We ran experiments with an increased liquid flow rate of 20 mL/min to minimize the possible drying of liquid inside the module at these high gas flow rates. Two runs were conducted using a model flue gas with an initial composition of 2210 ppm SO_2 , 3% O_2 , 9.9% CO_2 and balance N_2 . The results are presented in the last two rows of Table 4-1. Both runs had incoming gas humidified. The first run (No. 12) reached steady state after 5 h. The effluent SO_2 concentration was 65 ppm. The SO_2 removal was 97%. The following run (No. 13) was conducted to reproduce the preceding run. After about 5 h, Run 13 achieved steady state and yielded reproducible results. The effluent had 96% SO_2 removed. The operating temperatures of these two runs differed by 5°C , which probably caused the variation in the final values in K_g .

As mentioned before, we had difficulty obtaining steady state runs using 5-10 mL/min of liquid flow rate. Runs 1, 2, 6, and 7 achieved steady state using dry gas. The K_g values increased when the liquid flow rate was changed from 5 to 10 mL/min while the gas flow rates were between 1810-2260 sccm. The increase is probably related more to the increased absorption capacity of a higher liquid flow rate. Run 11 was an attempt to reproduce Run 10. A pseudo-steady-state condition was obtained at 5-7 h where the SO_2 level at the exit gas oscillated near 290 ± 20 ppm. Although the incoming gas was humidified, the process performed poorly as indicated by the low value of K_g . We concluded that it was not a reproducible run.

Three runs (10, 12, and 13) achieved steady state conditions using humidified incoming gas at a flow rate of 2713 sccm. The operating temperature of run 10 was high at 29°C and

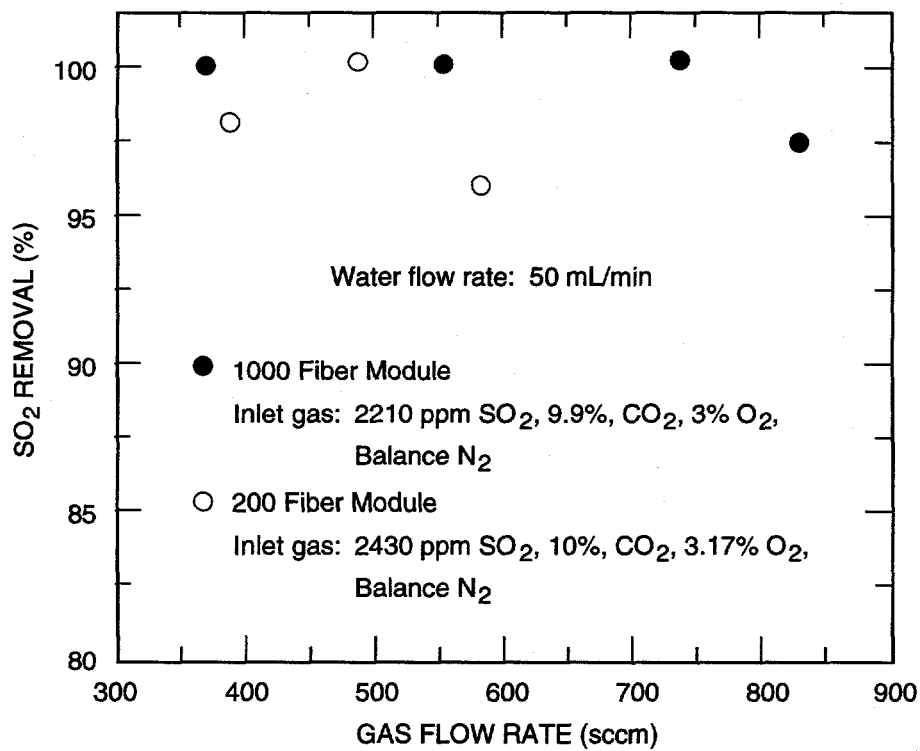
probably caused an increased reaction. A comparison of the K_g values of these runs shows that the changes in the liquid flow rate from 10 to 20 mL/min did not contribute significantly to the overall SO_2 absorption. This suggests that the mass transfer may not be controlled by the liquid-phase at 0.2 M sulfite concentration. The gas phase controlled transfer can likely be achieved by using this or higher levels of Na_2SO_3 in the scrubbing liquor.

Hence, we performed additional experiments. The liquid flow rate was at 20 mL/min and the gas flow rate was increased from 2713 to about 4500 sccm. The K_g values should increase; if that increment is significant, then gas phase control is indicated. Similar gas flow rates were used in a separate set of experiments where the liquid flow rate was 30 mL/min. Due to increased absorptive capacity at that liquid flow rate, all SO_2 can get absorbed. However, we expect to obtain a steady state condition at much higher gas flow rates and some SO_2 in the exit gas stream. Such results, at two different liquid flow rates and at several high gas flow rates, can highlight the role of gas phase control in SO_2 transfer.

To continue to characterize the operational characteristics of the 1000-fiber module, we also performed several SO_2 absorption experiments using DI water as the scrubbing medium. A model flue gas was supplied to the tube side and water was pumped through the shell side. The flue gas contained 2210 ppm SO_2 , 3% O_2 , 9.9% CO_2 , and balance N_2 . Gas flow rates of 370-840 sccm and a water flow rate of 50 mL/min were used. Very high removal for SO_2 was observed, mostly 100%. The results are plotted in Figure 4-23, describing the percent SO_2 removal efficiency. The plot also includes the results obtained previously, for the 200-fiber module in similar experiments using the same water flow rate. Another experiment, not shown in the plot, was conducted with 25 mL/min of water flow rate and 370 sccm of gas flow rate. It achieved 98% SO_2 removal efficiency.

NJIT's main objectives were to conduct experiments for removing SO_2 and NO_x from flue gas at various conditions and for regenerating the SO_2 scrubbing liquor, namely, the spent aqueous Na_2SO_3 solution obtained from a simultaneously run absorption experiment.

The removal of SO_2 and NO_x involves SO_2 scrubbing followed by NO_x scrubbing using separate liquors. We performed extensive studies on SO_2 absorption with aqueous sulfite solution using a model flue gas containing 2300 ± 200 ppm SO_2 , $3.1 \pm 0.1\%$ O_2 , $10.1 \pm 0.2\%$ CO_2 and balance N_2 . These gas mixtures did not have any NO . However, the power plant flue gases contain both SO_2 and NO . Because wet scrubbing of SO_2 will be the first of the two absorption processes, it is important to examine how the absorption of SO_2 by the aqueous sulfite liquor is influenced by the presence of NO in the gas stream. For that purpose, we



CM-3501-42

Figure 4-23. SO₂ removal with water.

conducted an experiment using 0.2 M aqueous Na_2SO_3 solution and a feed gas containing 520 ppm NO, 2475 ppm SO_2 , 10.3% CO_2 , and balance N_2 . A gas mixture containing O_2 and NO is not stable over days; so we excluded O_2 from the model flue gas used in the run.

The cross-flow module containing 200 fibers was used. The feed gas was introduced to the tube side of the unit at a flow rate of 3000 cc/min. The aqueous sulfite liquor was pumped through the shell side at 20 mL/min. The experimental parameters are identical to those used in standard runs for absorption of SO_2 with 0.2 M Na_2SO_3 solution. The GC cannot detect the presence of NO. We employed an infrared analyzer (Lira Model 202, Mine Safety Appliances, Minnesota) to detect NO at the inlet-outlet streams of the HFC absorber module. The feed gas was initially passed through the infrared analyzer, showing the presence of NO. The composition of other components in the inlet feed gas was checked by injecting a sample into the GC. As the run progressed, the effluent gas was passed periodically through the infrared analyzer to indicate possible changes in the concentration of NO. The effluent gas composition was also monitored in the GC. The infrared analyzer requires dry gas for sampling. Two Nafion membrane driers were employed in series to remove moisture from the effluent stream prior to sending the gas to the infrared analyzer. However, we could not achieve a complete removal of the moisture from this stream.

The GC readings of the residual composition of SO_2 at the outlet gas stream showed a constant value of 40 ppm after about 3 h of run time. This reading indicated that the steady state condition for absorption of SO_2 was reached. The run was continued for two or more hours. The readings of the infrared analyzer showed that the concentration of NO in the outlet stream increased somewhat from that of the feed inlet value of 527 ppm NO. This was due to the reduction of SO_2 and CO_2 concentration in the outlet gas stream. The SO_2 removal was 98%, a result obtained repeatedly in similar runs with model flue gas mixtures having no NO. We concluded that 527 ppm of NO in the feed gas did not influence the absorptive process of removing SO_2 via an aqueous sulfite solution.

To study the regeneration of the SO_2 scrubbing liquor, we used the 1000-fiber HFC module for the liquid-liquid extraction (LLE) run and the 200-fiber HFC module for SO_2 absorption. The major reasons for using this arrangement are as follows: Because the walls of the fibers are hydrophobic, water does not wet the fiber walls, and the pores within the fiber walls are filled with gas, ensuring rapid diffusion. A small contactor, therefore, suffices in this operation. However, during LLE, the organic liquid will penetrate the hydrophobic fiber walls and fill their pores. Diffusion through these liquid-filled pores will be several orders of magnitude smaller than diffusion through the gas-filled pores. Hence, (LLE) needs a larger module. Details of the (LLE) runs are provided later. The extracting organic solvent

dimethylaniline (DMA) wets the fiber material. Its removal from the module could be difficult and time consuming. Therefore, the 1000-fiber module was used for extraction runs only. Prior to starting the extraction runs, this 1000-fiber unit was used for a series of CO₂ absorption experiments. In previous runs, the values of the overall MTC (K_{Olm}) in pure CO₂ absorption were smaller than those obtained for a gas mixture of 10% CO₂ and balance N₂. The effort described below was directed toward examining that issue.

Pure CO₂ was fed into the tube side of the 1000-fiber unit. The scrubbing liquid was DI water obtained from a Barnstead E-pure water purification system. The water was pumped through the shell side of the module. The shell side contained a large volume of water, which absorbed CO₂ coming through the fiber pores. The experimental system was allowed to reach a steady state, defined by a constant gas flow rate at the exit. Previous runs took 2-3 h to reach steady state. We duplicated those runs first.

In the first run (No. 1, Table 4-2), the water flow rate was 100 mL/min. A pseudo-steady-state condition was observed at the end of 5 h. In the second run, we monitored the gas-side pressure drop within the module using a manometer between the entrance and exit of the module. The manometric liquid was water, colored with microgram quantities of KMnO₄. The run reached a steady state between 2 and 3 h and was ended after 4 h. The manometer showed an increase of pressure drop by 30%-40%. Several experiments were then run for about 4 to 5 h. Often, the manometer showed increased pressure drops at the tube side as the run progressed. These may be attributed to blockage of pores by water vapor. Typically, a run was ended when such pressure drops became twice the initial pressure drop. Table 4-2 is a summary of these results. The MTCs K_{Olm} values are calculated from readings obtained at the steady state condition. Occasionally, we noticed a minor drift as time passed.

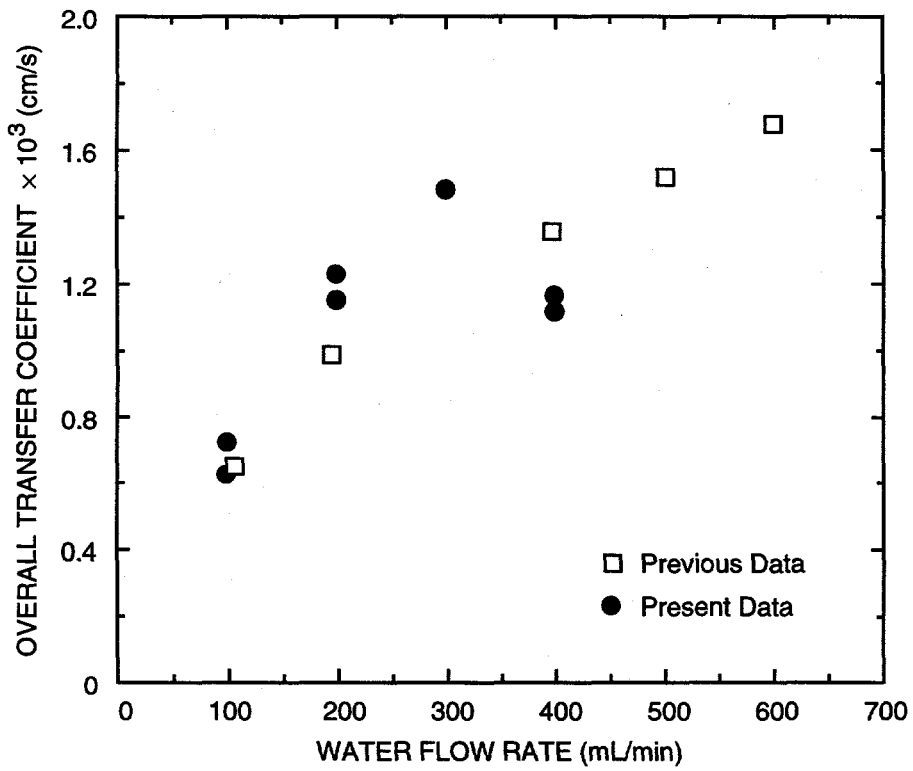
The above results are plotted in Figure 4-24. Earlier data on CO₂ absorption using the 1000-fiber module are also plotted. The values are similar to previous results. Despite some scatter, the experimental results are reproducible. The values of K_{Olm} in absorption of pure CO₂ turned out to be smaller than those obtained with a mixture of 10% CO₂ and balance N₂. We observed some increase in the pressure drop on the gas side. Such increased pressure drop indicated possible pore blockage, which might have affected the experimental results with pure CO₂ by reducing the mass transfer rate. We know that there is no gas phase resistance in absorption of pure CO₂ in water. So the liquid side resistance prevails. If pore blockage becomes significant, then the resistance to liquid-side mass transfer will increase during a run.

Table 4-2
SUMMARY OF RESULTS ON CO₂ ABSORPTION IN THE 1000 FIBER UNIT

Run No.	Water Flow Rate (mL/min)	Percent Increase from Initial Pressure Drop by Manometer Reading	MTC	
			Present Result	Earlier Result
1	101	No manometer	0.73	---
2	100	30	0.63	---
	108	---	---	0.65
3	200	20	1.23	---
4	200	60	1.15	---
	200	---	---	0.99
5	300	20	1.48	---
6	400	60	1.16	---
7	400	50	1.12	---
	400	---	---	1.36
	500	---	---	1.52
	600	---	---	1.68

We also conducted work on simultaneous absorption of SO₂ by an aqueous solution of Na₂SO₃ and regeneration of the spent liquor by extraction with DMA. A few runs were not useful because of the problems in pumping liquid at a low flow rate and difficulties in handling DMA. Three runs were completed. Results of the LLE are presented in a later section. In this section, we provide details on the absorption in each of these three runs.

The first trial run used aqueous 0.2 M Na₂SO₃ solution as the absorbent. It was pumped through the shell side of the 200-fiber module at 20 mL/min. The residual composition of SO₂ at the outlet of this module was measured by sampling the treated flue gas in a GC. When a steady state condition for absorption was reached, the composition of SO₂ in the effluent attained a constant level. Such steady state conditions were reached after 6 h. The effluent sulfite



CAM-3501-45A

Figure 4-24. Pure CO₂ absorption in the 1000 fiber module.

solution was then fed into the tube side of the 1000-fiber module and liquid DMA was pumped through the shell side of this extractor unit. We monitored the pH of both the aqueous effluent from the absorption unit and that from the liquid-liquid extraction unit.

We anticipated that the pH of the stream after the extraction step would increase because SO₂ was removed from it by DMA. We did not notice any such change (see results of Run 1 in Table 4-2). The SO₂ concentration in DMA at the exit was determined by wet chemistry, which indicated SO₂ flux across the organic phase to be 4.6×10^{-10} mol/cm² s. The corresponding SO₂ flux from the flue gas to the aqueous phase in the absorption step was 1.02×10^{-8} mol/cm² s. The low fraction of SO₂ recovered by LLE suggested that there was less free SO₂ available for removal at this step. A significant part of the SO₂ in the aqueous phase probably reacted with Na₂SO₃ to form NaHSO₃.

In the following runs, the procedure for sampling the organic phase was improved. Also in these runs, sulfite solution was not used to absorb SO₂. Instead, DI water was used. We expected that more free SO₂ would be available for removal by LLE. Also, it might be easier to monitor the pH changes of the acidic aqueous solution as SO₂ is removed from it by DMA. Table 4-3 is a summary of results relating the absorption part of these experiments. Water was used as absorbent in Runs 2 and 3. Run 2 did not show much change of pH in the aqueous effluent caused by extraction with DMA. The next run with a higher water flow rate showed noticeable change.

Our purpose in conducting absorption-only experiments was to obtain a situation where the resistance to mass transfer shifts to the gas phase. We assume that a sulfite concentration of 0.2 M aqueous Na₂SO₃ was suitable to bring out that condition. In this type of experiment, the liquid flow rate was 20 mL/min and the gas flow rate was increased from about 2700 to 4500 sccm. There could be drying of sulfite solution near the pores inside the module at high gas flow rates, giving rise to an unsteady process and poorer performance in the contactor. Humidification of the incoming model flue gas prevented such drying of liquid inside the module.

Two absorption-only experiments were conducted using 0.2 M Na₂SO₃ solution under identical conditions and using a model flue gas with an initial composition of 2400 ppm SO₂, 3% O₂, 10% CO₂, and the balance N₂. One run was conducted with humidified incoming flue gas, and the other used dry gas from the cylinder. The purpose was to examine if steady state and good performance from the contactor could be achieved without humidifying the flue gas. Such experiments were not conducted earlier using the sulfite liquid flow rate at 20 mL/min. The results are presented in Table 4-3, which also includes results of previously obtained steady state runs using a liquid flow of 20 mL/min. The runs are numbered accordingly. The inlet gas was

Table 4-3
SUMMARY OF ABSORPTION DATA IN SIMULTANEOUS ABSORPTION-EXTRACTION RUNS

Run No.	Aqueous Absorbent		Flow Rate (sccm) (Humidified)	Flue Gas		Absorptive Flux of SO ₂ (mole/cm ² s)	Steady State pH of Aqueous Stream	
	Type	Flow Rate (mL/min)		SO ₂ Composition (ppm)			After Absorption	After Extraction
				Inlet	Outlet			
1	0.2 M Na ₂ SO ₃	20	2722	2260	105	1.02 x 10 ⁻⁸	7.4	7.4
2	Water	22	901	2400	617	2.78 x 10 ⁻⁹	5.0	5.05
3	Water	50	908	2400	207	3.41 x 10 ⁻⁹	2.8	5.4

not humidified in Run 16. Run 14, in Table 4-4, describes the absorption part of the above absorption-extraction run with sulfite solution. The performance of the HFC in absorbing the model flue gas with Na_2SO_3 appears reproducible at this liquid flow rate, as evidenced by the reproducible values of K_g .

To evaluate the performance of the HFC in absorbing a model flue gas, we studied the extent of several reactions that occur simultaneously between the component gases and the sulfite liquor. We analyzed the results of some experiments with 0.2 M Na_2SO_3 . Specifically, the conversions of SO_2 and CO_2 were compared. The reaction between SO_2 and aqueous Na_2SO_3 was rapid; it could be considered instantaneous. Preliminary analysis of steady state data showed that a ratio of about 4:1 was maintained between the amount reacted for SO_2 and CO_2 . Typically in a run, the composition of SO_2 dropped from an initial value of 2200 ppm to a value less than 100 ppm. The amount of CO_2 consumed in a parallel reaction was approximately 500 ppm. The initial concentration of CO_2 was close to 10% by volume. Thus, its depletion can be considered less significant with respect to that of SO_2 .

COMBINED ABSORPTION AND EXTRACTION

Initially, we conducted one absorption-only run and six simultaneous absorption runs of SO_2 by an aqueous solution of Na_2SO_3 and regeneration of the spent liquor by extraction with DMA. Details on the absorption part of these runs are presented in this section.

The sulfite liquor was pumped through the shell side of the 200-fiber module. The first three runs, AE-4 to AE-6, used a model flue gas with an initial composition of 2300 ppm of SO_2 , 2.9% O_2 , 10.5% CO_2 , and the balance N_2 . The second three runs, AE-7 to AE-9, used a model flue gas with an initial composition of 2170 ppm of SO_2 , 3.13% O_2 , 10.8% CO_2 , and the balance N_2 . The residual composition of SO_2 at the outlet of this module was measured by sampling the treated flue gas in a GC. A steady state condition for the absorption process was reached after about 5-6 h. The effluent sulfite solution was then fed into the tube side of the 1000-fiber module and liquid DMA was pumped through the shell side of this extractor unit. The SO_2 concentration in the DMA at the exit was determined by wet chemistry, from which its flux at the extraction stage was calculated. The corresponding SO_2 flux from the flue gas to the aqueous phase in the absorption step was obtained from the material balance. Table 4-5 presents the run-parameters and the absorptive fluxes.

In run AE-4, the flue gas was humidified before being fed into the module. Dry gas from the cylinder was used in runs AE-5 and AE-6. The flow rate of the sulfite liquor was changed to 10 mL/min in run AE-6 to examine its effect on the extraction process. We monitored the pH of

Table 4-4
RESULTS OF SO₂ ABSORPTION RUNS USING 0.2 M Na₂SO₃ AT 20 mL/min

Run No.	Temp. (°C)	Liquid Flow Rate (mL/min)	Gas Flow Rate (sccm)	SO ₂ Composition (ppm)			SO ₂ Removal (%)	Kg (cm/s)
				Dry	Humid	Outlet		
12	28	20	2713	2210	2050	65	97	0.349
13	23	20	2713	2210	2082	71	96	0.337
14	20	20	2723	2400	2260	105	96	0.324
15	22	20	2705	2400	2243	67	97	0.345
16	20	20	2723	2400	---	58	98	0.367

Table 4-5

SUMMARY OF ABSORPTION DATA IN SIMULTANEOUS ABSORPTION-EXTRACTION RUNS

Run No.	Aqueous Absorbent		Flue Gas		Absorptive Flux of SO ₂ (mole/cm ² s)	Steady State pH of Aqueous Stream		
	Type	Flow Rate (mL/min)	Flow Rate (sccm)	SO ₂ Composition (ppm)		After Absorption	After Extraction	
AE-4*	0.2 M Na ₂ SO ₃	20	2722 (Humidified)	2250	69	1.02 x 10 ⁻⁸	7.35	7.4
AE-5*	0.2 M Na ₂ SO ₃	20	2704 (Dry)	2300	43	1.05 x 10 ⁻⁸	7.7	7.8
AE-6**	0.2 M Na ₂ SO ₃	10	2732 (Dry)	2300	100	1.038 x 10 ⁻⁸	7.3	7.3
AE-7*	0.2 M Na ₂ SO ₃	20	2732	2170	44	0.996 x 10 ⁻⁸	7.55	7.75
AE-8*	0.2 M Na ₂ SO ₃	20	2732	2170	60	0.990 x 10 ⁻⁸	7.4	7.5
AE-9***	0.2 M Na ₂ SO ₃	30	5000	2170	142	1.721 x 10 ⁻⁸	7.3	7.65

* DMA flow rates were different at the extraction stage.

** The liquid flow rate at the absorption part was decreased.

*** Both the gas and liquid flow rates at the absorption part were increased.

both the aqueous effluent from the absorption unit and that from the extraction unit. An increase in the pH of the stream after extraction was anticipated because SO₂ was removed at this step. We did not observe any significant change (see Table 4-5). Dry gas from the cylinder was used in runs AE-7, AE-8, and AE-9. The flow rate of the DMA was varied at the extraction stage; otherwise the absorption segment of runs AE-7 and AE-8 were similar to that of Runs AE-5 and AE-6. In run AE-9, the flow rate of the sulfite liquor was increased to 30 mL/min to examine its effect in reducing the boundary layer resistance at the downstream extraction process.

We increased the gas flow rate to 5 seem to adapt to the increased liquid flow rate and to help attain a low residual concentration of SO₂ at the outlet of the absorption unit. After about 3 h, the SO₂ level in the treated flue gas reached a value of 144 ± 5 ppm. It remained there for the rest of the run time of 4 h, which included the extraction process. It was the highest gas flow rate we ever used. A steady absorption process was in effect with an increased flow of aqueous sulfite liquor. The high flow rate of the liquid allowed the operation without any pore drying, although the incoming flue gas was not humidified. We monitored the pH of both the aqueous effluents from the absorption unit and that from the extraction unit. A minor increase in the pH of the stream after extraction was observed in these three runs. See Table 4-5.

To continue our efforts to obtain a situation where the resistance to mass transfer shifts to the gas phase, we conducted two absorption-only experiments. The first, A-17, was run with the flow rate of the humidified incoming flue gas set at approximately 3630 sccm. The other conditions were identical to those absorption-only runs reported previously. The model flue gas had an initial composition of 2300 ppm SO₂, 2.9% O₂, 10.5% CO₂, and the balance N₂. The results are presented in Table 4-6, which also includes results of the absorption part of the above absorption-extraction runs with the sulfite solution.

In the second absorption-only experiment, Run A-18, the model flue gas had an initial composition of 2170 ppm SO₂, 3.13% O₂, 10.8% CO₂, and the balance N₂. It was humidified before being fed into the module. The flow rate of this incoming flue gas was 4500 sccm. An increase of the gas flow rate was in line with the experimental pattern we adopted in recently completed absorption-only runs when other conditions were identical. The incoming flue gas was humidified by passing it through the tube side of two HFC modules whose shell sides were filled with water maintained at 10 psig. The high gas flow rate of 4500 sccm introduced a larger amount of moisture in the stream. It was difficult to remove this moisture completely from the sample effluent going into the GC by the Nafion membrane drier. After 3 h, the effluent compositions of SO₂, other components, and water vapor attained a constant level. The SO₂ composition was 148 ± 8 ppm with repetitive fluctuations showing a steady state run condition.

The results are presented in Table 4-6, which includes results of the absorption part of the above extraction-absorption runs.

The steady state condition for the absorption process was achieved in many runs, using a flow rate of 20 mL/min for the aqueous sulfite solution and gas flow rates varying between 1800 and 4500 sccm. Most runs used liquid and gas flow rates of 20 mL/min and about 2700 sccm, respectively, a combination often used in absorption-extraction runs. Typical values of the MTC obtained from some of these runs are plotted in Figure 4-25 against the corresponding gas flow rates. Sample values are from Table 4-6. The plot shows a pattern in which K_g increases with the gas flow rate, and that dependency becomes smaller at higher gas flow rates. The data trend is toward gas-phase controlled mass transfer.

Previously, an analysis of results of some flue gas absorption experiments with 0.2 M Na_2SO_3 was reported. We compared the conversions of SO_2 and CO_2 that occurred simultaneously. The analysis suggested that the reaction between SO_2 and aqueous Na_2SO_3 can be considered instantaneous. Typically, a ratio of about 4:1 was maintained between the amount reacted for SO_2 and CO_2 . The depletion of CO_2 was less significant with respect to that of SO_2 .

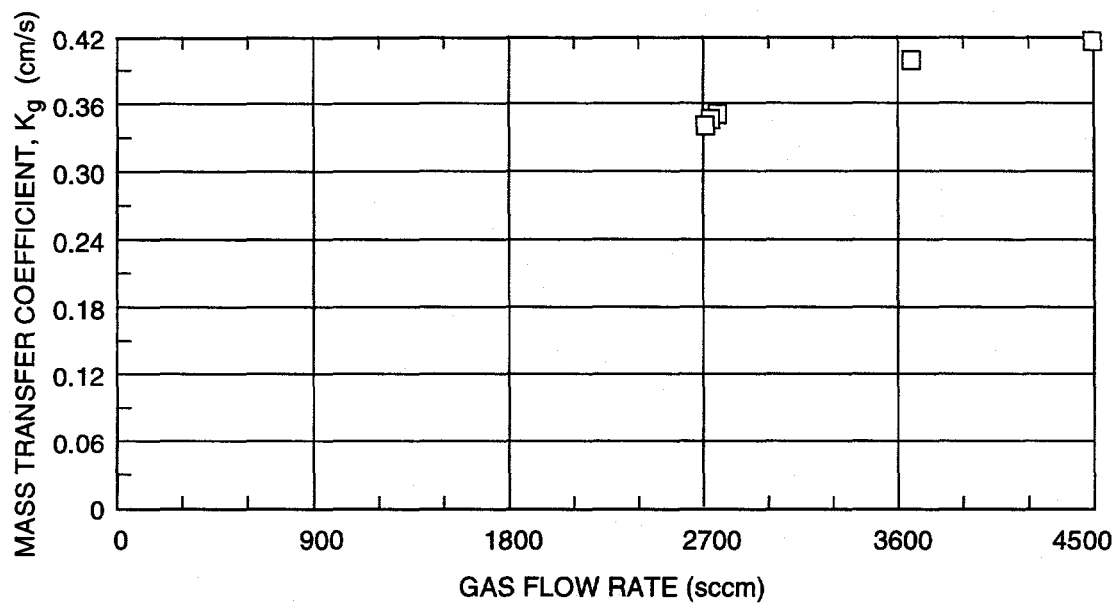
A separate run was also conducted using 0.2 M Na_2SO_3 to absorb a gas mixture of CO_2 - N_2 containing 9.89 % CO_2 . A model flue gas usually consists of about 2500 ppm SO_2 , 10% CO_2 , 3% O_2 , and the balance N_2 . The purpose in this experiment was to gather data on the extent of reaction that could occur between CO_2 and the sulfite liquor in the 200-fiber contactor in the absence of SO_2 and O_2 . The gas flow rate was about 2700 sccm and the liquid flow rate was 20 mL/min, similar to those of a typical run in absorbing flue gas. A steady state condition was obtained after about 2 h, and the run continued for an additional hour. An estimation of GC results indicated that 4.34% of the incoming CO_2 reacted with the sulfite solution. It amounted to a removal of 4290 ppm from 98,900 ppm of inlet CO_2 . In the case of flue gas absorption, the SO_2 composition dropped typically from about 2300 to 50-80 ppm. The amount of CO_2 consumed in a parallel reaction was estimated to be approximately 500 ppm. The selectivity of reactions with sulfite is favored for SO_2 . We plan to continue to examine the speed of the reactions of SO_2 with the sulfite solution.

Earlier, an experiment was conducted on absorption of SO_2 by DI water and its simultaneous recovery by extraction with DMA. The absorption part of Run AE-11 is similar to that part of Run AE-3 using water as the absorbent. These two runs differed in their LLE segments. The flow rate of the organic phase was 40 mL/min in run AE-11 and 6 mL/min in AE-3. The extraction part of Run AE-11 resembles the extraction part of Run AE-10. The purpose of using a high flow rate of DMA was to examine its effect in removing SO_2 from the aqueous phase. We also developed an experimental setup to find the values of the distribution

Table 4-6
RESULTS OF SO₂ ABSORPTION RUNS USING 0.2 M Na₂SO₃ AT 20 mL/min

Run No.*	Temp. (°C)	Liquid Flow Rate (mL/min)	Gas Flow Rate (sccm)	SO ₂ Composition (ppm)				SO ₂ Removal (%)	Kg (cm/s)
				Inlet		Outlet			
				Dry	Humid	Dry	Humid		
AE-4	19	20	2732	2300	2250	69	97	0.345	
AE-5	22	20	2704	2300	---	43	98	0.395	
AE-6	19	10	2723	2300	---	80	97	0.332	
A-17	20	20	3630	2300	2243	100	96	0.397	
AE-7	19	20	2732	2170	---	44	98	0.384	
AE-8	19	20	2732	2170	---	60	97	0.354	
AE-9	19	30	5000	2170	---	142	93	0.465	
A-18	18.5	20	4500	2170	2150	148	93	0.416	
A-15	22	20	2704	2400	2243	67	97	0.345	
A-12	28	20	2713	2210	2050	65	97	0.349	

*AE indicates absorption-extraction run, A indicates absorption-only run.



CM-3501-59

Figure 4-25. Variation of mass transfer coefficient with gas flow rates at an aqueous sulfite solution flow of 20 mL/min.

coefficient (m_i) for SO₂ in organic-aqueous phases. We present results of these LLE runs and such flow assembly under Task 6, after describing the absorption part of these runs.

The aqueous phase (DI water/sulfite liquor) was pumped through the shell side of the 200-fiber module. The runs used a model flue gas with an initial composition of 2230 ppm of SO₂, 3.13% O₂, 11.0% CO₂, and the balance N₂. Both runs AE-10 and AE-11 used dry gas from the cylinder. When the absorption process reached steady state, the aqueous effluent was fed into the tube side of the 1000-fiber module used for LLE. In this extractor unit, liquid DMA was pumped through the shell side. The flow rate of the DMA (~40 mL/min) was the highest value used so far. Table 4-7 presents the run parameters and the absorptive fluxes.

The absorption part of run AE-11, similar to that part of run AE-3 using water as the absorbent, had a flow rate of incoming flue gas of 908 sccm. The flow rate of water on the shell side of the HFC unit was 50 mL/min. A steady state for the absorption was achieved in about 3 h with a SO₂ concentration in the treated gas of 150 ± 5 ppm. The pH value of the aqueous effluent from the absorption unit was 2.7. When LLE operation was initiated at 5 h, the pH of this stream beyond the extraction unit increased to 5.6. Evidently, a high removal of SO₂ from the aqueous stream was occurring. The run continued for about 8 h. Table 4-7 summarizes the results. The absorption performance of the current run AE-11 matches that of run AE-3. The two runs differed in LLE segments only.

In the absorption part of run AE-10, the gas flow rate was 2459 sccm. The absorption segment of this run was partly similar to a previously completed run AE-6. The flow rate of the sulfite liquor was 10 mL/min instead of the usual 20 mL/min to raise the level of SO₂ in the aqueous phase. After about 3 h, the SO₂ level in the treated flue gas reached a value of 40 ± 5 ppm. Such a steady state condition remained for the rest of the run time of 7 h, which included the extraction process. We monitored the pH of both aqueous effluent from the absorption unit and that from the extraction unit. We did not observe any significant change. The higher concentrations of SO₂ in the aqueous phase and an increased residence time for the aqueous phase in the LLE module were expected to cause high recovery by extraction. (See Table 4-7.)

Additional experiments were conducted to measure the distribution coefficient (m_i) of SO₂ between the aqueous and organic phases. The procedure involved contacting and thus establishing equilibrium between constant volumes of SO₂-rich aqueous phase and fresh DMA. This was attained by operating two HFCs. In the first unit, a steady state condition for absorption of SO₂ into an aqueous phase was obtained. The tube side of the second module was fed with a constant volume of this SO₂-laden effluent. A constant volume of fresh DMA was then introduced at the

Table 4-7
ABSORPTION DATA IN RECENT ABSORPTION-EXTRACTION RUNS USING HIGH AND LOW FLOW RATES OF DMA

Run No.	Aqueous Absorbent		Flow Rate (sccm)	Flue Gas SO ₂ Composition (ppm)		Absorptive Flux of SO ₂ (mole/cm ² s)	Steady State pH of Aqueous Stream	
	Type	Flow Rate (mL/min)		Inlet	Outlet		After Absorption	After Extraction
	AE-10*	0.2 M Na ₂ SO ₃		10	2459		2230	40
AE-6**	0.2 M Na ₂ SO ₃	10	2732	2300	100	1.038 x 10 ⁻⁸	7.3	7.3
AE-11*	Water	50	908	2230	147	3.25 x 10 ⁻⁹	2.7	5.4
AE-3**	Water	50	908	240	207	3.41 x 10 ⁻⁹	2.8	5.4

* DMA flow rate during extraction ~40 mL/min.

** DMA flow rate during extraction ~6 mL/min.

shell side of that unit. Continuous contacting between both these phases was maintained by keeping them in two, separate, closed-loop circulations. A LLE process operated, transferring SO₂ from the aqueous to the organic phase in batch mode. The experiment was continued for a long time (between 6 and 24 h), ensuring that equilibrium had been reached between the phases. The composition of SO₂ in each phase changed gradually and reached a constant value. The final concentration of SO₂ in DMA was measured. Its initial composition in the aqueous phase was known beforehand from the mass balance of the absorption process.

We present results of these new runs and their procedures in the section on Task 6, after describing the absorption part of these runs. The runs are numbered as AEM-1 and AEM-2. The aqueous phase (DI water/sulfite liquor) was pumped through the shell side of the 200-fiber module. The runs used a model flue gas with an initial composition of 2230 ppm of SO₂, 3.13% O₂, 11.0% CO₂, and the balance N₂. Both runs AEM-1 and AEM-2 used dry gas from the cylinder. When the absorption process reached a steady state, a known volume of the aqueous effluent was fed into the tube side of the 1000-fiber module. A four-way valve was used to disengage the first module. The shell side of the extractor unit was filled with fresh DMA. After introducing a constant volume of DMA, another four-way valve was used to disengage inflow of new DMA. Two pumps were run simultaneously to circulate the aqueous phase and the organic phase in two separate loops. The fibers were wetted by DMA. The contacting of the phases took place in the tube side of the extractor. Table 4-8 presents the run parameters and the absorptive fluxes.

We conducted three experiments. Two involved measuring the distribution coefficient (m_i) of SO₂ between the aqueous and organic phases. The objective was to measure accurately such m_i values and obtain reproducibility of the results with those reported earlier. The runs are numbered AEM-3 and AEM-4. Details of the procedure are similar to the runs performed earlier. The third run, AE-12, involved absorption of SO₂ in 0.2 M Na₂SO₃ solution and its simultaneous recovery by extraction with DMA. The flow rate of the organic phase was 102 mL/min. The purpose of using such a high flow rate of DMA was to achieve complete recovery of SO₂. This is in line with one of the milestones of the project (i.e., achieving 99% SO₂ recovery at the LLE stage). As stated before, the results and procedures of the LLE stage will be discussed under Task 6 in this report.

The m_i -runs AEM-3 and AE-4 used a model flue gas having the following composition: 2230 ppm SO₂, 3.13% O₂, 11.0% CO₂, and the balance N₂. Run AE-12 used a gas containing 2300 ppm of SO₂, 3.22% O₂, 11.0% CO₂, and the balance N₂. All three runs used dry gas from a cylinder. We present the run parameters and the absorptive fluxes in Table 4-7.

Table 4-8
ABSORPTION DATA TO DETERMINE DISTRIBUTION CONSTANT (m) USING HFCs FOR ABSORPTION-EXTRACTION

Run No.	Aqueous Absorbent		Flue Gas		pH of Aqueous Stream		Concentration of SO ₂ in Aqueous Phase (mole/cm ³)		
	Type	Flow Rate (mL/min)	Flow Rate (scfm)	SO ₂ Composition (ppm)		Initial		Final	
				Inlet	Outlet				
AEM-1	0.2 M Na ₂ SO ₃	20	2732	2230	43	9.4	7.3	4.43 x 10 ⁻⁶	13.3 x 10 ⁻⁶
AEM-2	Water	45	908	2230	85	5.6	3.0	1.45 x 10 ⁻⁶	1.9 x 10 ⁻⁶
AEM-3	Water	45	908	2230	116	5.6	3.2	1.43 x 10 ⁻⁶	1.9 x 10 ⁻⁶
AEM-4	0.2 M Na ₂ SO ₃	20	2718	2230	44	9.4	7.3	4.42 x 10 ⁻⁶	13.3 x 10 ⁻⁶
AE-12	0.2 M Na ₂ SO ₃	20	2718	2300	42	9.3	7.3	4.57 x 10 ⁻⁶	13.7 x 10 ⁻⁶

We made a module to conduct process studies on a contained liquid membrane technique to regenerate the aqueous absorbent. Details of the construction are presented under Task 6 in this report.

TASK 5: MASS TRANSFER RATE STUDIES FOR NO_x SCRUBBING IN HOLLOW FIBER CONTACTORS

The objective of this task was to determine the mass transfer characteristics of hollow fiber contactors (HFCs) for scrubbing NO_x from a simulated flue gas. NO and N₂ are blended at controlled rates, passed through a humidifier, checked for composition, heated, and fed into the lumens of the hollow fibers. The scrubbing liquid is pumped at a controlled flow rate, filtered, heated, and fed into the shell-side of the hollow fiber module. Pressure and temperature probes at various locations allow us to monitor and control the experimental conditions.

Initially we used aqueous solutions of [Fe^{II}(EDTA)]²⁻ as the scrubbing solution. The chelate is known to complex with NO according to the liquid-phase reaction



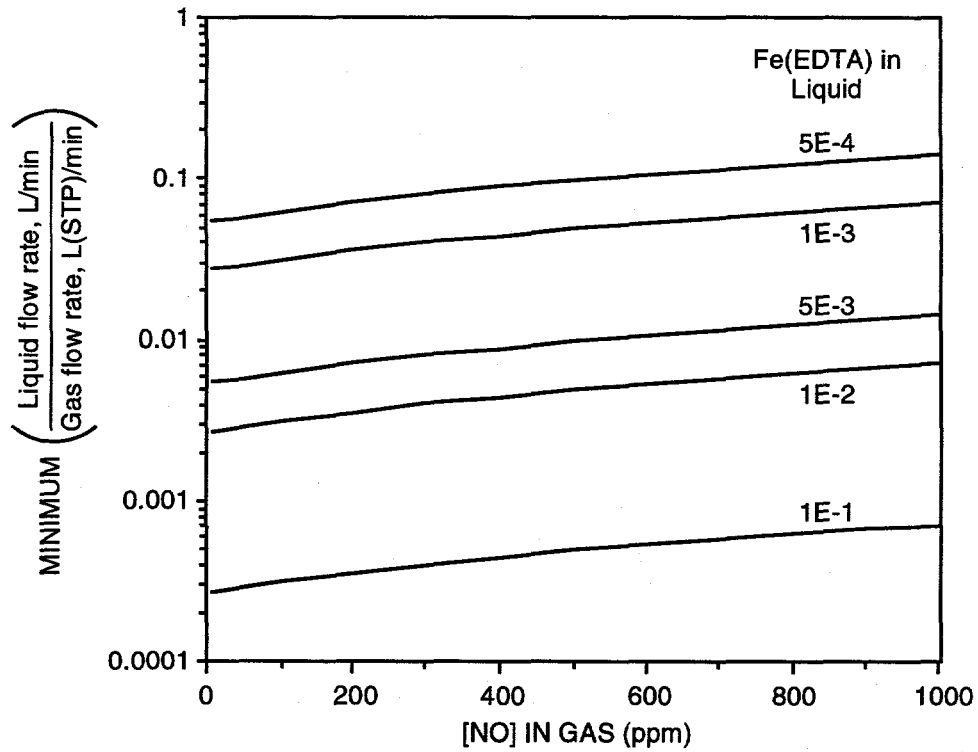
Based on this expression and assuming counter current flow, Appendix E shows that the minimum liquid flow rate necessary to treat a given gas flow rate is given as

$$\frac{\text{Liquid flow rate; L/min}}{\text{Gas flow rate; L (STP)/min}} = \frac{10^{-6}}{22.4} \frac{1 + K\alpha[\text{NO(g)}][\text{Fe}^{\text{II}}(\text{EDTA})^{2-}(\text{l})]_{\text{initial}}}{\alpha\{1 + K\alpha[\text{NO(g)}] + K[\text{Fe}^{\text{II}}(\text{EDTA})^{2-}(\text{l})]_{\text{initial}}\}} \quad (5-2)$$

where K is the equilibrium constant of the reaction shown in Eq. (5-1) and α is the partition coefficient between gas and liquid phase NO.

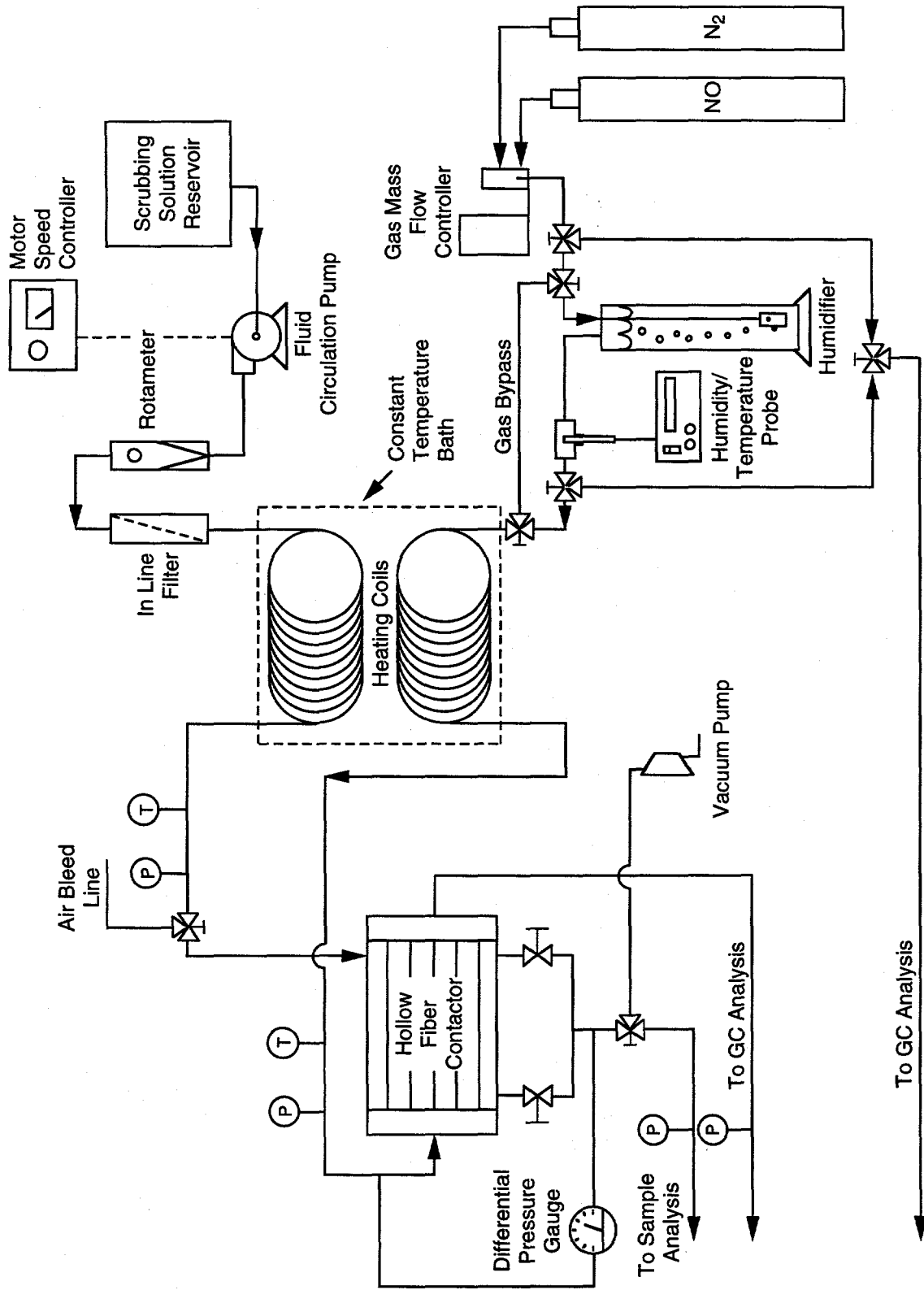
From literature, we obtained the value of K as 9.90×10^5 L/mol and the value of α as 1.788×10^{-9} mol/L-ppm. Figure 5-1 shows the results of calculations using Eq. (5-2). A higher initial Fe^{II}(EDTA)²⁻ concentration in the liquid phase allows a higher gas to liquid ratio to be used. These data were used to help design the HFC apparatus.

From these data, we completed construction of the HFC test apparatus, shown in Figure 5-2, and moved it to a hood to alleviate safety concerns. While waiting for a NO_x analyzer from DOE, we duplicated early experiments reported by NJIT under Task 3 of this project. Successful duplication would ensure that our test apparatus was performing similarly to that of other researchers.



CM-3501-91

Figure 5-1. Minimum liquid-to-gas flow rate ratio needed to obtain equilibrium.



CAM-3501-39

Figure 5-2. Schematic diagram of HFC apparatus.

CO₂ SCRUBBING

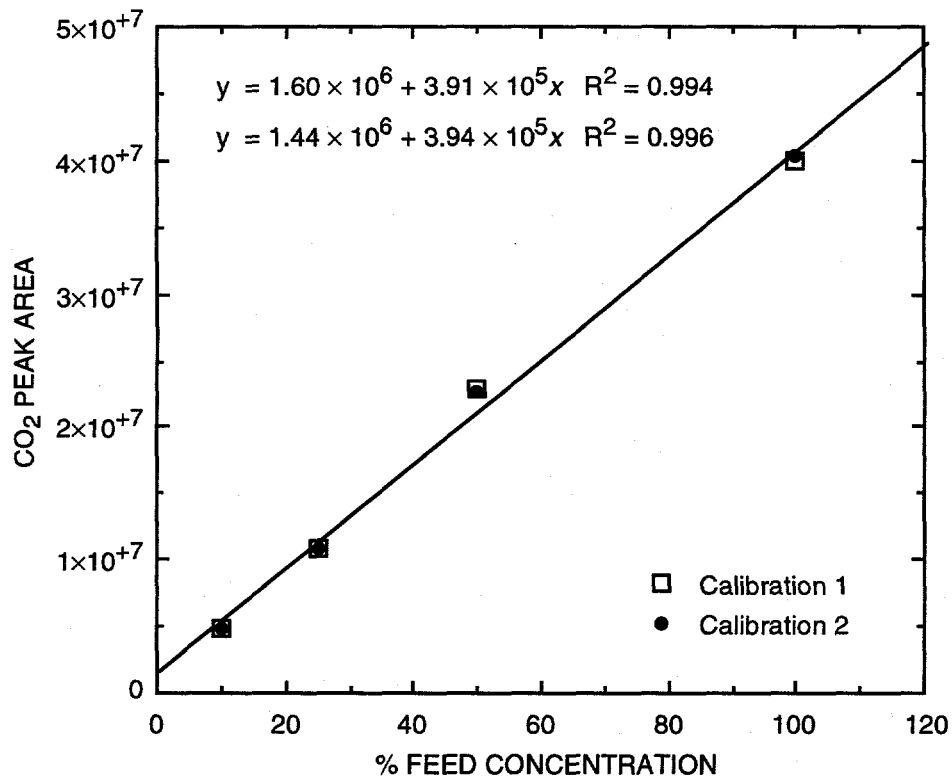
The first experiments we repeated were those using a 1000-fiber HFC with 300- μ m-OD and 240- μ m-ID fibers and an active length of 23 cm. Our experiments, like those at NJIT, focused on CO₂ scrubbing with water. Two sets of experiments were conducted at room temperature. The first was with a 1.99% CO₂, 2.01% N₂, and the balance He gas mixture from a cylinder (Liquid Carbonic, Chicago, IL) flowing through the fiber lumens and DI water (Milli-Q, Millipore Corporation, Medford, MA) flowing in the shell side. The gas flow rate was set at 80 sccm and the water flow rate varied between 25 and 100 mL/min. The second set of experiments was conducted identically to the first, except that the gas feed was 50% CO₂ in N₂, obtained by blending pure CO₂ and pure N₂ from cylinders. Overall mass transfer coefficients (MTCs) were calculated for both sets of experiments.

We produced a GC calibration gas by blending known flow rates of the feed cylinder gas with known flow rates of N₂ from a cylinder. The blended gas of known composition was then sampled with a GC (Hewlett Packard Model 5890), resulting in a calibration curve like the one shown in Figure 5-3. These calibrations were made frequently, especially at the end of a run.

Our results, along with those of NJIT (see Task 4) are plotted in Figure 5-4. Two observations are immediate. First, in our modules, the MTCs with 1.99% CO₂ were lower than the ones with 50% CO₂. This indicates the existence of a gas phase resistance. Conversely, the MTC reported by NJIT was the same for 100% CO₂ and 10% CO₂, which indicates no gas phase resistance in their module. Hence, our results and NJIT results differ in gas phase resistances. The second immediate observation is that the magnitude of MTC we measured was about 3-8 times lower than that reported by NJIT. Hence, our results and NJIT results differ in magnitude of MTCs.

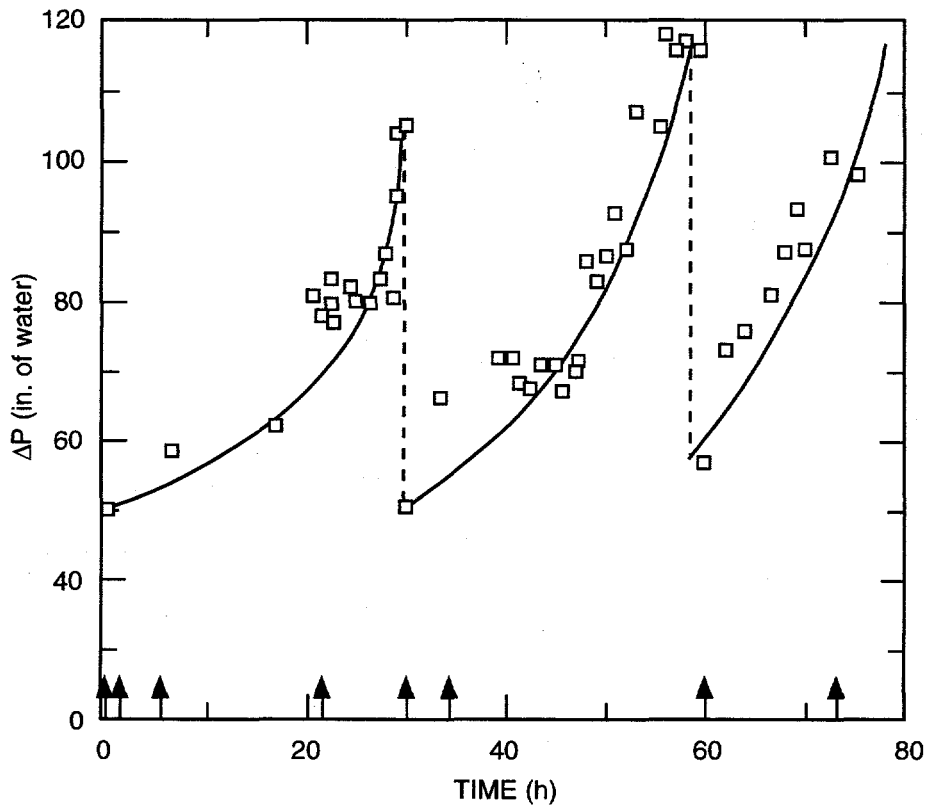
Clearly, these two differences indicate that our modules and NJIT modules are different. We visually inspected our module under a microscope and noted that up to 10%-15% of the fiber ends were blocked. The blockage appeared to be epoxy or fiber material sheared during manufacturing. Although the percent blockage was low, it may have changed the hydrodynamics within the module to yield different results.

Since then, we contacted Hoechst Celanese to learn how to open the fiber ends and we removed the 1000-fiber module from our process line. In the meantime, we conducted the same experiments with the 200-fiber HFC.



CAM-3501-37

Figure 5-3. Calibration using a 1.99% CO₂ cylinder.



CM-3501-138

Figure 5-4. Pressure drop across the HFC during an 80-h period.

Arrows indicate halting the deposition, measuring the mass transfer coefficient, and restarting the deposition.

Dashed lines indicate a back pulse of air.

Before continuing the experiments, we photographed the ends of both the 200-fiber and the 1000-fiber HFCs. These are shown in Figure 5-5. We counted 301 fibers in the "200"-fiber HFC and 1155 fibers in the "1000"-fiber HFC. Moreover, as shown in Figures 5-5.1 and 5-5.2, the 301-fiber module has all of its fiber ends completely open. However, as shown in Figures 5-5.3 and 5-5.4, the 1155-fiber module has about 10%-15% of its fiber ends blocked. As we will show below, we believe the blockage leads to unsatisfactory performance of the 1155-fiber HFC. We sent this module back to HC with copies of our photographs, and they agreed to replace the 1155-fiber HFC at no additional cost.

We also completed a series of experiments: scrubbing gases of various concentrations of CO₂ with water using the 301-fiber HC HFC. These experiments were essentially duplicates of those performed earlier at the NJIT in Task 4 of this project. DI water in our experiments was obtained from a Millipore Milli-Q water purification system (Millipore Corp., Bedford, MA). Three gas compositions were used: 1.91% CO₂/2.01% N₂/balance He, 50% CO₂/balance He, and 99.99% CO₂. Scrubbing experiments were conducted at room temperature with water flow rates between 25 and 160 mL/min and a gas flow rate of 80 sccm.

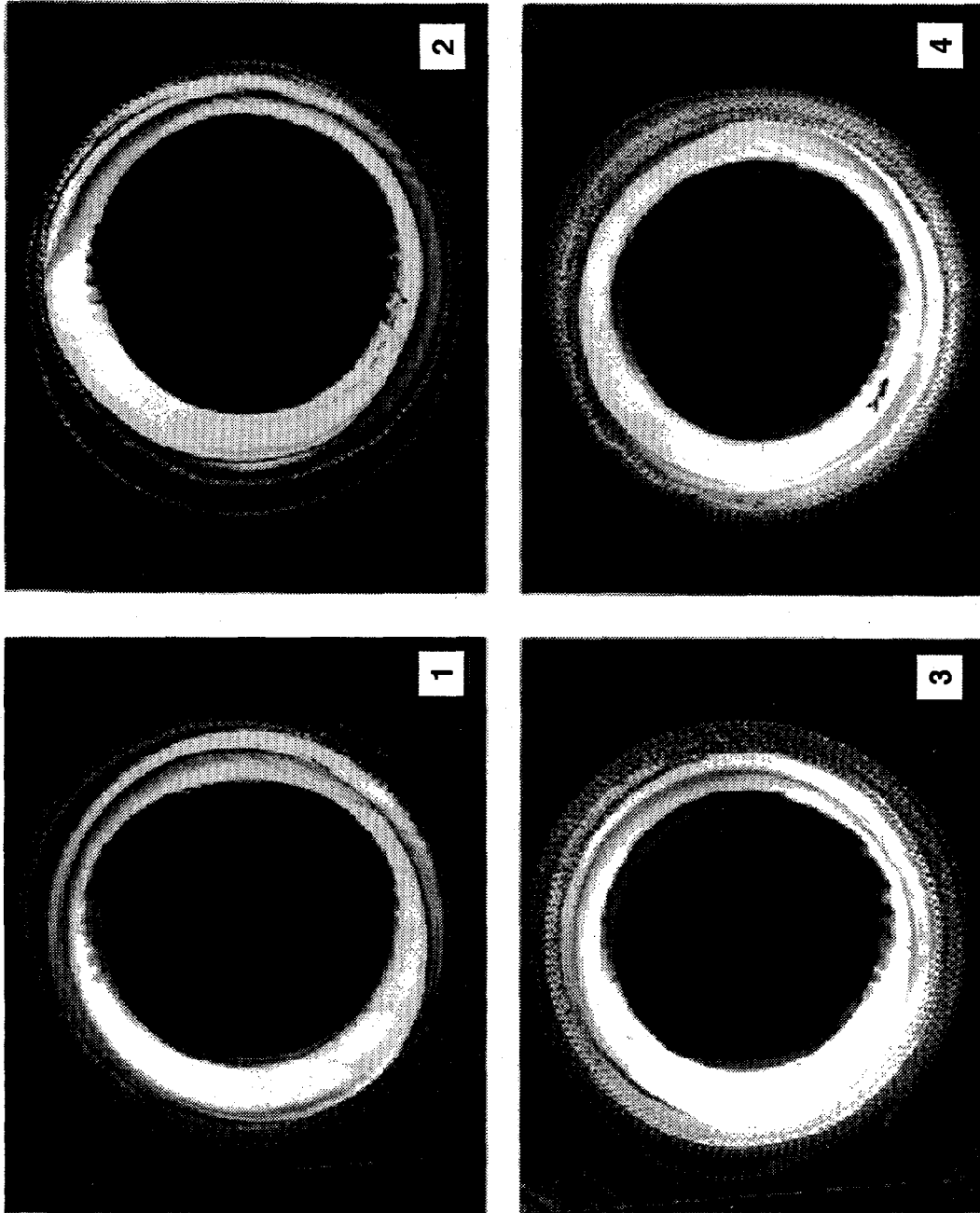
For the three gas compositions, the overall liquid MTC (K_{Olm}) versus water flow rate is plotted in Figure 5-6; earlier data reported by NJIT are also plotted. The K_{Olm} of the 1.91% CO₂ and the 50% CO₂ experiments at SRI are fairly similar, but K_{Olm} of the pure CO₂ experiment is slightly higher. This indicates a slight gas-side resistance, unlike NJIT data. Still, the gas phase resistance is small.

The overall MTCs and liquid flow rates were reduced to Sherwood numbers and Reynolds numbers (based on OD) and are plotted in Figure 5-7 along with NJIT results (see Task 4). From this figure, our results for the 301-fiber HFC appear to be similar to NJIT results, especially at higher Reynolds numbers. The relatively flat slope of these data points indicates that the overall resistance does not depend much on the liquid flow rate.

As reported earlier, we conducted an additional set of experiments with CO₂ with the "1000"-fiber HFC, but many fibers in this module were blocked. The effect of these blocked fibers can be seen in the low Sherwood numbers found in Figure 5-7. As a result, we believe that the 1000-fiber HFC was not performing adequately.

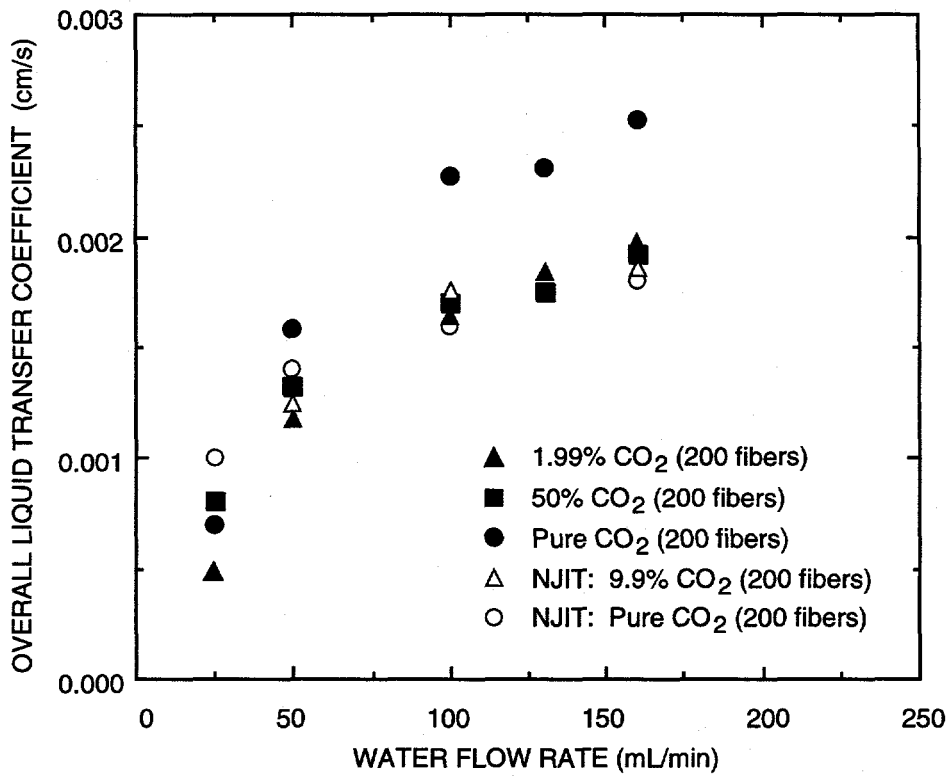
SO₂ SCRUBBING

Next, we tested the performance of our 301-fiber HFC with a simulated flue gas containing 1.46% SO₂ and a balance of N₂. This was done to compare our HFC's performance with the one used by NJIT. Before doing any experimental runs, we calibrated our GC (Hewlett-Packard



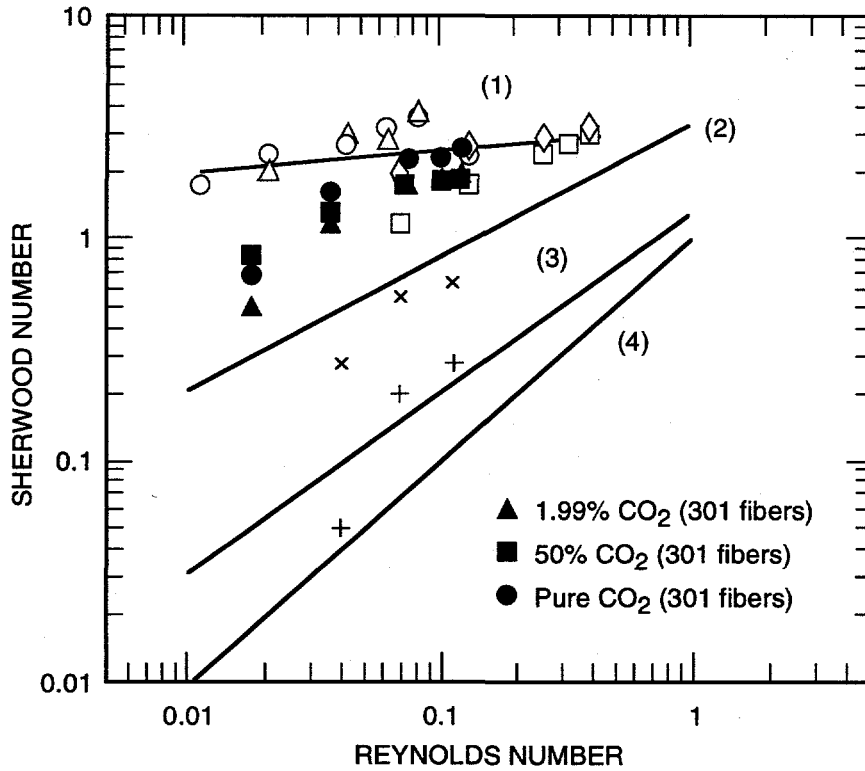
CPM-3501-52

Figure 5-5. Fiber openings for 200 - fiber module (top 1 and 2) and 1000 - fiber module (bottom 3 and 4).



CAM-3501-43

Figure 5-6. Overall liquid mass transfer coefficient versus liquid flow rate.



Module	Pure CO ₂		CO ₂ -N ₂		
	NJIT	SRI	NJIT, 9.9%	SRI, 1.99%	SRI, 50%
200 Fibers	○		△		■
301 Fibers		●		▲	■
1000 Fibers	□		◇		
1155 Fibers				+	×

(1) NJIT Combined Data
 $Sh = 0.38 \quad Re^{0.08} \quad Sc^{0.33}$

(2) Kreith and Black, 1980
 $Sh = 0.39 \quad Re^{0.59} \quad Sc^{0.33}$

(3) Wickramasinghe et al., 1992
 $Sh = 0.15 \quad Re^{0.8} \quad Sc^{0.33} \quad \text{for } Re > 2.5$

(4) Literature correlation (Yang and Cussler, 1986)
 $Sh = 0.39 \quad Re^{1.0} \quad Sc^{0.33} \quad \text{for } Re > 2.5$

CM-3501-49A

Figure 5-7. Sherwood number versus Reynolds number for CO₂ absorption in water.

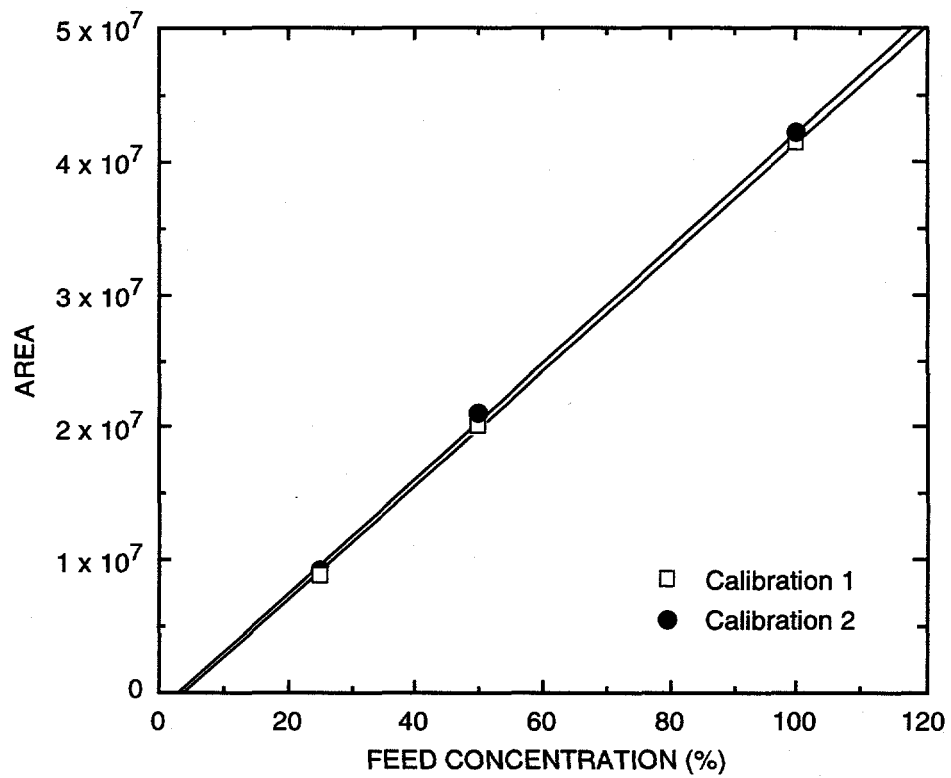
Model No. 5890) with this gas mixture blended with N₂. The results of the calibration can be seen in Figure 5-8, which shows that the calibration is linear and nearly goes through the origin. Next, we planned to duplicate the procedures from the SO₂ experiments completed at NJIT. Therefore, the flue gas flow rate was set at 44.5 sccm, and the chosen range of the water flow rate was 25-125 mL/min. According to NJIT's findings, 98% removal of SO₂ from a 1.6% SO₂ flue gas was obtained at a liquid flow rate of 50 mL/min. At higher liquid flow rates, 100% removal of SO₂ was observed. When we performed the same experiment with our HFC, we found that 100% of the SO₂ was scrubbed from the simulated flue gas at a liquid flow rate of only 25 mL/min. As a result, we decided to keep the water flow rate at 25 mL/min and to increase the gas flow rate until SO₂ could be detected in the exiting gas stream. Assuming that the MTC obtained from the CO₂/H₂O experiments would be the same for an SO₂/H₂O system, we calculated that to get 10%, 25%, and 50% of the SO₂ feed concentration in the exiting gas stream, gas flow rates of 148 sccm, 240 sccm, and 460 sccm, respectively, would be needed at a water flow rate of 25 mL/min. Three experiments with SO₂ were completed based on the previous calculations.

With a gas flow rate of 148 sccm and a water flow rate of 25 mL/min, no SO₂ was detected at the gas outlet. At a gas flow rate of 240 sccm, 92.9% removal of SO₂ was observed. Also, with the gas flow rate increased to 427.4 sccm, 73.8% of the SO₂ was removed from the flue gas. Figure 5-9 shows these results. Because the actual amount of SO₂ removal is higher than that predicted by the previous calculations, the overall MTC at 25 mL/min of H₂O for SO₂ scrubbing differs from the one for CO₂ scrubbing.

NO_x SCRUBBING

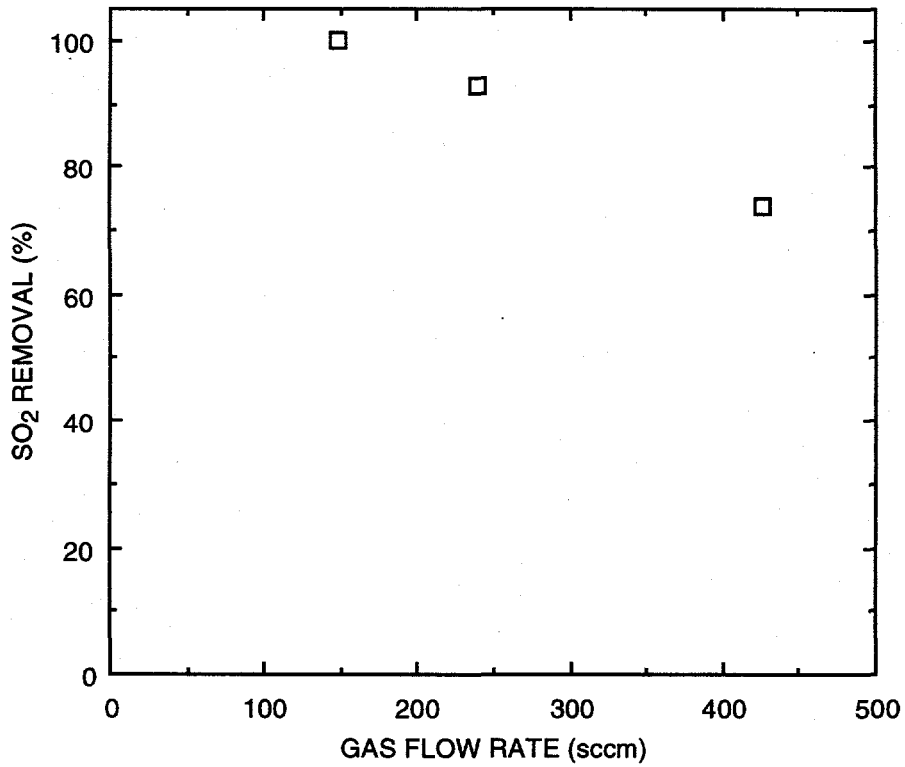
Later, we received the NO_x analyzer from another DOE contractor. It was calibrated with a 1.04% NO/balance N₂ gas cylinder blended with N₂. The calibration curve, shown in Figure 5-10, is linear.

We began studying NO_x removal from a simulated flue gas stream using our 301-fiber HFC. For these experiments, we blended 1.04% NO with N₂ to arrive at a 100-ppm gas mixture; 900 sccm of this mixture was sent through the HFC and then to the NO_x analyzer. For our first experiment, we used DI water set at either 25 or 50 mL/min as the scrubbing liquid. At both flow rates, none of the NO was removed from the flue gas. This was expected since NO is known to be insoluble in water.



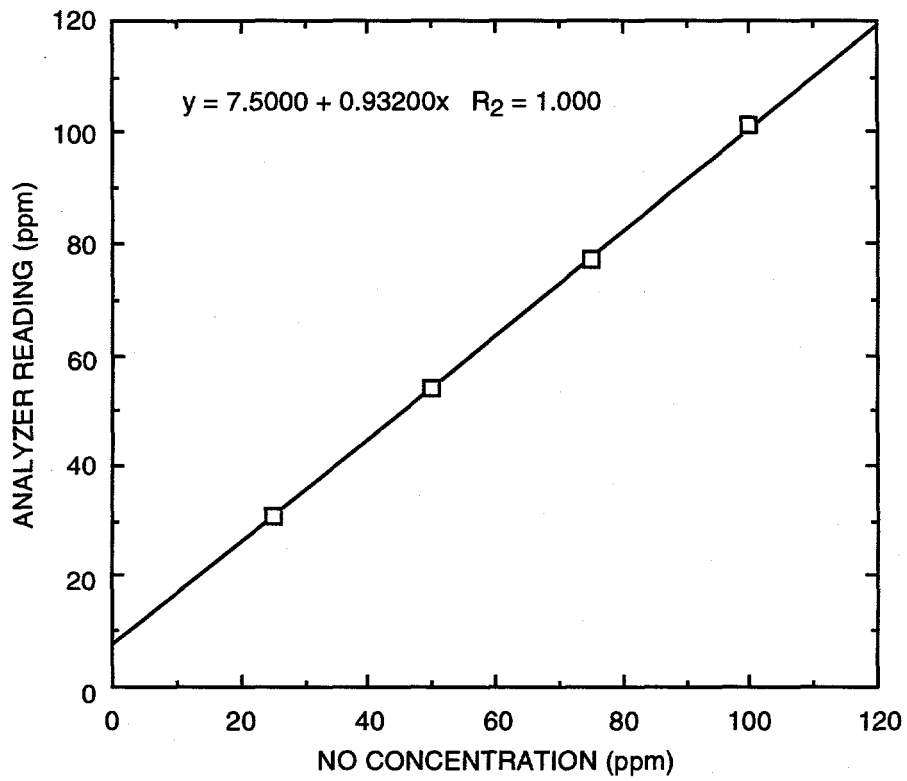
CAM-3501-46

Figure 5-8. GC calibration with 1.46% SO₂ in the N₂ feed.



CAM-3501-47

Figure 5-9. SO₂ removal water flow rate of 25 mL/min.



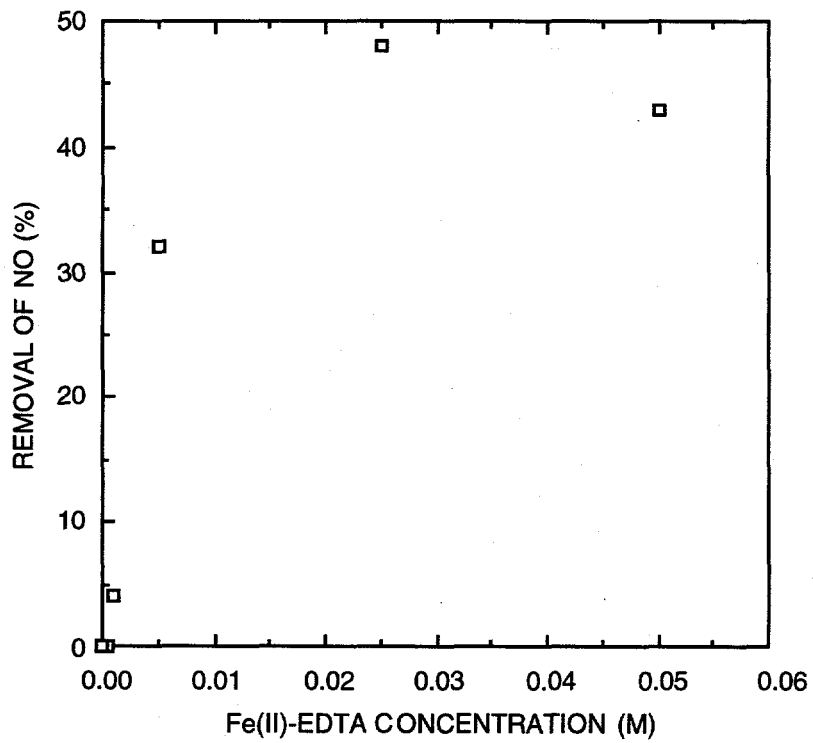
CAM-3501-50

Figure 5-10. Calibration curve of the NO_x analyzer.

In the next series of experiments, we used aqueous solutions of Fe(II)-EDTA as the scrubbing liquid. The range of Fe(II)-EDTA concentrations we used was 0.0005 to 0.05 M, and liquid flow rates between 25 and 300 mL/min. The results of these experiments are shown in Figure 5-11, where the percent removal of NO increases with increasing concentrations of Fe(II)-EDTA. For example, with a 0.0005-M solution, 0% of the NO is removed. Subsequently, with a 0.05-M solution, nearly 50% NO removal is achieved. Also, according to Figure 5-11, the absorption capacities of the 0.025-M and 0.05-M solutions are similar. This is because the Fe(II)-EDTA solution appeared to be saturated at these higher concentrations, meaning that the solubility limit was probably reached around 0.02-0.025 M. Therefore, increasing the Fe(II)-EDTA concentration any further would not necessarily improve the NO scrubbing performance of the HFC. We also found that increasing the liquid flow rates during all the experimental runs did not affect NO removal, indicating that the gas-side resistance dominates mass transfer.

Next, we decreased the gas flow rate of 100-ppm NO through the HFC from 900 sccm to 300 sccm. To meet the gas flow requirement for the NO_x analyzer, 600 sccm of N₂ was blended with the flue gas stream after it left the HFC. The scrubbing liquid was 0.02 M Fe(II)-EDTA at flow rates between 25 and 200 mL/min. The result of this experiment is that 79.9% of the NO was scrubbed from the simulated flue gas—independent of the liquid flow rate. Next, we decreased the flue gas flow rate through the HFC to about 200 sccm. Consequently, 700 sccm of N₂ had to be blended with the flue gas after the HFC to keep the 900-sccm flow rate requirement for the analyzer. The same concentration of Fe(II)-EDTA and liquid flow rates were used in this experiment. In this case, 85% of NO was removed from the flue gas—independent of the liquid flow rate. Because increasing the liquid flow rates does not significantly affect the percentage of NO removal, the gas-side resistance seems to dominate mass transfer in these experiments. Achieving 85% NO_x removal was milestone 5 for this project; we met that milestone.

After completing these runs, we calculated the overall liquid-side MTCs (K_{oLm}) for the 301-fiber HFC by using the experimental results from the NO_x-absorption runs (Task 2). After determining the equilibrium constant (K) for the 100-ppm NO/20-mM Fe(II)-EDTA run, we calculated and plotted the total concentration of NO absorbed in the liquid solution as a function of the NO concentration in the gas. At the lower gas phase concentrations of NO, the curve is fairly linear. As a result, the partition coefficient (H) for a 20 mM Fe(II)-EDTA solution was estimated to be the slope of the curve at the lower NO gas phase concentrations. The slope would equal H, and this was calculated to be 6.961×10^{-5} mol/L-atm. With H, we determined the K_{oLm} for the 301-fiber HFC. This calculation was performed using the data from the HFC experiments where 80%-85% NO removal was observed.



CAM-3501-55

Figure 5-11. Percent removal of NO versus Fe(II)-EDTA concentration.

In the experiment with 20 mM Fe(II)-EDTA and a gas flow rate of 290 sccm, about 80% of the NO was scrubbed from the flue gas. K_{Olm} calculated for this experiment is 7.15×10^{-6} cm/s. Also, for the experiment with a 200-sccm gas flow rate, more than 85% NO removal was achieved. The K_{Olm} for this experiment was calculated to be 7.51×10^{-6} cm/s. Because these values of K_{Olm} are much lower than that obtained using CO₂, we decided to continue characterizing the 301-fiber HFC with Fe(II)-EDTA as the scrubbing solution. The lower K_{Olm} values may be caused by pore condensation between runs or perhaps deposition of Fe(II)-EDTA crystals onto pores during a run.

Also, we received a new 1000-fiber HFC from HC. The fiber openings on both ends of this HFC looked better than our original one. However, we found that HC sent us a module with a baffle at its center. Our previous 1000-fiber HFC did not have this baffle. Therefore, HC volunteered to make us a new HFC without a baffle. We received the new module, photographed the module ends, and counted 1169 fibers. We then proceeded to do similar experiments with this HFC.

After meeting Milestone 5, we concentrated our efforts on achieving 85% NO_x removal with an alternate scrubbing agent. From the reversible NO_x absorption experimental results (Task 2), we demonstrated that the SRI synthesized Co(II)-phthalocyanine compound functions as a suitable binding agent for NO. In addition, the enhanced activity of this chemical reagent in the presence of O₂ for reversible absorption of NO has given us an added incentive to further exploit the chemistry in HFCs. Accordingly, we conducted two process runs using the aqueous Co-phthalocyanine solution in the 301-fiber HFC.

We prepared simulated flue gas to the process by mixing appropriate amounts of NO, N₂, and O₂. The composition of the feed gas was 500 ppm NO, 4.5% O₂, and the balance N₂ to the HFC. The exiting NO concentration was constantly monitored. Key results from the experiments, summarized in Table 5-1, show that a NO removal rate as high as 51% was obtained with a nominal aqueous solution flow rate of 4.6 mL/min. This high performance of the module gave us the confidence that we could achieve 85% NO removal rates rather easily by changing key process parameters.

One observation made during the second experiment was that the module performance was unaffected by the variation of liquid flow rate. However, decreasing the feed gas flow rate by a factor of 9 (Table 5-1) increased the removal rate by a factor of 2.5 for about the same liquid flow rate. This behavior explains that the gas phase resistance is dominating the liquid phase resistance for the mass transfer. This observation agrees well with the earlier data on Fe(II)EDTA runs. In any event, additional experimental runs were necessary to identify the key

Table 5-1
EXPERIMENTAL RESULTS ON NO_x ABSORPTION USING HFCs

Run No.	Feed Gas		Flowrate (sccm)	Aqueous Solution		pH		Outlet NO Concentration	Steady State	Flux (mol/cm ² /s)	NO Transfer Rate (mol/s)	% Removal	
	NO (ppm)	O ₂ (%)		N ₂	Type	Concentration (mM)	Initial						Final
CP-1*	500	4.50	balance	900	Co-phth	20	6.10	3.60	407	Y	1.12×10^{-10}	7.33×10^{-9}	22
CP-2	500	4.50	balance	100	Co-phth	20	6.10	5.90	251	Y	2.83×10^{-11}	1.83×10^{-8}	51

* The concentration of Co-phthalocyanine solution is likely to be low because water was present in the HFC before the solution was introduced.

process parameters that effect the overall system performance and to achieve NO removal of 85% (target value). To do so, we calculated overall liquid side MTCs (K_{olm}) in the following manner.

The calculation of K_{olm} becomes somewhat involved when the solubility of NO in Co-phthalocyanine solution does not follow a linear relationship. Indeed, as can be seen in Figure 5-12 the equilibrium relationship is highly nonlinear. This relationship has been calculated from $K = 5.2 \times 10^6$ L/mol reported in Task 2 of this report. Thus, we cannot use the conventional log-mean driving force to calculate K_{olm} . Rather, the overall MTC is given as [Cussler (1984)]

$$K_{olm} = \frac{L}{Aaz} \int_0^{C_L} \frac{dC_L}{C^* - C_L} \quad (5-3)$$

Here, L denotes the volumetric liquid flow rate, A is the cross-sectional area of the module, a is the specific surface area of the contactor, z is the length of the module, C_L is the concentration of NO (physical and chemical) in liquid, and C^* is the liquid phase NO concentration that is in equilibrium with the gas phase NO partial pressure.

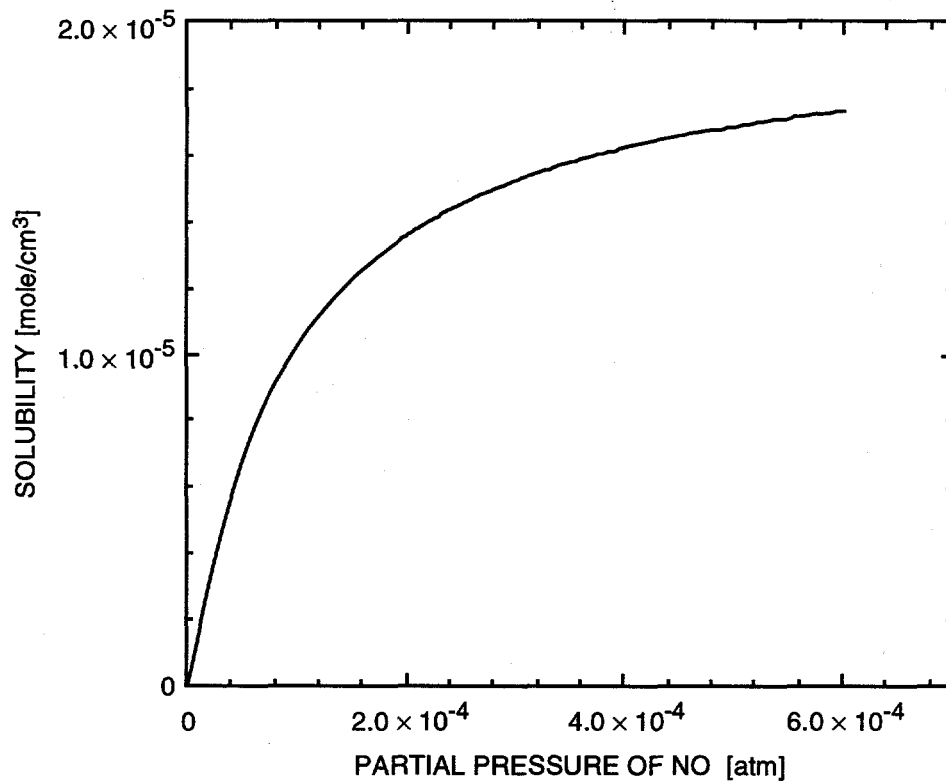
The integral in the above equation must be numerically evaluated after expressing C^* in terms of C_L . This can be accomplished by writing solute mass balance on the section of the module encompassing one end to any other point over the length. It can be written as

$$P_g = P_{ga} + \frac{RTL}{G} C_L \quad (5-4)$$

where P_g indicates the partial pressure of NO in gas phase, P_{ga} is NO partial pressure in the outlet gas stream, and G denotes the volumetric gas flow rate.

Now the integral in Equation (5-3) can be numerically calculated by using Eq. (5-4) and Figure 5-12 to determine K_{olm} . Using this method, the MTCs were obtained to be 6.74×10^{-6} and 1.78×10^{-6} cm/s, respectively, for the two experimental runs presented in Table 5-1. Again, these results compare well with the previous NO_x absorption runs using EDTA solutions.

Next, we focused our efforts on identifying and studying critical process parameters when using Co(II)-phthalocyanine solution. The overall mass transfer resistance for the absorption of NO into liquid can be characterized by three resistances contributed by the gas phase, the liquid phase, and the membrane pore stagnant gas phase. From the results of past studies, we believe that the membrane resistance is negligible compared with the other resistances. Therefore, we



CM-3501-63

Figure 5-12. Calculated solubility of NO in 20 mM Co-phthalocyanine solution at 25°C.

performed several experiments to study the mass transfer effects of the other (gas and liquid) phases.

Table 5-2 presents the experimental results along with calculated overall MTCs (K_{og}) based on the gas phase. K_{og} increases with increasing gas flow rate, which demonstrates the existence of a gas phase resistance to mass transfer. However, the percent removal of NO remains approximately the same. This behavior implies a need for a larger HFC to improve the percent NO removal.

Table 5-2
EXPERIMENTAL RESULTS ON THE NO_x SCRUBBING WITH 300 FIBER HFC

Feed Gas			Scrubbing Liquid 20 mM		% Removal	$K_{og} \times 10^3$ (cm/s)
NO (ppm)	O ₂ (%)	Flow rate (sccm)	Type	Flow rate (mL/min)		
500	4.5	100	3-Ph	4.6	51	1.9
2300	4.5	100	3-Ph	4.1	62	2.5
500	4.5	40	3-Ph	4.1	50	0.7
500	4.5	40	3-Ph	0.5	50	0.7

As shown in the table, liquid flow rate does not affect the mass transfer. This could be due to the solution having either a very high absorption capacity or a very low affinity toward binding NO. However, Task 2 results show that the former reasoning is incorrect, because the absorption rate (dC_L/dt) of NO with Co-phthalocyanine solution is slower than that using Fe(II)-EDTA solution.

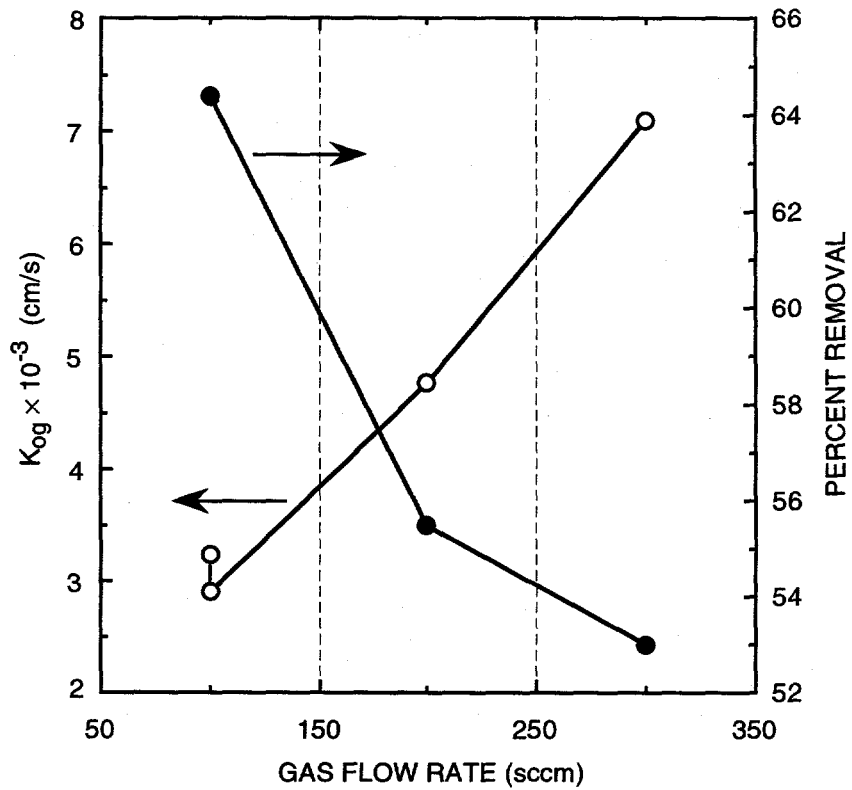
To increase the absorption rate, we conducted the experiments at 50°C. Also, we attempted to increase the NO absorption rates by increasing the Co(II)-phthalocyanine concentration. The results of these experiments are presented below.

The feed flue gas composition to the HFC was 500 ppm NO, 4.5% O₂, and the balance N₂. The liquid flow rate was approximately maintained at 1 mL/min. In the first set of experiments,

the liquid entering the HFC was heated to 50°C by an electrical tape wound around to the liquid-carrying 1/4-inch stainless steel tube. The temperature of the heating tape was controlled by a thermostat. An operation similar to the gas carrying tubing did not increase the temperature of the gas stream even at the maximum power output levels of the thermostat because of the low gas flow rates (~100 sccm) used for the experiments. Therefore, for all the runs, the entering gas stream was essentially at 25°C and the entering liquid stream temperature was 50°C.

Figure 5-13 shows the variation of the MTC (K_{og}) and the percent removal of NO with the gas flow rate. As mentioned earlier, the percent removal decreases with the increase in gas flow rate while K_{og} increases. This phenomenon is desirable for obtaining high NO flux rates into the liquid stream at even low driving forces. Thus, to obtain high percent removals, the operation requires a higher number of fibers in the module. The maximum NO removal obtained was 64.4%. For all these runs, the Co(II)-phthalocyanine concentration was 0.02 M.

Another approach we can adapt to increase the NO absorption capabilities is to increase the Co(II) phthalocyanine concentration in the liquid. We conducted a run at 0.1 M concentration of Co(II)-phthalocyanine. The gas flow rate was 100 sccm, the liquid inlet temperature was 50°C, and the remaining parameters were the same as in earlier runs. The observed percent removal of NO was 84.3%. This high removal capability of the aqueous Co(II)-phthalocyanine system at actual flue gas temperatures gave us confidence to set up a regeneration process for the Co(II)-phthalocyanine scrubbing solution.



CM-3501-72

Figure 5-13. Effect of gas flow rate on mass transfer coefficient and percent removal.

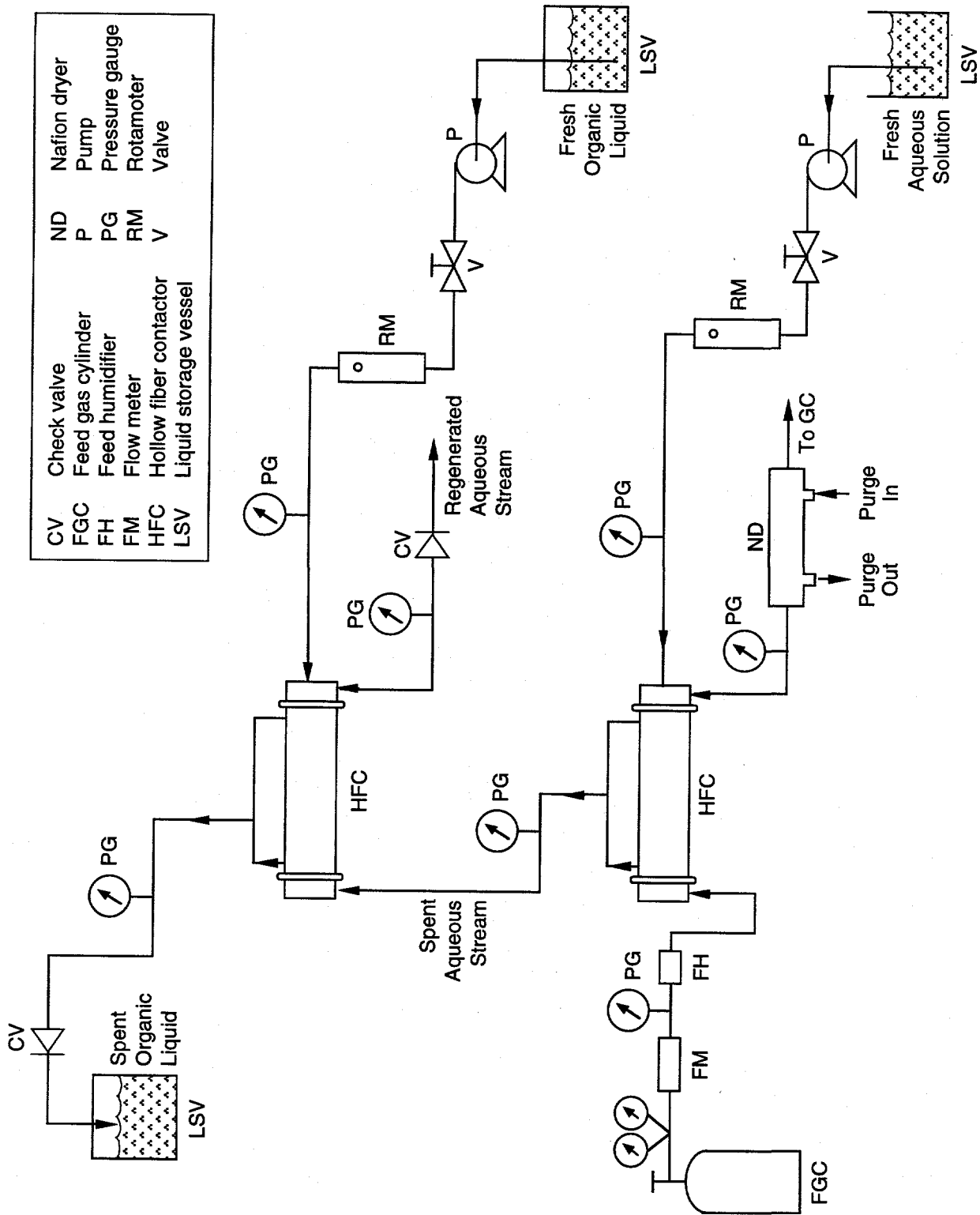
TASK 6: SO₂ LIQUOR REGENERATION

The objective of this task was to determine the fundamental mass transfer characteristics of HFCs for regenerating SO₂ scrubbing liquor with organic solvents having a high affinity for SO₂. Two alternative processes were suggested in the research proposal: liquid-liquid extraction (LLE) and extraction via hollow fiber contained liquid membrane (HFCLM). We proposed to use DMA and/or an oligomer of DMA as an organic extractant. In the first process, SO₂ was extracted from the aqueous solution into the organic liquid in a module having a single set of fibers, whereas in the second process the organic was used as a SO₂ selective membrane in a contained liquid membrane device that had two sets of fibers.

LIQUID-LIQUID EXTRACTION

Initially, we explored the LLE technique in a hollow fiber module. We conducted absorption of SO₂ with an aqueous solution in one hollow fiber module and regeneration of the spent aqueous solution in a second module. The experimental setup was designed for simultaneous operations of absorption and extraction. Figure 6-1 shows the modified combined setup. First, a model flue gas mixture (2400 ppm SO₂, 9.76% CO₂, 3.03% O₂, and the balance N₂) was humidified and sent through the tube side of a cross-flow module containing 200 hollow fibers (fiber ID and OD, 240 and 300 μ m, respectively). The feed gas flow rate was 2713 sccm and the gas composition after humidification was 2260 ppm SO₂, 9.76% CO₂, 3.03% O₂, and the balance N₂. An aqueous solution of 0.2 M Na₂SO₃ solution was pumped through the shell side at the rate of 20 cm³/min. The exit aqueous stream from the first module was sent through the tube side of the second hollow fiber module containing 1000 fibers (fiber ID and OD, 240 and 300 μ m, respectively). The exit pressure of the aqueous stream was maintained higher than 5 psig by a check valve provided at the outlet of the second module. However, the organic flow through the second module was not initiated at this time.

The pH of the fresh aqueous solution was measured at the beginning of the experiment, and the pH of the spent absorbent solution was measured at regular intervals during the experiment. The steady state of the absorption experiment was monitored by sampling the treated flue gas in a gas chromatograph. Normally, it took 5 to 7 h to achieve a steady state under these operating conditions. The flow of the organic (DMA) through the second HFC was started when a reasonable steady residual SO₂ composition was achieved at the first module outlet. The flow rate of DMA was set at about 6 cm³/min. The organic liquid spontaneously wets the pores of the hollow fibers. By keeping the organic phase pressure at 1/3 psig, we were able to maintain a



CAM-3501-40A

Figure 6-1. Schematic of combined absorption and liquor regeneration setup.

stable aqueous-organic interface at each pore mouth on the fiber ID. We anticipated that we could monitor the steady state of the LLE experiment by monitoring the change in pH of the exit aqueous solution stream at the second module outlet, but we did not notice any appreciable change in the solution pH.

The extraction experiment was continued for at least 2 h, and organic samples were collected and analyzed in the following manner. For a given period of time, the spent organic liquid line was directly introduced into a flask containing excess NaOH solution of known concentration. The SO₂ from the organic solution reacted with NaOH in the aqueous phase. The total mixture was then titrated with HCl solution using phenolphthalein as an indicator. The SO₂ concentration in DMA was calculated from the titration values to be 8.0×10^{-6} mol/cm³ and the flux of SO₂ was found to be 4.6×10^{-10} mol/cm² s. We are exploring other analytical techniques to determine the SO₂ concentration in the organic liquid. Analysis of the aqueous phase is preferred. Ion chromatography is a possibility for this purpose. SO₂ concentration in the organic liquid can then be determined from the difference in the aqueous phase concentrations at the module inlet and outlet.

We conducted further test runs on simultaneous absorption and extraction using DI water (instead of an aqueous solution of 0.2 M Na₂SO₃ solution) as an absorbing liquid and DMA as an organic extractant. The module having 200 hollow fibers (fiber ID and OD, 240 and 300 μm, respectively) was used for gas absorption. A certified gas mixture consisting of 2400 ppm SO₂, 9.76% CO₂, 3.03% O₂, and the balance N₂ was sent directly through the tube side without humidification, whereas DI water was allowed to flow through the shell side. The exit water stream was introduced to the tube side of the second, cross-flow, hollow fiber module having 1000 fibers (fiber ID and OD, 240 and 300 μm, respectively). We waited 3 to 4 h to achieve a steady state in the absorption apparatus.

The extraction part of the experiment was initiated with organic flow in the shell side when a steady outlet gas composition was achieved. The gas composition was monitored at a regular interval by a GC. In the first module (absorption section), water pressure was higher than the gas pressure to immobilize the gas-liquid phase interface on the OD of the fibers. In the other module, the aqueous-organic interface was immobilized on the ID of the fibers with higher water pressure in the tube side. The pH of the DI feed water and the outlet water streams of the first and second modules were measured. During the runs, we noticed a faint yellow color in the regenerated water stream, but the phase interface in the extraction section was stable and no emulsion was observed. At the end of each experiment, we disconnected the absorption module from the setup. The module was thoroughly washed with water and dried under vacuum conditions. No such cleaning procedure was adopted for the extraction module. However,

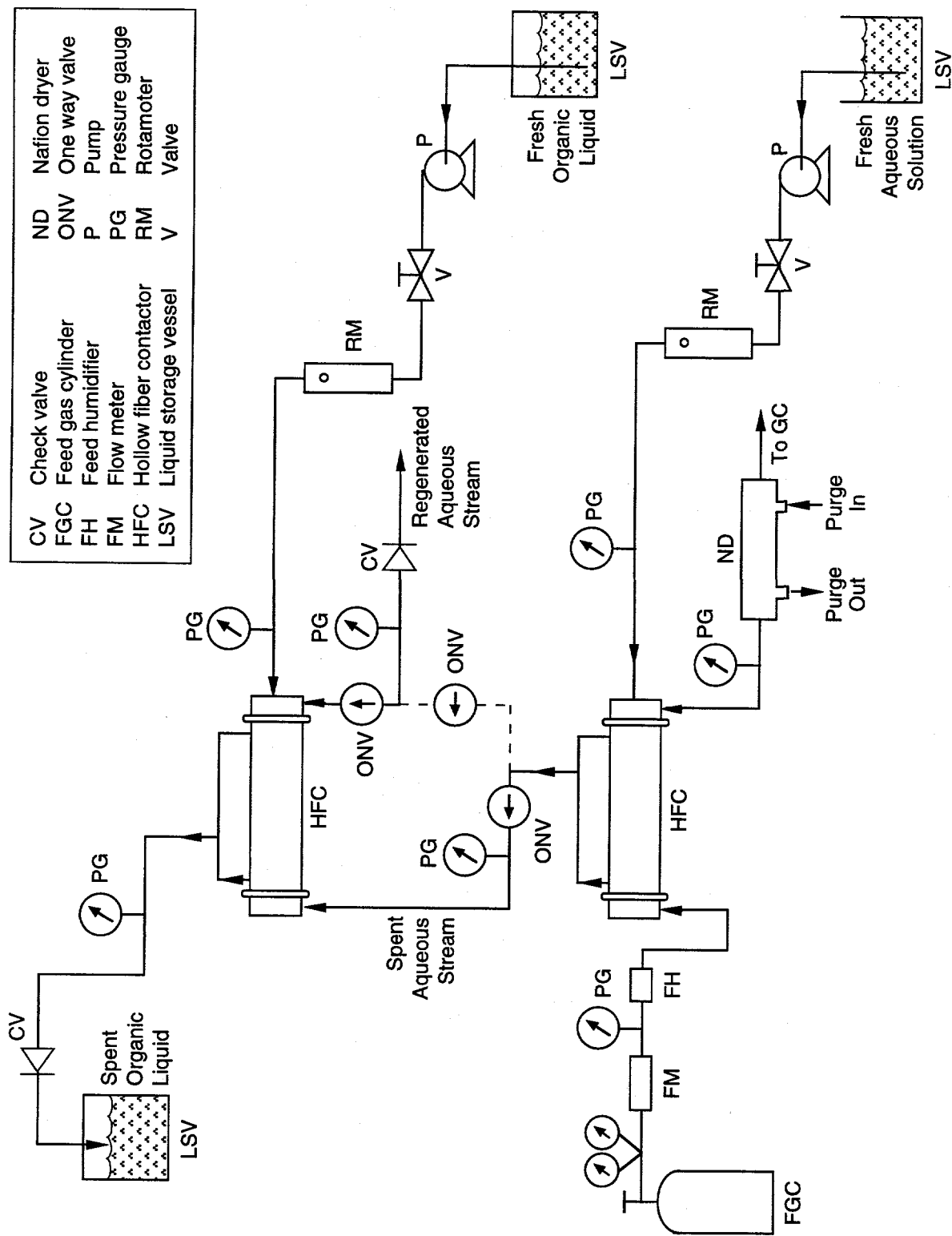
during an earlier absorption part of a run, water from the tube side of the second module penetrated through the fibers and appeared in the shell side outlet along with DMA. Apparently, some DMA from the fiber pores (left over from a previous run) dissolved in the aqueous phase.

To prevent this kind of failure, we modified the setup by installing three additional valves in the aqueous line. These valves allow the aqueous stream to bypass the second module (extraction) altogether when we run our experiment only in absorption mode (i.e., when we wait for a steady state to be achieved in the absorption apparatus). The liquid flow to the second module is initiated in the following order. First, the organic phase is allowed to flow through the shell side so that the fiber pores are wetted thoroughly and the organic appears in the lumen side. Then the aqueous flow at higher pressure is channeled through the tube side of the module to drive the organic liquid out. This method of operation appeared to overcome the problem.

Figure 6-2 shows the modified, combined absorption/extraction setup. A certified gas mixture consisting of 2300 ppm SO₂, 10.5% CO₂, 2.9% O₂, and the balance N₂ was sent through the tube side of the module containing 200 hollow fibers (fiber ID and OD, 240 and 300 μm, respectively). An aqueous solution of 0.2 M Na₂SO₃ was passed through the shell side. The exit aqueous stream was introduced to the tube side of the second, cross-flow, hollow fiber module containing 1000 fibers (fiber ID and OD, 240 and 300 μm, respectively) only when a steady state in the absorption apparatus was achieved. In all runs a constant model feed flue gas flow rate of ~2700 sccm was maintained. In the first run, (AE-4, Table 6-2), the feed gas was humidified, but in the other two cases, the model flue gas was introduced without humidification.

We also improved the procedure for measuring the SO₂ concentration in the organic phase. The spent organic liquid is discharged into the bottom section of a burette filled with excess NaOH solution. The procedure increases the contact time and enables the free SO₂ to react completely as the organic liquid travels upward through the aqueous solution. The SO₂ concentration in DMA is determined by titrating the total mixture with HCl solution. We made two successful experiments in which a constant feed gas flow rate of about 900 sccm was used. The water flow rates were varied from ~20 to 50 mL/min. In both cases, the flow rate of DMA was maintained at 6 mL/min. Table 6-1 summarizes the extraction data, including the SO₂ concentration in DMA and the flux of SO₂ during regeneration.

We did three runs: AE-4, AE-5, and AE-6. In runs AE-4 and AE-5 (Table 6-2), the flow rate of the aqueous solution was kept at 20 mL/min, but the organic flow rate was changed from 6.9 to 4 mL/min. At the higher organic flow rate, the SO₂ concentration in DMA was lower but the total SO₂ transfer was higher. Comparing runs AE-4 and AE-6, we see that the



CV	Check valve	ND	Nafion dryer
FGC	Feed gas cylinder	ONV	One way valve
FH	Feed humidifier	P	Pump
FM	Flow meter	PG	Pressure gauge
HFC	Hollow fiber contactor	RM	Rotameter
LSV	Liquid storage vessel	V	Valve

CAM-3501-40B

Figure 6-2. Schematic of combined absorption and liquor regeneration setup modified to allow aqueous stream to bypass the second module.

Table 6-1
SUMMARY OF EXTRACTION DATA IN SIMULTANEOUS ABSORPTION-EXTRACTION RUNS

Run No.	Aqueous Absorbent		Flue Gas Flow Rate (scfm)	SO ₂ Concentration in DMA (mol/cm ³)	Extractive Flux of SO ₂ (mol/cm ² s)	SO ₂ Transfer (mol/s)		Percent Recovery by Extraction
	Type	Flow Rate (mL/min)				Absorption	At Extraction	
1	0.2 M Na ₂ SO ₃	20	2722 (Humidified)	8.0×10^{-10}	4.6×10^{-10}	4.42×10^{-6}	7.98×10^{-7}	18
2	Water	22	901	1.45×10^{-5}	1.19×10^{-9}	1.2×10^{-6}	1.45×10^{-6}	~100
3	Water	50	908	8.85×10^{-6}	5.1×10^{-10}	1.48×10^{-6}	8.84×10^{-7}	59

Table 6-2
SUMMARY OF EXTRACTION DATA IN SIMULTANEOUS ABSORPTION-EXTRACTION RUNS

Run No.	Aqueous Absorbent		Flue Gas Flow Rate (sccm)	Flow Rate of DMA (mL/min)	SO ₂ Concentration in DMA (mol/cm ³)	Extractive Flux of SO ₂ (mol/cm ² s)	SO ₂ Transfer (mol/s)		Percent Recovery by Extraction
	Type	Flow Rate (mL/min)					Absorption	At Extraction	
AE-6	0.2 M Na ₂ SO ₃	10	2723 (Dry)	6.1	2.93 x 10 ⁻⁶	1.72 x 10 ⁻¹⁰	4.50 x 10 ⁻⁶	2.98 x 10 ⁻⁷	6.6
AE-4	0.2 M Na ₂ SO ₃	20	2732 (Humidified)	6.9	4.97 x 10 ⁻⁶	3.30 x 10 ⁻¹⁰	4.43 x 10 ⁻⁶	5.72 x 10 ⁻⁷	13.0
AE-9	0.2 M Na ₂ SO ₃	30	5000 (Dry)	6.4	6.21 x 10 ⁻⁶	3.82 x 10 ⁻¹⁰	7.46 x 10 ⁻⁶	6.62 x 10 ⁻⁷	8.9
AE-5	0.2 M Na ₂ SO ₃	20	2704 (Dry)	4.05	6.68 x 10 ⁻⁶	2.60 x 10 ⁻¹⁰	4.54 x 10 ⁻⁶	4.51 x 10 ⁻⁷	9.9
AE-7	0.2 M Na ₂ SO ₃	20	2723 (Dry)	16	2.67 x 10 ⁻⁶	4.11 x 10 ⁻¹⁰	4.32 x 10 ⁻⁶	7.12 x 10 ⁻⁷	16.5
AE-8	0.2 M Na ₂ SO ₃	20	2732 (Dry)	31	3.31 x 10 ⁻⁶	9.75 x 10 ⁻¹⁰	4.29 x 10 ⁻⁶	1.69 x 10 ⁻⁶	39.4
AE-10	0.2 M Na ₂ SO ₃	10	2459 (Dry)	38	3.33 x 10 ⁻¹⁰	12.17 x 10 ⁻¹⁰	4.01 x 10 ⁻⁶	2.11 x 10 ⁻⁶	52.6

SO₂ transfer rate decreased by about 50% when the aqueous flow rate was changed from 20 ml/min to 10 mL/min. A summary of extraction data and the flux of SO₂ during regeneration is shown in Table 6-2. In these runs only a maximum of 13% of the absorbed SO₂ was recovered by the organic liquid. In our earlier runs with water, we obtained much higher recoveries. Therefore, we performed further experiments at higher flow rates.

Next, to study the effect of organic and aqueous flow rates on the SO₂ transfer in the extraction process, we conducted additional test runs on simultaneous absorption and extraction with an aqueous solution of 0.2 M Na₂SO₃ as an absorbing liquid and with DMA as an organic extractant. In membrane solvent extraction, the overall resistance to solute transfer comes from three resistances in series: the aqueous resistance, the and organic film resistance and the membrane resistance. Increasing the fluid flow rates could reduce the aqueous and organic resistances and improve mass transfer.

In the next set of experiments, the gas mixture used as a feed to the absorption module had a composition of 2170 ppm SO₂, 3.13% O₂, 10.8% CO₂, and the balance N₂. These runs are numbered AE-7, AE-8, and AE-9 in Table 6-2. The aqueous and organic flow rates were varied systematically in the combined setup, and the SO₂ concentration in the DMA was determined. The effect of aqueous, absorbent, flow rate variation is presented in the first part of Table 6-1. In all runs except run AE-9, a constant feed flue gas flow rate of ~2700 sccm was maintained. We see an increase in SO₂ transfer in the extraction process (by a factor of 2.2) as the absorbent flow rate was increased from 10 to 30 mL/min, keeping the organic flow rate constant at ~6 mL/min. In run AE-9, the gas flow rate to the absorption module was 5000 sccm. This very high gas flow rate was used to obtain a reasonable amount of SO₂ at the exit gas stream. We anticipated that all the SO₂ present would be absorbed at the lower gas flow rate of ~2700 sccm and the aqueous Na₂SO₃ solution flow rate of 30 mL/min. A higher organic flow rate under these conditions would result in a higher percent recovery in the extraction process.

The second part of Table 6-2 presents the data obtained by varying the organic flow rate. In all these runs, the feed gas and the aqueous solution flow rates were maintained at constant values. The SO₂ transfer in the extraction process increased substantially as the organic flow rate was increased from 4 to 31 mL/min. We were able to recover about 40% of the absorbed SO₂ from the aqueous solution when the organic liquid flow rate was 31 mL/min. We can recover even more of the absorbed SO₂ by manipulating the aqueous and organic flow rates and by providing a larger contact area.

Finally, we conducted an additional run, AE-10. A certified gas mixture consisting of 2230 ppm SO₂, 11% CO₂, 3.20% O₂, and the balance N₂ was passed through the tube side of module containing 200 hollow fibers, without humidification. The flue gas flow rate was about 2450 sccm. An aqueous solution of 0.2 M Na₂SO₃ was passed through the shell side. The exit aqueous stream was allowed to bypass the extraction module during the time period needed to achieve a steady state in the absorption apparatus. Once a steady outlet gas composition was achieved, the extraction part of the experiment was initiated with DMA flow in the shell side and by introducing the exit aqueous stream to the tube side of the second cross-flow hollow fiber module containing 1000 fibers. Normally, it took 3 to 5 h to achieve a steady state in the absorption part of the experiment. However, out of three trial runs, we were able to achieve a steady state in only one. Two runs were abandoned when we did not get a constant outlet SO₂ composition in more than a 6-h period.

In our earlier experimental results, we saw that the SO₂ transfer in the extraction increased substantially with increase in organic flow rate. Therefore, in run AE-10, the organic flow rate was kept at a high value of 38 mL/min, whereas the aqueous flow rate was maintained at 10 mL/min as shown in Table 6-2. Under these conditions, we could recover more than 50% of the absorbed SO₂ from the loaded aqueous 0.2 M Na₂SO₃ solution. As the organic flow rate was increased from ~4 mL/min to 38 mL/min (9.4 times), the extractive flux of SO₂ increased from 2.60×10^{-10} to 12.17×10^{-10} mol/cm²/s (4.7 times). The total SO₂ transfer also increased from a value of 4.51×10^{-7} to 2.11×10^{-6} mol/s. Further increase in SO₂ recovery is possible with even higher organic flow rates. However, we do not plan to use higher organic flow rates at this time.

DISTRIBUTION COEFFICIENT

We systematically studied the absorption of SO₂ by an aqueous 0.2 M Na₂SO₃ solution and subsequent regeneration of the spent liquor by extraction with DMA. The results indicated that the SO₂ transfer in the extraction stage increases substantially with increase in organic flow rate. We were able to recover as much as 50% of the absorbed SO₂ from the loaded aqueous 0.2 M Na₂SO₃ solution into DMA (Run AE-10) using a 1000-fiber module. Further increase in SO₂ recovery is possible with even higher organic flow rates. However, to demonstrate that higher SO₂ recovery is achievable in the extraction unit, we used an alternative strategy. We switched back to water absorbent instead of aqueous 0.2 M Na₂SO₃ solution. To achieve a high removal efficiency (90+%) using 0.2 M Na₂SO₃, we would need to make the DMA circulation rate very high (see Runs AE-10 and AE-6 in Table 6-3), which is impractical in the laboratory.

Table 6-3
ABSORPTION DATA IN ABSORPTION-EXTRACTION RUNS USING HIGH AND LOW FLOW RATES OF DMA

Run No.	Aqueous Absorbent		Flue Gas Flow Rate (sccm) (dry)	Flow Rate of DMA (mL/min)	SO ₂ Concentration In DMA (mole/cm ³)	Extractive Flux of SO ₂ (mole/cm ² s)	SO ₂ Transfer (mole/s)		Percent Recovery by Extraction
	Type	Flow Rate, (mL/min)					At Absorption	At Extraction	
AE-10	0.2 M Na ₂ SO ₃	10	2459	38.0	3.33×10^{-6}	12.17×10^{-10}	4.01×10^{-6}	2.11×10^{-6}	52.6
AE-6	0.2 M Na ₂ SO ₃	10	2723	6.1	2.93×10^{-6}	1.72×10^{-10}	4.50×10^{-6}	2.98×10^{-7}	6.6
AE-11	Water	50	908	42.0	1.85×10^{-6}	7.55×10^{-10}	1.41×10^{-6}	1.31×10^{-6}	92.9
AE-3	Water	50	908	6.0	8.85×10^{-6}	5.1×10^{-10}	1.48×10^{-6}	8.84×10^{-7}	59

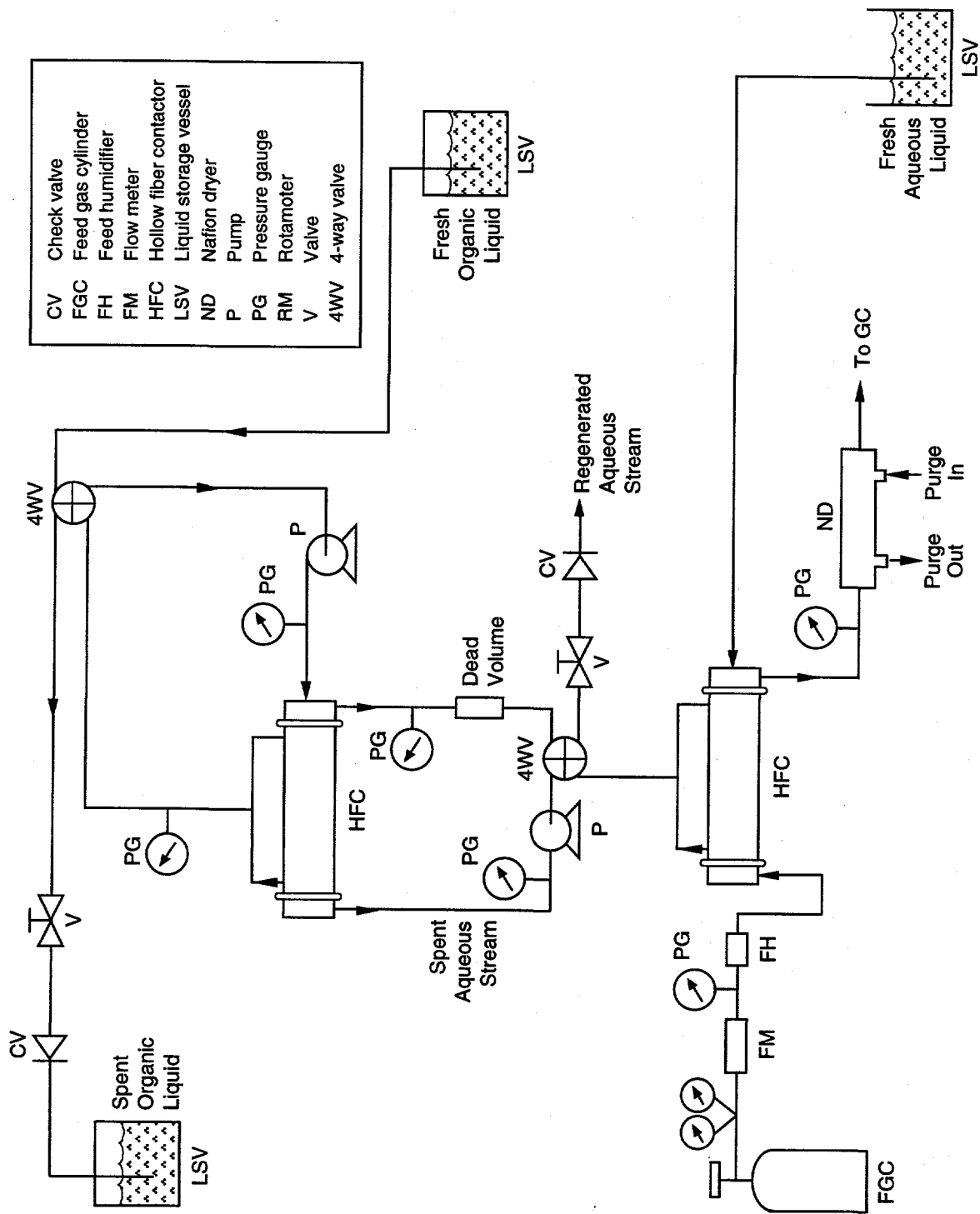
As a result, one alternative was that we absorb SO₂ with water (for the same SO₂ flux, a higher water flow rate is needed than for 0.2 M Na₂SO₃, because SO₂ is much more soluble in 0.2 M Na₂SO₃). The extraction of SO₂ from spent water is much easier than from spent 0.2 M Na₂SO₃ (SO₂ solubility is higher in 0.2 M Na₂SO₃), and this allows up to 93% of the SO₂ being extracted, while maintaining practical water and DMA flow rates.

Water was introduced to the shell side of the 200-fiber cross-flow module at a flow rate of 50 mL/min. A model flue gas mixture having 2230 ppm SO₂, 3.2% O₂, 11% CO₂, and the balance N₂ was passed through the tube side of the module without any humidification. The exit water stream loaded with SO₂ was then diverted to the tube side of the second cross-flow hollow fiber module containing 1000 fibers. DMA was passed through the shell side at a high flow rate of 42 mL/min. The SO₂ concentration in the DMA at steady state was determined in a manner described earlier.

The results of this water run are also shown in Table 6-3 (Run AE-11). Water has a lower absorption capacity of SO₂ than aqueous 0.2 M Na₂SO₃ solution. The SO₂ transfer in this particular absorption run is about 1.4×10^{-6} mol/s, which is much less than the $\sim 4 \times 10^{-6}$ mol/s obtained in general with aqueous 0.2 M Na₂SO₃ solution. But with a high DMA flow rate of ~ 40 mL/min, more than 90% of the SO₂ was extracted from the water stream into the DMA. For comparison, we also show a run (AE-3) taken with a lower DMA flow rate.

To analyze the extraction results in a meaningful manner and to predict the system behavior, we need to know the distribution coefficient of SO₂ between the aqueous and organic phases. Due to the volatility of the solute in this case, these measurements cannot be performed in the traditional manner (such as using a separatory funnel). Therefore, we conducted this measurement in a batch recirculation mode. Earlier, we modified the experimental setup for this particular measurement. Figure 6-3 shows the arrangement. The exit aqueous stream from the first module passes through a four-way valve before entering the tube side of the second module. Similarly, the organic stream in the shell side of the second module passes through a four-way valve. Flow meters from both lines have been removed and the position of the pumps has been changed. An additional dead volume is provided in the aqueous liquid line.

The absorption part of the experiment was conducted in the usual fashion. Once a steady state was achieved (as confirmed by the GC) in the absorption apparatus, the four-way valve in the aqueous solution exit line was switched to a batch recirculation mode for the second module. Fresh DMA was also pumped in a batch circulation mode in the shell side of the second module. The composition of SO₂ in each phase changed slowly but asymptotically to a final equilibrium value. The final concentration of SO₂ in DMA was determined by a titrimetric method described



CM-3501-61

Figure 6-3. Schematic of combined absorption and liquor regeneration setup modified for batch mode recirculation.

earlier. From the gas absorption measurement, the composition of SO₂ in the aqueous stream at the start of the recirculation experiment was known. The equilibrium SO₂ concentration in the aqueous phase may be determined from material balance equations and thus the distribution coefficient can be calculated.

Later, experiments were conducted to determine the distribution coefficient of SO₂ between the aqueous and organic phases. As stated earlier, the distribution coefficient measurement experiments cannot be conducted using the in a traditional separatory funnel method because the solute SO₂ is volatile. These measurements were conducted in a batch recirculation mode, as shown in Figure 6-4.

In this arrangement, a known volume of aqueous solution (V_w) loaded with a known initial composition of SO₂ (C) comes into contact with a known volume of fresh organic solvent (V_o) in a hollow fiber extraction module in cross-flow. The known fluid volumes of both phases are circulated through the module such that a part of the aqueous solution is in continuous contact with the organic solvent. The composition of SO₂ in two reservoirs (Figure 6-4) changes slowly and asymptotically to final equilibrium values. If the final compositions of the solute in aqueous and organic phases are C_w and C_o, respectively, then by material balance

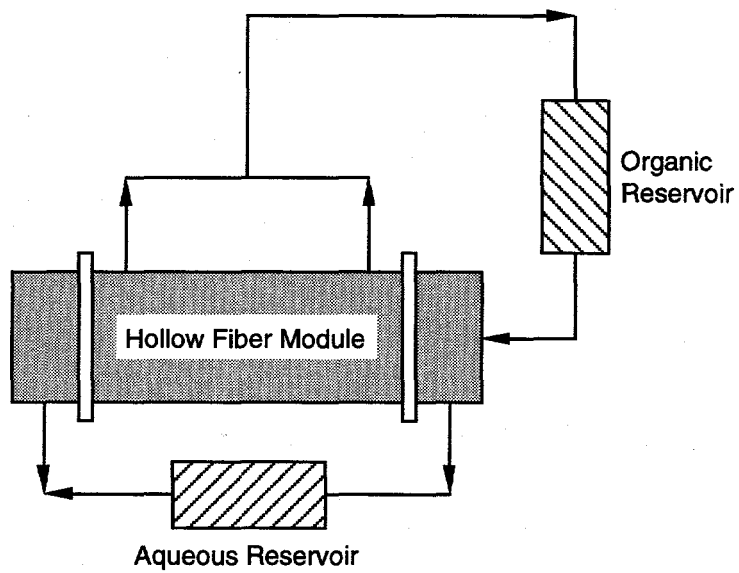
$$V_2 C_2^f = V_o C_o^f + V_w C_w^f \quad (6-1)$$

$$C_w^f = C_w^i - \frac{V_o}{V_w} C_o^f \quad (6-2)$$

If the final organic phase concentration, C_o^f, is measured from the experiment, the final aqueous phase concentration may be calculated from Eq. (6-2). Then the distribution coefficient (m_i) is determined from the following relation.

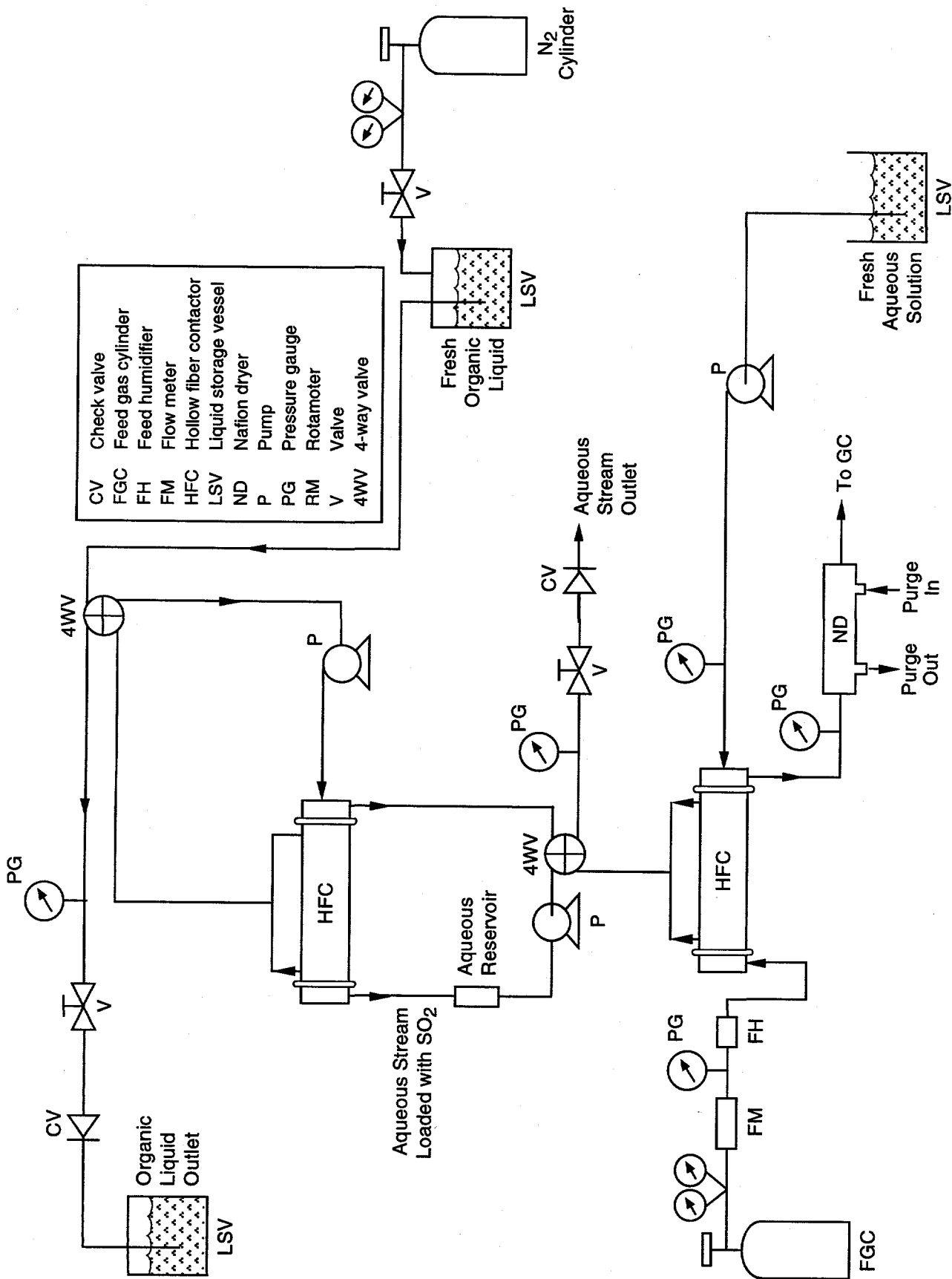
$$m_i = \frac{C_o^f}{C_w^f} \quad (6-3)$$

Figure 6-5 shows a modified diagram of the experimental setup used for the distribution coefficient measurement. The arrangement in Figure 6-5 supersedes the one shown in Figure 6-3. The setup and the procedure for the experiments were further modified because we found the earlier arrangement to be inadequate. The following experimental procedure was established after a few iterations.



CM-3501-64

Figure 6-4. Schematic of batch recirculation mode of operation using a hollow fiber contactor.



CM-3501-65

Figure 6-5. Modified absorption and liquor regeneration setup for distribution coefficient measurement.

A model flue gas mixture consisting of 2230 ppm SO₂, 11% CO₂, 3.13% O₂, and the balance N₂ was sent through the tube side, while an aqueous phase was pumped through the shell side, of the 200-fiber absorption module. The exit aqueous stream from this first module was passed through a four-way valve, then a second aqueous solution pump and an aqueous reservoir (volume of 75 mL) before entering the tube side, of the 1000-fiber extraction module. During the absorption part of the experiment, the aqueous line was not connected to the second hollow fiber module. Further, the second pump in the aqueous line was also not in operation. Once a steady gas composition was achieved at the flue gas outlet line (thus, the steady state SO₂ composition in the aqueous phase, C, was also known), the aqueous lines were connected to the second hollow fiber module. The system was allowed to run for another 30 min after which the four-way valve was switched to the batch recirculation mode of operation in the second module. The absorption part of the experiment was discontinued at this time. The second pump in the aqueous line was not yet turned on. The recirculation loop was filled with the aqueous solution, but there was no flow.

At this point, the organic flow through the shell side of the second module was initiated. The pump (placed after the four-way valve in the organic line) required priming by pressurizing the organic storage vessel with a N₂ cylinder. As soon as the hollow fiber module and the recirculation loop were filled with the organic solvent, the organic pump was shut off and immediately the four-way valve was switched to the recirculation mode of operation. Contacting of the two phases was then initiated by starting the aqueous phase flow and then the organic flow in the corresponding recirculation loop. The second module was operated under these conditions for about 2 h. After this, a known amount of DMA sample from the hollow fiber module was withdrawn from the module inlet line, directly into a burette containing excess NaOH solution of known concentration. The SO₂ from the organic solution reacted with NaOH in the aqueous phase. The total mixture was then back-titrated with standard HCl solution using phenolphthalein as an indicator. The SO₂ concentration in DMA (C₀) was calculated from the titration values. The volume of both aqueous loops (including module and dead volume) were measured accurately after the completion of the experiment to determine the final aqueous phase concentration via Eq. (6-2). The distribution coefficient was then calculated using Eq. (6-3).

Distribution coefficient measurement experiments were conducted both for aqueous 0.2 M Na₂SO₃ solution-SO₂-DMA and water-SO₂-DMA systems. For the aqueous Na₂SO₃ solution-SO₂-DMA system, the SO₂ concentration at the outlet of the absorption module was 13.3 x 10⁻⁶ mol/cm³ of solution. The SO₂ concentration in DMA after equilibration was 1.8 x 10⁻⁶ mol/cm³. A distribution coefficient value of about 0.2 was obtained.

From our earlier experience with water absorbent, we anticipated that a higher m_i value would result. However, we faced difficulty in determining m_i of the water-SO₂-DMA system. At the end of the experiment, the two phases were transferred into two separate vessels and water-oil emulsion was found in both phases. Although the extent of water contamination in DMA was not known, the SO₂ concentration in DMA was determined to develop a rough estimate of distribution coefficient. The change in SO₂ concentration in the water phase was large, whereas that in the organic phase was small. This led to an additional uncertainty in the concentration measurement. A very rough estimate of distribution coefficient would be ~10. Due to the large shell volume in the HFC itself, the organic volume in the recirculation loop is much larger than the aqueous volume. For the water-SO₂-DMA system, it is probably better to have an aqueous reservoir much larger than the organic reservoir. The reverse may be true for Na₂SO₃ solution-SO₂-DMA, because the SO₂ concentration in 0.2 M Na₂SO₃ solution is much larger to start with.

Earlier, we studied the absorption of SO₂ by water or by an aqueous 0.2 M Na₂SO₃ solution in a HFC and subsequent regeneration of the spent liquor in a second HFC via LLE with DMA. We reported preliminary results on the measurement of the distribution coefficient (m_i) of SO₂ in an experiment involving batch recirculation mode. We conducted additional measurements of distribution coefficients for both aqueous 0.2 M Na₂SO₃ solution-SO₂-DMA and water-SO₂-DMA systems. Further, to demonstrate 99% SO₂ liquor regeneration efficiency in laboratory modules, we conducted an extraction run for a very high DMA flow rate.

The experimental setup for m_i determination, shown in Figure 6-5, has gone through some minor changes in its operational procedure to prevent the formation of an aqueous-oil emulsion. In addition, the aqueous reservoir was larger than the organic reservoir for the water-SO₂-DMA system (Run AEM-3). For the aqueous 0.2 M Na₂SO₃ solution-SO₂-DMA system, a larger organic reservoir was used (Run AEM-4). We have confidence in these measurements because we did not see any breakthrough of phases at the end of the runs. Table 6-4 shows the results and the distribution coefficients.

For simultaneous absorption and extraction runs, a feed gas containing 2300 ppm SO₂, 3.22% O₂, 11% CO₂, and the balance N₂ was passed through the tube side of the 200-fiber module without any humidification. A constant feed gas flow rate of ~2700 sccm was maintained. An aqueous 0.2 M Na₂SO₃ solution was introduced into the shell side at a flow rate of 20 mL/min. Once a steady state was achieved in the absorption module, the exit aqueous flow was directed through the tube side of the second hollow fiber module containing 1000 fibers. The extraction part of the experiment was initiated with DMA flow in the shell side of the second

Table 6-4
DETERMINATION OF DISTRIBUTION COEFFICIENT (m_i)

Run No.	Aqueous Absorbent	Volumes in Circulation (mL)		Initial Concentration of SO ₂ in Aqueous Phase (C _{wⁱ}) (mole/cc)	Equilibrium Concentration of SO ₂		Distribution Coefficient m _i = C _o ^f /C _{w^f}
		Aqueous (V _w)	Organic (V _o)		Organic Phase (C _o ^f) (mol/cm ³)	Aqueous Phase (C _{w^f}) (mol/cm ³)	
AEM-3	Water	562	375	1.90 x 10 ⁻⁶	2.35 x 10 ⁻⁶	0.33 x 10 ⁻⁶	7.1
AEM-4	0.2 M Na ₂ SO ₃	145	368	13.3 x 10 ⁻⁶	2.86 x 10 ⁻⁶	6.04 x 10 ⁻⁶	0.47

module. The DMA flow rate was maintained at a high value of 102 mL/min (Run AE-12). Under these conditions, we were able to recover almost all of the absorbed SO₂ from the loaded aqueous 0.2 M Na₂SO₃ solution. The extractive flux of SO₂ was 26.87 x 10⁻⁶ mol cm²/s. The results are presented in Table 6-5 (along with other data representing higher SO₂ recovery by extraction). With this high flux, we achieved ~100% extraction efficiency, meeting a milestone in this task.

HOLLOW FIBER CONTAINED LIQUID MEMBRANE

In addition to LLE, the hollow fiber contained liquid membrane (HFCLM) technique may be used to regenerate aqueous SO₂ scrubbing liquor. An HFCLM permeator containing two sets of fibers was built. The first set of fibers were made of microporous hydrophobic polypropylene (Hoechst-Celanese, Charlotte, NC; Celgard X-10, ID: 240 μm, OD: 290 μm). The second set of fibers were made of silicone rubber (Baxter Healthcare Corp., Edison, NJ; silicone tubing, ID: 0.012 inch, OD: 0.025 inch). Following the method described in the literature (S. Majumdar et al., 1988), we prepared two separate fiber mats, one containing 200 Celgard fibers and another containing 100 silicone tubings. An integrated mat was then created by placing one mat on top of the other. Distilled water was spread over the integrated mat and the fibers were gathered gently and slowly to form a bundle.

The bundle was inserted directly into a specially constructed permeator shell where a Teflon pipe was used to keep the fibers in a defined volume. The two sets of fibers were separated at each end of the permeator through the openings of a Y-connection. The Celgard fibers were potted with two layers of resin mixtures, first with a silicone rubber (RTV 118, GE, Waterford, NY) and then with an epoxy resin (C4-D, Beacon Chemical Co., Mt. Vernon, NY). The silicone tubings were potted with an additional layer of silicone rubber (RTV 615A and 615B, GE, Waterford, NY). The effective length of the module is 18 inches.

We initiated process studies to determine the mass transfer characteristics of the newly built HFCLM module for regenerating aqueous SO₂ scrubbing liquor with organic solvent having a high affinity for SO₂. We tested the module with water at a pressure differential of 15 psi. The silicone tubule side showed leaks. We repotted the exterior end of that side with epoxy. The following trial with water at 15 psi did not show any leaks. We monitored the permeation of CO₂ through the module, in polymeric mode and using water as the CLM. The

Table 6-5
RESULTS OF RUN AE-12 AND OTHER RUNS WITH HIGHER RECOVERY OF SO₂ BY LLE

Run No.	Aqueous Absorbent		Flue Gas Flow Rate (sccm) (dry)	Flow Rate of DMA (mL/min)	SO ₂ Concentration in DMA (mol/cm ³)	Extractive Flux of SO ₂ (mol/cm ² s)	SO ₂ Transfer (mole/s)		Percent Recovery by Extraction
	Type	Flow Rate, (mL/min)					At Absorption	At Extraction	
AE-12	0.2 M Na ₂ SO ₃	20	2718	102	2.74 x 10 ⁻⁶	26.87 x 10 ⁻¹⁰	4.57 x 10 ⁻⁶	4.66 x 10 ⁻⁶	~100
AE-10	0.2 M Na ₂ SO ₃	10	2459	38	3.33 x 10 ⁻⁶	12.17 x 10 ⁻¹⁰	4.01 x 10 ⁻⁶	2.11 x 10 ⁻⁶	52.6
AE-11	Water	50	908	42.0	1.85 x 10 ⁻⁶	7.55 x 10 ⁻¹⁰	1.41 x 10 ⁻⁶	1.31 x 10 ⁻⁶	92.9
AE-3	Water	50	908	6.0	8.85 x 10 ⁻⁶	5.1 x 10 ⁻¹⁰	1.48 x 10 ⁻⁶	8.84 x 10 ⁻⁷	59.0

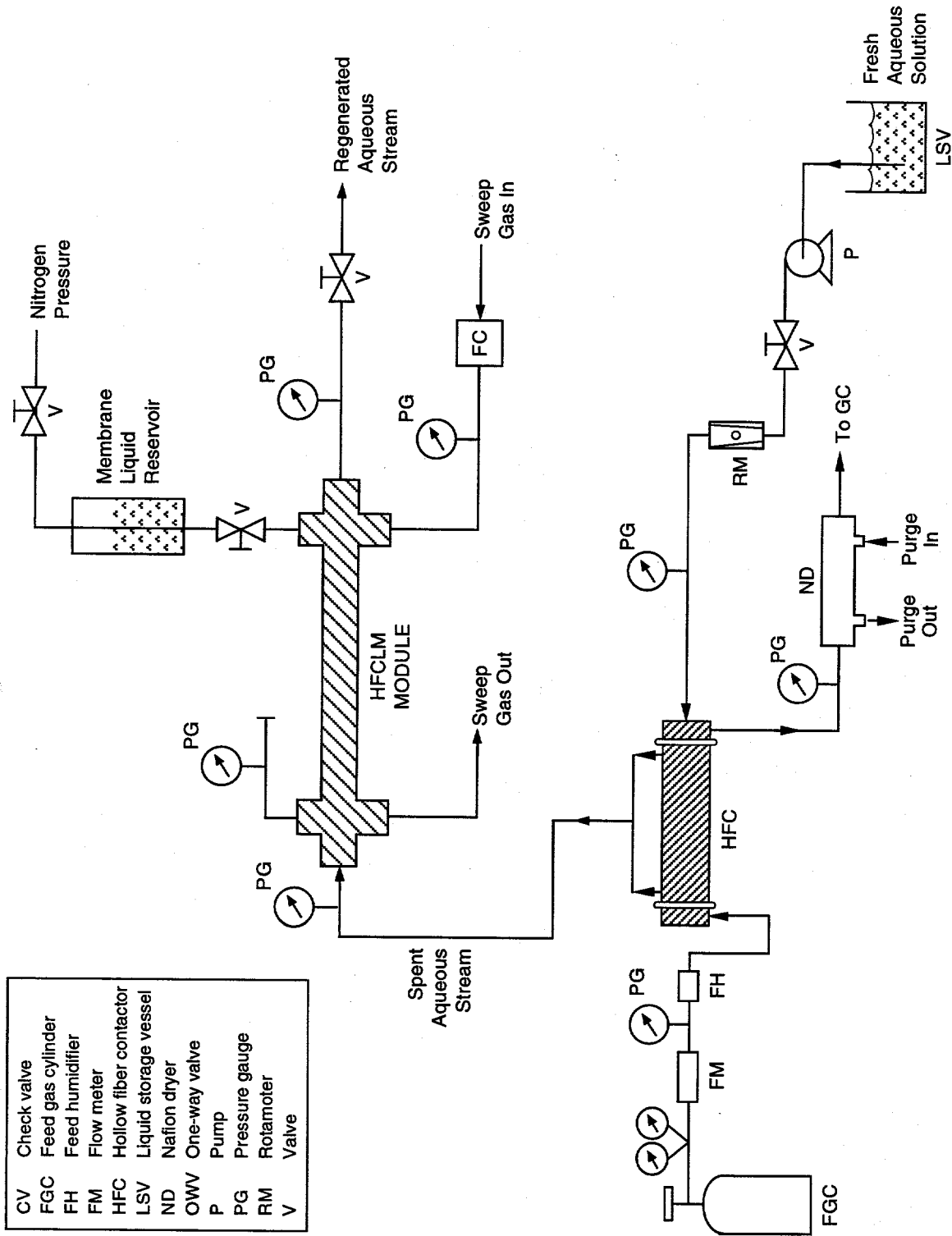
data yielded an effective membrane thickness of the CLM as 1050 μm . We then conducted experiments using aqueous sulfite solution-SO₂-DMA and water-SO₂-DMA systems. A typical absorption-HFCLM run comprises three simultaneous steps for the transfer of SO₂: absorption into aqueous solution, extraction with organic, and recovery by vacuum or sweep-gas. Figure 6-6 shows the experimental assembly, which is similar to one used in the absorption-extraction runs. We added line connections to allow the application of vacuum and/or the passage of sweep gas through the permeator and a reservoir for the organic liquid to maintain a constant volume for the liquid membrane. A feed gas containing 0.23% SO₂, 3.22% O₂, 11% CO₂, and the balance N₂ was passed through the tube side of the 200-fiber module without any humidification. The aqueous absorbent was introduced into the shell side. Once a steady state was achieved in the absorption module, the exit aqueous flow was directed through the tube side of the Celgard fibers in the HFCLM permeator. The extraction was in effect by the DMA at the shell side of the module, acting as the CLM. The pervaporation process is caused by application of a vacuum through the bore of the PDMS rubber tubules; it draws out the SO₂ from the DMA-CLM.

In exploratory runs, a constant volume of He was passed through the silicone tubules, acting as sweep gas. Such trials were done before adopting the vacuum mode of operation. Higher flow of He can establish a sizable gradient for the partial pressure of SO₂ so that the DMA phase strips off SO₂. It is possible that such a gradient attains the level available by using vacuum. The effluent sweep gas can be fed to a GC to determine its SO₂ content and to evaluate the performance of the pervaporation.

The first trial run used 0.2 M Na₂SO₃ solution as the absorbent at 20 mL/min and the model flue gas at 2730 sccm. Such combination is commonly used in our absorption experiments using the sulfite liquor. The run continued for 9 h. The volume of DMA inside the module as CLM was about 75 mL. The flow rate for He was initially at 150 mL/min and was then lowered to 50 and 10 mL/min, respectively. Under these conditions, the GC results did not show any trace amount of SO₂ at the effluent sweep gas. The possible causes were: SO₂ was not extracted from the SO₂-laden aqueous 0.2 M Na₂SO₃ solution, or the pervaporation did not recover SO₂ from the organic phase.

Previous LLE runs with DMA showed that it was easier to recover SO₂ from water than from the reactive sulfite solution. So in the next run, water was the absorbent instead of 0.2 M Na₂SO₃. The run used the most common parameters for absorption of SO₂ with water: 907 sccm of model flue gas flow rate and 50 mL/min of water flow rate. The run continued for 7 h. The GC measurements did not show SO₂ at the effluent sweep gas stream of He at 150, 50, and 10 cm³/min. A pH value of 5.8 was measured at 4 h onward for the aqueous stream collected at

CV	Check valve
FGC	Feed gas cylinder
FH	Feed humidifier
FM	Flow meter
HFC	Hollow fiber contactor
LSV	Liquid storage vessel
ND	Nafion dryer
OWV	One-way valve
P	Pump
PG	Pressure gauge
RM	Rotameter
V	Valve



CM-3501-65A

Figure 6-6. Schematic of combined absorption and liquor regeneration setup modified for HFCLM runs.

the exit of the HFCLM unit. Often we measured a pH of 3 for the outlet stream of the absorption unit after about 3 h. This occurs after the absorption process reaches a steady state condition under such experimental conditions. The neutral effluent of the HFCLM unit suggested that the DMA-liquid-membrane stripped SO_2 from the aqueous stream, but our measurement did not show the presence of SO_2 in the sweep gas.

For the next run, 100 mL of DMA was first contacted with SO_2 by purging with a gas mixture containing 1.65% SO_2 and balance N_2 for about 1/2 h under a pressure of 4 psig. Then the shell side of the HFCLM permeator was filled with this DMA solution. Otherwise, the run duplicated the preceding run. Again, the effluent sweep gas stream did not show traces of SO_2 . A preliminary estimate suggested that more time was required to make the DMA solution saturated with SO_2 in the above procedure.

We attempted to regenerate the aqueous SO_2 scrubbing liquor using the DMA again. A sample of fresh DMA was equilibrated with SO_2 in a flask by bubbling a model flue gas mixture containing 0.23% SO_2 , 3.22% O_2 , 11% CO_2 , and the balance N_2 . A sweep helium gas at a constant flow rate of 15 mL/min was then bubbled through the flask. The GC analysis of the helium stream showed SO_2 . Then we conducted a similar experiment using the HFCLM permeator to strip off SO_2 from SO_2 -enriched DMA. About 100 mL of DMA was first equilibrated with SO_2 by purging it with the model flue gas mixture. The shell side of the HFCLM permeator was then filled with the DMA solution. A constant flow rate of He was passed through the silicone tubules to strip the SO_2 from the CLM. A GC analysis of the effluent did not show traces of SO_2 . We concluded that the resistance of the thick silicone tubule wall was too high.

The module was then dried using vacuum followed by a flow of N_2 through the shell side (a regular procedure after each trial). After the above run, we found that the silicone rubber was so swollen that N_2 could not be passed through the lumen of the tubules even at a pressure of 15 psig. The module was washed with 50% acetone in water and then dried by applying vacuum to the shell side for one day. Still the silicone tubes did not allow any passage of N_2 . The rubber tubules were probably heavily swollen by long exposure to DMA and were then blocked inside at its potted sections. The module was inoperable.

Continuing our study, we used a separate HFCLM module available in our laboratory. It contains two sets of fibers: microporous Celgard and coated Celgard. An ultrathin nonporous skin of silicone rubber on the outside surface of the microporous hollow fibers provided the coating. Such a skin has a typical thickness of 1 μm , and so it will have a very high permeation rate for SO_2 in the above application. The permeator was thoroughly washed with a solution of acetone in water and then vacuum dried. Leak tests were performed, and no leaks were found. Table 6-6 gives details of the module.

Table 6-6

GEOMETRIC CHARACTERISTICS OF THE COATED FIBER MODULE FOR HFCLM

Effective length, cm	18	
ID of the shell, cm	0.238	
Fiber type	Coated Celgard	Celgard
	X-10	X-10
ID/OD, μm	100/142	100/142
Number	26	26
Transfer area, cm^2	17.7	32.5
Fiber details		
Tortuosity	3.5	
Porosity	0.2	
Packing Factor	0.18	

The new module was used to repeat the run with the HFCLM permeator containing silicone tubules, as described above. The GC analysis showed SO_2 in the effluent sweep of He. Obviously, the resistance of the thin skinned fiber was much lower than that of the silicone tubules. The results of this experiment established the feasibility of the CLM technique for extracting SO_2 from SO_2 -laden DMA solution.

A few runs were then conducted using water- SO_2 -DMA and aqueous sulfite solution- SO_2 -DMA systems. A model flue gas containing 0.23% ppm SO_2 , 3.22% O_2 , 11.0% CO_2 , and the balance N_2 was passed through the tube side of the 200-fiber absorption module without any humidification. The aqueous absorbent was introduced into the shell side of this unit. Once a steady state was achieved, a small fraction of the exiting aqueous stream of about 0.3-0.6 mL/min was directed through the tube side of the Celgard fibers in the HFCLM permeator. The HFCLM module had about 10-15 mL of SO_2 -laden DMA as the CLM. He gas was passed at a flow rate of 15 mL/min through the lumen of the coated fiber.

The first run used water as the absorbent at 45 mL/min and the model flue gas at 908 mL (STP)/min. Such a combination is commonly used in our absorption experiments using water. The run continued for 9 h. The GC results showed SO_2 at the effluent sweep gas from the HFCLM unit. However, a steady concentration of SO_2 in the sweep stream was not seen. The

possible cause was the unstable interface between water and liquid DMA membrane inside the HFCLM permeator. Water droplets were seen in the sample liquid membrane collected at the end of the experiment. We have experienced the limited miscibility of DMA in water before, and that caused difficulty in maintaining a stable interface.

In the next run, 0.2 M Na_2SO_3 served as the absorbent. The run employed the most commonly used parameters for absorption of SO_2 with sulfite liquor: a flow rate of 2686 mL (STP)/min of model flue gas and an aqueous flow rate of 17 mL/min. The model flue gas contained 0.225% SO_2 , 3.29% O_2 , 11% CO_2 , and the balance N_2 . The run continued for 7 h. The measured pH of the outlet stream from the absorption unit was 7.2 after about 3 h. This stream was then introduced to the HFCLM unit. After 1 h, a pH value of 7.3 was obtained in the aqueous stream collected at the exit of the HFCLM unit, after the absorption process reached a steady state condition. This was indicated by a constant value for the trace SO_2 concentration in the exit gas stream from the absorption module. Also, the GC measurement of the effluent sweep-gas stream from the HFCLM permeator showed a steady value for the concentration of SO_2 . The flow rate of the SO_2 -carrying sulfite solution through the HFCLM unit was 0.3 mL/min. A high pressure of about 18 psig was needed to pass the aqueous phase through the HFCLM permeator due to the very small number of fibers.

Our calculations showed that this experiment recovered about 1% of the SO_2 that was absorbed by the aqueous sulfite solution. Two days later, the experiment was repeated. Only the flow rate of the sulfite solution was different, which was at 0.6 mL/min. The rest of the parameters were similar to those of the preceding run. The run recovered about 0.7% of the SO_2 that was absorbed by the sulfite liquor. The use of coated fibers in these two runs demonstrated that it is possible to regenerate the aqueous SO_2 scrubbing liquor with organic DMA as the CLM in a larger unit.

TASK 7: PARTICLE DEPOSITION

The objective of this task was to determine whether deposition of particulate matter on the inside of the hollow fibers significantly affects the mass transfer efficiency and whether the effect, if any, is reversible. This study of particulate matter is essential because, in a coal-fired power plant application, even downstream of a high efficiency bag filter, there will be nearly 30 mg of particulate matter per cubic meter of flue gas (30 mg/m^3). Therefore, any SO_2/NO_x technology that purports to be practical must deal with this issue and must be robust in the presence of these low level particle concentrations. The size range of the particulate matter that needed to be considered here was 0.2 to 0.3 μm ; this size corresponds to the minimum in the efficiency curve of a bag filter in an actual power plant.

The methodology required to conduct this task in a systematic fashion consisted of six steps: (1) selection of suitable particle generation method to simulate a particle-laden flue gas stream, (2) procurement of typical fly ash material in the desired size range, (3) design of an experimental setup to aerosolize the particles into the flue gas feed stream to the HFC, (4) particle characterization and analysis equipment downstream of the HFC, (5) trial operation of the whole particle generation-analyzing system using inert gases, and (6) mass transfer studies in HFC using simulated flue gas. The most widely used techniques for generating solid particles into gas stream are dry dispersion and wet-particle dispersion. Dry powders are dispensed by dust feeding equipment (e.g., fluidized bed dust generator). Dust feeding systems are appropriate for generating particles of 0.5 to 100 μm with air flow rates ranging from 10 to 50 L/min. High operating air flows are required to minimize particle agglomeration especially at submicron particle ranges. However, the wet-particle generation method appears to be appropriate because of its flexibility involved with operating parameters, leading to increased control in designing the generating system.

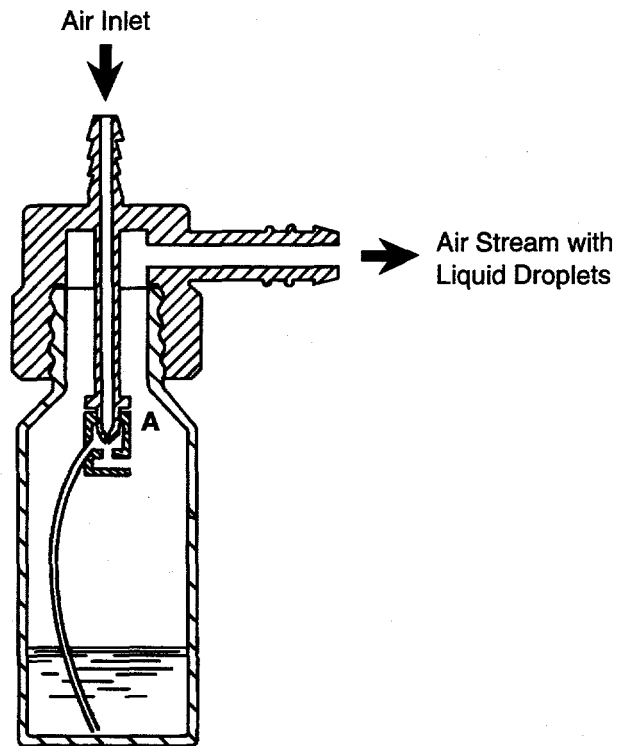
Liquid aerosol generation is one of the common methods for generating particles for inhalation and air pollution studies. Similar to these studies, when quantifying the effect of these particles on mass transfer in an HFC, two important parameters are concentration and size distribution of the particulate matter. These parameters dictate the selection of the type of liquid aerosol generator. Several techniques are available to mechanically disperse liquids to form aerosols. Some of the common methods are air nebulizers, spinning-disc atomizers, ultrasonic nebulizers, and vibrating orifice generators. We chose to work with the pneumatic nebulizers because of their ability to generate very fine droplets at suitable gas flow rates and cost-effectiveness.

In these pneumatic nebulizers, compressed air is used to atomize the liquid into droplets. In the Wright nebulizer, shown in Figure 7-1, air passes through a narrow tube to position A. The high velocity air emerging from this tube creates a low-pressure region at the tube exit, drawing liquid from the reservoir upward through a liquid feed tube. The emitted liquid is atomized by high-velocity air into small droplets. Large droplets impinge onto the upper wall of the curved exit duct, and the smaller droplets remain aerosolized. Clearly, the critical parameters in selecting a nebulizer are the liquid droplet size distribution, the liquid delivery rate, and the gas flow rate. Because numerous models and designs of medical nebulizers are available, choosing the appropriate type of nebulizer was difficult.

For the selection process, we completed some initial calculations to estimate key parameters. Table 7-1 shows the calculations. Each nebulizer, based on its design, will have a certain gas-to-liquid flow rate and a corresponding mass median aerodynamic diameter (MMAD). For the desired particle concentration and MMAD in the gas stream, the calculations shown in Table 7-1 are used to generate the required parameters for the nebulizer. The second half of the table gives lumped particle cluster size, assuming that the coalesced particles form a perfect sphere. The last row in the table indicates the particle size and particle concentration in gas stream suitable for the present study. Knowing the feasibility of particle generation, the next step was to acquire liquid-borne fly ash particles.

The fly ash material must be typical of that found in flue gas streams to produce realistic effects from our laboratory studies. The composition of coal ash typically contains about 58% silica, 27% alumina, and trace amounts of other metal oxides (EPRI Report #CS-2894). Because the majority of ash contains silica material, we decided to procure liquid samples of colloidal silica dispersion. A silica dispersion sample containing 30 wt% of solid particles was kindly supplied by CABOT Corporation, IL.

Other important factors that concerned us were the size range and the nature of the size distribution of these silica particles present in the liquid phase. We have used a Horiba particle analyzer to study the size range, and the results are given in Figure 7-2. About 50% of particles are in the range of 0.1 to 0.3 μm , which is the required size range. Results from Figure 7-2 are also plotted on log-normal probability axes to test the type of distribution (Figure 7-3). While the plot exhibits the bimodal behavior, the dashed line covers about 90% of particles. For all practical purposes, the trace amounts of particles above 90% can be neglected. Therefore, we assumed that the particles would follow the log-normal distribution. The distribution can be characterized by knowing two parameters: the geometric mean and the geometric standard deviation. The concentration of solids in the supplied colloidal silica dispersion was 30 wt% in deionized water. This liquid dispersion was diluted appropriately while using the nebulizers.



CM-3501-60A

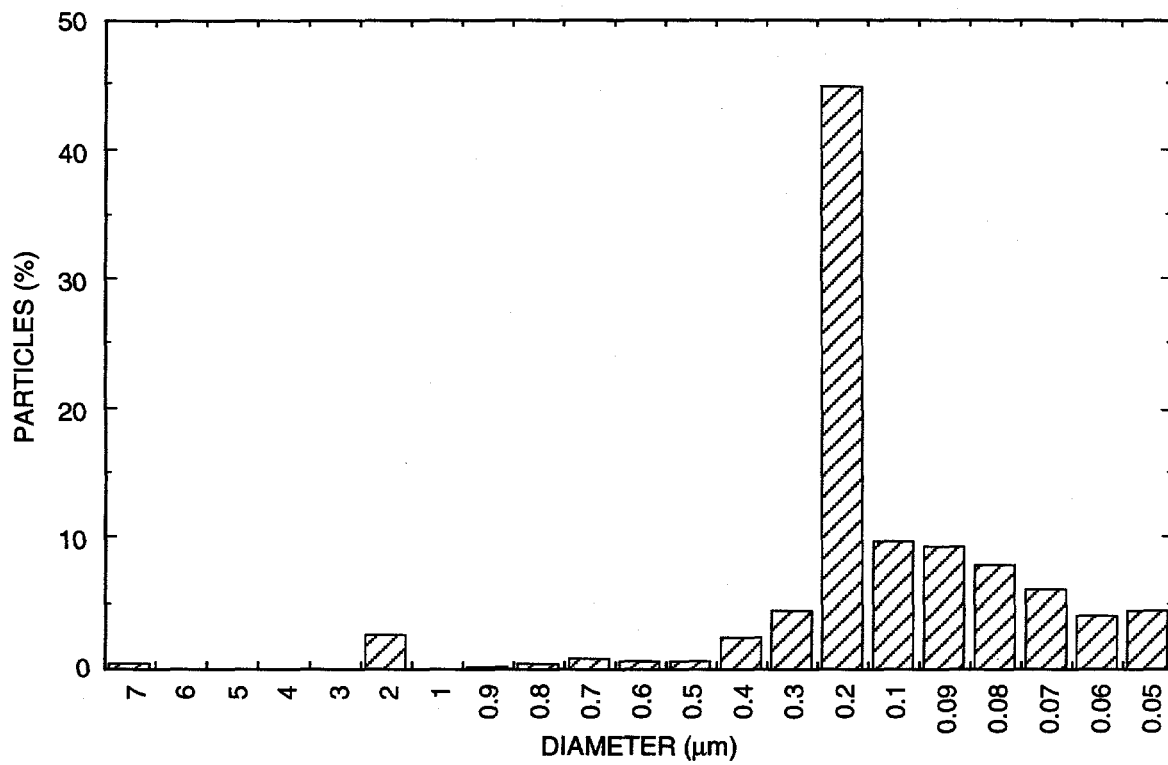
Figure 7-1. Schematic of Wright nebulizer.

Table 7-1
PARTICLE GENERATION USING NEBULIZERS

Gas flow (s/m)	12	Solid particle size (μ)	0.2
Liquid Delivery (mL/min)	0.3	Particle density (g/cm ³)	2.5
Liquid drop (μ m)	3	Mass of solid particle	1.048×10^{-11}
Rate of formation of droplets (#/min)	2.12×10^{10}		

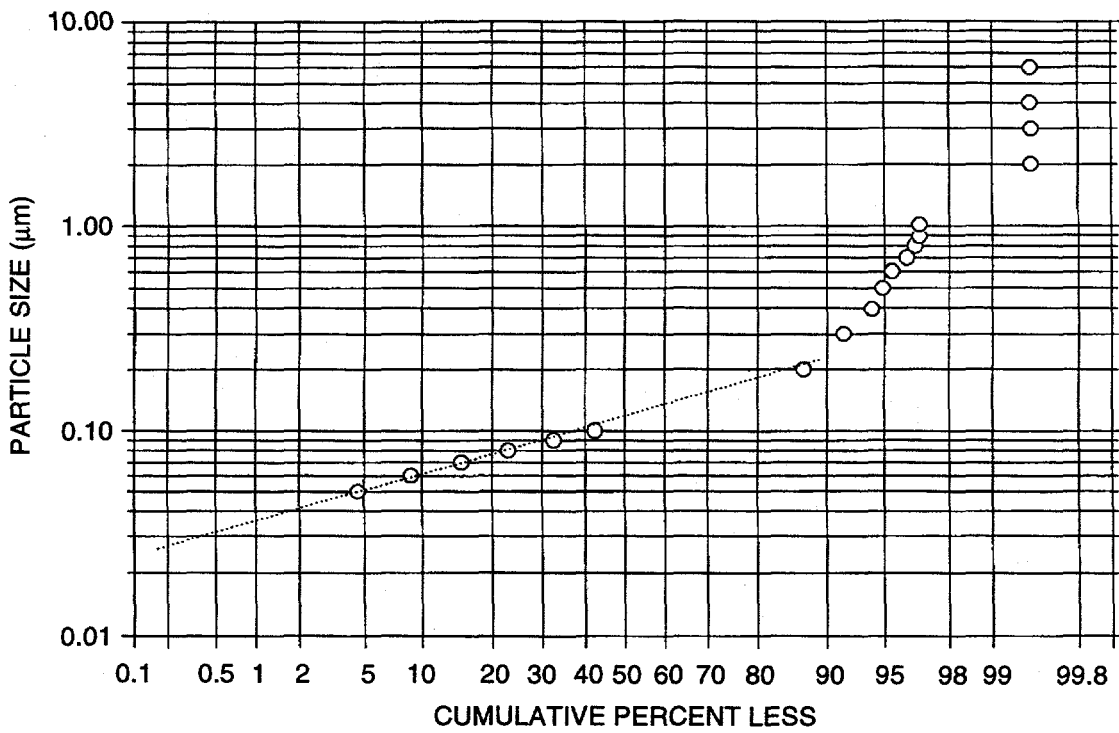
Desired Particle Conc. in Gas Stream (mg/m ³)	Particle Flow (mg/min)	Particle Conc. in Liquid (mg/gm of Water)	Calculations Based on Droplet Size		
			# Particle Flow Req. (#/min)	# Particle Per Water Droplet	Size of Particle Cluster (μ m)
300	3.6	12	3.436×10^{11}	16.20	0.570
200	2.4	8	2.291×10^{11}	10.80	0.498
100	1.2	4	1.145×10^{11}	5.40	0.395
50	0.6	2	5.727×10^{10}	2.70	0.314
25	0.3	1	2.864×10^{10}	1.35	0.249

Relative humidity of dry air (%)	12
Absolute humidity of dry (kg/kg dry)	0.002
Times supersaturated	1.054
Density of air (25°C) (kg/L)	0.001
Absolute humidity after nebu (kg/kg dry)	0.021



CAM-3501-66

Figure 7-2. Size distribution of dispersed silica particles.



CM-3501-67

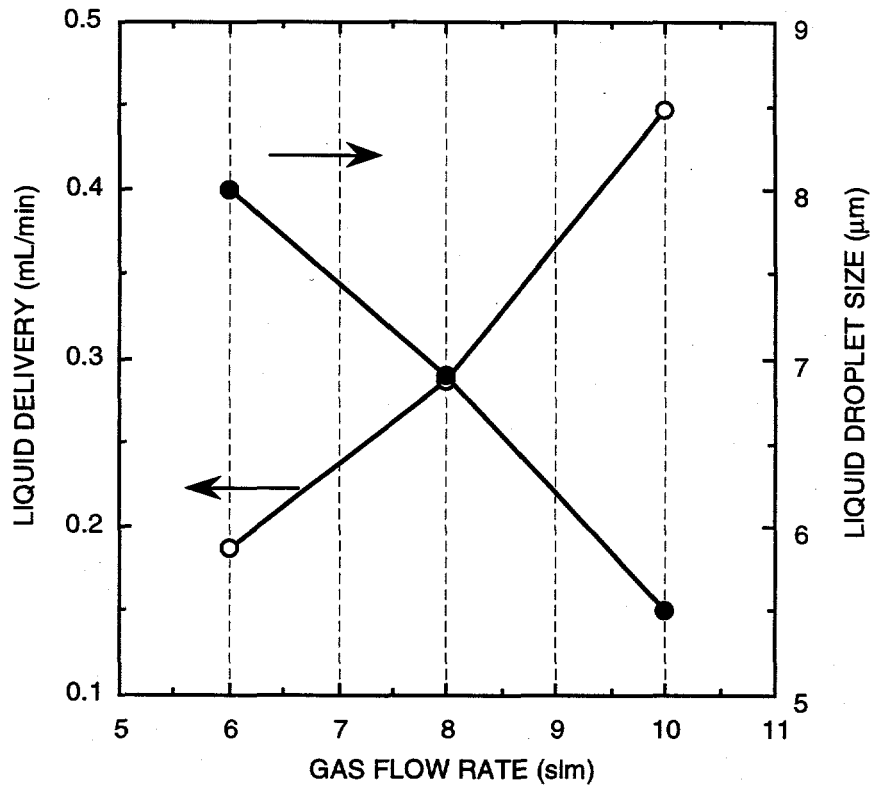
Figure 7-3. Log-normal distribution of dispersed silica particles.

We tested several nebulizers for their applicability to the present process. From Table 7-1, we can infer that to obtain the desired dry particle size (0.1-0.4 μm), the droplet size generated by a nebulizer must be as small as possible ($\sim 0.3 \mu\text{m}$). For all the nebulizers, based on their design, the liquid delivery rate is fixed for a certain gas flow rate. Typical performance characteristics of an Inspiron (Ominicare, Inc.) (400 cm^3) nebulizer are shown in Figure 7-4, which shows that an increase in the gas flow rate results in smaller droplet size, but also increases the liquid delivery rate. The droplet size distribution from the nebulizer was measured by Malvern Optical Instruments (laser aerosol spectrophotometer). While it is appropriate to get small droplets, it is undesirable to introduce high amounts of liquid into the gas stream because it creates difficulties in the particle analysis and alters the mechanism of particle deposition rates.

From our preliminary tests with several nebulizers, we successfully optimized the parameters, with an Acorn II nebulizer (Marquest Medical Products, Inc., Englewood, CO), for generating particles with a suitable size range. The inlet gas flow rate to the system was 11.7 L/min and the corresponding liquid delivery rate was 0.29 mL/min. These operating parameters also generated a liquid droplet size of 3.4 μm . The properties of the gas stream at the exit of the nebulizer were 100% relative humidity and 15°C dew point. A section of the gas tubing was heated by electrical heating tape to bring down the humidity levels of the gas stream. This heating became necessary to vaporize the liquid droplets and to condition further the solid particles.

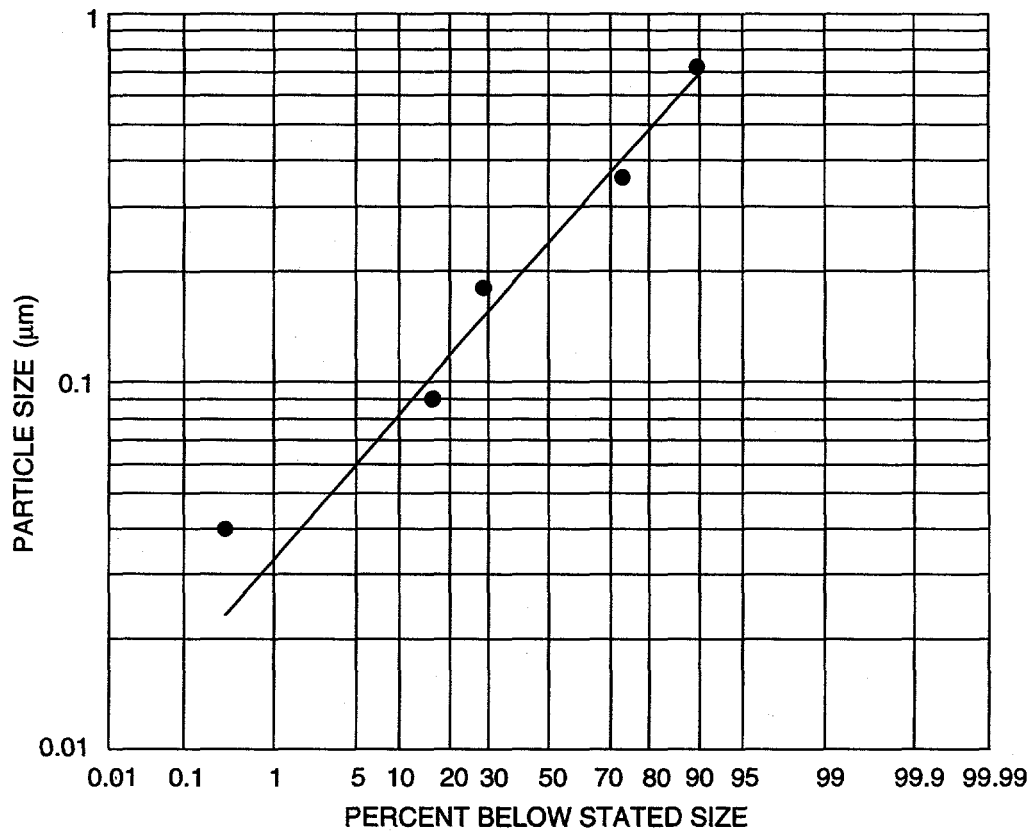
In an experiment, a known sample solution of silica dispersion was taken into the reservoir of the Acorn II nebulizer and was aerosolized with 11.7 L/min of gas flow rate. The wet particle-laden gas stream was heated and analyzed for particle size distribution. Silica dispersion sampling and characterization of aerosol was done using a Quartz Microscopic crystal cascade impactor. This instrument measures the size of the particles based on well established particle impaction theory. The instrument essentially contains a 10-stage cascade impactor equipped with quartz crystals. Depending on the entrance nozzle diameter and the distance between the crystal surface and nozzle outlet, only a certain size particles will be retained on the crystal surface. This retained particle mass is measured with electronic sensing meters. The sample to the meter was taken after the heated tube section. The gas properties at the sampling position are 72% relative humidity, 23°C dew point, and 28°C dry bulb temperature.

The sampling time to the instrument was varied from 1 to 20 s to verify the reproducibility of the results. Figures 7-5 and 7-6 show the size distribution curves from the same sample designed to produce a particle concentration of 30 mg/m^3 . The ordinate in the figure gives the particle size (μm) on a logarithmic scale, and the abscissa gives the cumulative percent below the



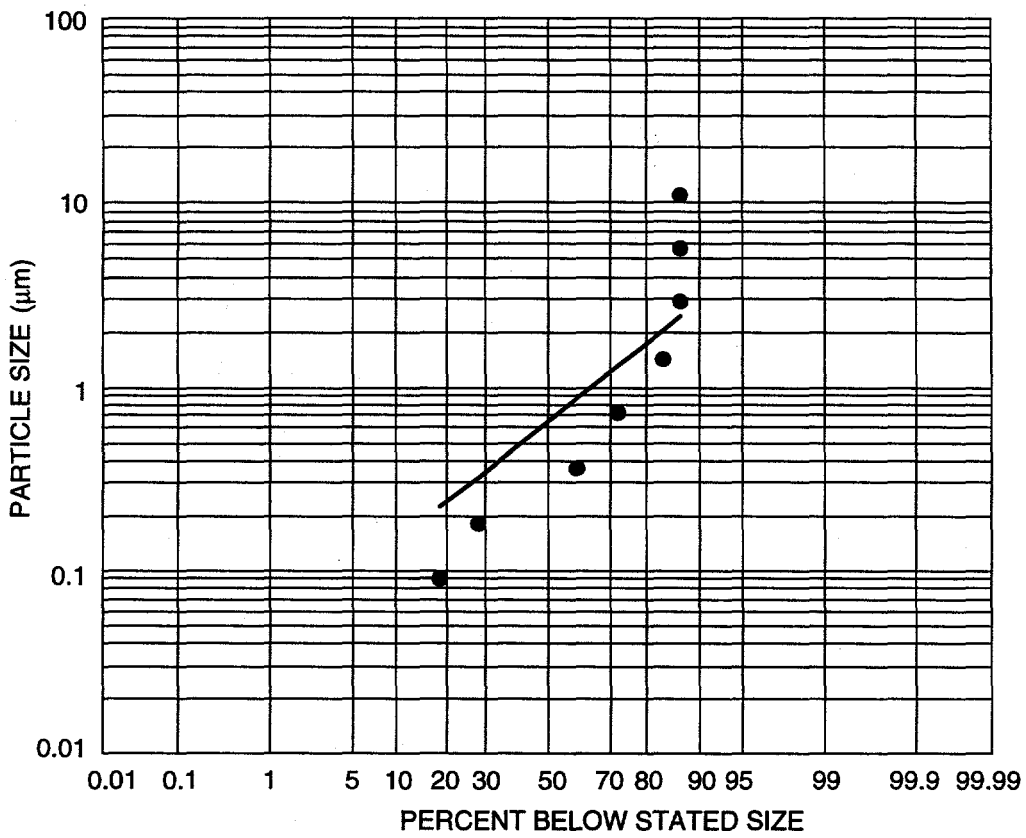
CM-3501-73

Figure 7-4. Inspirin (400 cm³) nebulizer performance characteristics.



CAM-3501-83

Figure 7-5. Particle size distribution for the sampling time of 1 s.



CAM-3501-84

Figure 7-6. Particle size distribution for the sampling time of 40 s.

stated size on a probability scale. The MMAD that corresponds to 50% on the abscissa, according to Figure 7-5, is 0.25 μm . In Figure 7-6, the size distribution is somewhat distorted with a few larger particles close to 10 μm . Considering the practical difficulties involved with accurate sampling and the method (e.g., mass based or number based) of analysis, one can neglect these few isolated particles. Then the MMAD for Figure 7-6 is about 0.4 μm . This kind of correction is not unusual in particle size analysis experiments.

The average particle size measured here is about 3 to 4 times larger than the silica dispersion size measurements conducted in the liquid form, indicating that the silica particles agglomerate in the gaseous media. Still, the particle sizes in the gaseous media fall in a range similar to that found downstream of a bag filter in a power plant. As a result, we estimated particle deposition rates before conducting the time-on stream tests with this particle generation technology.

Deposition of particles on the inner walls of hollow fibers can be estimated by using established theories. The gas flow inside the fibers is assumed to be laminar and the mechanism of particle deposition is varied according to the particle size. Figure 7-7 shows the deposition efficiency. Using the equations given by Fuchs (1964), the capture efficiency for 0.2- μm particles is about 1%, indicating that the time needed for a monolayer coverage is 290 h.

Our next step was to deposit the generated particles onto the inner walls of the hollow fibers and to further estimate the effect of this deposition on SO_2 mass transfer. To examine the change in mass transfer, we had to characterize the module immediately before the start of particle deposition. Then at suitable time intervals, we measured the mass transfer characteristics of the HFC repeatedly. This procedure allowed us to correlate the amount of particles deposited to the mass transfer efficiency of the module. In addition, we measured the mass of the particles in the exiting gas stream.

SO_2 absorption experiments were conducted in a 1000-fiber HFC. Water was shown (e.g., Task 4) to be a good absorbing solvent for SO_2 and hence was used as the absorption medium. The feed gas stream to the HFC contained 4000 ppm of SO_2 and balance N_2 . The exit gas stream from the HFC was monitored by a GC (HP 5890) equipped with a Porapak Q column (6 ft x 2 mm ID, Alltech Assoc., Deerfield, IL). Because the detectable limit for this system is approximately 500 ppm, the SO_2 inlet concentration of 4000 ppm was appropriate for analyzing the HFC exit gas stream.

We conducted experiments at various gas flow rates. Figure 7-8 shows the variation of the gas side overall MTC (K_{og}). The liquid flow rate was maintained at 11.2 mL/min. K_{og} increases rapidly (by a factor of 6) at the low gas flow rates and becomes almost flat at the high (>2 SLPM)

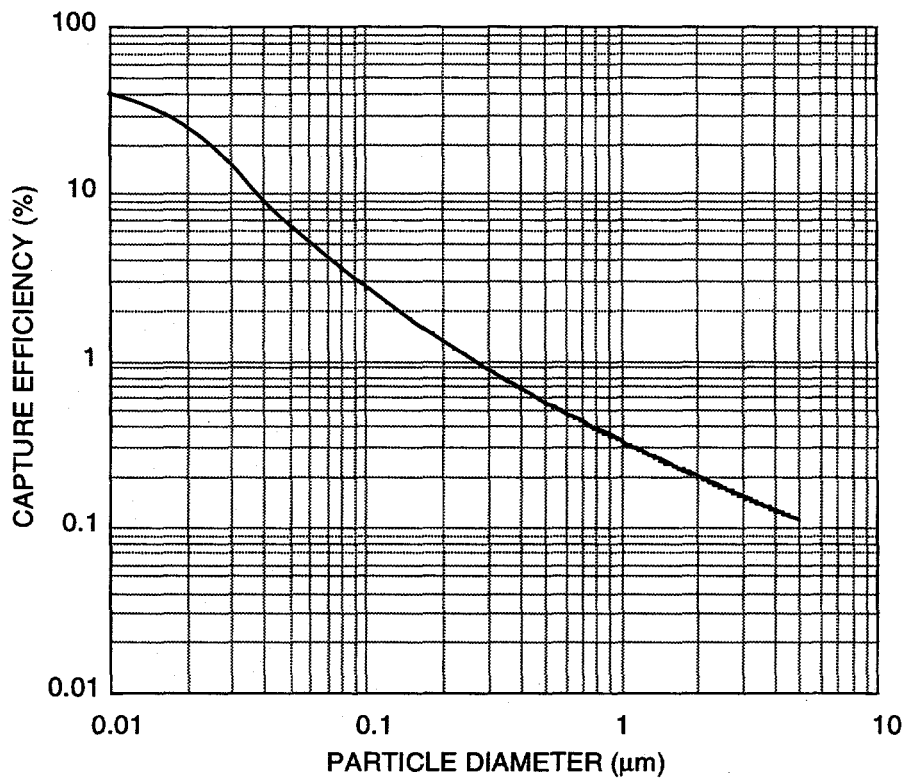
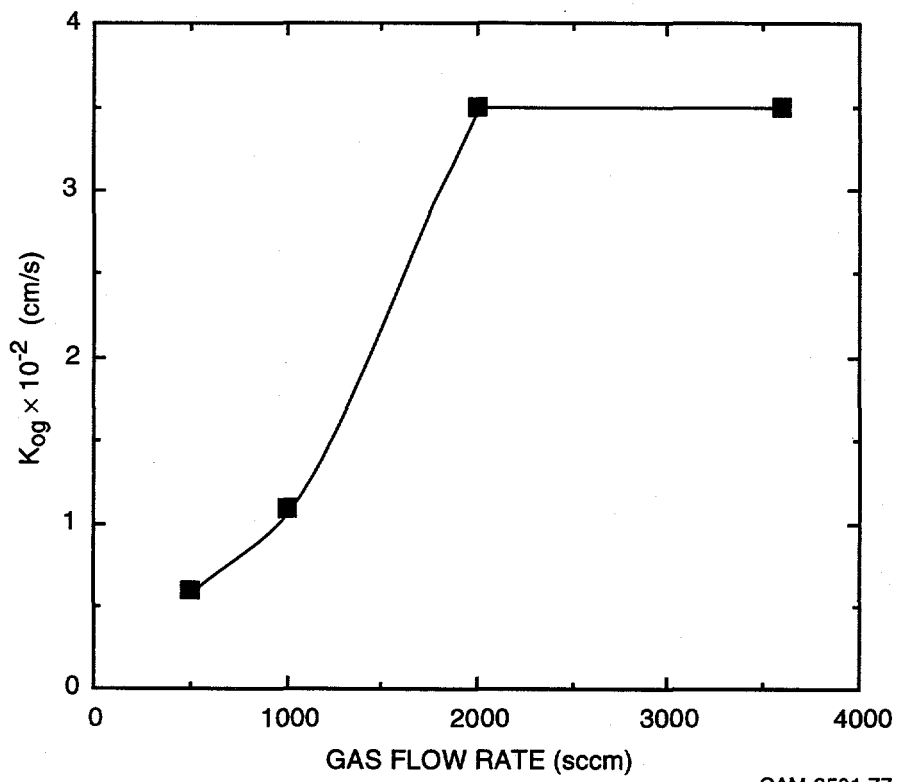


Figure 7-7. Particle capture efficiency in a HFC.

Fiber length: 23 cm, number of fibers: 1155, ID: 240 μm , gas flow: 11.7 slm.



CAM-3501-77

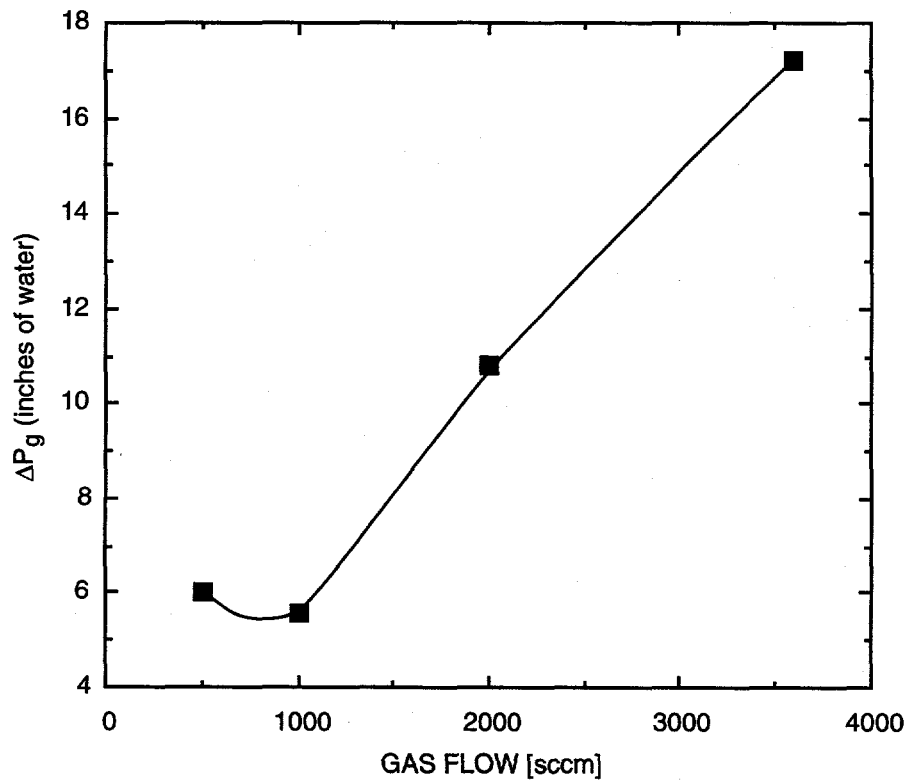
Figure 7-8. Variation of gas side, overall, mass transfer coefficient with gas flow rate.

almost flat at the high (>2 SLPM) gas flow rates. This behavior at the high gas flow rates is due to the attainment of equilibrium conditions for SO₂ in the liquid.

Another factor in this study was the gas pressure drop (ΔP_g) across the HFC. This drop is important because of its fourth power functional relationship with the diameter of the fiber (see Eq. 14-4, Task 14). Because the fiber diameter will change after repeated exposure to the particle-laden gas stream, ΔP_g will be greatly affected. The differential pressure across the HFC was measured with a digital pressure meter (Air-Neutronics, Ltd., Oxford, England). Figure 7-9 gives the dependency of ΔP_g on the gas flow rate. The overall trend is linear with laminar flow conditions, except for one 1000-sccm point, which could be due to a wrong zero set point in the pressure meter or a leak during the measurements. Again, these stated results will serve as baseline measurements for all the future work with the particle deposition system.

It was also critical to determine the mass of the particles in the outlet gas stream in order to quantify the amount of particles deposited on the walls of the hollow fibers. As noted above, accurate particle size measurements are very difficult with the smaller particles (< 1 μm). In an attempt to observe the particle collection efficiency using filters, we purchased an in-line, stainless-steel, filter holder and 0.2- μm pore size filter membranes from Millipore (Bedford, MA). The manufacturer claimed these filter membranes would show 99.99% particle collection efficiency.

The particle-laden stream was generated using an Acorn-II nebulizer system. Liquid containing a known amount of colloidal silica particles was pumped into the nebulizer reservoir using a peristaltic pump. The level of the liquid in the reservoir was maintained at about 4 mL to provide a constant liquid-delivery rate. This ensured a uniform particle generation and particle size range. The gas stream was heated to reduce the humidity level, and the particles were filtered using two 0.2- μm filters for 2 h. During the run, the amount of liquid being nebulized was also recorded. We calculated that only 90% of the generated particles were actually collected by the two filters. This 10% discrepancy, even for a simple generate-and-capture test, gives the error we may expect to have while generating and then depositing particles on an HFC. Our earlier calculations showed that 1% of the generated particles should be deposited on an HFC, which is well within our experimental 10% measurement error. As a result, we abandoned efforts to quantify the amount of particles deposited and focused only on its effects on mass transfer. Before presenting the test results, it is appropriate to compare the operating parameters of the present system with those of the actual power plant.



CAM-3501-78

Figure 7-9. Effect of gas flow on the pressure drop across the HFC.

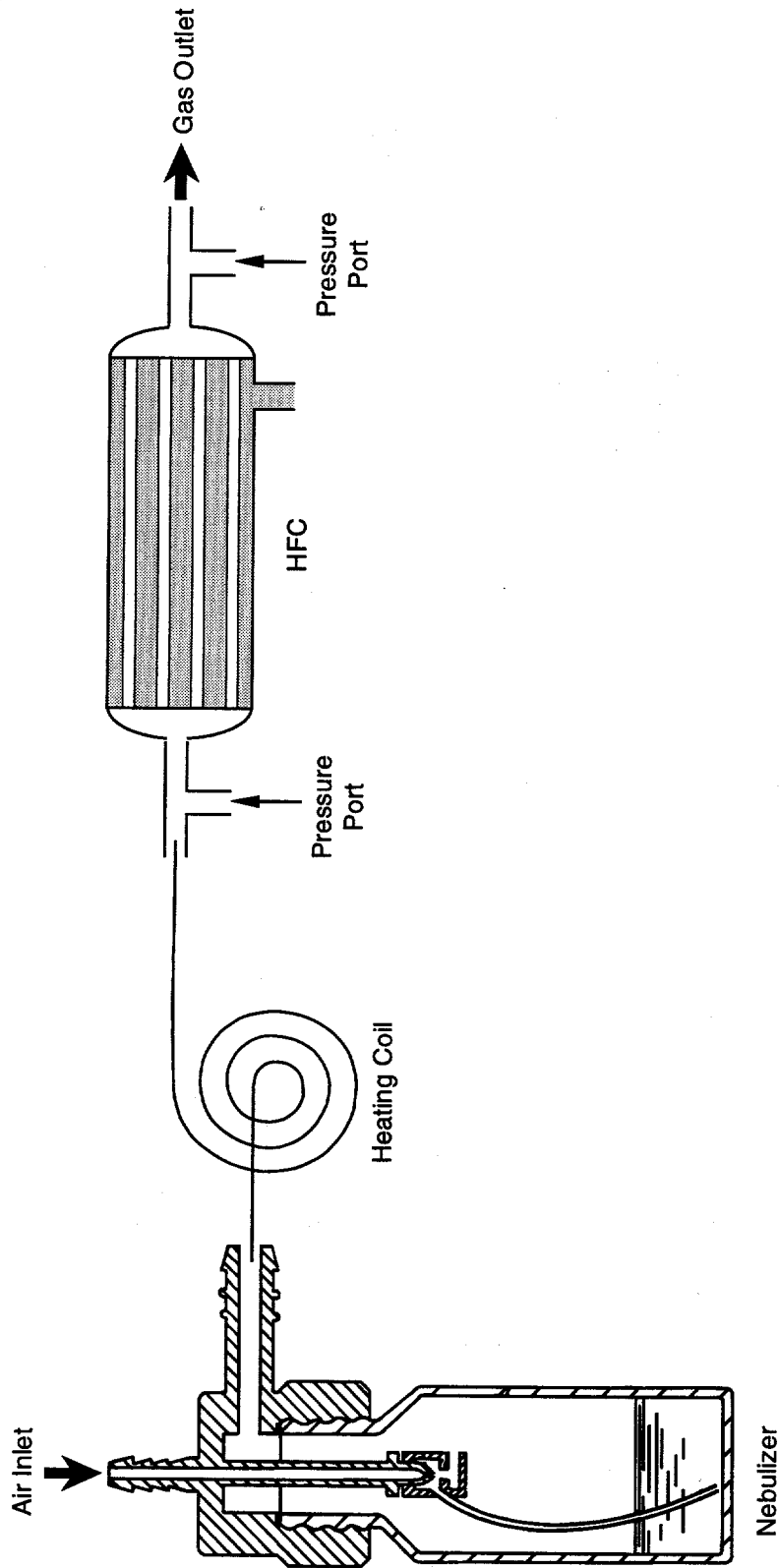
Gas flow rate through the fibers determines the residence time of a gas molecule and, therefore, affects the deposition of particulate matter. The flow rate for all the experiments was fixed at 11.7 SLPM. This flow rate was chosen only to generate an appropriate particle size distribution and not to simulate actual plant conditions. However, this flow gives a residence time of 0.053 s in contrast to a value of 0.073 s (based on 14-cm long, 240- μm -ID fibers, see Task 14) that corresponds to a more practical situation. Because these two values are within a difference of $\sim 25\%$, the flow rate under consideration fairly represents actual plant conditions.

The temperature of the gas stream affects the diffusion rates of particles. In our experiments, the gas stream entering the module was at about 40°C , as opposed to an approximate power plant flue gas temperature of 50°C . Humidity levels were indeed difficult to maintain as the temperature of the stream dropped along the module. At the inlet to the module, the relative humidity of the stream was about 70% and the exiting stream was at room temperature and completely saturated. Even water droplets were noticed occasionally at the outlet of the device, indicating the condensation of water. If the condensation occurs well into the module, it is very likely that this process alters the particle deposition phenomenon because of the high tendency of the particles to agglomerate. Keeping these factors in mind, we conducted time-on-stream studies. The results are presented below.

Figure 7-10 shows the experimental arrangement for generating particles. The liquid level in the Acorn II nebulizer reservoir was maintained at about 4 mL. The liquid sample was prepared by diluting the original colloidal silica dispersion so as to produce a particle concentration of 30 mg/m^3 . During initial stages of the particle deposition process, we measured the mass transfer frequently. We also monitored the pressure drop across the module (ΔP_g) periodically during particle deposition.

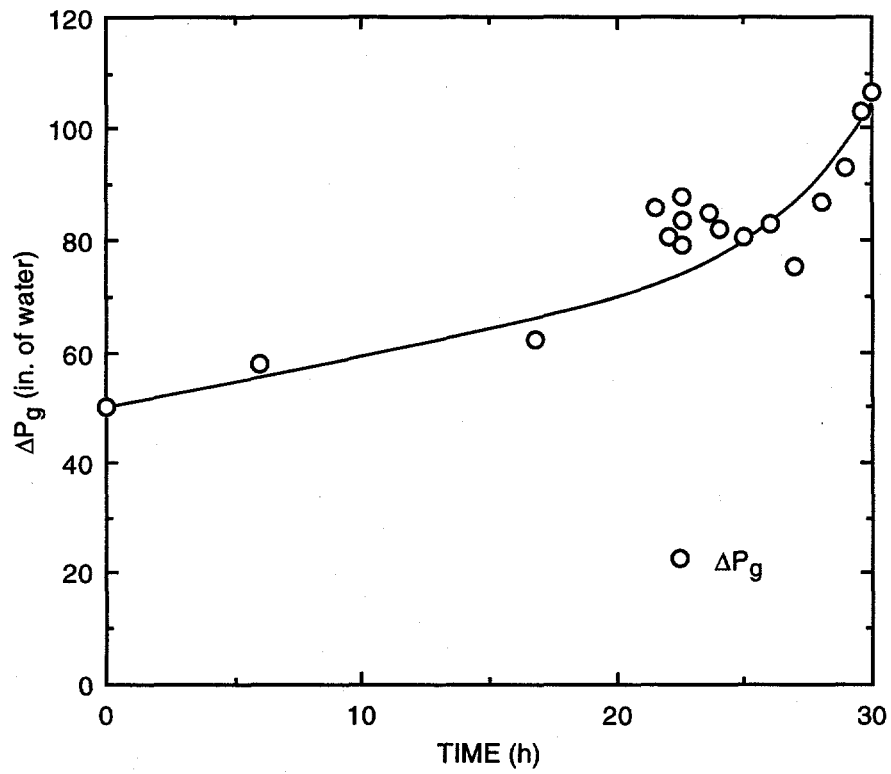
During the first 30 h, as can be seen from Figure 7-11, ΔP_g increased monotonically and reached about 115 inches of water. At this time, the particle deposition process was stopped and the module was dismantled to observe the fibers. We noticed a particle cake at the gas inlet end of the fiber bundle, which was an unexpected result. Figures 7-12 and 7-13 are photographs of the cake and fiber ends.

As shown earlier, the particle size generated could vary anywhere from 0.1 to 5 μm , with a mean around 0.2 μm . The large particles likely did not follow the gas stream lines. In this case, these particles clung onto the inner surface of the fibers, closer to the fiber inlets. As the experiment progressed, this obstructing particle started growing due to interception of other particles and further agglomeration. This process eventually led to blocking the fiber and the cake buildup. We believe that this blockage might run a few inches into the module from the gas inlet. The particle cake



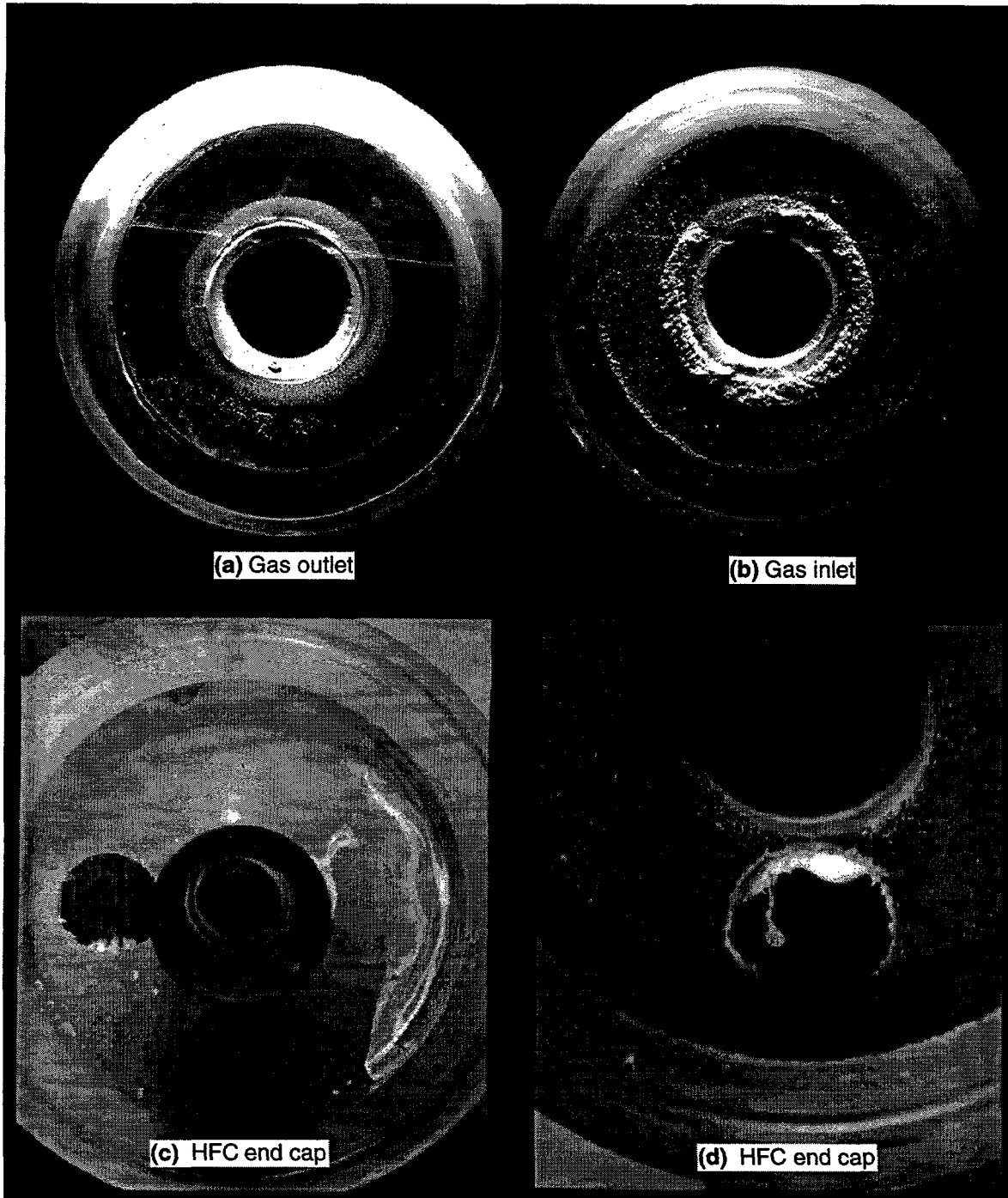
CM-3501-60B

Figure 7-10. Experimental setup for particle generation.



CM-3501-75A

Figure 7-11. Variation of ΔP_g across HFC.



CPM-3501-136

Figure 7-12. Pictures of HFC end caps (c), (d) and gas inlet (b) and outlet (a) ends of fibers. Particle cake (b) is formed at gas inlet end (b). A lump of particles is seen on the gas inlet (b) and magnified end caps (c) and (d).



CPM-3501-137

Figure 7-13. Enlarged view of a portion of particle cake formed at gas inlet end of HFC.

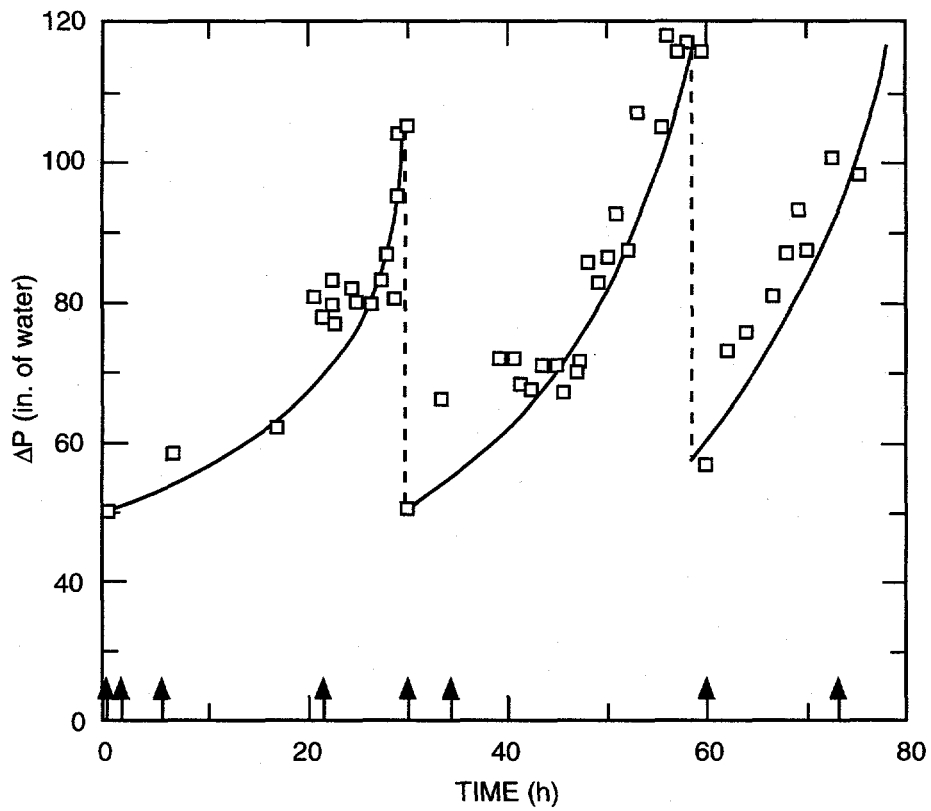
buildup is rather unexpected and we examined the problem from two different angles. First is the effect of this cake on the mass transfer efficiency. Secondly, we wanted to design a method to clear the particle cake and the blocked fiber bore.

We conducted mass transfer experiments using two different gas flow rates: 500 SCCM and 1000 SCCM. The composition of the simulated flue gas stream was 4000 ppm SO₂ and the balance N₂. The absorbing medium was water, which was maintained at a flow rate of about 10 mL/min. To observe the effect of the particle deposition on mass transfer, the mass transfer coefficient measurement experiments were conducted periodically during the particle deposition. Measurements were also made before and after the particle cake wash-out operation.

As shown in Figure 7-13, the particles were loosely packed to a thickness of about 1 mm. This formation was simply washed by using DI water. The rapid increase in pressure drop (ΔP) across the HFC (Figure 7-11) was due the fiber blockage and can, in principle, be cleaned by using a high pressure back-pulse jet. This operation was performed by a computer controlled solenoid (on-off) valve. The supply pressure was fixed at 80 psig. The valve settings were 1200 mSEC on and 500 mSEC off. The duration of the operation was 5 min. The ΔP across the HFC was noticed to drop down to normal pressures after back pulsing.

For every 30 h of particle deposition operation, ΔP was observed to reach close to 150 inches of water and the process was stopped for cleaning. Figure 7-14 shows these data. Visual observation after 60 h of deposition indicated that the cake formed is less severe compared with the first 30 h of operation. The reason could be the variation in particle size distribution that is being generated from the nebulizer and also the prevailing humidity conditions.

Several mass transfer experiments were conducted during the 80 h of operation. The resulting mass transfer coefficients (K_{og}) are plotted against time in Figure 7-15. The filled circles indicate the data with a 1000 SCCM gas flow, and the open circles indicate the trend with a 500 SCCM flow rate. At 30, 60, and 76 h, the experiments were conducted before and after the cleaning step. The decrease in K_{og} due to cake formation is about 5% to 8%. This cake formation is mostly due to plugging of the fiber bore. The cleaning step seems to reverse the phenomenon. Considering the overall trends of the two sets of data, the K_{og} is decreased by 20, which has two possible explanations. The first explanation, that the fibers are blocked, parallels the explanation of the pressure drop changes. However, if this were the case, because the pressure resets, the MTC should also reset to its initial value after every back pulse. Clearly it does not. Therefore, fiber blockage does not seem to account for the decrease in MTC. The second explanation, that some of the particles deposit on the fiber walls, implies that particles coating the fiber walls may reduce the mass transfer efficiency of the HFC. This explanation is more complex and merits further discussion.

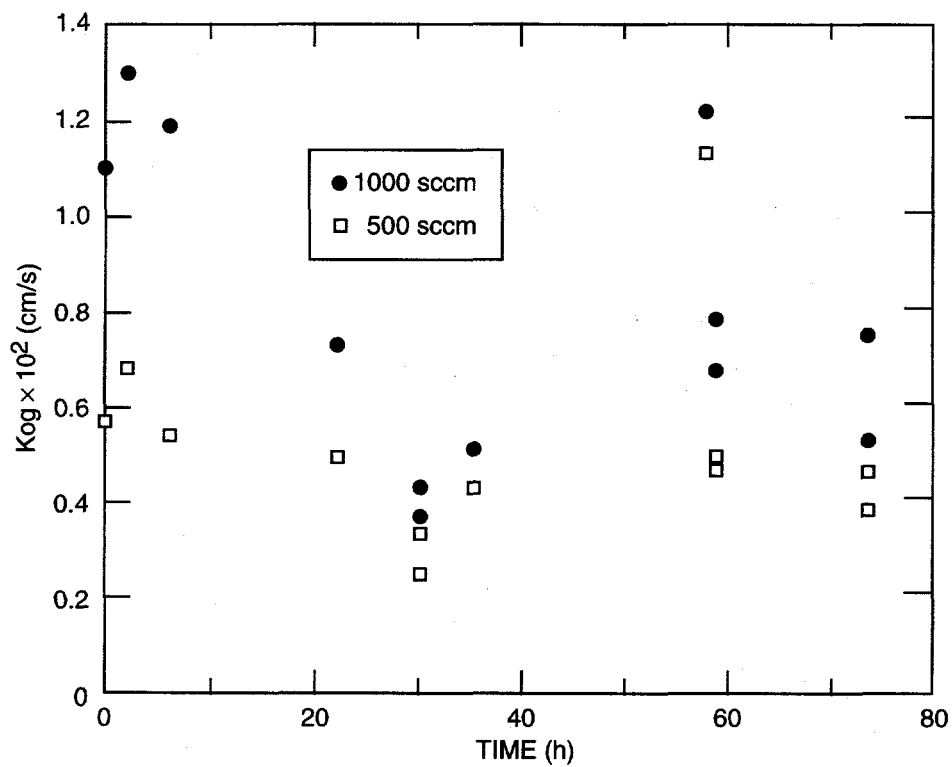


CM-3501-138

Figure 7-14. Pressure drop across the HFC during an 80-h period.

Arrows indicate halting the deposition, measuring the mass transfer coefficient, and restarting the deposition.

Dashed lines indicate a back pulse of air.



CAM-3501-139

Figure 7-15. Influence of particle deposition on the MTC.

Inlet gas SO₂ concentration = 4000 ppm. The MTC drops approximately 20% overall after 80 h of deposition.

Particles coating a porous membrane wall will reduce the mass transfer area of the membrane (we assume negligible changes in tortuosity due to the monolayer). The two parameters to consider are: the porosity of the monolayer itself and the extent to which the particles block the membrane pores underneath. The first parameter will affect the monolayer deposition time, while the second will affect the mass transfer area.

We approximate the monolayer to be a close packed structure (containing $0.25 \mu\text{m}$ particles) with a porosity of 0.2. The precise value of the porosity is largely unknown. Figure 7-7 shows the capture efficiency to be 1% for a $0.25 \mu\text{m}$ particle. We can use this efficiency to calculate the time required for a monolayer deposition of particles along the fiber's inner wall as:

$$t = \frac{\left(3.27 \times 10^{12} \frac{\text{particles}}{\text{monolayer}}\right) \left(2.05 \times 10^{-14} \frac{\text{g}}{?}\right)}{(0.01)(3.51 \times 10^{-4} \text{ g/min})} = 318 \text{ h} \quad (7-1)$$

where the number of particles in a monolayer is given by the ratio of the module surface area (based on the fiber inner diameter) covered by the monolayer [$2003 \text{ cm}^2 (1-0.2) = 1602$] to the cross-sectional area of a $0.25 \mu\text{m}$ particle ($4.9 \times 10^{-10} \text{ cm}^2$), the weight of a particle is given by the product of the particle density (2.5 g/cm^3) and the particle volume ($8.2 \times 10^{-15} \text{ cm}^3$), and the particle feed rate is given by the product of the gas flow rate ($11.71/\text{min}$) and particle concentration in the gas (30 mg/m^3). Hence, we estimate a monolayer deposition time of 318 h, assuming a monolayer porosity of 0.2.

The extent to which the particles of this monolayer block the membrane pores underneath is more difficult to determine. We know only the particles size distribution in the feed gas (see Figure 7-15) and not the pore size distribution of the membrane wall. Precise calculations for the effect of monolayer coverage on the reduction of mass transfer area requires knowledge of both distributions, not knowledge of just one. To be sure, the average particle size ($0.25 \mu\text{m}$) is larger than the average size of the fiber wall pores ($0.05 \mu\text{m}$), but we do not have information on the precise surface coverage characteristics of the particle monolayer.

If we assume the extreme case that a particle blocks all membrane pores underneath it, then the change in mass transfer area is directly proportional to the monolayer porosity. Specifically, the mass transfer area is reduced by 80% when the monolayer porosity is 0.2. As a result, the apparent MTC will drop 80% in 318 h, and we therefore infer the MTC will drop 20% in 80 h. However, if we assume that a particle only partially blocks the membrane pores underneath it, then the reduction in mass transfer area will be less. For example, if the monolayer reduces the mass

transfer area by only 30%, then the time for monolayer deposition would still be 318 h, but the MTC decreases only by 7.5% in 80 h.

Experimentally, we observed a drop in the MTC of approximately 20% in 80 h, corresponding to the extreme case of complete blockage. Hence, we suspect that the particles probably do coat the membrane surface and reduce the mass transfer efficiency of the fibers as implied in these calculations, even though the particle feed rate used in Eq. (7-1) is high, because all the particles did not enter the HFC as shown in Figures 7-12 and 7-13. The precise reduction remains difficult to quantify and correlate, because the fiber pore structure and particle size/shape are unknown, and these influence the nature and severity of the mass transfer changes.

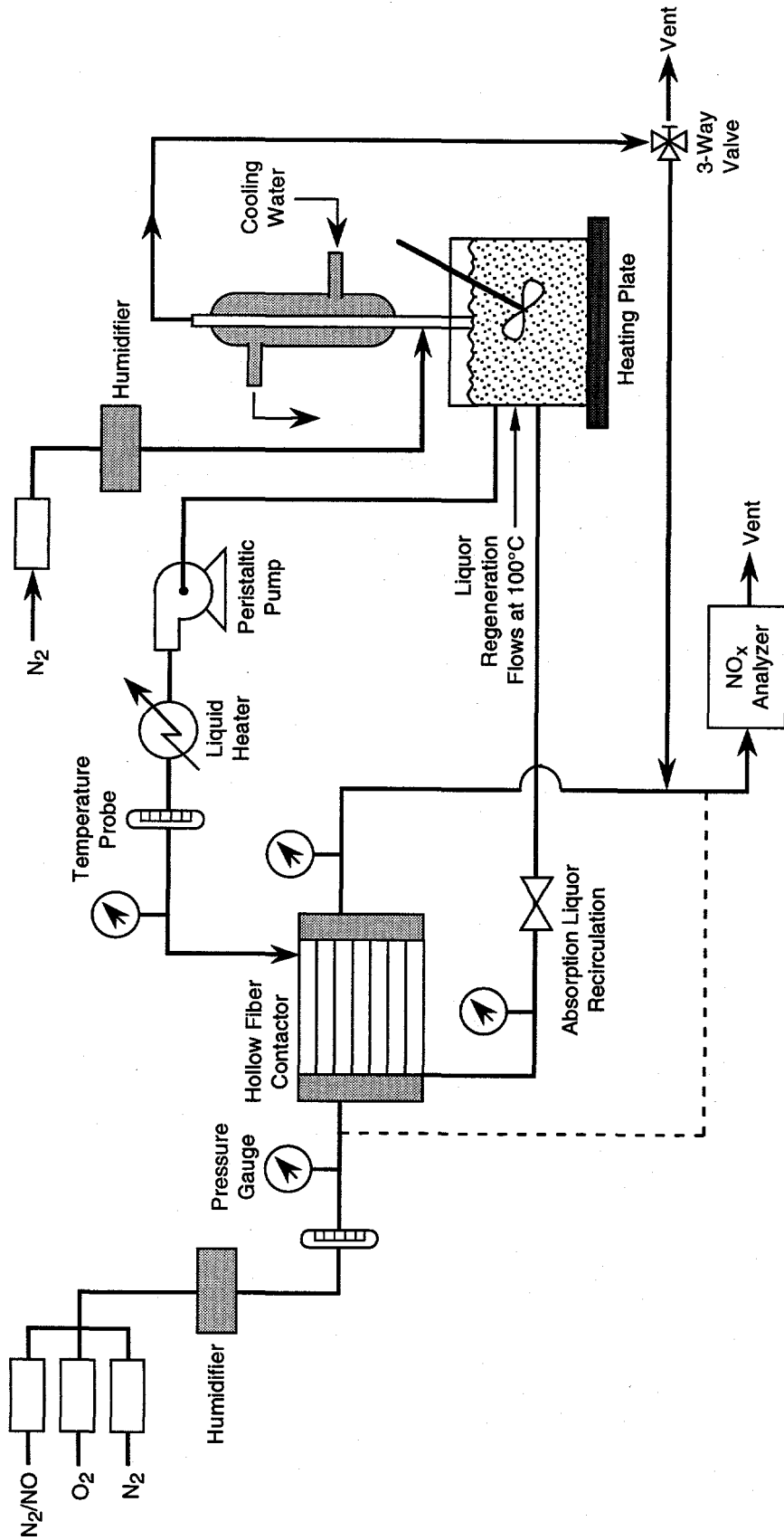
TASK 8: INTEGRATED NO_x LIFE TESTS

Liquid scrubbing systems for NO_x have traditionally been plagued by degradation of performance over time, with a subsequent need for convoluted liquor regeneration schemes. Therefore, it is essential to determine whether or to what extent there is any loss with time in the performance of the NO_x absorption/desorption system. In Task 2, we showed Co(II)-phthalocyanine as a promising candidate for NO_x absorption in the presence of O₂. In Task 5, we demonstrated the superior mass transfer characteristics of a Co(II)-phthalocyanine scrubbing system in a 300-fiber HFC. Consequently, the objective in Task 8 was to devise a continuously operating system for determining if the NO_x absorption/desorption chemistry has the potential to be commercially robust.

For the integrated tests, we used the absorption part of the experimental scheme from Task 5. Ideally, we needed to operate the desorption system and not impede the absorption process at the steady condition. This implies that by using the desorption process, one has to desorb the same amount of NO as is being absorbed by the aqueous NO_x scrubbing solution. We chose to operate the desorption apparatus at about 100°C and to design a system that condenses back any water that is being evaporated from the Co(II)-phthalocyanine solution.

For the NO desorption process, we looked at several possibilities (such as indirect steam stripping and using direct inert gas contacting). Use of inert gas was appealing because we can pass this gas through the NO_x analyzer to determine the NO concentration. In this fashion, we can observe the efficiency of the designed system and also its integrity. Knowing these factors, we devised a scheme for this closed-loop operation, as illustrated in Figure 8-1. The heart of the desorption process is a three-necked flask (200 mL) that acts as a reservoir for the NO_x scrubbing solution. This solution is recirculated between this flask and the HFC using a peristaltic pump. Two of the three ports of the flask are used for liquid entry and exit. The third port is fitted with a condenser and also serves as the NO stripping gas inlet and outlet section, as shown in Figure 8-1. The contents in the flask are maintained at 100°C using a hot plate, and vigorous stirring is accomplished by a magnetic stirrer.

We conducted a combined absorption and desorption test using the above experimental arrangement. Co(II)-phthalocyanine solution (0.1 M) was recirculated between the 300-fiber HFC and the desorption flask at a flow rate of about 3 mL/min. The gas flow through the lumens of



CM-360583-32B

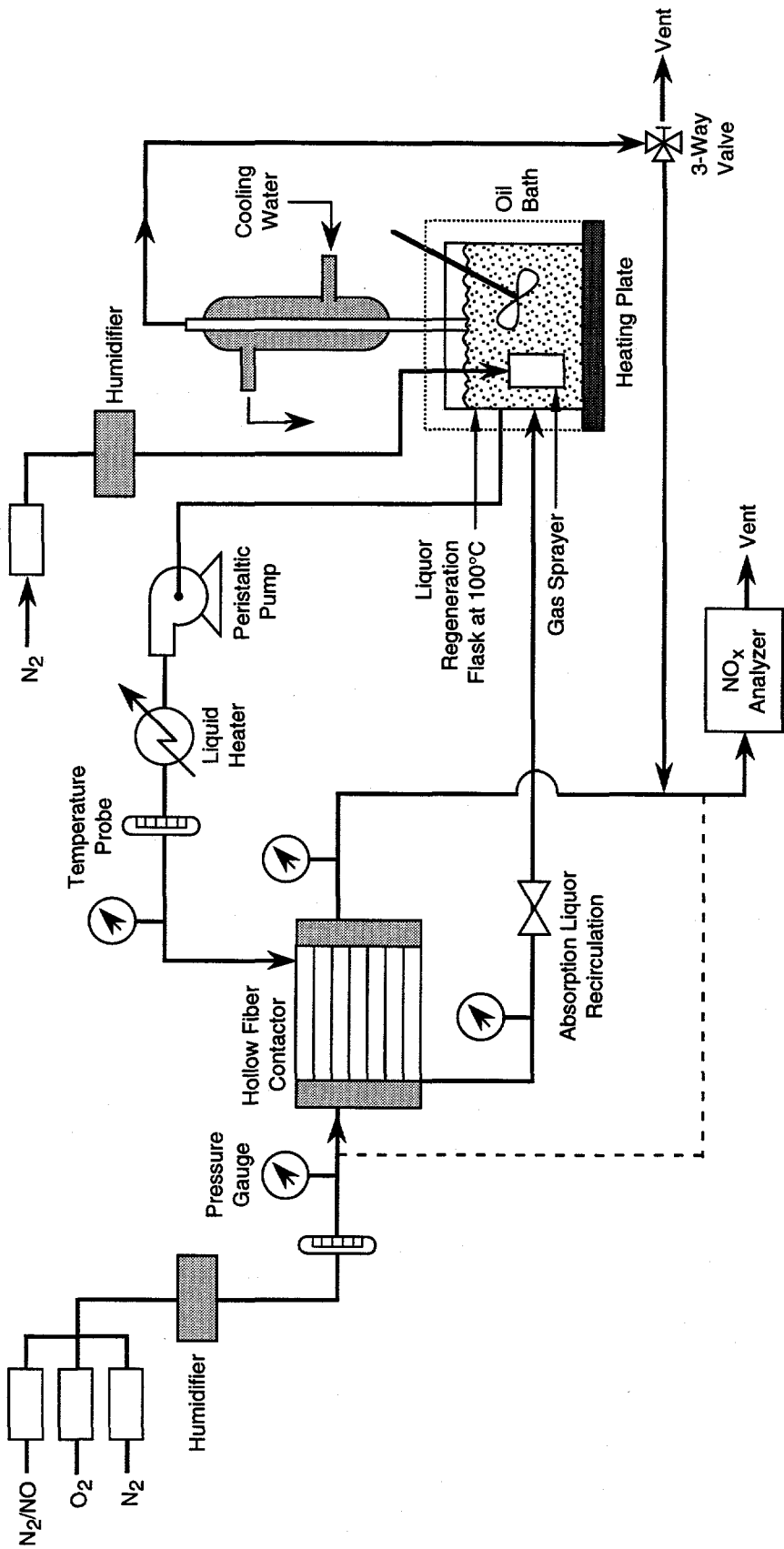
Figure 8-1. Schematic of the NO_x absorption and desorption experiment.

HFC was 100 sccm. This feed gas mixture was prepared by blending appropriate amounts of NO, O₂, and N₂. The composition of gas was 500 ppm NO, 4.5% O₂, and balance N₂. Pure N₂ was flowed to the bottom of the condenser section of the desorption apparatus at a rate of 20 sccm. The temperature of the desorption flask was maintained at 100°C with a heated oil bath. The liquid inlet temperature into HFC was 45°C and that of the gas stream was 25°C.

The duration of the run was about 6.5 h. During the experiment, both the HFC exiting gas stream and the desorption exiting stream were monitored for their NO concentration. The NO removal rate in the HFC was almost steady at 72% (absorption rate = 2.67×10^{-8} mol/s) during the run. However, the desorption rate was ten times lower than the absorption rate (desorption rate = 2.8×10^{-9} mol/s). Under steady operating conditions, the absorption and desorption rates must be equal. A possible explanation of this lack of equality is that the desorption process is too slow because of the mass transfer resistances. These mass transfer resistances occur because the decomplexed NO has to travel to the surface of the liquid to be swept away by the gas stream. Another explanation is that the capacity of Co(II)-phthalocyanine is so high that the system is running under pseudo steady state conditions. A simple calculation (assuming no mass transfer resistances in desorption) shows that the latter explanation can be ruled out. Therefore, to accelerate the desorption rate of the process, we modified the experimental scheme as shown in Figure 8-2. In this arrangement, the gas stream is sparged in the liquid contained in the desorption flask. Also, the gas flow is increased to 300 sccm to increase the driving force between the liquid and the gas.

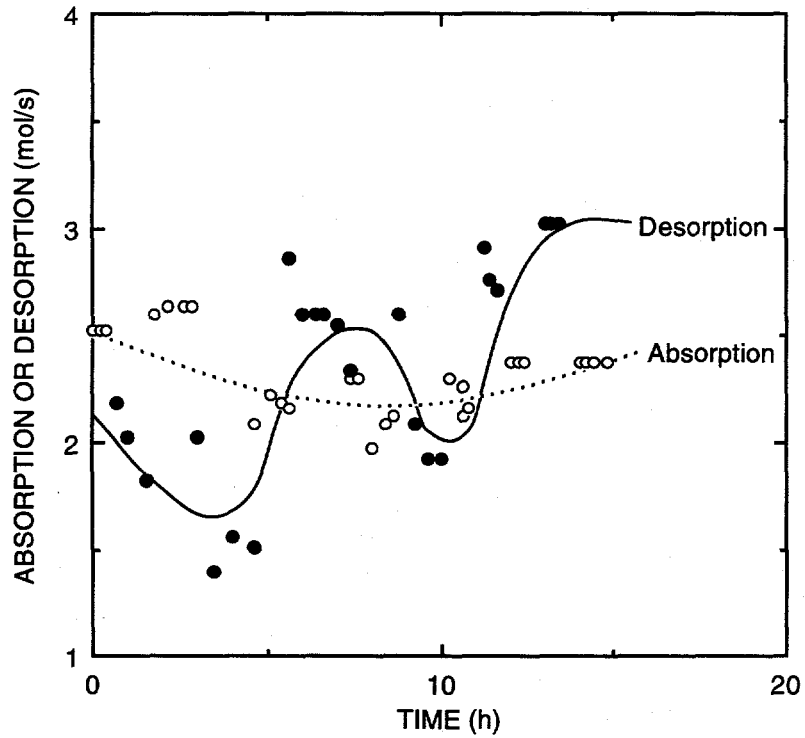
Both absorption and desorption results are shown in Figure 8-3. During this 15 h of operation, we did not observe any deactivation of Co(II)-phthalocyanine. Also, the rate of absorption and desorption are approximately equal. At the end of 4 h of operation, we observed some leaks of Co(II)-phthalocyanine spilling into the oil bath causing fluctuations in our readings (see Figure 8-3). We fixed the leaks and steady operating conditions were maintained during the entire operation.

Problems related to the desorption step were fixed and we continued collecting data using the combined absorption-desorption apparatus. The 100 mM Co(II)-phthalocyanine solution was recirculated between the 300-fiber HFC and the desorption flask (250 mL) at a 3 ml/min flow rate. The flue gas flow rate through the lumens of the HFC was 100 sccm. This feed gas stream had a composition of 500 ppm NO, 4.5% O₂, and balance N₂. Pure N₂ (sweep gas) after humidification was sparged into the liquid contained in the desorption flask. The sweep gas stream flow rate was maintained at 300 sccm. This high-flow rate compared to feed was used to create a higher driving force for NO between the liquid phase and the sweep gas phase.



CM-360583-32D

Figure 8-2. Schematic of the modified NO_x absorption and desorption experiment.



CM-3501-94

Figure 8-3. Simultaneous NO_x absorption and desorption tests using Co(II)-phthalocyanine.

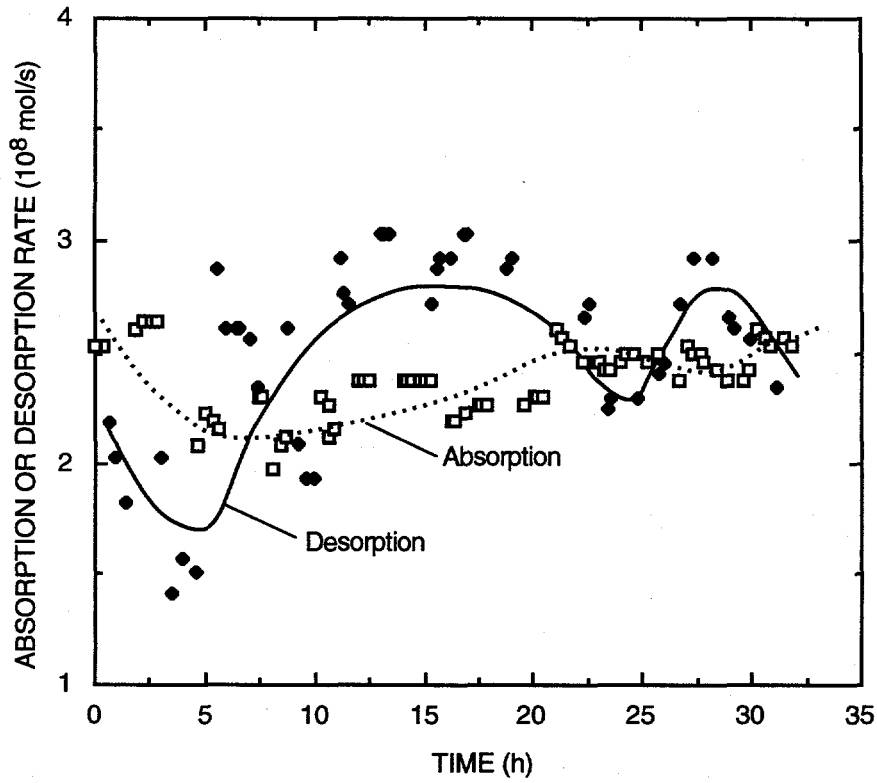
The outlet gas streams from both the 300 HFC and the desorption flask were monitored for NO concentration. The results are plotted in Figure 8-4. The evaporation losses due to repeated exposure of the liquid to the gas stream in the HFC, as well as in the desorption flask, were monitored by watching the liquid level in the flask. The losses were small. However, the fluctuation in data points could be attributed somewhat to these concentration changes that were due to the evaporation of water. Figure 8-5 shows an additional 10 h worth of data on the simultaneous absorption/desorption of NO. Despite some fluctuations, both absorption and desorption rates are approximately equal to one another.

Further experimentation was hampered by the NO_x analyzer. The analyzer began drifting by about 5% per hour, leading to false readings. We suspended testing and sent the analyzer out for repair.

During the time the analyzer was being repaired, we set the apparatus up for automatic data acquisition and control. Specifically, the absorption/desorption output from the NO_x analyzer and the temperature and pressure of all streams were set up to be continuously monitored. A safety feature was also incorporated to shut the system down when any abnormal behavior is detected. With this automatic data acquisition and control system, individual ('single-stretch') runs of 24 to 48 h (instead of 8-10 h as previously required) or more were continuously monitored, thus improving the efficiency and quality of data collection.

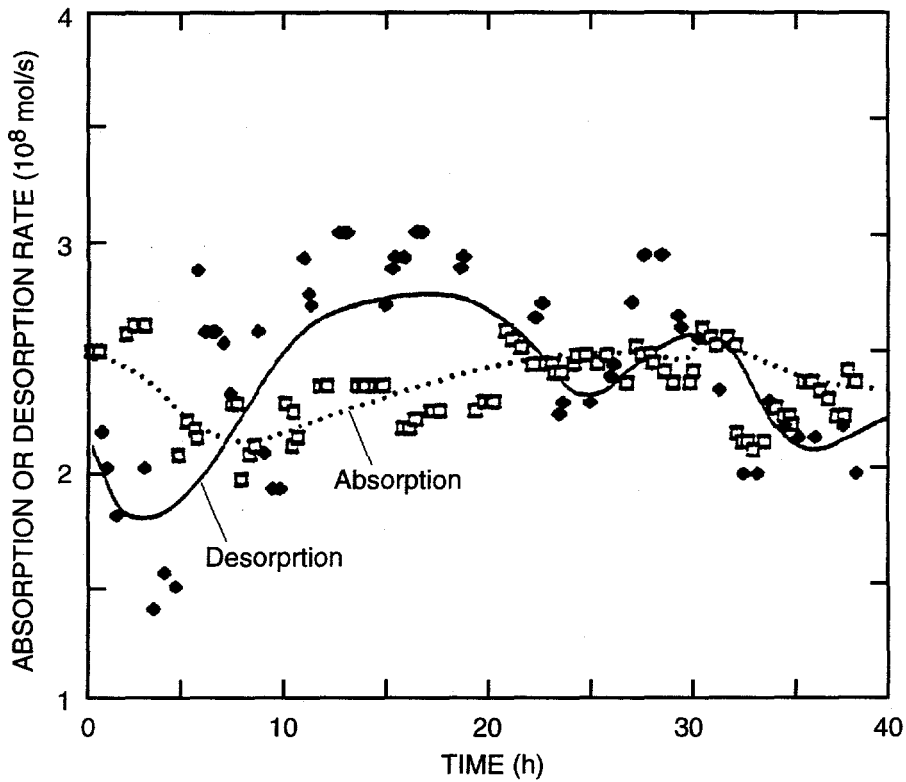
Figure 8-6 shows the data acquisition and control setup using a computer. One of the important features of this automated system is to circulate the warm fluid (Co(II)-phthalocyanine solution) continuously through the absorber (300-fiber HFC). This circulation operation prevents precipitation inside the fibers, leading to decreased efficiency of the HFC. As shown in Figure 8-6, the peristaltic pump is connected to the computer and will automatically shut off if any system anomalies are detected (i.e., sudden pressure decreases or increases). The computer also saves the data to a file that can be opened and analyzed in a spreadsheet or other computer program (Labview or Excel).

We tested the analyzer, upon its return from the repair shop, to make sure it was in working condition. A calibration gas (Liquid Carbonic, Menlo Park, CA) of 480 ppm NO was used to calibrate the unit. A second calibration gas of 48 ppm was used to test the consistency of the unit. A reading of 46 ppm was obtained; about a 4% error. Given that the range of the first calibration gas is ten times greater than that of the second, the error is acceptable. For all the experiments, the unit was calibrated using the 48 ppm standard cylinder, since this is in the vicinity of the process conditions.



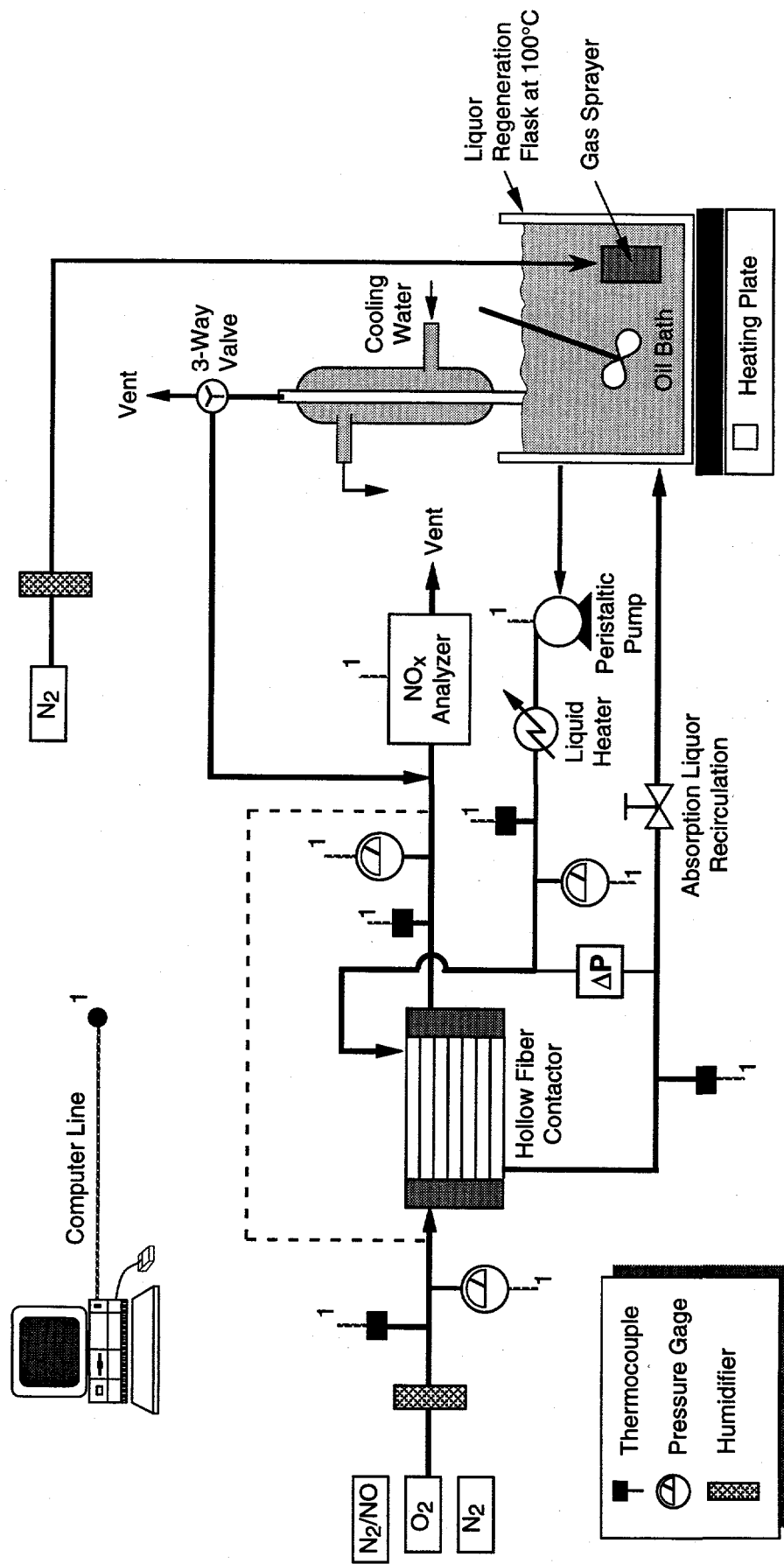
CAM-3501-96

Figure 8-4. Simultaneous NO_x absorption and desorption tests using Co(II) - phthalocyanine (30 h of operation).



CM-3501-97

Figure 8-5. Simultaneous NO_x absorption and desorption tests using Co(II)-phthalocyanine (40 h of operation).



CM-360583-32E

Figure 8-6. Schematic of the modified NO_x absorption and desorption experiment.

The automated data acquisition system includes six mass flow controllers that were calibrated to give the desired flow. Table 8-1 shows the function, desired flow, and required setting for each controller.

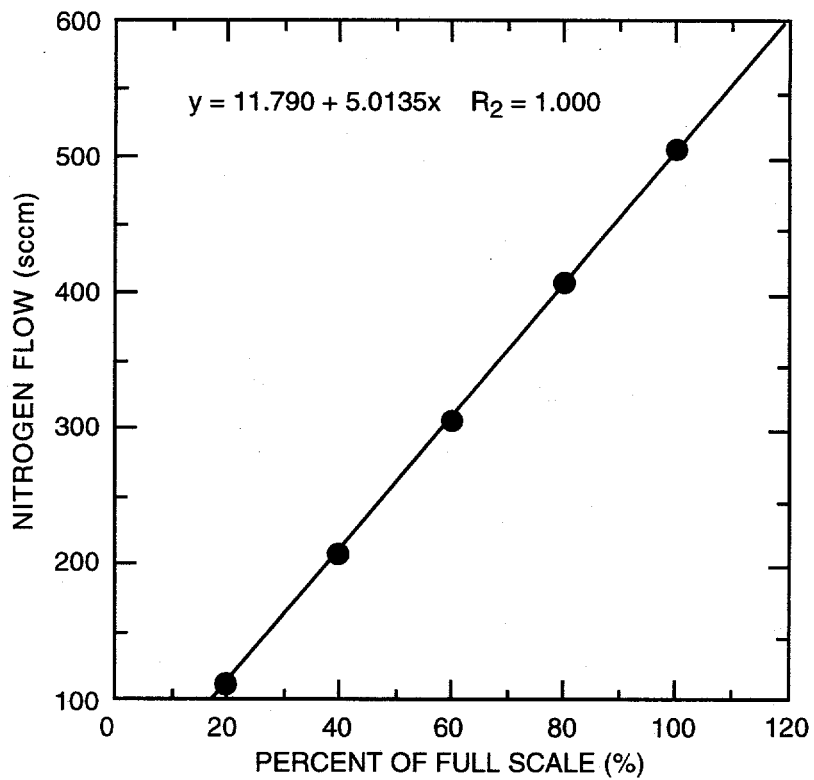
Table 8-1
MASS FLOW CONTROLLER (MFC) AND SETTINGS

MFC Number	Function	Type of Gas Used	Desired Flow	Required Setting
1	NO Feed	1% NO in N ₂	4.9 SCCM	4.4 SCCM
2	N ₂ Feed	Nitrogen	90.6 SCCM	84.2 SCCM
3	O ₂ Feed	Oxygen	4.5 SCCM	16.5% FS
4	Make-up Stream	Nitrogen	500 SCCM	94.7% FS
5	Make-up Stream	Nitrogen	100 or 300 SCCM	24.9% or 82.7% FS
6	Stripping Gas	Nitrogen	300 SCCM	283 SCCM

As shown in Table 8-1, MFC 5 has 2 desired settings, because the NO_x analyzer requires a constant flow of 900 SCCM. When the exit stream from the absorber (100 SCCM) is analyzed, a make-up gas flow of 800 SCCM is required. This flow is achieved by MFC 4 in parallel with MFC 5 set in the 300 SCCM mode. When, on the other hand, the stream from the desorber (MFC 6 at 300 SCCM) is analyzed, a make-up gas flow of 600 SCCM is obtained by MFC 4 in parallel with MFC 5 set in the 100 SCCM mode. Figure 8-7 is a representative calibration curve for MFC 5.

We developed a method to determine the concentration of Co(II)-phthalocyanine in scrubbing solution. Standard solutions at different concentrations were prepared and analyzed on a UV spectrophotometer. Appropriate absorption peaks were determined (based on the standards) to be at 218 and 320 nm wavelengths. A standard curve for each wavelength was plotted and shown to have excellent linearity (Figure 8-8). Therefore, these standard curves were used to analyze unspent scrubbing solution as discussed below.

The UV spectrophotometer method consists of obtaining a small sample (about 400 µL) of solution and diluting it with water to obtain 1 L total solution. A portion of the diluted sample is



CM-3501-101

Figure 8-7. Flow calibration curve.

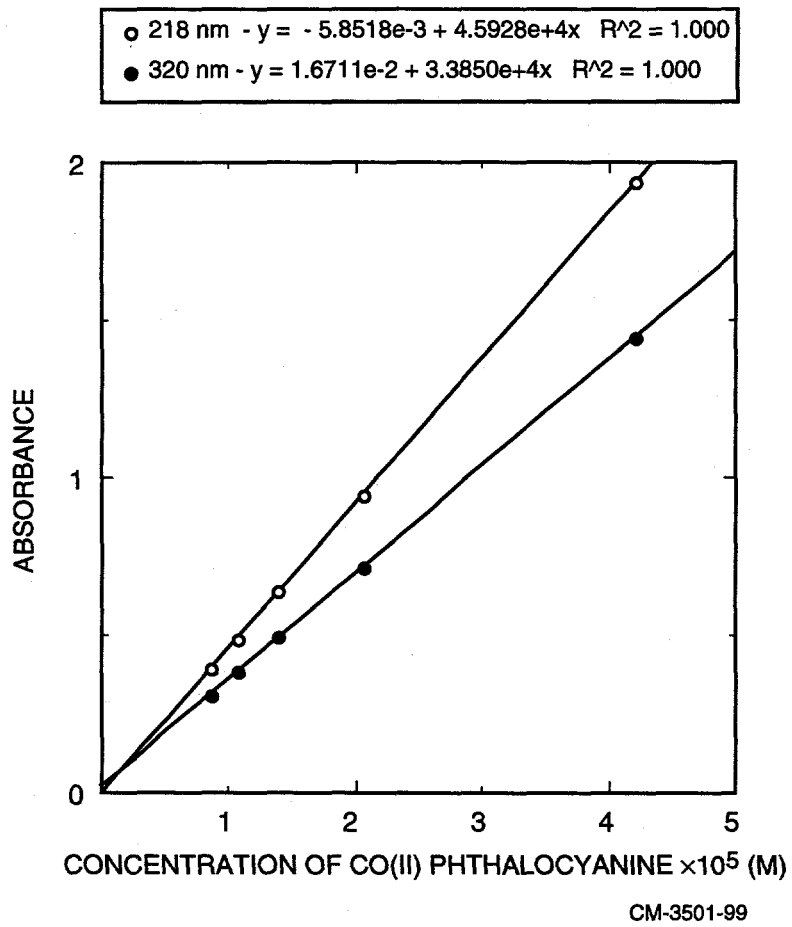


Figure 8-8. Co(II) phthalocyanine - standard curves.

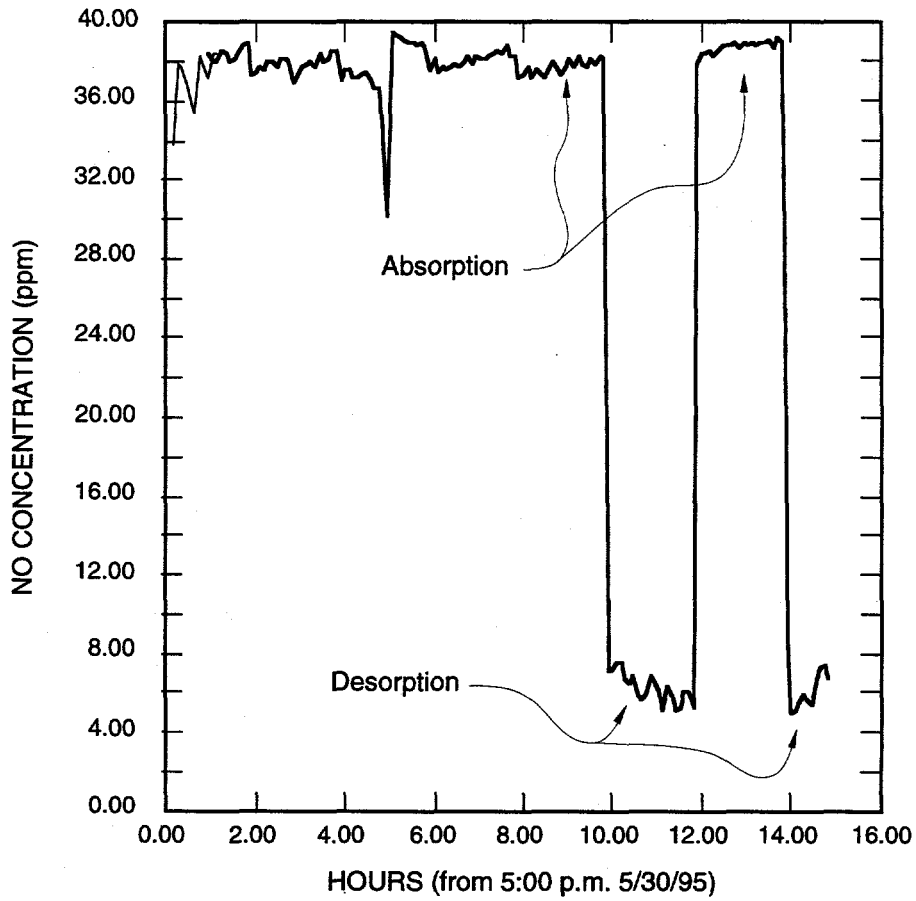
analyzed on a Hewlett Packard 8452A diode array spectrophotometer. The absorbance at 218 and 320 nm is recorded and compared to a known standard curve. The prepared solution for the experiment was determined to be about 95 mM Co(II)-phthalocyanine. The solution inside the contactor, however, was determined to be about 75 mM. This discrepancy is from a small volume of water that remained in the contactor from our initial leak tests with water.

On May 16, 1995, we began the first run using NO and the Co(II)-phthalocyanine solution. The exit stream from the absorber was monitored for NO content. Initially, the readings were around 2-3 ppm, which was expected. The reading did not increase, however, for several hours. At this point, we thought that because of the large volume of liquid (about 450 mL) and the dilute (500 ppm NO and 100 SCCM) feed stream, the system would take an exceedingly long period of time to reach steady state. We decided to increase the feed concentration to 1800 ppm NO. The system was run in this configuration overnight. The exit gas from the desorber the next morning showed only 10 ppm NO. A simple calculation showed that the system was still not at steady state (mass balance closure was only about 30%), yet the concentration of the exit stream from the absorber was fairly constant over a 16 h period (about 11-12 ppm). To check the gas leaks in the plumbing, we decided to shunt the gas side of the HFC. This exercise revealed no such problem.

After placing the contactor back in line, however, the behavior of the system changed. The exit stream from the absorber was about 1350 ppm (feed is 1800 ppm), while the exit after the desorber was about 30 ppm. Encouraged by this change, we set the feed back down to 500 ppm NO and let the system run for about 15 h (total time now logged by the liquid is about 126 h). As shown in Figure 8-9, the absorption and desorption characteristics are completely opposite of what was expected. We expected that, at a steady state, the exit gas stream after absorption would contain only about 20%-30% of the NO in the feed. For this test, about 70% of the NO in the feed was noticed after the absorber. In addition, the mass balance closure was only about 80%.

Either the absorber plumbing system is faulty (including leaks, plugged fibers, etc.) or the liquor is completely saturated with NO. The former seems more plausible than the latter because previous tests of about 40 h showed that no degradation of the Co(II)-phthalocyanine solution occurred.

In an attempt to close the mass balance between absorption and desorption processes, we tried using a simple glass flask in place of the HFC and sparging the NO gas stream through the scrubbing liquid (water) contained in the flask. This operation posed serious difficulties in maintaining a constant amount of liquid in the flasks. These difficulties arose because the gas and liquid are directly in contact with one another (unlike HFC operation) and therefore the recirculation (flow) of liquid between absorption and desorption flasks depended on several



CM-3501-100

Figure 8-9. Absorption and desorption processes exiting gas NO concentrations as a function of time.

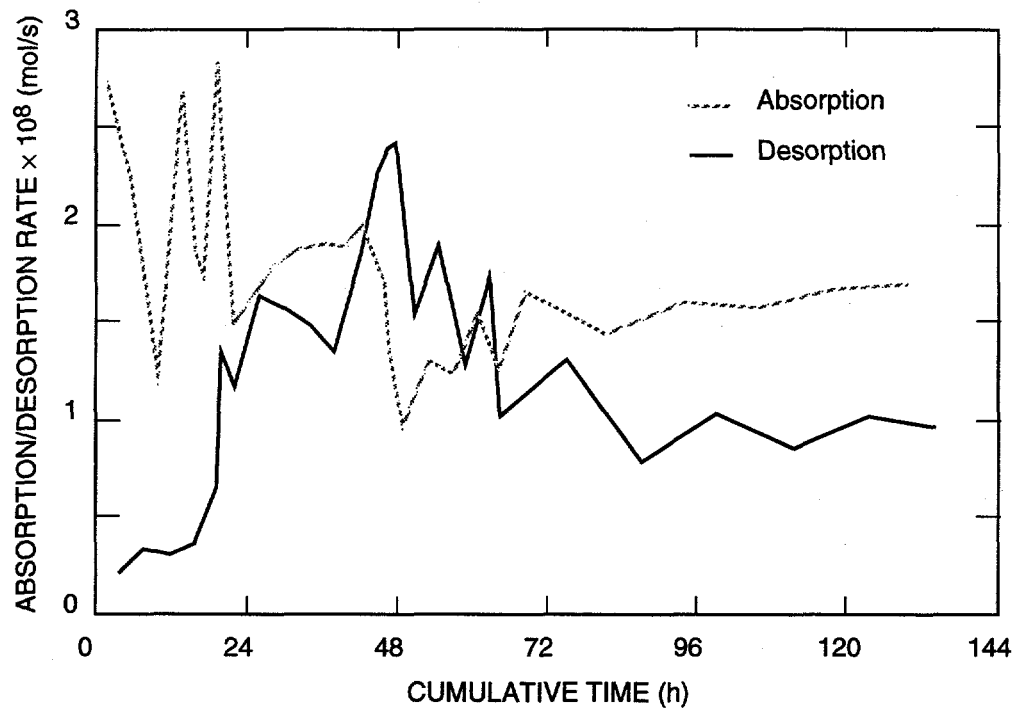
factors: (1) the pressure differential generated by the peristaltic pump, (2) the pressure of gas contained in the head space of each flask and, 3) the gravitational pressure head. Therefore, we could not maintain the flow between the processes. However, thorough cleaning and testing of the HFC seemed to solve the problem, as the mass balance of the system approached closure after several hours of operation.

We obtained data for a period of about 140 h (cumulative time logged on the scrubbing liquor). Figure 8-10 shows the absorption/desorption characteristics of the liquid over this time. As expected, during the starting period, the absorption rate is complete (100%) and the desorption rate is zero. By the end of the second day of the operation, both absorption and desorption rates became stabilized. From the data shown, the average NO removal rate calculated is 50%. However in Task 5, 85% NO removal rates were demonstrated using the same 300-fiber HFC. Therefore, we believe that the desorption process is limiting the overall efficiency of the system.

To increase the efficiency of the desorber, the operation was made counter-current and the mass transfer area was increased with the help of baffles. Figure 8-11 is a schematic of this arrangement. The stripping section has a condenser affixed at the top that is filled with glass beads. The glass beads are supported by a fritted glass barrier, allowing gas to flow up and liquid to flow down. Shortly after fabricating and installing the stripping section, we experienced difficulties in calibrating the NO_x analyzer due to some scrubbing liquid entrained into the equipment. We hope to resolve the problem by simply dismantling and cleaning the affected parts.

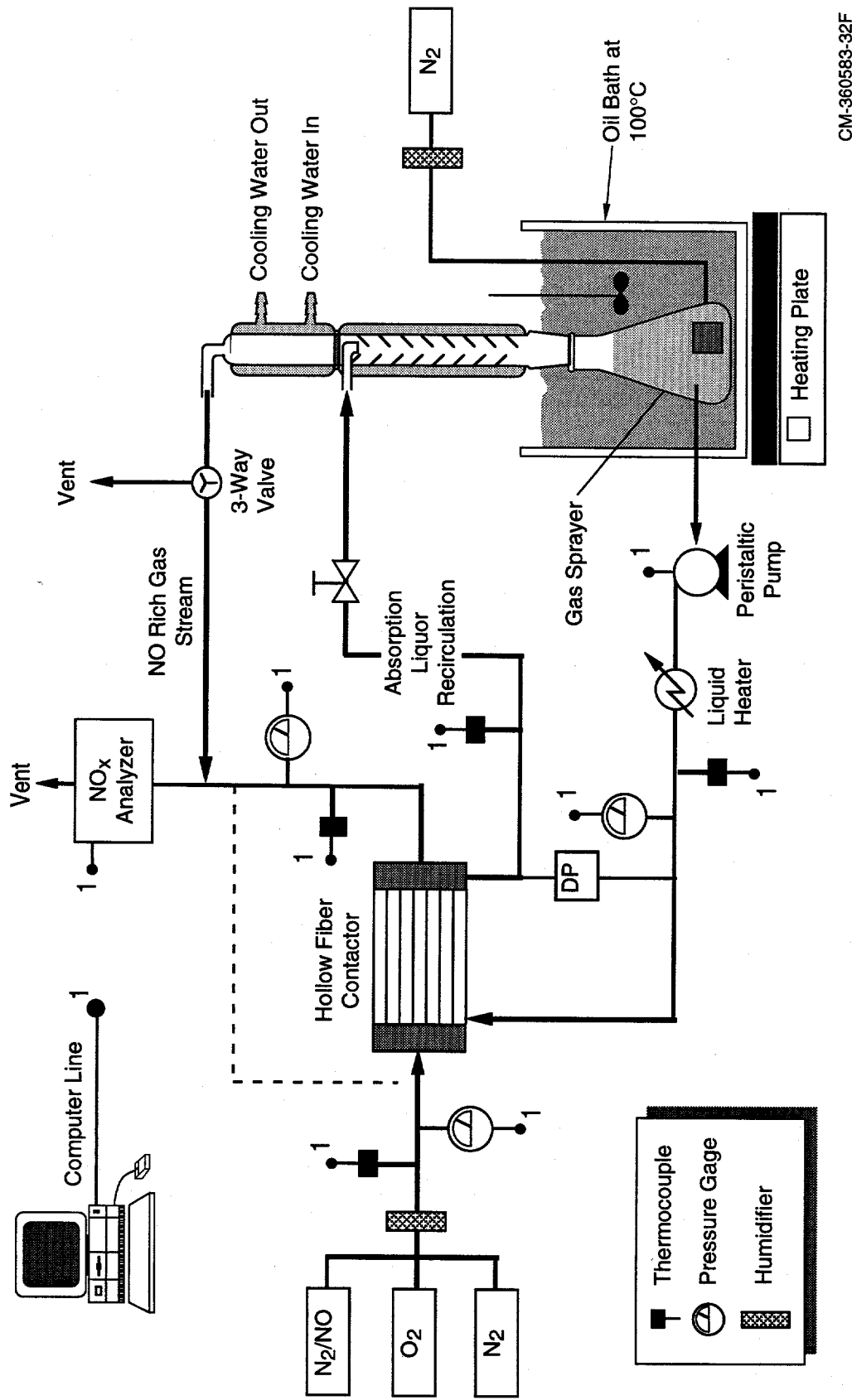
After restarting the system, we noticed that the removal of NO from the feed stream by the HFC was very poor. Examination of the contactor revealed that solid precipitate had clogged fiber pores, resulting in lower mass transfer area. Cleaning the contactor proved a much harder job than originally anticipated. After thorough cleaning, we noticed a water leak from the shell side to the tube side. This was due to either a broken fiber or to hydrophilic pores. Subsequent testing of the contactor pointed to the change in characteristics of the fiber; the breakthrough pressure was 5-10 psig for water. If a fiber was broken, the breakthrough pressure would be much less than this. A new HFC was located in our lab and tested. The new contactor has 1155 fibers, and has a slightly different liquid flow configuration. The breakthrough pressure of this contactor is approximately 70 psig. This contactor was installed into the NO_x absorption/desorption system.

Meanwhile, we also synthesized about 40 g of the 4-4'-4"-4''' tetra sodium salt of Co(II)-sulfophthalocyanine for our future requirements. (See Task 16).



CM-3501-102

Figure 8-10. NO_x scrubbing solution lifetime data.



CM-360583-32F

Figure 8-11. NO_x absorption and desorption experimental setup (enhanced desorption operation).

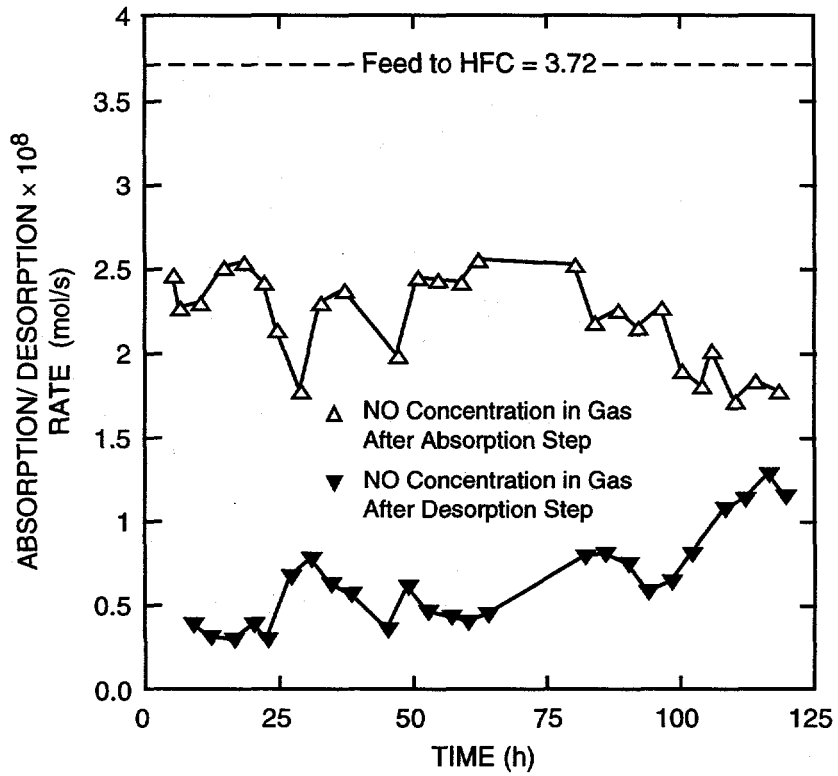
We leak tested the apparatus with a 1150 fiber HFC and determined that it was suitable for our purposes. We resumed testing of the NO_x scrubbing solutions and logged an additional 120 h (see Figure 8-12). The horizontal (broken) line in the figure represents the NO concentration in the feed stream to HFC. The top and bottom curves represent NO concentration in the gas streams from absorption (HFC) and desorption devices, respectively. At steady state, the sum of NO concentrations exiting the absorption and desorption devices must equal the feed concentration. Therefore, from the figure, we can infer that the process is at an unsteady condition and, with an increase in time, the scrubbing solution capacity for NO absorption will also increase. The NO removal after 120 h of operation was about 54%. This behavior demonstrates that the solution is not deactivating.

We installed some additional safety features (i.e., check-valves) that allowed us to run for longer continuous periods of time. We collected an additional 400 h of experimental data using the modified NO_x absorption/desorption system. Figure 8-12 shows the overall lifetime of the solution to date. Figure 8-13 indicates the absorption rate in the HFC and also the desorption rate in the stripping device. Despite some noise due to either the change of the contactor or the shut-off of the apparatus, the trend in absorption/desorption behavior is steady. Therefore, we believe that the Co(II)-phthalocyanine solution performance is unchanged during this test period (650 h). The low removal rates can be attributed to the inefficiency of the stripping device; the rate limiting step.

As pointed out by DOE, this presents a problem during the characterization of the subscale prototype modules. The most reasonable solution would be to use another HFC in place of a conventional stripper. However, the maximum operating temperature for polypropylene fibers is about 70°C. Therefore, use of another HFC as a stripper is not possible by a polypropylene fiber contactor because of the higher temperatures (~100°C) involved in the stripping system.

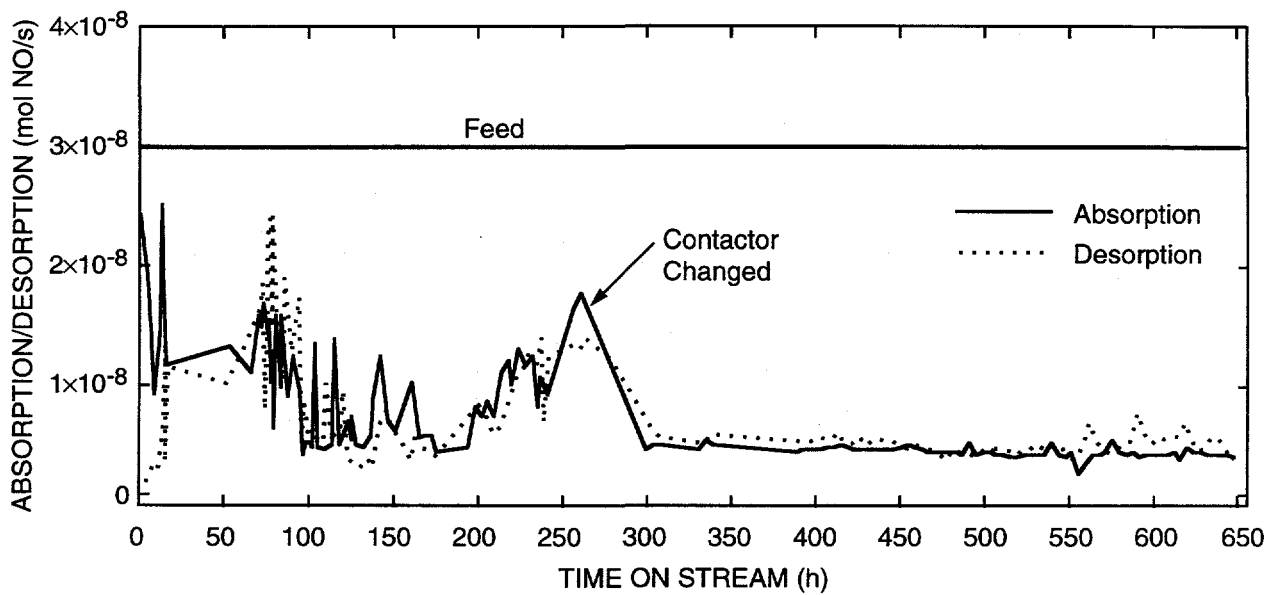
Because the desorption operation is conducted at about 100°C, a large, packed, tower (e.g., packed with glass beads) seems a feasible alternative. The glass beads would provide higher, gas-liquid, interfacial areas leading to sufficient desorption rates. In our previous Co(II)-phthalocyanine regeneration tests, we employed the gas sparging arrangement.

In summary, the lifetime studies of the NO_x stripping liquor show that little or no deactivation occurs over time. Our data looks promising and gives precedent for large scale testing.



CM-3501-117

Figure 8-12. NO_x scrubbing lifetime studies (August 1995).



CAM-3501-125A

Figure 8-13. NO_x scrubbing solution lifetime data.

TASK 9: PERFORMANCE OF SCALABLE MODULES

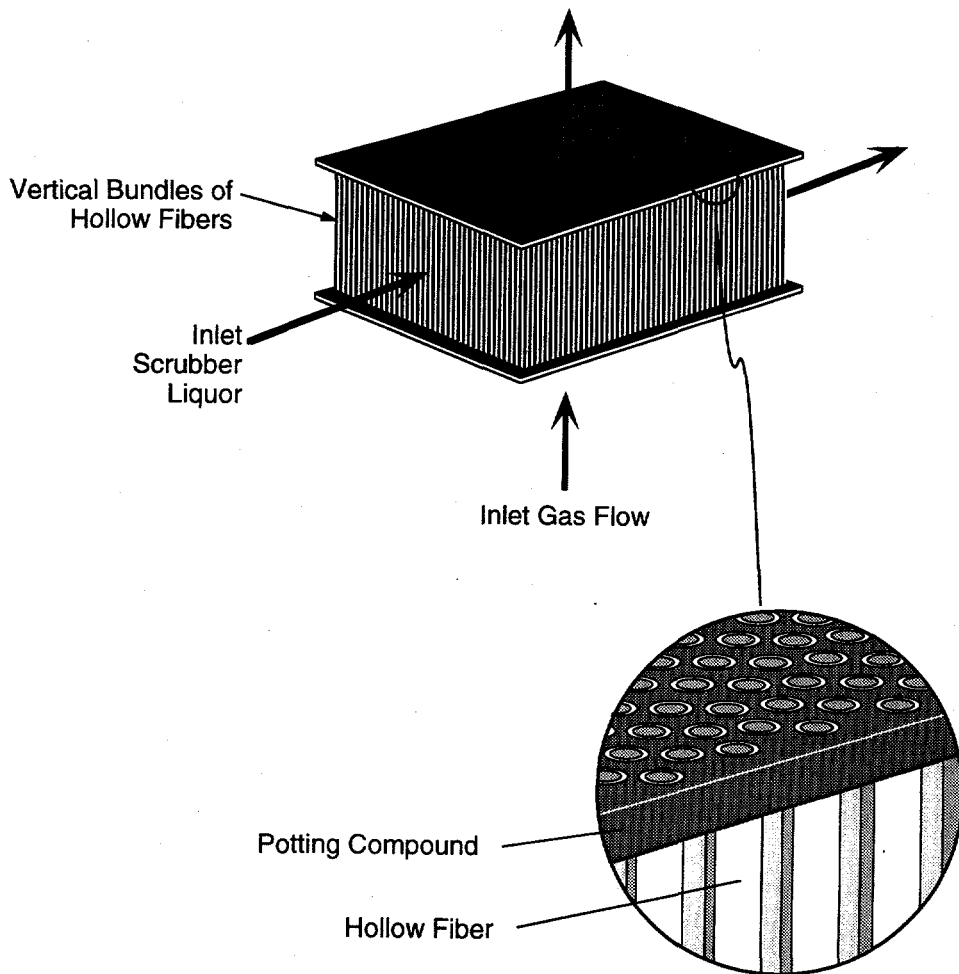
Because of the need for billions of (approximately 30 cm long) fibers to treat the flue gas from a 500 MW(e) plant, it is critical to establish the mass transfer characteristics of a module that can be scaled up to a prototypical size. To appreciate this point, one must recognize that approximately 250,000 modules of 2 inch diameter would be required to provide one billion fibers. Such an arrangement would provide a ducting, plumbing, and maintenance nightmare in a full-scale plant and clearly would not be economical or workable. A new design concept, such as rectangular modules, is needed for a full-scale plant. Therefore, the objective of Task 9 was to develop the mass transfer fundamentals of rectangular modules.

The term "scalable module" is an important concept because it influences our ability to think about an eventual application of HFC devices to a 500 MW(e) power plant. We use the term to mean a module that exhibits the important phenomena that would appear in modules of the 500 MW(e) plant. For example, mass transfer in the rectangular (square) module will be different than that in the cylindrical modules because the flow pattern in a large-scale rectangular module absorber or liquid-liquid extractor will be cross-flow, not counter-current, as shown in Figure 9-1. Probably more importantly, flow distribution and liquid pressure drop behavior will be much different in a large "scalable" module than in our laboratory modules. Therefore, Task 9 was designed to obtain the fundamental mass transfer behavior, including issues of flow distribution and pressure drop, on modules that reflect these basic features of large-scale modules with gas and liquid flow rates in the range of 5-10 cfm and 1-5 L/min, respectively.

DESIGN OF RECTANGULAR MODULES AND EXPERIMENTAL APPARATUS

We began a preliminary evaluation of the efficacy of the rectangular modules. The assumptions involved in the calculations and the fiber dimensions are given below.

- Rectangular module dimensions: 0.8 ft x 1 ft x 1 inch.
- Packing density of fibers = 40%.
- Fiber dimensions: ID - 240 μm ; OD - 300 μm .
- Maximum pressure drop along the length of the fiber = 10 inches of water.
- Gas flow through the fiber is laminar.



CM-360583-52

Figure 9-1. Cross-flow pattern of gas and liquid flow in a rectangular hollow fiber cassette (module).

The number of fibers that can be placed in rectangular

$$\begin{aligned} \text{geometry} &= \frac{(\text{Cross sectional area of shell}) \text{ Packing density}}{\text{Cross sectional area of fiber based on OD}} \\ &= 43,000 \text{ fibers} \\ \text{Gas flow per fiber} &= \frac{\pi \Delta P d_i^4}{128 \mu_g L} \end{aligned} \quad (9-1)$$

where

ΔP = Pressure drop along the length of fiber = 24866 dynes/cm²

d_i = ID of fiber = 240 μm

μ_g = Viscosity of gas = 1.7×10^{-4} g/cm·s

L = Length of fiber = 24 cm.

Upon substitution of the above parameter values into Eq. (9-1), we get

$$Q_g/\text{fiber} = 3.0 \text{ cc/min}$$

Gas flow through the module, $Q_g = Q_g/\text{fiber}$ (total number of fibers)

$$= 125 \text{ L/min}$$

Because this gas flow rate is within the range mentioned above, it is of further interest to see the gas scrubbing capacities of the module. From experimental data obtained so far (see Task 14), the mass transfer correlation is given as

$$K_{og} = 0.079257 \text{ Re}^{0.33211} \quad (9-2)$$

where Re is the gas side Reynolds number and is given as

$$\text{Re} = \frac{4 \rho_g (Q_g/\text{fiber})}{\pi \mu_g d_i} \quad (9-3)$$

Here ρ_g indicates gas density.

From Eqs. (9-2) and (9-3), we obtain K_{og} to be 0.23 cm/s.

The equilibrium calculation for the $\text{Na}_2\text{SO}_3/\text{SO}_2$ system indicates that the partial pressure of SO_2 (p^*) in equilibrium with the liquid is very small compared with the actual partial pressure (p) and therefore the mass balance yields

$$\ln \frac{P_O}{P_L} = K_{og} \pi d_o LN/Q_g \quad (4)$$

Here P_O and P_L indicate the partial pressures of SO_2 in the entering and exiting gas streams, respectively.

From Eq. (9-4), we estimate that the SO_2 removal rate is more than 99%. In summary, these approximate estimations indicate that a rectangular module with dimensions of 0.8 ft x 1 ft x 1 inch containing 240 μm ID fibers will effectively function as an SO_2 scrubber.

Ten membrane companies were approached to solicit their interest in this project. A summary of events is given in Table 9-1. Based on these consultations with different membrane module manufacturers, Separation Equipment Technologies, Inc. (Setec), Livermore, CA, was identified as a suitable supplier for the rectangular modules, and two modules were ordered.

Previously, we indicated that the rectangular HFCs with dimensions of 0.8 ft x 1 ft x 1 inch will take out 99% SO_2 from flue gas streams. These calculations were based on the HC fibers. However, the Setec hollow fiber characteristics vary substantially compared with those of HC fibers. Therefore, we had to design our experimental system based on the Setec fibers.

The specifications and performance characteristics of the module, which we obtained from Setec, are listed below:

- Rectangular module dimensions = 12 x 4 x 1 inches
- Packing density of fibers = 70%
- Fiber dimensions: ID - 600 μm ; OD - 1000 μm
- Maximum pressure drop along the length of the fiber = 10 inches of water
- Number of fibers in module = 2300
- Gas flow through the module = 200 SLPM

Table 9-1

DISCUSSIONS WITH MEMBRANE MANUFACTURERS

Manufacturer	Date(s) of Correspondence	Comments	End Result
Hoechst-Celanese Charlotte, NC	1990 - Sept. 1994	Hoechst-Celanese was initially the membrane company that showed interest in commercializing these modules. For business reasons, they decided not to pursue it further.	Not a feasible option.
TNO, Netherlands	Sept. 1994 - Jan. 1995	Already makes rectangular modules. Ideal candidates. Prototype module would cost approx. \$30,000 for lab-scale. Already trying to commercialize.	Too expensive, but may be feasible later.
Compact Membrane Systems, Inc. (CMS) Wilmington, Delaware	Nov. - Dec. 1994	Rectangular lab-scale module is priced at \$36,000.	Too expensive, but may be feasible later.
LSR Technologies Massachusetts	Nov. - Dec. 1994	Rectangular lab-scale module is priced at \$9,000.	Does not have a reliable fiber supplier, no prior expertise with microporous fibers, and modules are expensive.
Innovative Membrane Systems, Inc. (IMS) Massachusetts	Nov. - Dec. 1994	No business interest in fabrication of microporous fiber modules.	_____
W.L. Gore & Associates, Inc. - Elkton, Maryland	July - Sept. 1994	Interested to use their PTFE (Teflon) fibers; Gore had also received the cost estimates under a nondisclosure agreement.	No Response. Probably because the process becomes too expensive with PTFE fibers.
Mitsubishi, Japan	Nov. 1994	Manufactures microporous hollow fibers.	No response.
Toyobo, Japan	Nov. 1994	Same as above.	Same as above.
Nitto Denko, Japan	Nov. 1994	No good fibers for the project.	_____
Setec, Inc. Livermore, CA	Nov. 1994 - present	Rectangular lab-scale module is priced at \$8,000.	Prior expertise with microporous polypropylene fibers. We placed an order for 2 modules.

- Estimated mass transfer coefficient $K_{Og} = 0.52 \text{ cm/s}$
(calculated using a correlation obtained from previous experimental data)
- Estimated SO_2 removal $> 95\%$

We predict that the above mentioned rectangular HFC will effectively treat gas flow rates up to 200 SLPM for gas containing a 3000 ppm SO_2 concentration. To calculate the scrubbing liquid flow rate, we assumed 99% SO_2 removal and a 50% approach to equilibrium SO_2 solubility in the liquid.

The rate of SO_2 absorption into the scrubbing liquid =

$$\frac{(\% \text{SO}_2 \text{ removal}) (\text{concentration SO}_2 \text{ in flue gas})}{(\text{flue gas flow rate})} = 0.027 \text{ mol/min} \quad (9-5)$$

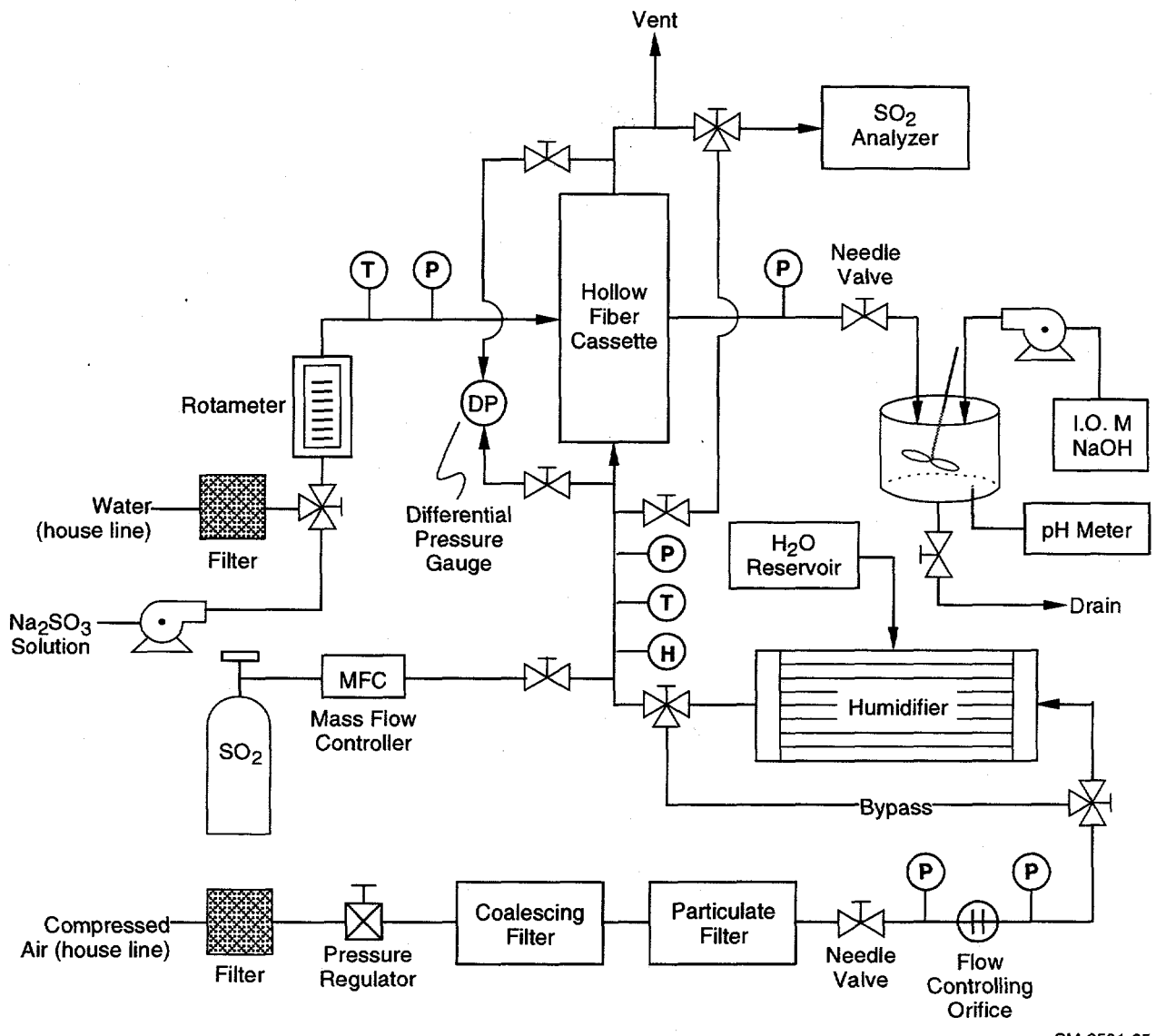
Equilibrium SO_2 solubility in water at 3000 ppm = 0.0108 mol/L.

$$\begin{aligned} \text{Water flow rate} &= \frac{(\text{Rate of SO}_2 \text{ absorption})}{(\text{Equilibrium SO}_2 \text{ solubility}) (\% \text{ approach to equilibrium}/100)} \\ &= 5 \text{ L/min} \end{aligned}$$

Equilibrium SO_2 solubility in 0.2 M Na_2SO_3 at 3000 ppm = 0.204 mol/L.

The Na_2SO_3 solution (0.2 M) flow rate = 0.3 L/min.

Based on these evaluations, we designed an experimental system to treat a simulated flue gas flow rate of 200 SLPM, an SO_2 concentration of 3000 ppm, and a scrubbing liquid flow rate of 5 L/min, as shown in Figure 9-2. Because of the magnitude of these flow rates, the most reasonable way to obtain the gas and liquid supply was to use the house lines. The house water was used only for those experiments using pure water as the scrubbing liquid. Aqueous sodium sulfite solution, with a flow rate at least an order of magnitude lower than that of water, was pumped from a reservoir. Both the gas and liquid lines were equipped with filters to remove particulates down to 0.1 μm from the water and 0.01 μm from the air. The air flow was controlled by a 0.08-inch-diameter orifice in which the critical flow rate was obtained by maintaining the absolute pressure upstream at least twice as high as the absolute pressure downstream .



CM-3501-95

Figure 9-2. Apparatus for scalable module testing.

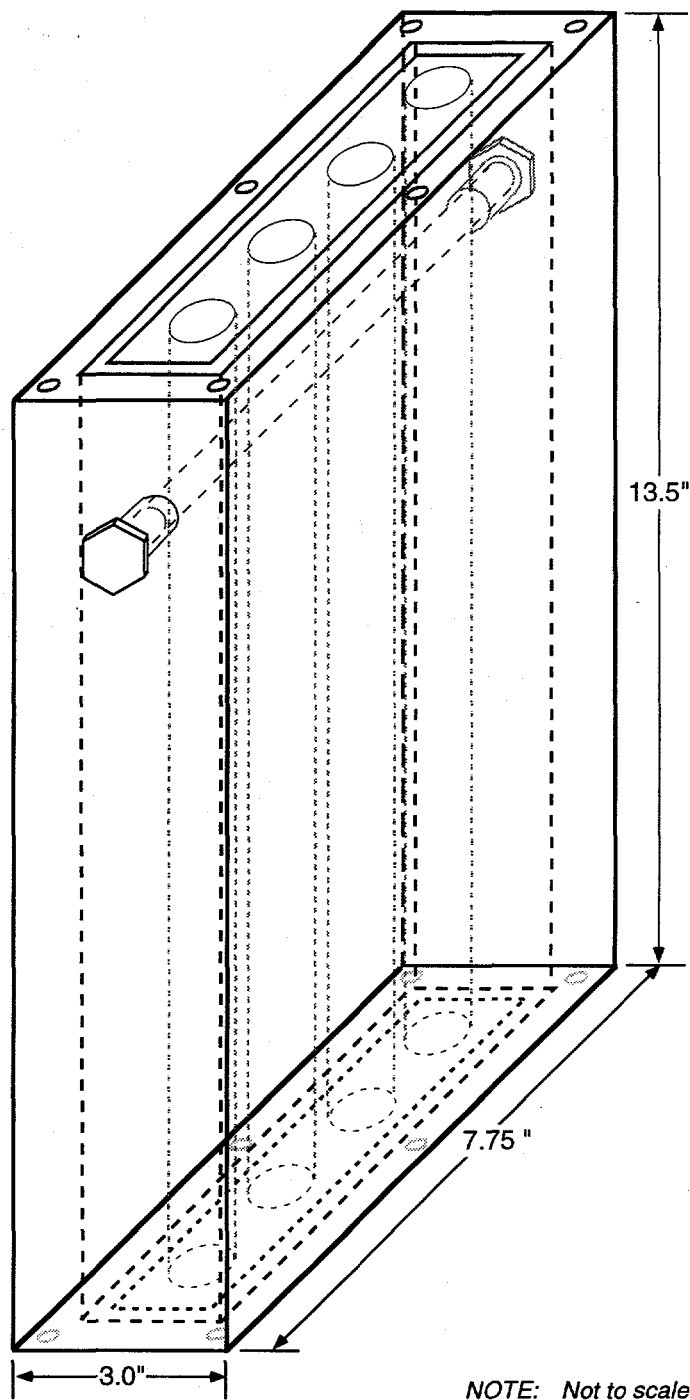
We humidified the air (except in the pure water experiments) prior to passing it through the module, because dry air will pick up water from the sodium sulfite solution and change its effective concentration. The humidification was accomplished by using another cylindrical type HFC. The air flows through the tube side of the HFC, and the shell side is filled with water. This shell side water is kept at a higher pressure, with the help of a pressurized tank, to avoid bubbling the air into the shell side water. SO₂ was added after humidification of the air stream, which prevented the absorption of SO₂ by the humidifier.

We used an SO₂ analyzer to measure the concentration of the gas both at the inlet and the outlet of the module. We also periodically monitored the pressure drop across the length of the fibers using a differential pressure gauge to ensure that it did not exceed the maximum value of 10 inches of water. The liquid on the shell side of the fibers was maintained at a higher pressure than the gas (but not at more than the allowable transmembrane pressure of 22 psi) by placing a needle valve on the liquid outlet.

The exiting solution, containing dissolved SO₂, had a pH of approximately 2.5 or 3. To comply with environmental regulations, we are required to neutralize this stream before draining the liquid. Therefore, the liquid outlet flowed into a stirred tank, where it was combined with sodium hydroxide (1.0 M) and monitored with a pH meter.

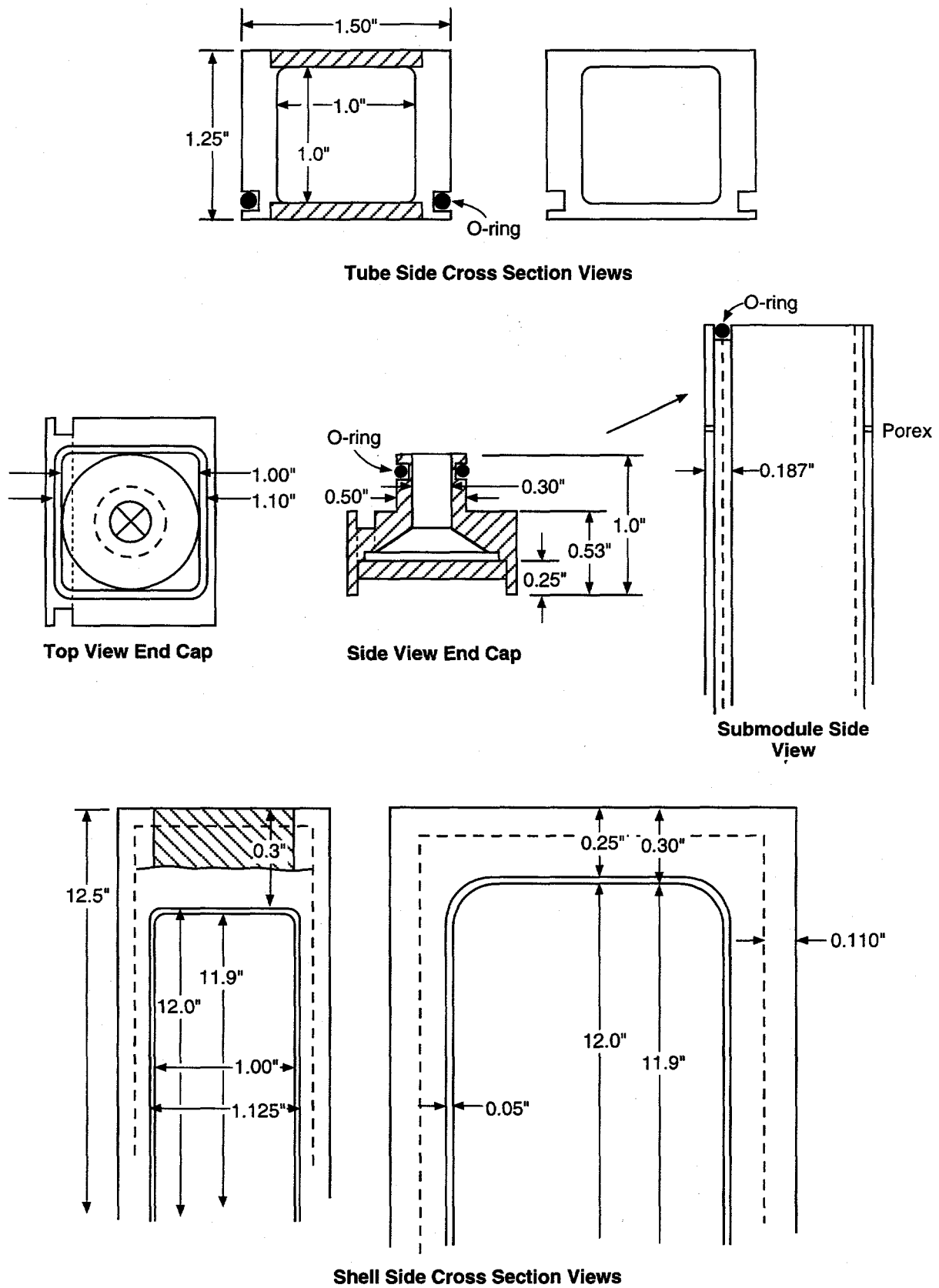
After constructing a substantial portion of the apparatus for testing rectangular HFCs, we received one of the rectangular HFCs from Setec. The design details are discussed below.

The dimensions of the housing are 13.5 x 7.75 x 3.0 inches, as shown in Figure 9-3. The housing is designed to hold four 'submodules', each with dimensions of 12.5 x 1.5 x 1.25 inches. Figure 9-4 illustrates the design features of one submodule. The submodule contains 700 microporous polypropylene fibers, each with a length of 12 inches, an OD of 1 mm, an ID of 0.6 mm, and a pore size of about 0.2 μm. At the fiber ends, a cap is designed (see Figure 9-5 for a side and top view of the cap) to uniformly collect the gas stream to each submodule. At the center of the plate, gas enters through a 3/8 inch port and flows into a manifold that runs along the width (7.75 inch side) of the housing and allows the gas to flow into four 1/16 inch orifices, each one leading to a submodule. Thus, the pressure drop across the orifices ensures a uniform flow distribution among all four units. In addition, a 0.25 inch porex (sintered) material is used at the gas inlet of each submodule to equally distribute the gas stream into the fiber bundle. The gas outlet of the housing has the same design as the inlet, except that no porex material is inside the submodule. The housing is polycarbonate.



NOTE: Not to scale
CM-3501-140

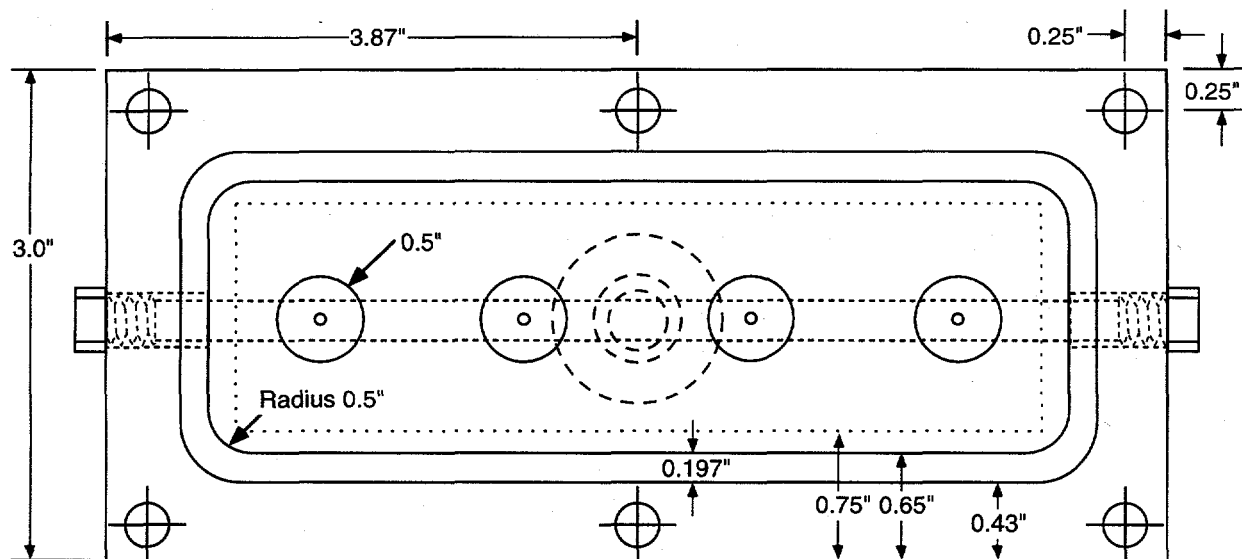
Figure 9-3. Drawing of rectangular housing.
Dimensions in inches.



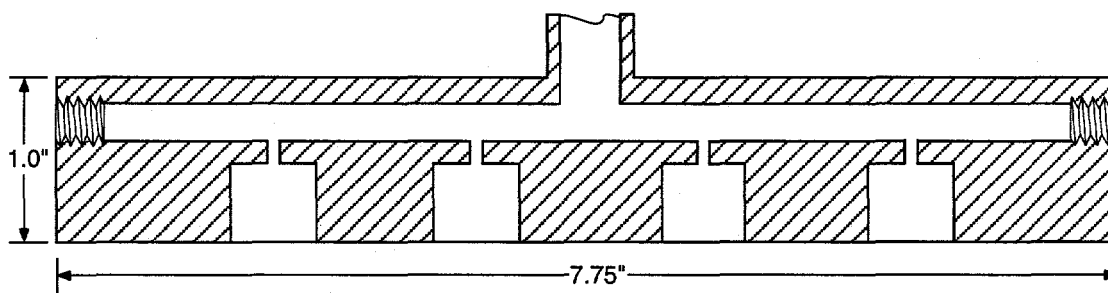
CM-3501-141

Figure 9-4. Design features of a submodule (dimensions in inches).

POLYCARBONATE HOUSING



(a) Top



(b) Side

CM-3501-142

Figure 9-5. Gas-side end plates of housing.

The liquid side of the housing has a similar design to the gas side, also with a manifold at the inlet that runs along the length of the module and separates the flow into twelve 1/16 inch orifices. On the inlet side of each submodule is a 12 x 1 inch piece of porex. A polycarbonate slab on the outlet side contains about 36 orifices (approximately 1/8-inch diameter) for the liquid to flow out of and then into the porex of the next subunit. The liquid outlet of the housing has the same design as the inlet.

Before completing fabrication of the housing and the submodules, we were given a "tester" submodule that enabled us to measure the pressure drop across the length of the fibers at various air flow rates. The results showed that we can flow up to 35 SLPM of air through the unit without exceeding the maximum pressure drop desired (10 inches of water). Therefore, it is possible to treat 140 SLPM using all four submodules.

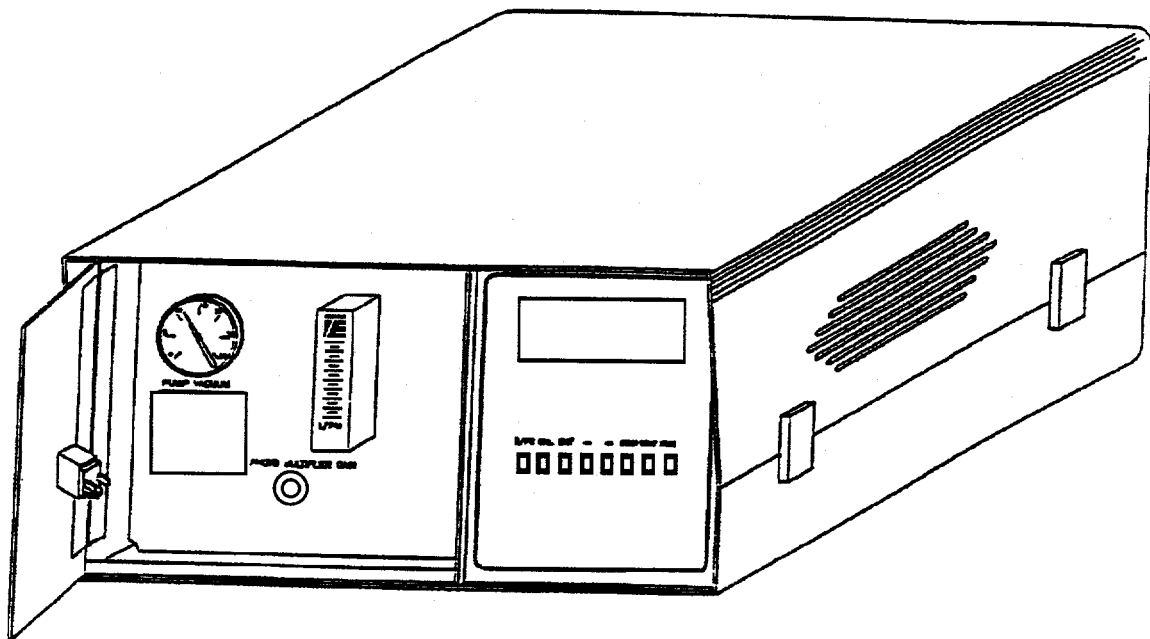
Upon receipt of the housing and all four submodules, we began testing the module using filtered water and filtered air. We encountered some problems with the housing; the ports on all four sides were unstable and broke off several times, and water leaked at some places in end plate joints. We sent the housing back to Setec to fix these problems.

In the meantime, we acquired a Model 40B SO₂ analyzer from Thermoenvironmental, Inc., Franklin, MA, through our internal resources. Figure 9-6 is a schematic of the equipment. The analyzer detects SO₂ based on pulsed UV-fluorescence. This equipment is used as a continuous monitoring system, with a sample gas flow rate of about 1 SLPM.

Following repairs at Setec, the rectangular module was returned to SRI. After testing again with air and water, the only problem we encountered was a small water leak at one corner of the housing, which cannot be corrected unless the housing is rebuilt. The leak produces only about one drop every 10 min, which is negligible compared with the liquid flow rates of about 1-5 L/min.

SO₂ SCRUBBING EXPERIMENTS

We conducted an experiment with 100 SLPM gas flow rate. The SO₂ concentration in the feed gas was 3000 ppm. The liquid (pure water) flow rate was maintained at 4.2 L/min. The SO₂ removal rate was measured to be 50%. The flow rates were somewhat limited by pressure drop. Although we believed the gas pressure drop through the fibers to be less than 10 inches of water at a flow rate of 100 SLPM (see the "tester" submodule data above), we could only measure the differential pressure across the entire housing, including the orifices and the porex material, which is about 5 psi. Similarly, we noticed pressure drops on the liquid side of about 11-12 psi for a flow rate of 5 L/min. Because the transmembrane pressure should not exceed 22 psi, we were



CAM-3501-143

Figure 9-6. SO₂ analyzer for continuous monitoring of gas streams.

somewhat restricted on using higher flow rates of liquid. One solution to this problem is to increase the size of the orifices (particularly those at the outlet, which are not really necessary for flow distribution).

We continued testing the rectangular module using pure water as the scrubbing liquid for SO₂ removal. The results of these experiments are summarized below.

The first set of experiments was conducted using a constant gas flow rate of 100 SLPM and varying water flow rates from 0.6 to 5 L/min. The SO₂ concentration in the feed gas was 3000 ppm. Figure 9-7 shows the percent of SO₂ removed as a function of water flow rate. In the second set of experiments, the liquid flow rate was held constant at 4.2 L/min, while the gas flow rate (still at 3000 ppm) was varied between 20 and 100 L/min. Figure 9-8 shows the removal results obtained for the various gas flow rates.. The highest SO₂ removal, about 85%, was obtained with a gas flow rate of 20 L/min and a liquid flow rate of 4.2 L/min.

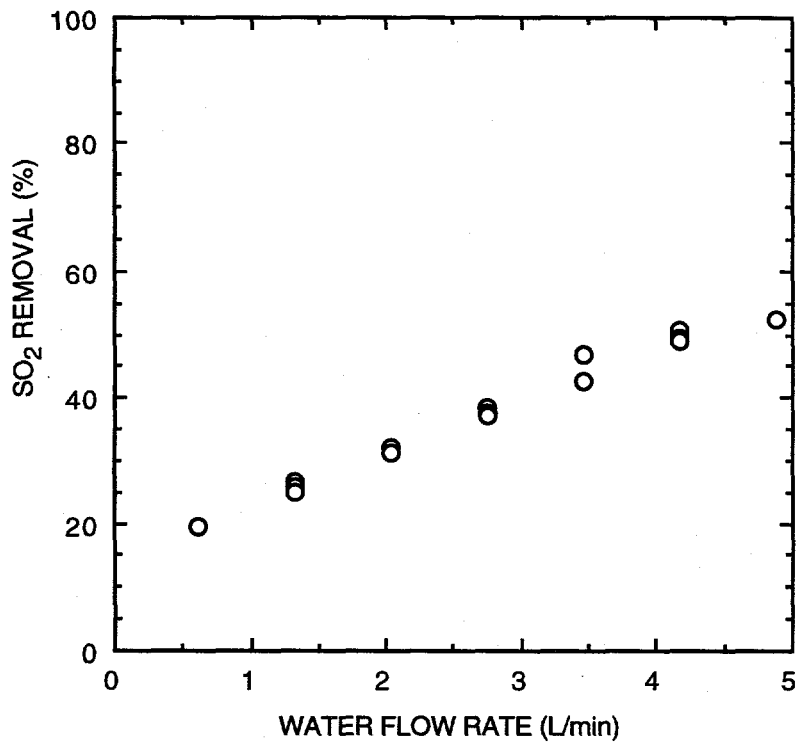
The mass transfer coefficients for these experiments were calculated as follows:

$$K_{og} = \frac{J_{SO_2}RT}{\Delta p_{lm}} \quad (9-6)$$

where K_{og} is the overall MTC in cm/s, J_{SO_2} is the flux of SO₂ across the membrane in mol/s-cm², R is the gas-law constant, T is the temperature in Kelvins, and Δp_{lm} is the log-mean partial pressure difference in atm. The calculations were based on counter-current flow, and therefore the log-mean difference was defined as

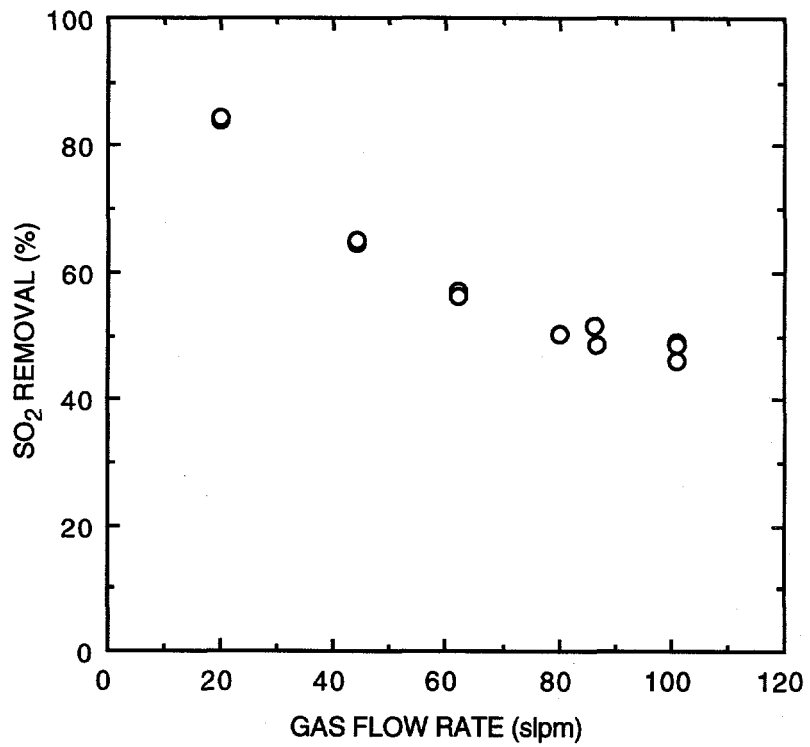
$$\Delta p_{lm} = \frac{(p_{in} - Hx_{out}) - (p_{out} - Hx_{in})}{\ln \left[\frac{(p_{in} - Hx_{out})}{(p_{out} - Hx_{in})} \right]} \quad (9-6)$$

where p_{in} is the partial pressure of SO₂ in the gas stream entering the contactor, p_{out} is the partial pressure of SO₂ in the exiting gas, x_{in} is the mole fraction of SO₂ in the entering liquid, x_{out} is the mole fraction of SO₂ in the exiting liquid, and H is Henry's law constant for the SO₂-water system in atm/mole fraction. The value for Henry's constant was determined to be 9596 mm Hg/mole fraction (12.6 atm/mole fraction) at 23°C from the equilibrium data shown in Figure 9-9 (Geankoplis, 1978).



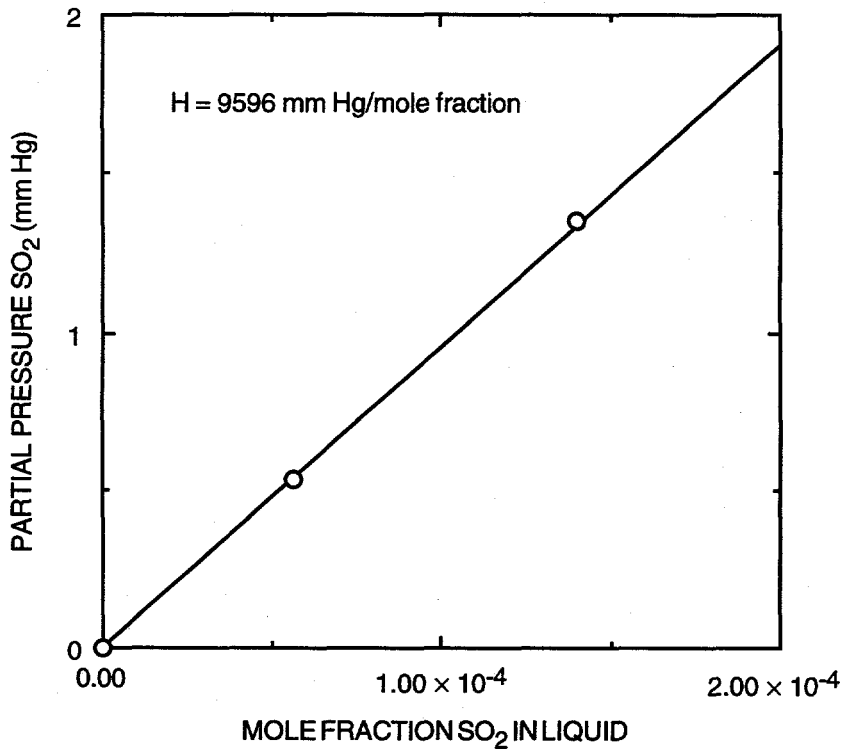
CAM-3501-105

Figure 9-7. Percent SO₂ removal versus water flow rate.



CAM-3501-106

Figure 9-8. Percent SO₂ removal versus gas flow rate.



CAM-3501-107

Figure 9-9. SO₂-water equilibrium curve.

The calculated overall MTCs as a function of water flow rate and of gas flow rate are shown in Figures 9-10 and 9-11, respectively. The graphs show that both the water flow and gas flow have an effect on the MTC.

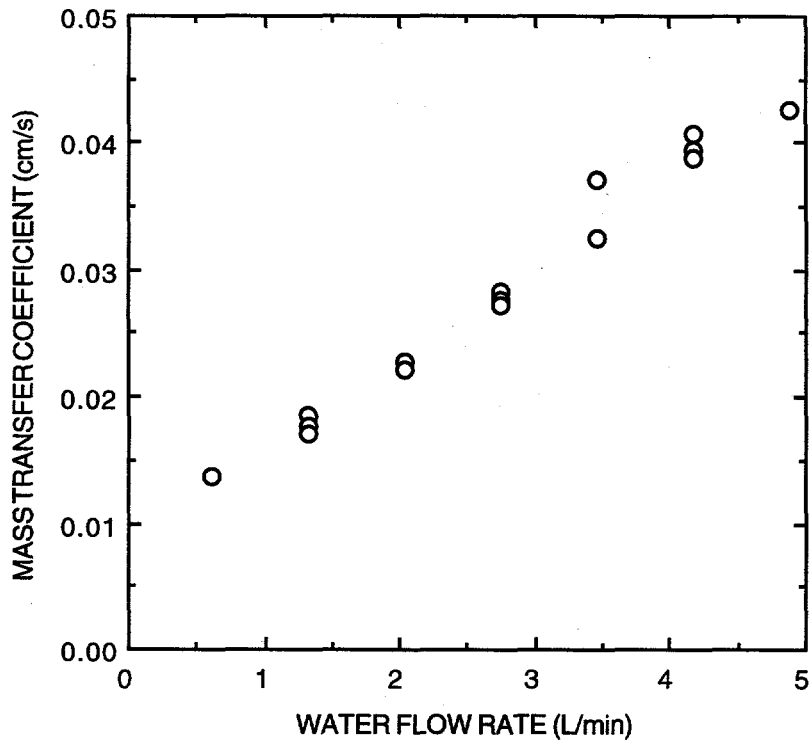
Next we tested the rectangular module using various sodium sulfite solutions as the scrubbing liquid for SO₂ removal. The results of these experiments are summarized below.

The experiments were performed in a manner similar to that used with pure water as the scrubbing liquid. We conducted the first set of tests using a constant gas flow rate of 100 SLPM, varying liquid flow rates, and the following concentrations of sodium sulfite in the liquid: 0.01M, 0.05M, 0.2M, and 0.5M. The SO₂ concentration in the feed gas was 3000 ppm. Figure 9-12 shows the percent of SO₂ removed as a function of liquid flow rate for the various sodium sulfite solutions and for pure water. In the second set of experiments, the liquid flow rate was held constant at 1 L/min and the gas flow rate was varied. The sodium sulfite concentrations used for these experiments were 0.05M and 0.2M. Figure 9-13 shows the removal results obtained for the various gas flow rates (the data for pure water is not included because the experiments were performed at a different liquid flow rate). The highest SO₂ removal, about 98%, was obtained with a gas flow rate of 20 L/min, a liquid flow rate of 1 L/min, and a sodium sulfite concentration of 0.02M.

The MTCs for these experiments were calculated in the same way as described for the pure water tests. The difference, however, lies in the calculation of Henry's coefficient. The value for the SO₂-water system was determined from experimental data, but for the SO₂-Na₂SO₃(aq) system, we had to calculate the value based on both the physically dissolved SO₂ and the sulfite/bisulfite ions. By performing a charge balance for various SO₂ concentrations, we were able to construct equilibrium curves for the different sodium sulfite solutions, as shown in Figure 9-14. (We also used this method to calculate an SO₂-water equilibrium curve, which is shown in Figure 9-14 along with the experimental data that was used for the SO₂-water calculations.) For each curve shown in the figure, there is a "threshold" value of the mole fraction SO₂ in the liquid below which the partial pressure of SO₂ in the vapor is essentially zero. In our experiments, the concentration of SO₂ absorbed in the liquid was always below this threshold value, so we assumed $H_{x_{out}} = 0$ when determining the log-mean partial pressure difference.

The calculated overall MTCs as a function of the liquid flow rate and of the gas flow rate are shown in Figures 9-15 and 9-16, respectively. The graphs show that the mass transfer appears to depend upon the liquid flow rate, but is independent of the gas flow rate near 100 SLPM.

Although the fibers are not demonstrating removal percentages as high as expected, we believe this may be due to specific problems with the housing design, rather than problems with



CAM-3501-108

Figure 9-10. Mass transfer coefficient versus water flow rate.

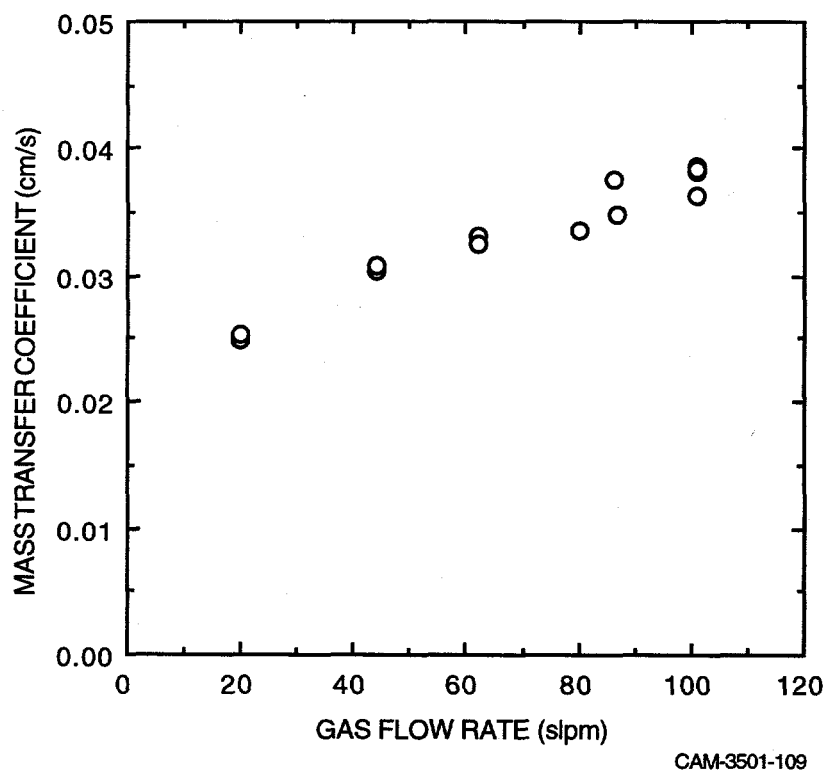
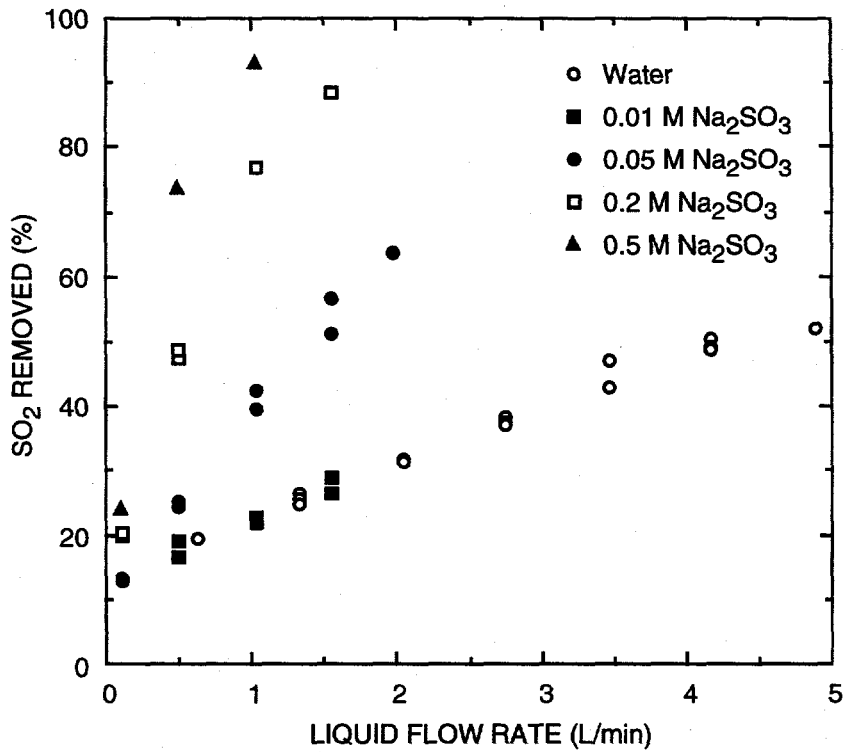
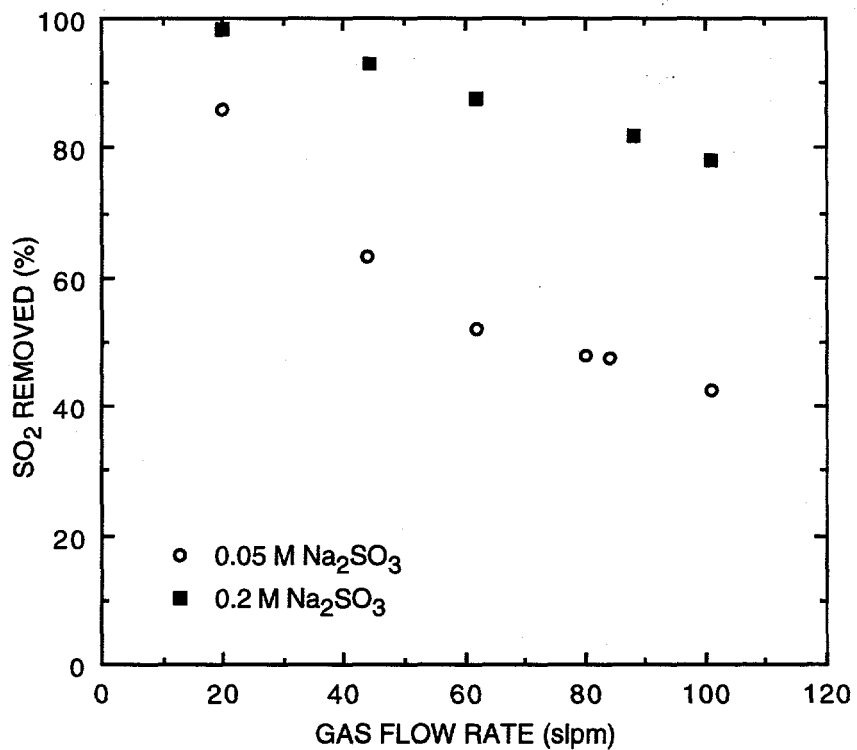


Figure 9-11. Mass transfer coefficient versus gas flow rate.



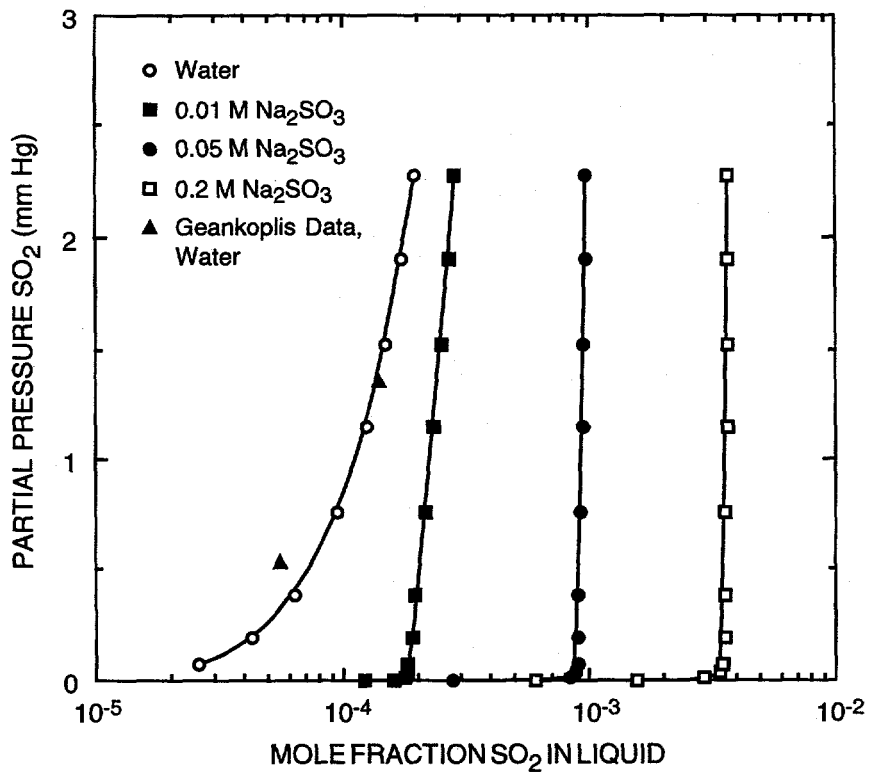
CAM-3501-114

Figure 9-12. Percent SO₂ removal versus liquid flow rate.
Gas flow rate = 100 slpm.



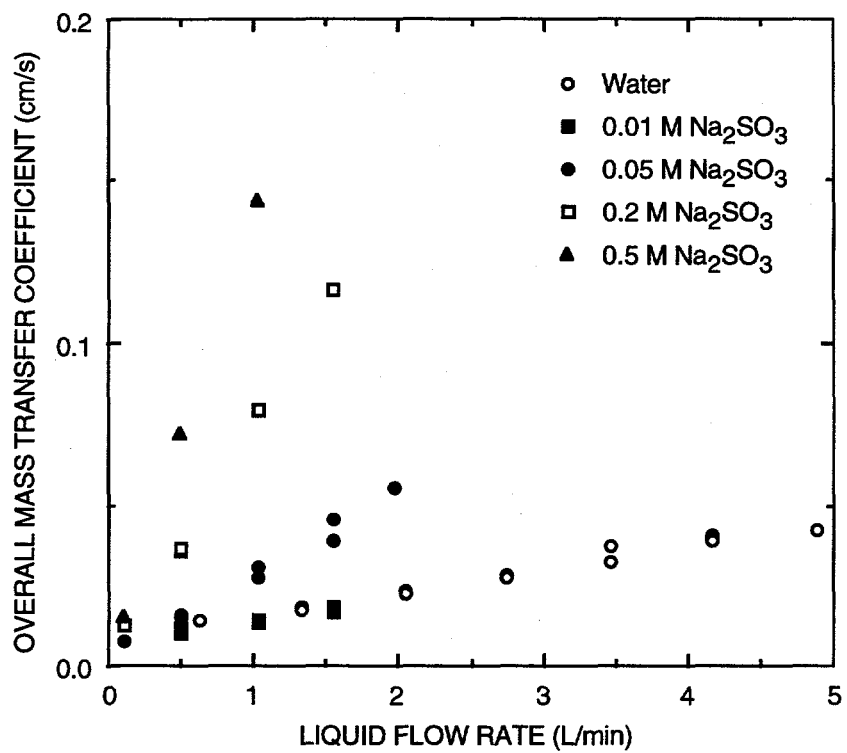
CAM-3501-115

Figure 9-13. Percent SO₂ removal versus gas flow rate.
Liquid flow rate = 1 L/min.



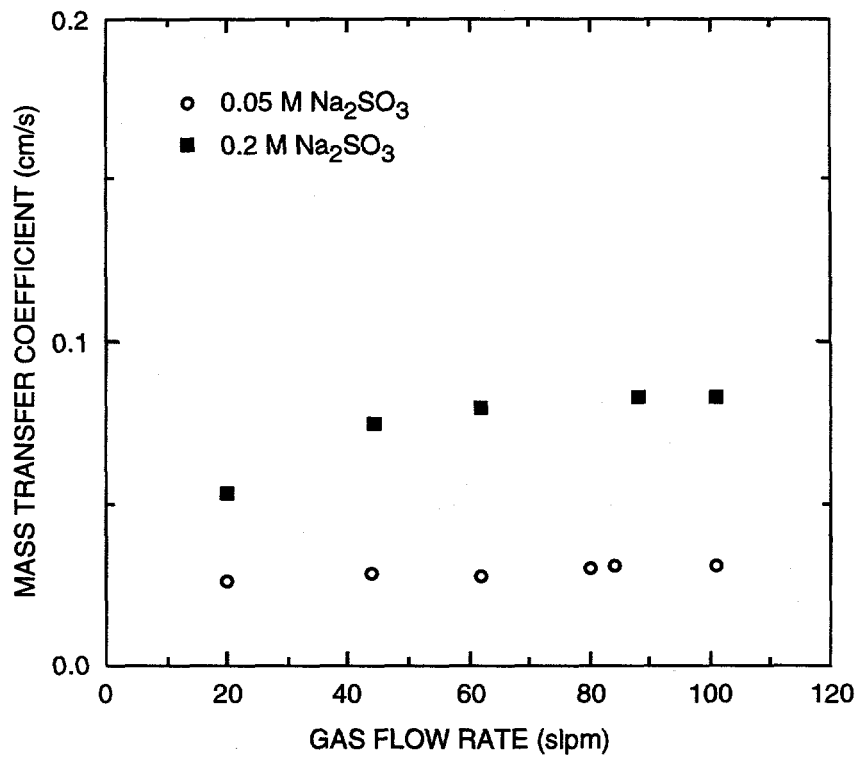
CAM-3501-113

Figure 9-14. SO₂ equilibrium curves in various sodium sulfite solutions.



CAM-3501-111

Figure 9-15. Overall mass transfer coefficient versus liquid flow rate.
Gas flow rate = 100 slpm.



CAM-3501-112

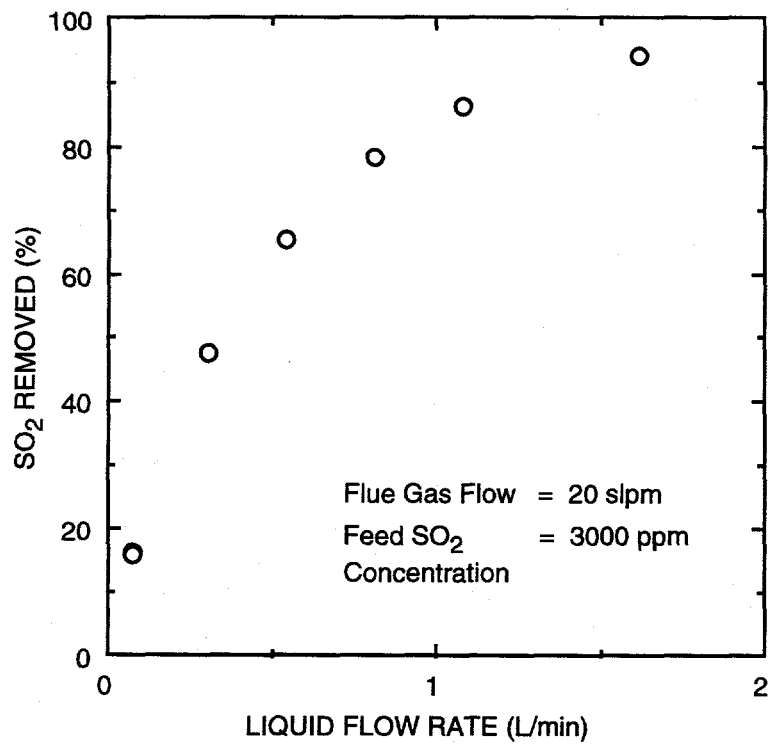
Figure 9-16. Overall mass transfer coefficient versus gas flow rate.
Liquid flow rate = 1 L/min.

the cross-flow geometry or the fibers themselves. Some of the liquid may be flowing around and outside of the submodules instead of through them. We have seen evidence of this flow pattern by performing tests with colored dye. In addition, the high packing density (85%) may also be causing flow channeling within the submodules, rather than allowing even flow around the fibers. To eliminate the possibility of flow channeling around the submodules, we tested one submodule welded permanently into its own housing.

We obtained one submodule (12.5 x 1.5 x 1.25 inches) welded permanently into a polypropylene housing. We performed one set of experiments with this submodule using pure water as the scrubbing liquid for a flue gas concentration of 3000 ppm SO₂. The liquid flow rate was varied while the gas flow rate was maintained constant at about 20 SLPM. Although this is slightly different than the previous flow rate of 25 SLPM (total flow in four-unit module = 100 SLPM), we believe this is a reasonable comparison because the mass transfer is independent of gas flow at these flow rates.

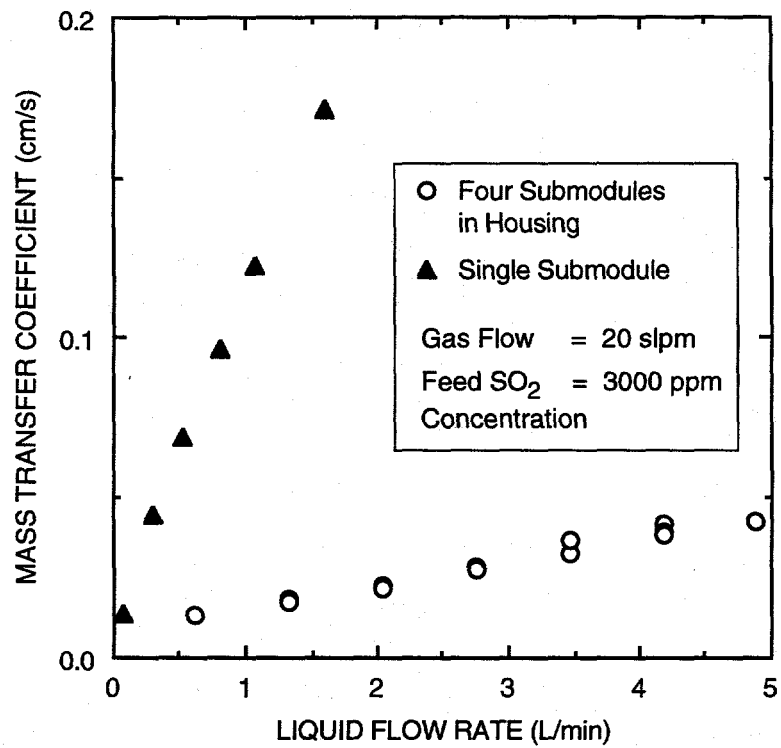
Figure 9-17 shows the percentage of SO₂ removed as a function of the liquid flow rate for the single submodule. The graph shows that the highest removal achieved was 97% at a water flow rate of 1.7 L/min. Figure 9-18 compares the MTCs measured for both the welded submodule and the previous device (housing with four submodules). The MTC is shown as a function of liquid flow rate because it should be independent of the gas flow rate. The MTCs obtained with the single submodule are almost an order of magnitude higher than those measured with the four submodules in the housing. These results show that the problem was in fact due to the housing design, which allowed liquid to flow around the modules rather than through the fiber bundle.

We also studied combined SO₂ absorption/scrubbing liquor regeneration using the cross-flow modules. Figure 9-19 shows the apparatus we designed for these experiments. Sodium sulfite solution is pumped from a reservoir through the first hollow fiber module to absorb SO₂ from the flue gas stream. The scrubbing liquor then passes into the second module, where the liquor is regenerated by the organic (d-DMA). The pH of the scrubbing liquor stream is monitored at the outlet of both modules. We must continuously regenerate the d-DMA stream because of the high synthesis costs involved. After passing through the second hollow fiber module, the SO₂-rich organic liquid is heated to about 125-150°C and the SO₂ is desorbed by a nitrogen stream bubbling into the liquid. The d-DMA is then pumped through a cooler to lower the temperature to about 25°C before entering the regenerator module. The feed gas, the gas exiting the scrubber, and the gas leaving the d-DMA stripper are all monitored by the SO₂ analyzer.



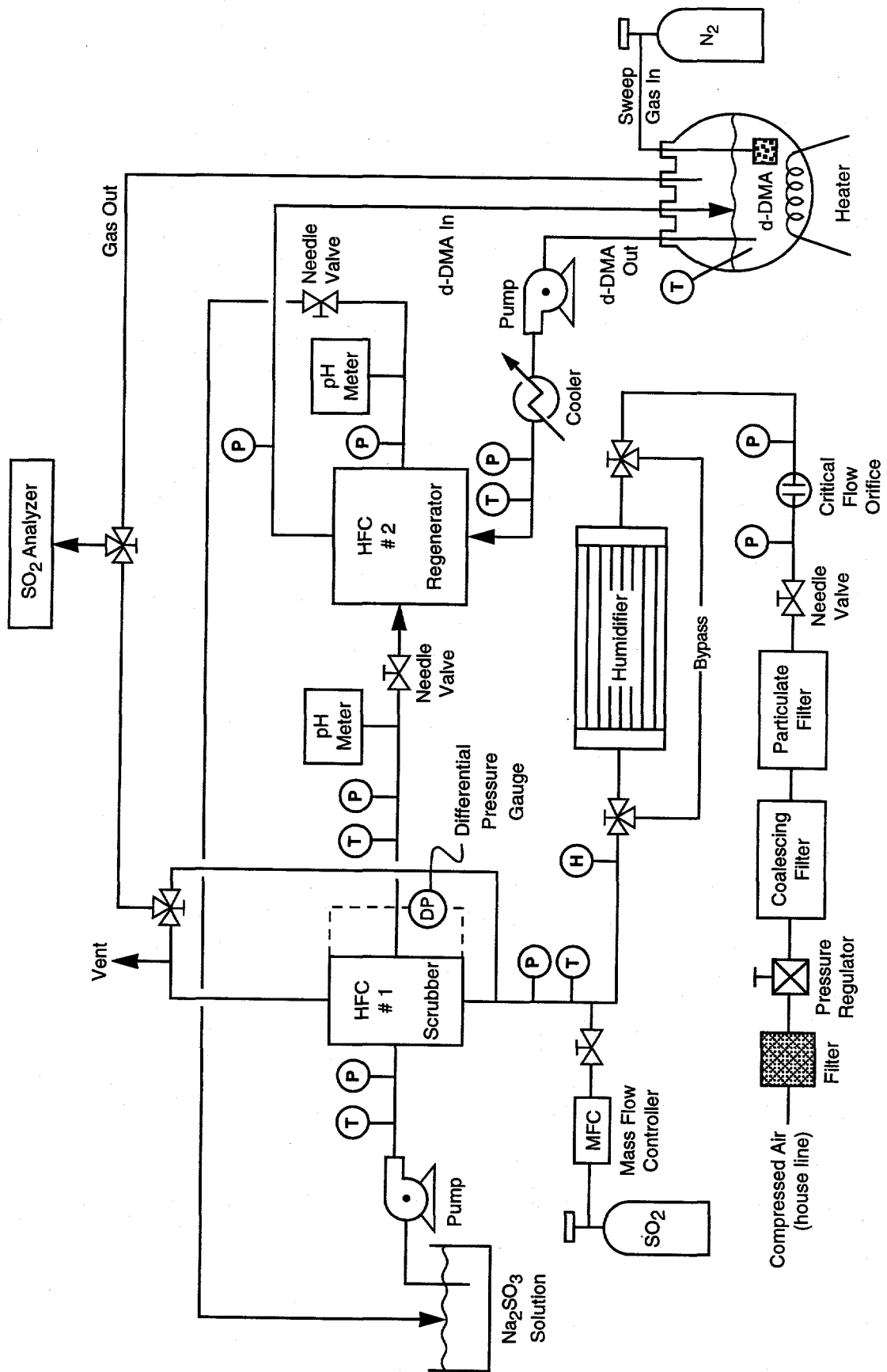
CM-3501-115A

Figure 9-17. Percent removal versus water flow rate.



CM-3501-116A

Figure 9-18. Mass transfer coefficient versus water flow rate.



CM-3501-95A

Figure 9-19. Apparatus for scalable module testing.

We indicated above that a single submodule in a welded polypropylene housing out-performs the previous rectangular HFC because of channeling the liquid flow. After the pure water experiments, we continued testing the single submodule using varying concentrations of sodium sulfite as the scrubbing liquid.

Tables 9-2 to 9-5 show our results of the experiments. In these experiments, we studied the effect of gas flow rate, liquid flow rate, and sodium sulfite concentration on the performance of HFC for SO₂ removal. All the experiments were conducted at room temperature and the inlet flue gas contained about 3000 ppm of SO₂.

Table 9-2 presents data using water as the scrubbing medium. The WG series represent experiments using a constant gas flow rate and the WL series represent experiments using a constant liquid flow rate. The highest removal achieved was 98% at a water flow rate of 1.7 L/min and a gas flow rate of 20 SLPM (Run WG22). Table 9-3 summarizes the results obtained by scrubbing with 0.01M Na₂SO₃ solution. We conducted experiments with a constant gas flow and chose not to study this concentration extensively because the results were very similar to those obtained with water. We were, however, able to remove 99.9% of the SO₂ from a 20 SLPM flue gas stream with a liquid flow rate of 0.9 L/min (Run S01G8). When removal rates are this high (~99.9%), we cannot calculate the MTC because of the log-mean concentration term involved in the calculations.

The data shown in Table 9-4 was obtained using 0.05M Na₂SO₃ scrubbing solution. At this concentration level, we studied two constant liquid flow rates; 20 ml/min and 65 mL/min (represented by Runs S05L20 and S05L65, respectively). A SO₂ removal rate of 99.9% from a flue gas stream of 20 SLPM was obtained using 360 mL/min of liquid flow (Run S05G2). Table 9-5 shows data from experiments performed using 0.2M Na₂SO₃, the highest concentration studied, as the scrubbing medium. In these experiments, 99.9% removal was achieved with a gas flow rate of 20 SLPM and a liquid flow rate of 65 mL/min (Run S2G13).

In addition to the percent removal and MTCs, we have represented the data in terms of the dimensionless Reynolds number and Sherwood number in order to scale up the data to Phase III of the program. The Reynolds number, calculated for both the gas and liquid, is given by

$$Re = \frac{\rho v D}{\mu} \quad (9-8)$$

where ρ is the fluid density, μ is the fluid viscosity, D is the inner diameter of the fiber (gas side) or outer diameter (liquid side), and v is the fluid velocity. For the liquid side, the velocity was

Table 9-2
RESULTS OF SO₂ ABSORPTION IN WATER

Run No.	Temp. (C°)	Liquid Flow (mL/min)	Gas Flow (SLPM)	Inlet SO ₂ Composition (ppm)	Outlet SO ₂ Composition (ppm)	Percent SO ₂ Removed	Kog (cm/s)	Re (gas)	Re (liquid)	Sh
WG1	24.6	72	20.3	2924	2441	17	0.0135	71.5	5.4	80
WG2	24.5	72	20.3	2914	2446	16	0.0130	71.5	5.4	76
WG3	24.5	302	20.3	2914	1521	48	0.0442	71.5	22.7	260
WG4	24.5	302	20.3	2914	1521	48	0.0442	71.5	22.7	260
WG5	24.5	538	20.3	2924	1018	65	0.0684	71.5	40.5	402
WG6	24.5	807	20.3	2924	635	78	0.0961	71.4	60.9	565
WG7	24.4	1081	20.3	2919	403	86	0.122	71.4	81.4	718
WG8	24.5	1615	20.3	2919	170	94	0.171	71.4	122	1006
WG9	23.5	96	20.3	3014	2198	27	0.0263	71.6	7.3	155
WG10	23.5	368	20.3	3024	1168	61	0.0660	71.6	27.7	388
WG11	23.5	591	20.3	3019	705	77	0.0962	71.6	44.5	566
WG12	23.5	846	20.3	3014	403	87	0.129	71.6	63.7	756
WG13	23.6	96	20.3	3029	2178	28	0.0282	71.6	7.3	166
WG14	23.7	368	20.3	3029	1212	60	0.0631	71.6	27.7	371
WG15	23.5	591	20.3	3033	789	74	0.0882	71.6	44.5	519
WG16	23.5	846	20.3	3038	412	86	0.178	71.6	63.7	751
WG17	26.6	77	20.2	3068	2317	25	0.0255	71.2	5.8	150
WG18	26.6	358	20.2	3068	1242	60	0.0628	71.2	27.0	370
WG19	26.7	590	20.2	3073	750	76	0.0934	71.2	44.5	550
WG20	26.8	877	20.2	3073	422	86	0.127	71.2	66.1	745
WG21	26.7	1169	20.2	3073	232	92	0.161	71.2	88.1	947
WG22	26.5	1740	20.2	3073	76	98	0.224	71.2	131	1317
WL1	26.7	590	20.2	3054	772	75	0.0900	71.2	44.5	529
WL2	26.9	590	15.3	3029	552	82	0.0827	53.9	44.5	486
WL3	26.9	590	12.2	3024	355	88	0.0817	42.9	44.5	481
WL4	27.1	590	9.6	3043	112	96	0.0987	33.8	44.5	581
WL5	27.3	590	22.1	3043	834	73	0.0935	77.8	44.5	550
WL6	24.5	590	20.3	3038	765	75	0.0900	71.4	44.5	530
WL7	24.7	590	15.3	3033	556	82	0.0819	54.0	44.5	482
WL8	24.7	590	12.2	3029	344	89	0.0823	42.8	44.5	484
WL9	25.1	590	9.7	3033	118	96	0.0973	34.1	44.5	572
WL10	23.2	590	20.3	3043	790	74	0.0877	71.3	44.5	516
WL11	23.2	590	16.1	3038	536	82	0.0889	56.9	44.5	523
WL12	23.3	590	13.2	3038	313	90	0.0947	46.5	44.5	557
WL13	23.5	590	9.7	3048	101	97	0.102	34.1	44.5	601

Table 9-3
RESULTS OF SO₂ ABSORPTION IN 0.01M Na₂SO₃ SOLUTION

Run No.	Temp. (C°)	Liquid Flow (mL/min)	Gas Flow (SLPM)	Inlet SO ₂ Composition (ppm)	Outlet SO ₂ Composition (ppm)	Percent SO ₂ Removed	Kog (cm/s)	Re (gas)	Re (liquid)	Sh
S01G1	24.5	77	20.3	2974	1919	35	0.0241	71.4	5.8	142
S01G2	24.6	77	20.3	2984	2128	29	0.0186	71.4	5.8	109
S01G3	24.8	358	20.3	2994	894	70	0.0664	71.4	27.0	391
S01G4	24.8	590	20.3	2994	453	85	0.104	71.4	44.5	610
S01G5	24.1	77	20.3	3004	2028	32	0.0215	71.4	5.8	126
S01G6	22.9	77	20.3	3004	2098	30	0.0196	71.4	5.8	115
S01G7	23.0	77	20.3	3004	2011	33	0.0122	71.4	5.8	129
S01G8	23.0	877	20.3	3004	3.4	99.9	-	71.4	66.1	-
S01G9	23.2	77	20.3	2994	1984	34	0.0226	71.4	5.8	132
S01G10	23.3	590	20.3	2994	126	96	0.172	71.4	44.5	1013
S01G11	23.4	358	20.3	3004	620	79	0.0859	71.4	27.0	506

Table 9-4
RESULTS OF SO₂ ABSORPTION IN 0.05M Na₂SO₃ SOLUTION

Run No.	Temp. (C°)	Liquid Flow (mL/min)	Gas Flow (SLPM)	Inlet SO ₂ Composition (ppm)	Outlet SO ₂ Composition (ppm)	Percent SO ₂ Removed	Kog (cm/s)	Re (gas)	Re (liquid)	Sh
S05G1	26.9	77	20.3	3004	645	79	0.0850	71.4	5.8	500
S05G2	27.3	358	20.3	3043	2.1	99.9	-	71.4	27.0	-
S05G3	27.3	590	20.3	3004	1.7	99.9	-	71.4	44.5	-
S05G4	27.1	77	20.3	3004	844	72	0.0703	71.4	5.8	413
S05G5	24.4	110	20.2	3003	522	83	0.0956	71.2	8.3	562
S05G6	24.6	20	20.2	3003	2336	22	0.0138	71.2	1.5	81
S05G7	24.8	43	20.2	3013	1759	42	0.0295	71.2	3.2	174
S05G8	24.7	65	20.2	3013	1271	58	0.0473	71.3	4.9	278
S05G9	24.7	88	20.2	3013	863	71	0.0685	71.3	6.6	403
S05L201	23.1	20	20.3	3043	2466	19	0.0115	71.3	1.5	68
S05L202	23.3	20	16.8	3033	1426	20	0.0102	59.2	1.5	60
S05L203	23.4	20	14.0	3003	2346	22	0.0094	49.3	1.5	55
S05L204	23.6	20	12.0	3013	2366	21	0.0079	42.2	1.5	46
S05L205	23.7	20	14.0	3003	2441	19	0.0079	49.3	1.5	46
S05L206	23.8	20	9.7	3013	2326	23	0.0068	34.1	1.5	40
S05L207	23.8	20	20.2	2993	2585	14	0.0080	71.3	1.5	47
S05L208	24.0	20	16.8	3033	2495	18	0.0089	59.2	1.5	52
S05L651	23.0	65	20.3	3033	1322	56	0.0454	71.5	4.9	297
S05L652	23.2	65	20.3	3043	1342	56	0.0447	71.4	4.9	263
S05L653	23.2	65	17.0	3024	1098	64	0.0466	60.0	4.9	274
S05L654	23.4	65	14.1	3033	322	73	0.0499	49.7	4.9	294
S05L655	23.4	65	12.0	3033	559	82	0.0550	42.2	4.9	323
S05L656	23.6	65	11.9	3029	623	79	0.0512	42.0	4.9	301
S05L657	23.8	65	9.7	3033	347	89	0.0575	34.3	4.9	338

Table 9-5
RESULTS OF SO₂ ABSORPTION IN 0.2M Na₂SO₃ SOLUTION

Run No.	Temp. (C°)	Liquid Flow (mL/min)	Gas Flow (SLPM)	Inlet SO ₂ Composition (ppm)	Outlet SO ₂ Composition (ppm)	Percent SO ₂ Removed	Kog (cm/s)	Re (gas)	Re (liquid)	Sh
S2G1	23.3	77	20.3	3024	1.7	99.9	-	71.4	5.8	-
S2G2	23.3	77	20.3	3024	1.5	99.9	-	71.4	5.8	-
S2G3	23.2	358	20.3	3029	1.4	99.9	-	71.4	27.0	-
S2G4	23.1	77	20.3	3033	1.1	99.9	-	71.4	5.8	-
S2G5	26.1	110	20.2	2994	1.4	99.9	-	71.3	8.3	-
S2G6	25.9	20	20.2	3004	1097	63	0.0555	71.3	1.5	326
S2G7	25.7	43	20.2	3024	79	97	0.200	71.3	3.2	1176
S2G8	25.8	20	20.3	2914	1023	65	0.0577	71.4	1.5	339
S2G9	25.7	43	20.3	2914	68	98	0.206	71.4	3.2	1214
S2G10	25.5	43	20.2	3003	198	93	0.149	71.3	3.2	877
S2G11	25.1	20	20.2	3003	1251	58	0.0481	71.3	1.5	283
S2G12	25.4	54	20.2	3003	36	99	0.241	71.3	4.1	1418
S2G13	25.3	65	20.2	3003	2.8	99.9	-	71.3	4.9	-
S2G14	23.9	43	20.2	3063	140	95	0.168	71.3	3.2	990
S2G15	24.2	43	20.2	3013	136	96	0.169	71.3	3.2	995
S2G16	24.2	110	20.2	3013	1.1	99.9	-	71.3	8.3	-
S2G17	24.1	20	20.2	3018	1246	59	0.0484	71.3	1.5	285
S2L1	23.2	20	20.3	3043	1073	65	0.0570	71.4	1.5	335
S2L2	23.4	20	26.8	3014	760	75	0.0624	59.0	1.5	368
S2L3	23.8	20	23.7	3033	442	85	0.0718	48.4	1.5	422
S2L4	23.9	20	11.9	3033	260	91	0.0798	42.1	1.5	470
S2L5	24.2	20	9.7	3024	58	98	0.104	34.0	1.5	612

determined by calculating the smallest space between the fibers and determining the velocity through that area (the maximum velocity of the liquid). The Sherwood number is given by

$$Sh = \frac{K_{og}D}{D_{AB}} \quad (9-9)$$

where K_{og} is the overall MTC, D is the outer diameter of the fiber, and D_{AB} is the diffusion coefficient of SO_2 in water.

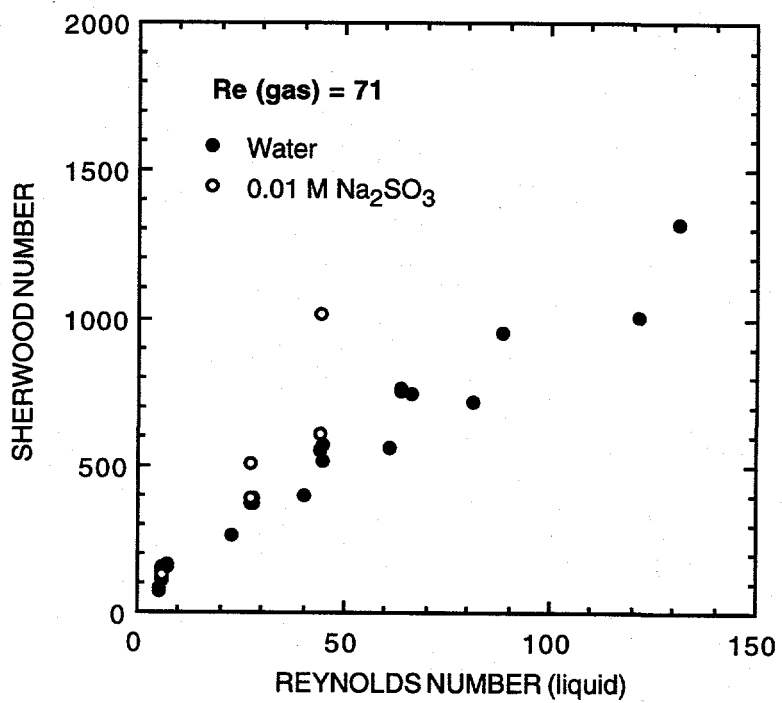
Figure 9-20 and 9-21 show variation of the Sherwood number as a function of the liquid side Reynolds number for a constant gas flow rate. Figures 9-22 to 9-24 show the Sherwood number versus the gas side Reynolds number for three liquid flow rates. The graphs illustrate that the MTC is dependent primarily on the liquid flow rate rather than on the gas flow rate. This is a rather surprising result for us, since our original laboratory work (Task 4) indicated the gas side dependence of the MTC.

For the combined SO_2 absorption and scrubbing liquor regeneration step, we intend to use 0.05M Na_2SO_3 solution. We believe that 0.01M Na_2SO_3 solution will not allow enough absorption and that 0.2M Na_2SO_3 solution will be too difficult to regenerate. There may be some additional problems with 0.2M Na_2SO_3 , including pore-wetting and oxidation of sulfites to form sulfates. We are investigating the latter possibility, which is likely a result of using house air in the simulated flue gas stream, which contains 21% oxygen instead of the 3%-4% found in actual flue gas.

We are expecting the arrival of a new HFC in October that will contain four submodules welded together in a fashion similar to the single unit we have been testing. This module will serve as the regenerator, with the aqueous phase on the shell side and the organic phase on the tube side. We intend to run some SO_2 absorption tests with this module before beginning the regeneration step in order to ensure that the MTCs are consistent with those obtained for the single submodule. We will then proceed to build the apparatus for the combined absorption/regeneration process.

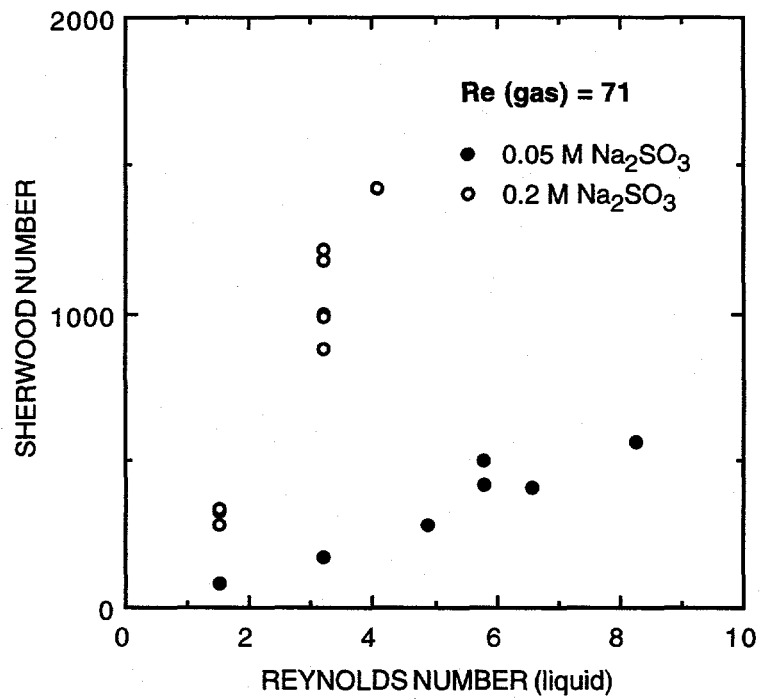
In the meantime, we finished testing the single welded submodule. We conducted additional experiments using 0.2M Na_2SO_3 as the scrubbing liquid, and investigated the possibility of sulfite oxidation by oxygen in the house air.

Table 9-6 shows all the results using 0.2M Na_2SO_3 solution. The run numbers S2G (constant gas flow) and S2L (constant liquid flow) represent runs using house air blended with SO_2 . Experiments using nitrogen blended with SO_2 are designated by S2NL.



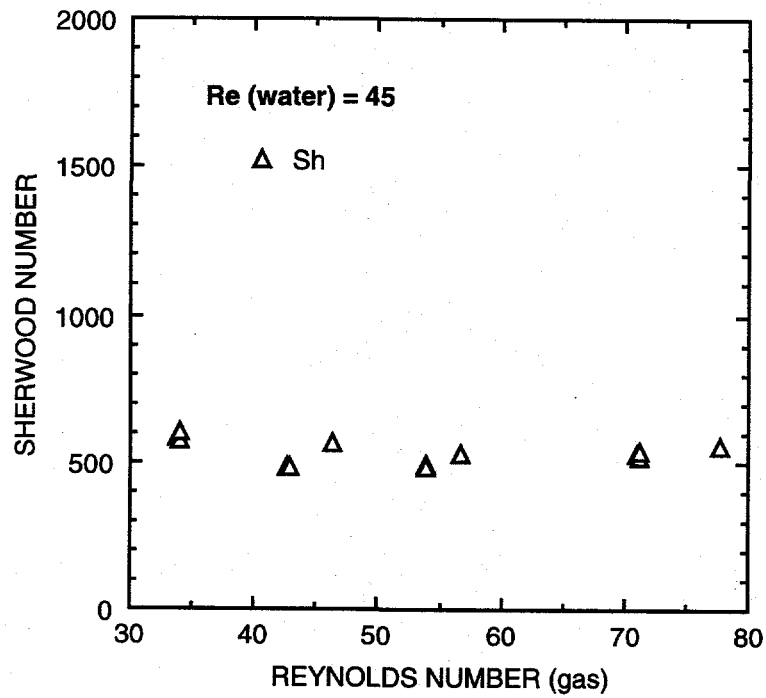
CAM-3501-130

Figure 9-20. Sherwood number versus Reynolds number (liquid).



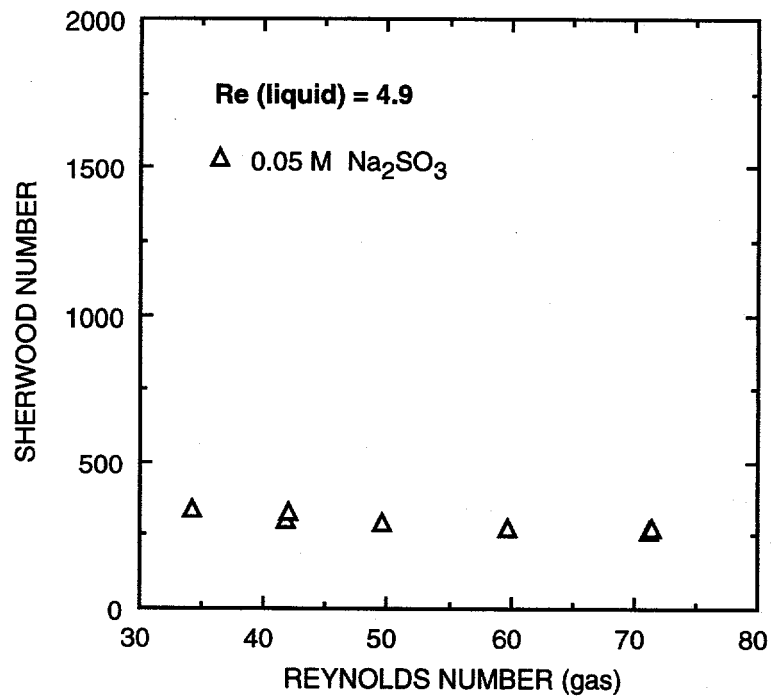
CAM-3501-129

Figure 9-21. Sherwood number versus Reynolds number (liquid).



CAM-3501-128

Figure 9-22. Sherwood number versus Reynolds number (gas).



CAM-3501-127

Figure 9-23. Sherwood number versus Reynolds number (gas).

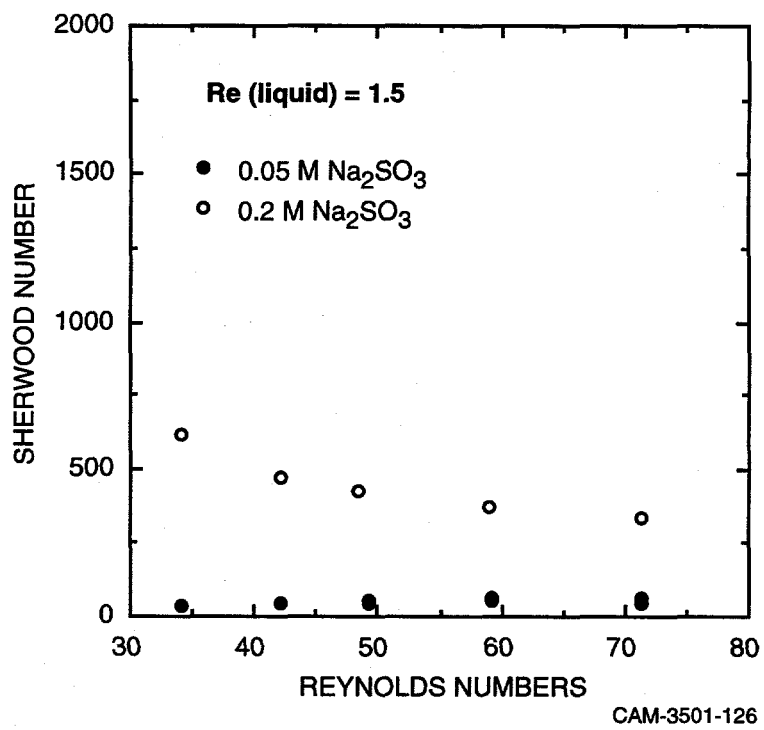


Figure 9-24. Sherwood number versus Reynolds number (gas).

Table 9-6
RESULTS OF SO₂ ABSORPTION IN 0.2M Na₂SO₃

Run No.	Temp. (C°)	Liquid Flow (mL/min)	Gas Flow (SLPM)	Inlet SO ₂ Composition (ppm)	Outlet SO ₂ Composition (ppm)	Percent SO ₂ Removed	Kog (cm/s)	Re (gas)	Re (liquid)	Sh
S2G1	23.3	77	20.3	3024	1.7	99.9	-	71.4	5.8	-
S2G2	23.3	77	20.3	3024	1.5	99.9	-	71.4	5.8	-
S2G3	23.2	358	20.3	3029	1.4	99.9	-	71.4	27.0	-
S2G4	23.1	77	20.3	3033	1.1	99.9	-	71.4	5.8	-
S2G5	26.1	110	20.2	2994	1.4	99.9	-	71.3	8.3	-
S2G6	25.9	20	20.2	3004	1097	63	0.0555	71.3	1.5	326
S2G7	25.7	43	20.2	3024	79	97	0.200	71.3	3.2	1176
S2G8	25.8	20	20.3	2914	1023	65	0.0577	71.4	1.5	339
S2G9	25.7	43	20.3	2914	68	98	0.206	71.4	3.2	1214
S2G10	25.5	43	20.2	3003	198	93	0.149	71.3	3.2	877
S2G11	25.1	20	20.2	3003	1251	58	0.0481	71.3	1.5	283
S2G12	25.4	54	20.2	3003	36	99	0.241	71.3	4.1	1418
S2G13	25.3	65	20.2	3003	2.8	99.9	-	71.3	4.9	-
S2G14	23.9	43	20.2	3063	140	95	0.168	71.3	3.2	990
S2G15	24.2	43	20.2	3013	136	96	0.169	71.3	3.2	995
S2G16	24.2	110	20.2	3013	1.1	99.9	-	71.3	8.3	-
S2G17	24.1	20	20.2	3018	1246	59	0.0484	71.3	1.5	285
S2L1	23.2	20	20.3	3043	1073	65	0.0570	71.4	1.5	335
S2L2	23.4	20	26.8	3014	760	75	0.0624	59.0	1.5	368
S2L3	23.8	20	23.7	3033	442	85	0.0718	48.4	1.5	422
S2L4	23.9	20	11.9	3033	260	91	0.0798	42.1	1.5	470
S2L5	24.2	20	9.7	3024	58	98	0.104	34.0	1.5	612
S2L6	25.0	20	9.8	2974	164	94	0.0773	34.3	1.5	455
S2L7	25.0	20	14.7	3024	760	75	0.0553	51.8	1.5	325
S2L8	24.7	20	19.8	3004	1188	60	0.0499	69.9	1.5	294
S2L9	23.2	20	20.0	3014	1367	55	0.0427	70.5	1.5	251
S2L10	23.5	20	14.8	3004	952	68	0.0461	52.0	1.5	271
S2L11	23.3	20	20.0	3004	1118	63	0.0534	70.6	1.5	314
S2L12	23.5	20	14.8	3033	680	78	0.0599	52.0	1.5	352
S2L13	23.8	20	9.6	3024	148	95	0.0792	33.9	1.5	466
S2L14	24.7	20	20.0	3019	1153	62	0.0523	70.6	1.5	308
S2L15	25.5	20	9.6	2984	101	97	0.0893	33.9	1.5	526
S2L16	22.7	20	35.2	3033	1791	41	0.0494	124	1.5	291
S2L17	22.7	20	20.1	3033	1171	61	0.0516	70.8	1.5	303
S2L18	22.9	20	9.6	3004	141	95	0.0799	33.9	1.5	470
S2L19	22.8	20	20.1	3004	1171	61	0.051	70.8	1.5	300
S2L20	22.4	20	35.2	3029	1786	41	0.0495	124	1.5	291
S2NL1	24.6	20	9.7	3014	9	99.7	-	34.2	1.5	-
S2NL2	24.0	20	9.8	3014	51	98	0.109	34.5	1.5	641
S2NL3	24.1	20	19.9	3014	1123	63	0.0532	70.2	1.5	313
S2NL4	23.9	20	14.7	3024	655	78	0.0611	51.8	1.5	359
S2NL5	23.8	20	9.9	3014	97	97	0.0926	34.9	1.5	545
S2NL6	23.3	20	20.0	3004	1118	63	0.0534	70.6	1.5	314
S2NL7	24.0	20	14.8	3043	493	84	0.0730	52.0	1.5	429
S2NL8	24.2	20	9.6	3014	23	99.2	-	33.9	1.5	-

Figure 9-25 is a comparative plot (Sherwood number versus Reynolds number) of the house air and nitrogen experiments. Although the removal rates were slightly higher with nitrogen, there is not a significant difference between the two. Therefore, the figure indicates that oxidation of sulfites to sulfates (less desirable species for SO₂ absorption) by the house air is not a serious concern.

We received a new contactor from Setec that contained four submodules welded together in the same way as the single submodule. We conducted experiments using water and 0.2M Na₂SO₃ as the scrubbing media and compared the results with those of the single welded module.

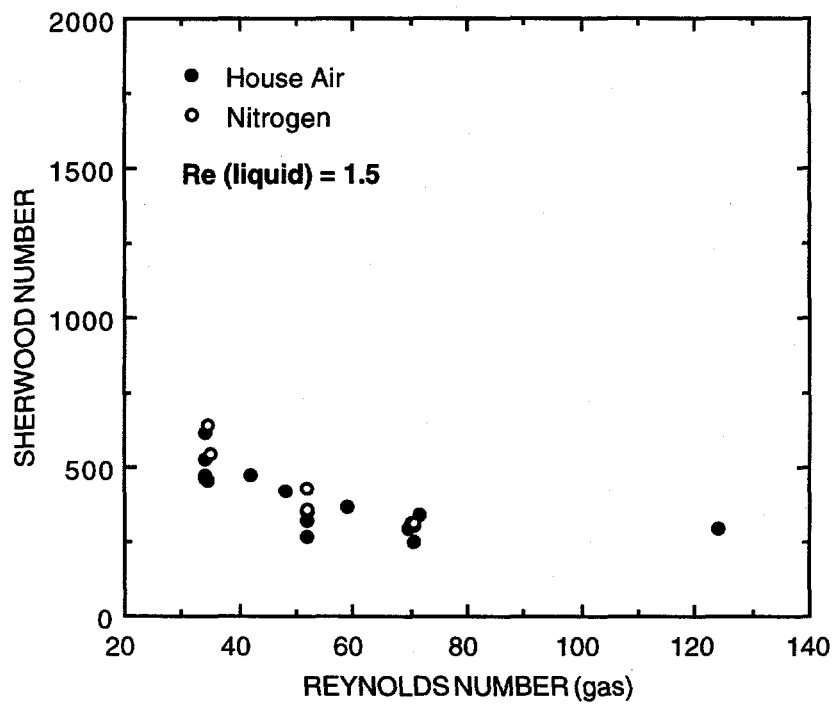
Figures 9-26 and 9-27 show the results obtained for these experiments. The observed MTCs with the four-unit module were significantly lower than those obtained using the single subunit module for both scrubbing liquids. The values were about 50% lower using water (Figure 9-26) and 70%-80% lower using 0.2M Na₂SO₃ solution (Figure 9-27).

We believe this discrepancy may be partly due to poor flow distribution of the gas among subunits in the module. To investigate this, we measured the flow through each of the individual modules using a mass flow meter. The total gas flow rate was 80 SLPM, the same rate that was used for the SO₂ scrubbing experiments. The flow through each module is shown in Table 9-7, with the submodule numbers indicating the direction of flow (i.e., the scrubbing liquid contacts No. 1 first and No. 4 last). The table shows that the flow distribution is not even among the four submodules. We investigated ways to correct this problem.

Table 9-7
GAS FLOW DISTRIBUTION IN FOUR-UNIT WELDED MODULE

Submodule No.	Flow (SLPM)
1	17.1
2	13.1
3	21.0
4	28.1

As we approached the portion of Task 9 that involved combined SO₂ absorption/scrubbing liquor regeneration, there were some issues we had to address. The first involved the design of the experimental apparatus. Although we were using HFCs for both the SO₂ absorption and the scrubbing liquid regeneration, the organic (d-DMA) regeneration was performed by bubbling sweep gas through a sparger. Because the sparger is not as efficient as the hollow fibers in providing mass



CM-3501-133

Figure 9-25. Sherwood number versus Reynolds number.

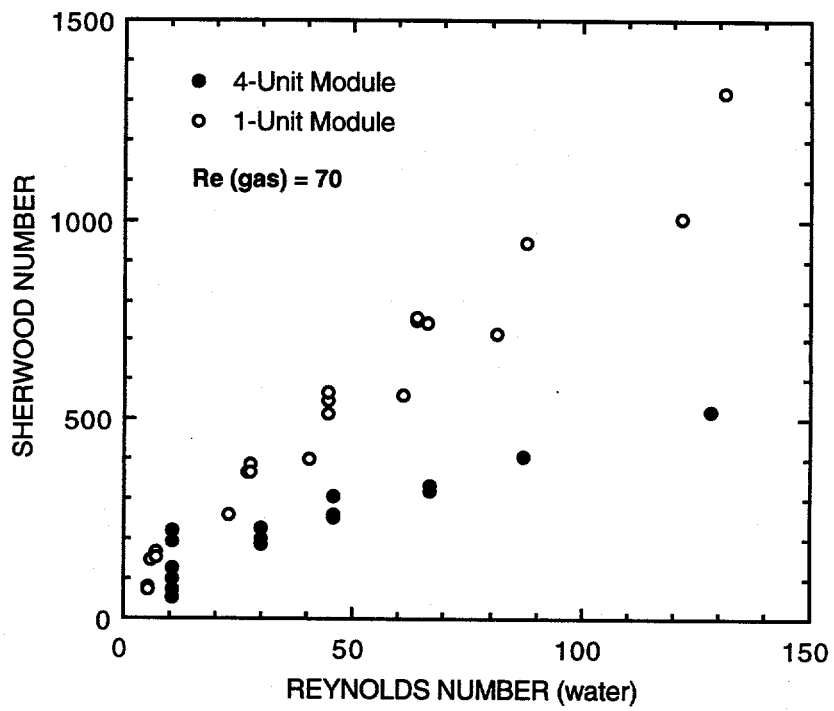
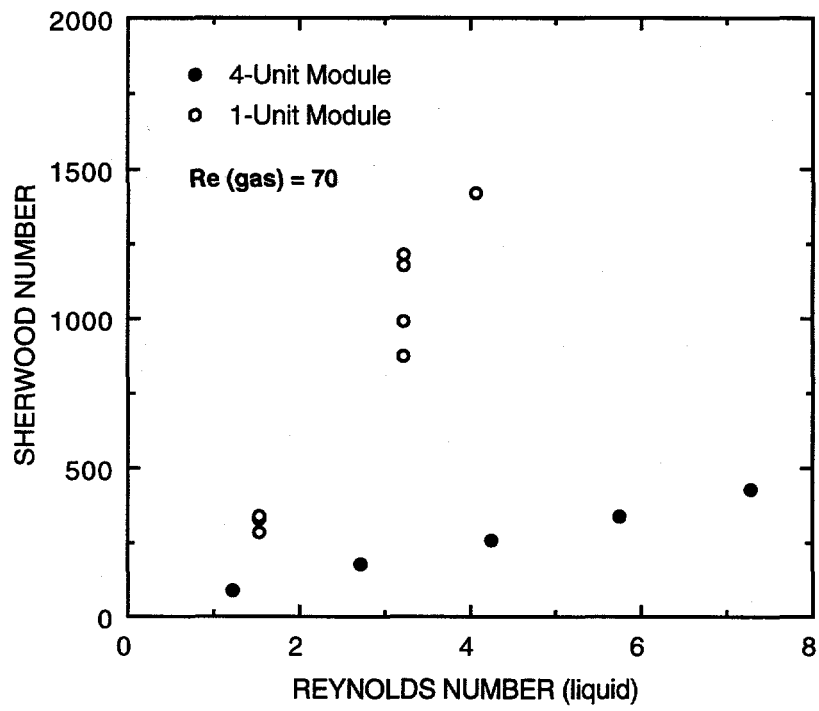


Figure 9-26. Sherwood number versus Reynolds number (water).



CAM-3501-132

Figure 9-27. Sherwood number versus Reynolds number (0.2 M Na₂SO₃).

transfer areas, we expected the regeneration of the organic liquid to be the factor that limited SO₂ removal. Possible solutions to this problem included the use of a distillation column rather than the sparger or operation of the experiment in a batch process as an alternative to regenerating the organic. Due to the time and expense involved in implementing either of the options, we performed the experiments as planned and evaluated the results with regard to the limitation imposed by the sparger.

The second issue stems from the results of the d-DMA synthesis. The final product exhibited some properties that were different from the properties of material synthesized and tested in Task 3. This new material was solid at room temperature, but melted at about 30°-40°C. The previously tested material was a low-viscosity liquid at room temperature. It seems that the amount of impurities in the d-DMA may determine the final form of d-DMA we obtain. The larger scale product was about 90% pure. We do not have any information on the earlier product, but we suspect it has a lower purity, causing a lower melting temperature. We planned on using the scaled-up synthesis product for the combined SO₂ absorption/scrubbing liquor regeneration step, but had to operate at slightly elevated temperatures. Another option was to dissolve this material in a high-boiling point solvent, such as sulfolane.

Lastly, it was important to address the safety issues regarding the d-DMA. Little is known about the toxicity of the compound. However, several of the reagents used are toxic and that the synthesized product is likely toxic and/or contains residual amounts of toxic compounds. In addition, some possibly carcinogenic solvents were used in the synthesis, so there may be a residue of suspect carcinogens. Therefore, care had to be taken to ensure that the d-DMA was not ingested, inhaled, or contacted with skin. Safety glasses, gloves and adequate ventilation had to be used at all times when handling the material. The material had to be stored and disposed as a hazardous organic substance.

We encountered some difficulties with the four-unit, welded module, in addition to the observed poor gas flow distribution as mentioned above. One of the four submodules had a liquid leak into the fiber lumens (gas side), and we also observed some deposits on the porex; the module was sent to Setec for repairs. We requested that they check the leaky submodule (and replace it if necessary), replace the soiled porex, and implement a more efficient flow distribution mechanism.

We completed construction of the apparatus for combined SO₂ absorption/scrubbing liquor regeneration in December 1995 (see Figure 9-19). Because the d-DMA melts above room temperature, we need to heat it slightly and continually circulate it through the process lines. For this reason, we could not start up the system in December, because the apparatus would have been left unattended for ten days during SRI's holiday closing. We began testing upon receipt of the repaired module.

The following is a summary of the changes made to the module during repairs. The leak we had observed in one of the submodules was repaired. The porex at the inlet, which had begun to appear soiled, was replaced with clean material. The new porex was circular rather than square in an attempt to create a better seal. In addition, we were given removable orifices in diameters of 1/16 inch and 3/32 inch to enable us to distribute the flow more evenly among the submodules.

The module was not returned to us until late January, at which time we spent several days drying the pores. We also determined the best configuration of the inlet orifices to obtain a good flow distribution. We chose to use no orifice on the first two submodules, a 3/32 inch orifice on Submodule 3 and a 1/16 inch orifice on Submodule 4. The distribution (shown in Table 9-8), although not perfectly even, was much improved.

Table 9-8
FLOW RATE DISTRIBUTION IN FOUR-UNIT WELDED MODULE

Submodule No.	Flow (SLPM)
1	19.0
2	18.2
3	17.4
4	24.8

Next, we performed SO₂ scrubbing tests with the repaired four-unit welded module. We also prepared to begin combined SO₂ absorption/scrubbing liquor regeneration, determined physical properties of the organic extractant, and performed one combined absorption/extraction experiment.

Figure 9-28 shows the results of the SO₂ scrubbing experiments, in which we used water as the scrubbing liquid. The Reynolds versus Sherwood plot is given for the repaired four-unit module along with the single-unit module and the four-unit module before repairs. This graph shows that the performance of the module did not change after the repairs. At first, one may expect the mass transfer to improve with a better gas flow distribution, but because mass transfer is

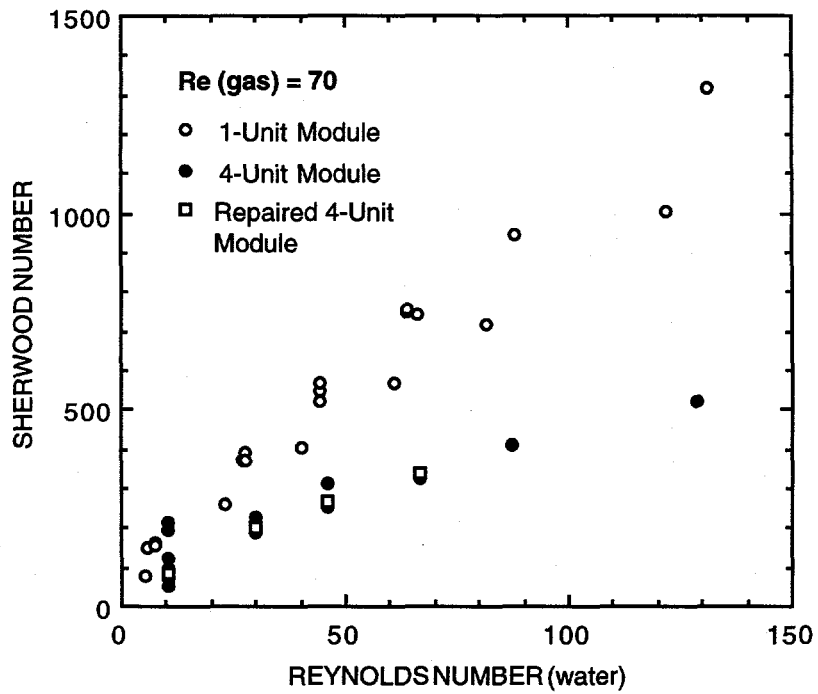


Figure 9-28. Sherwood number versus Reynolds number (water).

dominated by the liquid flow rate, a better gas flow distribution may not improve performance. Regardless, the four-unit module was still performing poorly when compared with the single-unit module. We believe that this is due to poor liquid flow distribution. One possible means to improve flow distribution was to change the module mounting from vertical to horizontal. In earlier work performed at NJIT, the module orientation was found to have an impact on the MTC (see Figure 4-11).

COMBINED SO₂ ABSORPTION/SCRUBBING LIQUOR REGENERATION

We measured several physical properties of the organic SO₂ extractant (d-DMA); these are shown in Table 9-9. We used Batch 1 in our experiments because of its lower melting point and lower viscosity.

After completing all of the pump, rotameter, mass flow controller, and orifice calibrations and testing the apparatus for leaks while pressurized at 15 psig, we began combined SO₂ absorption/scrubbing liquor regeneration experiments. We used the welded single-unit module to scrub the flue gas with the aqueous sodium sulfite solution, and the welded four-unit module to contact the aqueous solution and the organic extractant.

Table 9-9
PHYSICAL PROPERTIES OF d-DMA

Property	Batch 1	Batch 2
Measured	(distilled 10/19/95)	(distilled 10/25/95)
Melting Temperature	29.5 - 31°C	39 - 44°C
Range		
Density at 59°C	0.990 g/mL	1.001 g/mL
Viscosity at 39°C	17.7 cP	23.2 cP
Viscosity at 59°C	8.40 cP	10.1 cP

We were able to run the process for about 2 h, but did not reach steady state. Initially, SO₂ removals were high (>99%) but then began to decline gradually. The behavior was expected, as we anticipated the desorption of the d-DMA to be the limiting factor. Removal rates continued to decrease as the d-DMA came closer to saturation with SO₂.

During the experiment, we observed the sodium sulfite solution turning an orange color; we suspected that the solution was extracting an impurity in the d-DMA that was soluble in water/sodium sulfite. We analyzed the material to determine its chemical structure. We did not expect the impurity to cause problems in the process. However, when we shut down between tests we always replaced the sodium sulfite with fresh solution.

The next major obstacle we faced stemmed from the higher melting point of the d-DMA. After running the experiment, we flushed the contactor with methanol but still noticed a brown hue inside the module. We used a better solvent, trichloroethylene, which removed most traces of d-DMA. Because the solvent cleaning and vacuum drying process was so time consuming, it was not conceivable to clean the module between runs. Instead, we kept it heated in an oven to prevent the d-DMA from solidifying. This technique may have increased the likelihood of emulsions forming during experiments, but we did not expect this to cause any major problems.

The experiment we performed indicated that it would probably take several days to reach steady state conditions. Therefore, we focused our efforts on improving the integrity of the system to allow for longer periods of continuous operation.

During our second attempt at running the experiment, we observed a significant leak in the absorber module, causing the sodium sulfite solution to pass through the pores into the gas side. This was probably because the absorber module was not completely dry (we cleaned both modules with TCE and methanol after the first run). The next problem we encountered was a pressure buildup on the d-DMA inlet to the regenerator module. This seemed to be caused by d-DMA solidifying in the module before reaching its steady-state temperature. We prevented this from happening by preheating the cooling liquid to ensure that the d-DMA left the cooler at around 40°C, instead of slowly increasing from room temperature to the steady-state temperature.

The final concern we had to address before running the experiment continuously was an emergency shutdown system. Initially, we tried to use a thermal dispersion flow switch to detect a d-DMA leak, but this was not effective at detecting flow of the organic liquid. We then set up a system to detect a catastrophic leak based on temperature readings; if the temperature begins to drop in the d-DMA lines, this indicated that flow has ceased due to a leak and the pump would be shut off.

We analyzed (by NMR) the orange material that was extracted into the aqueous phase out of the organic phase. This indicated that some of the d-DMA had degraded; the ether bond was broken and an alcohol was formed. We did not have any quantitative information on what fraction of the d-DMA had reacted, but we found that after several water extractions on a small sample, we were able to completely remove the new compound. This extraction procedure would have been

quite lengthy and complicated if we performed it on the entire volume of d-DMA, so we used the d-DMA we had "as is." We did not expect the alcohol to have much effect on SO₂ absorption, but it probably increased the vapor pressure of the organic material. Still, the overall effect of degradation on the process was expected to be very minor.

In the next experiment, we planned to leave the system running for at least 24 consecutive hours, as we believe that it might take a few days to reach steady-state conditions. We were able to circulate d-DMA through the tube side of the regenerator module for several days without problems. The sodium sulfite solution was not flowing through the shell side, because we were still experiencing difficulty keeping the aqueous material from leaking into the tube side of the fibers, so we were unable to flow the solution for long periods of time. Previous to this experiment, we had observed that the d-DMA was not flowing through the fiber pores, perhaps because of its high surface tension. This observation led us to believe that we could circulate d-DMA inside the fibers without the pressurized aqueous solution on the outside. In case of a leak, however, we closed the valves on the shell inlet and outlet.

After a few days of d-DMA circulation, we began flow of the sodium sulfite solution. We opened the valves on the shell inlet and outlet of the LLE module and attempted to pump the aqueous solution through the shell side. However, we were unable to get any liquid through the shell side of the module. We noticed that d-DMA had traveled through the pores and collected in the inlet and outlet ports of the shell side of the module, where it solidified. We are not sure why the d-DMA came through the pores; possibly the fibers were weakened due to the pressure buildup we experienced earlier or the higher temperature of d-DMA decreased the surface tension low enough to flow through the pores. In any case, we needed to get the solidified d-DMA out of the ports, so we used heating tape on a low setting. Once the d-DMA melted, we planned to attempt to flow sodium sulfite solution again. However, we were unable to prevent the organic liquid from coming into the aqueous lines after it melted; even the flue gas scrubbing module was contaminated with d-DMA. At this point, we decided that the high melting point of the d-DMA was causing too many problems and we investigated other options. We chose to switch to dimethylaniline (DMA) as the organic extractant. We should be able to use the DMA data to make predictions for system performance using d-DMA.

While waiting for our DMA order to arrive, we thoroughly cleaned the d-DMA out of both the absorber and extractor modules. We then performed one experiment using 0.05M sodium sulfite as the scrubbing solution and DMA as the SO₂ extractant. We were unable to run the experiment long enough to collect any valid data due to several problems we experienced. First, the sodium sulfite solution was leaking through the pores of both the absorber and the extractor module. This caused loss of sodium sulfite through the gas line and into the DMA reservoir, and

also caused inaccurate analyzer readings from sodium sulfite in the sample lines. We had experienced this problem with this module for a year and were still unable to find a way to prevent leaking. In addition, we noticed that the air bubblers in the DMA flask were causing foaming of DMA, leading to overflow and foam in the process lines. Because of these problems, we had to shut down the experiment.

This task was not completed due to a stop work order from the DOE.

TASK 10: DEVELOPMENT OF COMPUTATIONAL MODEL

The purpose of this task was to develop a fundamental computational model for the performance of the rectangular HFC and HFCLM modules using the fundamental mass transfer and thermodynamic data obtained in Tasks 2 through 9. This computational model would account for fiber ID, fiber OD, fiber packing density, liquid and gas flowrates, liquid phase chemistry and other such parameters as may seem pertinent. Nevertheless, the model would be only as detailed as can be tested experimentally in the observed mass transfer behavior of the system. We therefore would not attempt to solve the simultaneous three-dimensional flow fluid and conservation of mass equations. Rather, we would take a correlative approach typical of chemical engineering practice (using dimensionless numbers such as Reynolds number, Schmidt number, Peclet number) to produce a fundamentally-based and yet workable model. Examples of such correlative approaches have been given by Cussler and co-workers (Wickramasinghe, et al., 1991; Yang and Cussler, 1986; Qi and Cussler, 1985).

We were unable to develop correlations based on the Task 9 results because of our experimental difficulties, which led to insufficient data. We did, however, produce correlations based on results from earlier tasks. This is discussed in detail in Section 14.

TASK 11: CONSTRUCTION OF SUBSCALE PROTOTYPE SYSTEM

The objective of this task was to devise and build a test stand for conducting flue gas scrubbing with approximately 100 acfm of synthetic flue gas and for conducting scrubber liquor regeneration with the attendant liquid flowrates (about 0.1 to 1.0 gal/min). This test stand would include (1) a system for generating synthetic flue gas with SO₂ concentrations ranging from 0 to 3000 ppm, NO_x concentrations ranging from 0 to 60 pm, and with CO₂, O₂, N₂, and water vapor in a relatively narrow range typical of flue gas; (b) automatic data acquisition for recording flowrates, temperatures, pressures, and gas and liquid compositions; (c) a support structure for holding the SO₂ absorber and NO_x absorber cassettes[†]; (d) a support structure for holding SO₂ liquor regeneration cassette; (e) a vessel for regenerating the NO_x liquor (also for regenerating organic SO₂ extractant if option A is chosen for SO₂ liquor regeneration); and (f) attendant pumps, valves, gauges, ducting, and the like.

We did not execute this task due to the stop work order.

[†] We mean the hollow fiber contactors which, in module form, will likely be rectangular; in a full-scale plant these modules would likely be arranged horizontally (as in Appendix A) with a height of about 1 to 2 feet and a 100' x 100' cross section. Hence, these modules stack like cassette tapes, hence, the term cassettes.

TASK 12: OPERATION OF SUBSCALE PROTOTYPE SYSTEM

In this task, the objective was to determine the mass transfer behavior of our absorber cassettes and regenerator cassettes in our subscale prototype system. This system would present us with the opportunity for the first time to test modules for SO₂ absorption, NO absorption, and SO₂ regeneration that are of such a geometry and size that are conceivably scalable to a proof-of-concept test at the 5 MW(e) size (10,000 acfm, not part of this research). Therefore, we could obtain enough mass transfer data to achieve confidence in the design fundamentals of this system. Because of the size of the liquid flows necessary to obtain such mass transfer data, it would be essential to regenerate the scrubber liquors so as not to incur substantial chemical expenses. Therefore, we would aim for practical purposes to operate the system as an integrated SO₂/NO_x scrubber/regenerator, but would not insist on doing so. In this sense, basic mass transfer data on the individual components would take precedence over simply operating the system. Nevertheless, we would aim for a continuous integrated run of approximately one month duration towards the end of Task 12.

Because of the geometry of the HFC absorbers, it would be possible to stack the NO_x HFC absorber ("cassette") on top of the SO₂ "cassette". With our "stacked cassette" SO₂/NO_x scrubber and individual vessels for SO₂ and NO_x liquor regeneration, we would test a range of simulated flue gas compositions (e.g., 1500 to 4000 ppm SO₂, 300 to 600 ppm NO_x) at a variety of flowrates (e.g., 50 to 200 acfm). We intended to study the efficiency and mass transfer behavior of the individual absorbers and regenerator components of the system. We would use at least three different SO₂ and NO_x HFC absorbers and hollow fiber SO₂ regenerators in our studies, each with different fiber packing densities and fiber inside diameters (e.g., 240-400 μm ID). We would also do pure component inert gas tests so as to isolate the liquid-side mass transfer coefficient phenomena independent of the gas-side phenomena. In this way, we could obtain enough mass transfer design data that we would be able to understand the system and, along with our previous tasks, could create a computational design model that can be used with confidence (task 13).

We did not execute this task due to the stop work order.

TASK 13: REFINEMENT OF COMPUTATIONAL DESIGN MODEL

The purpose of this task was to use all of the data taken in our subscale prototype system tests to adjust and refine the computational model devised in Task 10. The result of Task 13 would be a design computer program, fundamentally-based, that could be used to guide scale up of this process to the proof-of-concept stage.

We did not execute this task due to the stop work order.

TASK 14: ECONOMIC EVALUATION

The objective of this task was to perform increasingly detailed economic analyses of the overall process to guide the research to the most critical problems and to assist management decision points.

We estimated the size and cost major battery limit equipment and the results for Option A (LLE of SO₂).

Figure 14-1 shows the process flow sheet with all the major equipment labeled. Table 14-1 gives the design basis for our 500-MW(e) plant. Given these design specifications, we proceeded with the sizing and costing of various equipment. The calculations for the absorbers (SO_x and NO_x) and the liquid-liquid extractor are presented in detailed below.

SO₂ ABSORBER

Based on the mass transfer data from Task 4, the important parameters and thermodynamic conditions are

SO ₂ absorbing liquid:	0.2 M Na ₂ SO ₃
Approach to equilibrium:	50% (assumed)
Liquid flow rate:	2.88 x 10 ⁴ L/min (98% removal basis)
Assumption:	p* <<< p (liquid has significant absorption capacity)
Mass transfer correlation:	

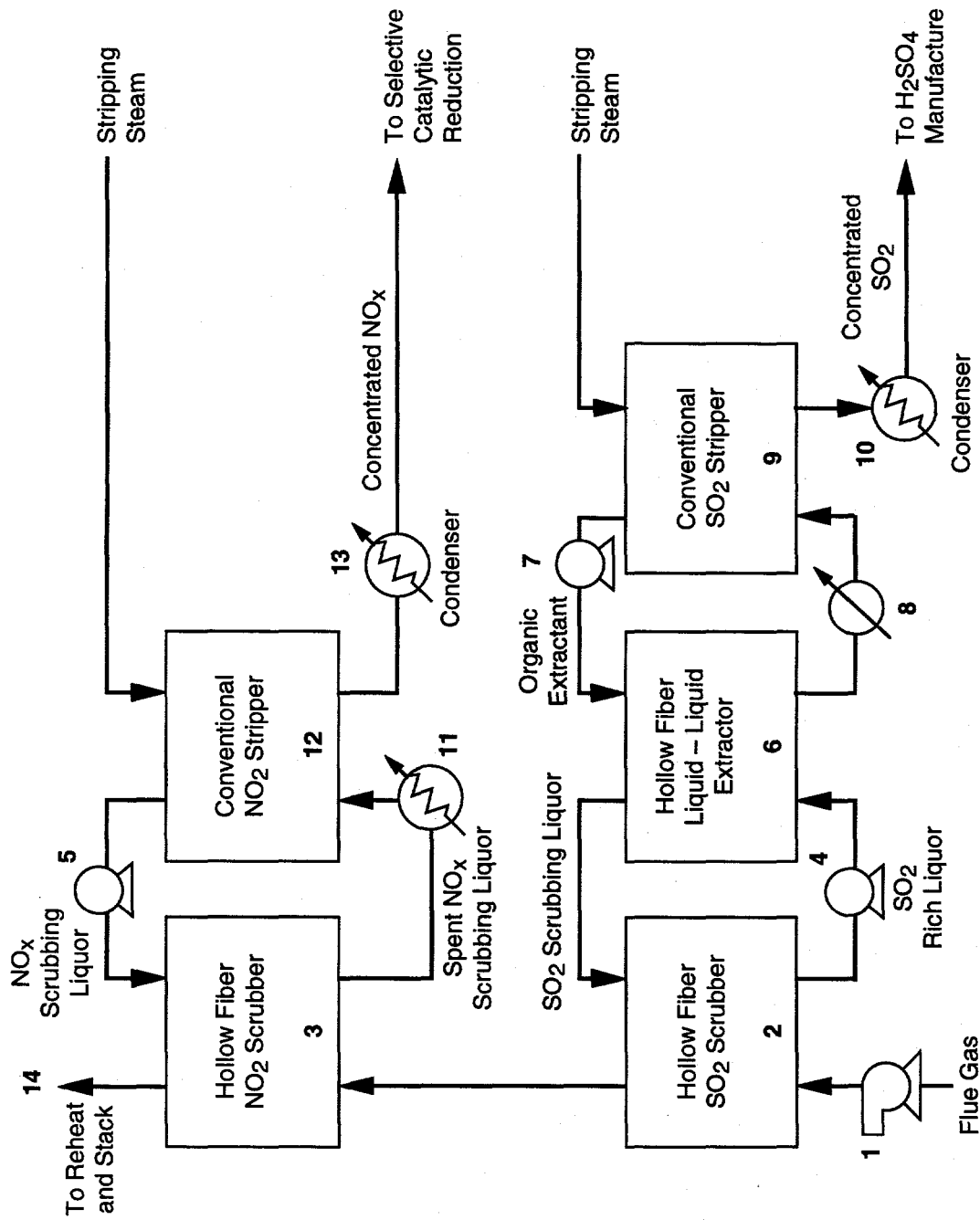
$$K_{Og} = 0.079257 Re^{0.33211} \quad (14-1)$$

where Re is the gas-side Reynolds number and is given as

$$Re = \frac{4 \rho_g Q_g}{\pi \mu_g d_i N} \quad (14-2)$$

where

ρ_g	=	gas density (g/cm ³)
Q_g	=	volumetric gas flow rate (cm ³ /s)
μ_g	=	viscosity of flue gas (g/cm s)
d_i	=	ID of the fiber (cm)
N	=	number of fibers



CM-360583-49D

Figure 14-1. Proposed SO₂/NO_x wet scrubbing with hollow fiber contacting devices. Option A for SO₂ liquor regeneration.

Table 14-1
BASIS FOR EXAMPLE DESIGN OF 500-MW(e) SO_x/NO_x PLANT

Flue gas flow rate	1 million actual ft ³ /min (2.25 x 10 ¹⁰ sccm)
Flue gas temperature	160°F
Flue gas pressure	760 mmHg
Flue gas composition	
SO _x	3000 ppm(v)
NO _x	450 ppm
CO ₂	14%
H ₂ O	8%
O ₂	3.3%
N ₂	74.4%
Fraction of SO _x /NO _x removed in absorbers	
SO _x	98%
NO _x	85%
Pressure drop	
SO _x scrubber (flange to flange)	10 inches H ₂ O
NO _x scrubber (flange to flange)	10 inches H ₂ O

Equation (14-1) is obtained from the experimental results of Task 4. Our equilibrium calculations for Na₂SO₃/SO₂ systems indicate that the partial pressure of SO₂ (p*) in equilibrium with the liquid is much lower than the actual partial pressure (p). For these conditions, the mass balance yields

$$\ln \frac{p_0}{p_L} = K_{og} \pi d_o L N / Q_g \quad (14-3)$$

where p₀ and p_L indicate the partial pressures of SO₂ in the entering and exiting gas streams, respectively.

The pressure drop in the module should not exceed 10 inches of water, and this constraint is imposed using the Hagen-Poiseulle equation (Bird et al., 1960).

$$Q_g = \frac{\pi d_i^4 \Delta P N}{128 \mu_g L} \quad (14-4)$$

where

$$\begin{aligned}\Delta P &= \text{pressure drop [dynes/cm}^2\text{]} \\ L &= \text{length of the fiber [cm]}\end{aligned}$$

Using the above four equations, we can explicitly find the number of fibers and then the length of the fiber, given the ID of the fiber. Commercially available 400- μm -ID is chosen to report cost information. The cost of the membrane is taken as \$0.20/ft² as per the arguments presented in our proposal (PYU 90-167).

NO_x ABSORBER

The key assumptions and conditions are

Absorbing liquid:	0.1M Co(II)-phthalocyanine
Approach to equilibrium:	10% (assumed based on the lab data)
Liquid flow rate:	48115 L/min (85% removal basis)

The mass transfer correlation (from Task 5) is

$$K_{og} = 0.0011907 \text{ Re}^{1.0307} \quad (14-5)$$

The mass balance equation for NO at any point in the absorber is given as

$$Q_g \int_{p_L}^{p_0} \frac{dp}{p - p^*} = K_{og} \pi d_o L N \quad (14-6)$$

The integral value in Eq. (14-6) is calculated by a numerical scheme and is a fixed number for a constant NO removal desired (85%). Similar to SO₂ absorber calculations, Eq. (14-5) and (14-6) are to be used in association with Eq. (14-3) and (14-4) to estimate the membrane area requirements.

LIQUID-LIQUID EXTRACTOR

The spent aqueous SO₂ liquor flow rate and SO₂ concentration in the solution are known from SO₂ absorber calculations. The partition coefficient from Task 6 is obtained as 0.5 (C_{org}/C_{aq}). Again, organic phase (DMA) is assumed to approach 50% equilibrium corresponding to the aqueous liquor inlet SO₂ concentration. Therefore,

DMA flow rate:	1.146 x 10 ⁵ L/min (99% removal basis)
----------------	---

From the laboratory data, the relation between organic side overall MTC ($K_{ov,org}$) and the shell side Re is given as

$$K_{ov,org} = 0.044754 Re^{1.3829} \quad (14-7)$$

However, using the proposed rectangular type modules with a length of 50 cm, the Re numbers turn out to be in the range of a few hundreds, leading to unacceptably high MTCs. In a situation where organic side and aqueous side resistances are negligibly small, we have the stagnant membrane phase (pore) resistance. This membrane resistance can be fairly well calculated using the following relation:

$$K_{ov,org} = \frac{D_{SO_2}}{t} \quad (14-8)$$

where

t = membrane wall thickness (cm)

D_{SO_2} = diffusion coefficient of SO_2 (cm^2/s)

Now, using the above $K_{ov,org}$ value and the log-mean concentration (ΔC_{ln}) driving force, the membrane area requirements can be calculated as

$$J_{SO_2} = K_{ov,org} \pi d_o L N \Delta C_{ln} \quad (14-9)$$

where J_{SO_2} = rate of SO_2 transfer (mole/s)

Knowing the gas and liquid flow rates at each point in the process, we can estimate the sizing of pumps and their costs using the simulation program, ASPEN. Likewise, the flue gas blower, stack gas reheating system, heat exchangers, and conventional strippers are designed and the corresponding utility costs are estimated. These details are given in Table 14-2.

Following the research that was completed in Task 9, the process costs were updated and are displayed in Table 14-3. The only costs that have changed were those related to the SO_2 extractant stripping section. This was due to a recently discovered error in the technical proposal. In Appendix A, page IA-10, the equilibrium K-factor was listed as 82.2. This is an incorrect calculation; the actual K-factor at $100^\circ C$ is about 2.7. This led to an increase in the required steam flow rate, which in turn greatly increased the cost of the extractant steam stripper and the condenser after the SO_2 stripper. By operating the stripper at a higher temperature, these costs are reduced, but the cost of the extractant heat exchanger is increased. We studied several cases and found an economic optimum using a 10-stage stripper at $125^\circ C$.

Table 14-2

**COST OF MAJOR EQUIPMENT AND UTILITY ITEMS IN OPTION A
FOR A 500-MW(e) POWER PLANT¹ (CORRECTION)
(Liquid-Liquid Extraction of SO₂ Liquor)**

<u>Item No.</u>	<u>Item Name</u>	<u>Capital Cost (dollars)</u>	<u>Utility Cost (dollars/h)</u>
1	Flue gas fan	\$750,000	\$170
2	SO ₂ scrubber	916,000	—
3	NO _x scrubber	2,060,000	—
4	SO ₂ liquor pump	27,000	7
5	NO _x liquor pump	34,000	4
6	SO ₂ extractor	500,000	—
7	Extractant pump	87,000	18
8	Extractant heat exchanger	424,000	1,560
9	Extractant steam stripper	400,000	100
10	Condenser after SO ₂ stripper	50,000	9
11	NO _x heat exchanger	473,000	1,880
12	NO _x steam stripper	188,000	484
13	Condenser after NO _x stripper	219,000	156
14	Stack gas reheating system	<u>1,729,000</u>	<u>231</u>
	Total	\$7,857,000	\$4,619

¹Integrating items 8 and 10 will eliminate item 10 and reduce the utility cost of item 8 to \$1307/h. Likewise, integrating items 11 and 13 will eliminate item 13 and reduce the utility cost of item 11 to \$1307/h.

Table 14-3

**COST OF MAJOR EQUIPMENT AND UTILITY ITEMS IN OPTION A
FOR A 500-MW(e) POWER PLANT^{1,2} (CORRECTION)
(Liquid-Liquid Extraction of SO₂ Liquor)**

Item No.	Item Name	Capital Cost (dollars)	Utility Cost (dollars/h)
1	Flue gas fan	\$750,000	\$170
2	SO ₂ scrubber	916,000	—
3	NO _x scrubber	2,060,000	—
4	SO ₂ liquor pump	27,000	7
5	NO _x liquor pump	34,000	4
6	SO ₂ extractor	500,000	—
7	Extractant pump	87,000	18
8	Extractant heat exchanger	853,000	2,291
9	Extractant steam stripper	589,000	907
10	Condenser after SO ₂ stripper	369,000	311
11	NO _x heat exchanger	473,000	1,880
12	NO _x steam stripper	188,000	484
13	Condenser after NO _x stripper	219,000	156
14	Stack gas reheating system	<u>1,729,000</u>	<u>231</u>
	Total	<u>\$8,794,000</u>	<u>\$6,459</u>

¹Coolers for recycling the organic extractant back to the SO₂ extractor (item 6) and the NO_x scrubbing liquor back to the NO_x scrubber (item 3) were not included in the original design proposal and, hence, are not included in this design. These are estimated to add an additional capital cost of \$3,100,000 and an additional utility cost of \$491/h.

²Integrating items 8 and 10 will eliminate item 10 and reduce the utility cost of item 8 to \$1422/h. Likewise, integrating items 11 and 13 will eliminate item 13 and reduce the utility cost of item 11 to \$1307/h.

We did not update the costs of the HFC modules because of inconclusive lab data in Task 9. The rectangular modules were exhibiting unusual mass transfer characteristics that were probably due to liquid side flow channeling. For this reason, we were unable to obtain a reliable correlation to size the full-scale modules. Therefore, the costs have been reported based on Phase I results.

TASK 15: REPORTING AND DELIVERABLES

Deliverables for this project were the documents specified in the Reporting Requirements Checklist, DOE F 1332.1. Copies of each report were mailed to the Document Control Center at the Pittsburgh Energy Technology Center (P.O. Box 10940, MS 921-118, Pittsburgh, PA 15236-0940).

TASK 16: CHEMICAL SYNTHESIS FOR PROCESS SCALE-UP

This task consisted of the synthesis efforts that were necessary for providing sufficient SO₂ liquor regeneration chemicals and NO_x scrubbing chemicals to allow proper study and operation of the NO_x life tests (Task 8) and of the scalable modules (Task 9).

The synthesis procedure for d-DMA [2,2'-bis(N-methyl-N-phenyl)ethyl ether] is described in SOP 340.3064 in Appendix F. We synthesized about 10 L of d-DMA for Task 9.

We synthesized a second batch of the tetrasodium salt of Co(II) 4,4',4'',4'''-tetrasulfophthalocyanine 2-hydrate according to a modified method of Weber and Busch (1965). A 2 L, three-necked, reaction flask fitted with a stirring rod and condenser was placed in an oil bath at room temperature. Monosodium salt of 4-sulfophthalic acid (120 g) was ground with a pestle and mortar and added to the reactor. Urea (163 g) was ground and added to the reactor. Ammonium chloride (13 g) was ground and added to reactor. Ammonium molybdate (2 g) was ground and added to the reactor. Co(II) sulfate hydrate (20 g) was ground and added to the reactor. Nitrobenzene (240 mL) was added to the reactor. The reaction vessel was heated at 180°C with stirring for 6 h. After the reaction time, the oil bath was shut off and the resulting cake was allowed to cool. The reactor was then destroyed to remove the hardened cake. The cake was ground and washed several times with methanol to remove most of the nitrobenzene. Additional purification was accomplished by stirring the product for 24 h in a large volume (~2L) of methanol and then filtering it. The washing and filtering steps were repeated. The product was dried in a vacuum oven at 60°C for 24 h to drive off the residual solvent. Forty-one grams of product was obtained. (UV spec: $\lambda_{\text{max}} = 660 \text{ nm}$, $\epsilon = 3.4 \times 10^3 \text{ M}^{-1} \text{ cm}^{-1}$).

REFERENCES

- Bird, R. B., W. E. Stewart, and E. N. Lightfoot (1960) *Transport Phenomena* (John Wiley and Sons).
- Cussler, E. L. (1984) *Diffusion* (Cambridge Press).
- Dean, J. A., Ed. (1979) *Lange's Handbook of Chemistry*, 12th ed. (McGraw-Hill, New York), p. 10-5.
- Demyanovich, R. J., and S. Lynn (1987) *Ind. Eng. Chem. Res.* **26**, 548-555.
- EPRI (Electric Power Research Institute) Report CS-2894 (Electric Power Research Institute, Palo Alto, CA).
- Fuchs, N. A. (1964) *Mechanics of Aerosols* (Pergamon Press, London), pp. 205-206.
- Geankoplis, C. (1978), *Transport Processes and Unit Operations* (Allyn and Bacon, MA).
- Karoor, S. (1992) "Gas Absorption Studies Using Microporous Hollow Fiber Membranes," Ph.D. Thesis, Stevens Institute of Technology, Hoboken, NJ.
- Kreith, F., and W. Z. Black (1980) *Basic Heat Transfer* (Harper and Row, Cambridge).
- Majumdar, S., et al. (1988) *AIChE J* **34**, 1135.
- Sada, E., H. Kumazawa, and Y. Takada (1984) *Ind. Eng. Chem. Fund.* **23**, 60-64.
- Weber, J. H. and Busch, D. H. (1965) *Inorganic Chemistry* **4**, 470.
- Wickramasinghe, S. R., M. J. Semmens, and E. L. Cussler (1992) "Hollow Fiber Modules Made with Hollow Fiber," *AIChE J.*
- Yang, M. C. and E. L. Cussler (1986) "Designing Hollow-Fiber Contactors," *AIChE Journal* **32**, 1910-1916.

Appendix A
INITIAL PRESSURE

INITIAL PRESSURE

In the test absorption apparatus, the sample cell is initially evacuated to a low pressure $P_{SC}(0)$, higher than the test adsorbent's vapor pressure. At this point, the sample cell contains N_2 and the adsorbent's vapor. The sample cell is then isolated and the headspace evacuated to a lower pressure $P_{HS}(0-)$, containing pure N_2 . The headspace is then pressurized to $P_{HS}(0)$ with a SO_2/N_2 gas mixture containing y^0 mole fraction SO_2 . At this point, the total moles of each gas is

$$\text{moles } N_2(0) = [P_{SC}(0) - P_V] \left[\frac{V_{SC} - V_L}{RT} \right] + P_{HS}(0) \frac{V_{HS}}{RT} + (1-y^0) [P_{HS}(0) - P_{HS}(0-)] \frac{V_{HS}}{RT} \quad (A-1)$$

$$= [P_{SC}(0) - P_V] \left[\frac{V_{SC} - V_L}{RT} \right] + (P_{HS}(0) - y^0 [P_{HS}(0) - P_{HS}(0-)]) \frac{V_{HS}}{RT} \quad (A-2)$$

$$\text{moles } SO_2(0) = y^0 [P_{HS}(0) - P_{HS}(0-)] \frac{V_{HS}}{RT} \quad (A-3)$$

where P is the pressure, V is the volume, P_V is the adsorbent's vapor pressure, R is the gas constant, and T is the absolute temperature. The subscripts HS, SC, and L refer to the headspace, sample cell, and liquid adsorbent, respectively.

At time 0, the headspace and the sample cell are connected by opening a valve. Here, we make two assumptions: (1) the gases in the headspace and sample cell instantly mix, and (2) the liquid adsorbent instantly exerts a vapor pressure in the headspace and sample cell. Thus, the partial pressure of each gas is given by

$$P_{N_2}(0) = \frac{[\text{moles } N_2(0)] RT}{V_{HS} + V_{SC} - V_L} \quad \text{and} \quad P_{SO_2}(0) = \frac{[\text{moles } SO_2(0)] RT}{V_{HS} + V_{SC} - V_L} \quad (A-4)$$

and the total pressure is given by

$$P(0) = P_{N_2}(0) + P_{SO_2}(0) + P_V \quad (A-5)$$

Substituting Eqs. (A-2) and (A-3) into Eq. (A-4) and then into Eq. (A-5) yields

$$P(0) = \frac{[P_{SC}(0) - P_V] [V_{SC} - V_L] + P_{HS}(0) V_{HS}}{V_{HS} + V_{SC} - V_L} + P_V \quad (A-6)$$

Note the absence of $P_{HS}(0-)$ from Equation (A-6). The initial mole fraction of SO_2 , $y_{SO_2}(0)$ is given by

$$y_{SO_2}(0) = \frac{P_{SO_2}(0)}{P(0)} = \frac{y^0 [P_{HS}(0) - P_{HS}(0-)] V_{HS}}{[P_{SC}(0) - P_V] [V_{SC} - V_L] + P_{HS}(0) V_{HS} + P_V (V_{HS} + V_{SC} - V_L)} \quad (A-7)$$

Appendix B

CALCULATION OF H AND H*

CALCULATION OF H AND H*

The partition coefficient, H, is defined as

$$H = \frac{P_{\text{SO}_2(\text{f})}}{x_{\text{SO}_2(\text{l})}} = P_{\text{SO}_2(\text{f})} \left[1 + \frac{\text{moles adsorbent}}{\text{moles SO}_2 \text{ in liquid}} \right] \quad (\text{B-1})$$

where $P_{\text{SO}_2(\text{f})}$ is the equilibrium partial pressure of SO_2 , and $x_{\text{SO}_2(\text{l})}$ is the mole fraction of SO_2 in the liquid adsorbent at equilibrium. At equilibrium, we can also write a SO_2 mass balance:

$$\frac{P_{\text{SO}_2(\text{f})}}{RT} [V_{\text{HS}} + V_{\text{SC}} - V_{\text{L}}] + \frac{P_{\text{SO}_2(\text{f})} C_{\text{L}} V_{\text{L}}}{H - P_{\text{SO}_2(\text{f})}} = y^{\circ} [P_{\text{HS}(0)} - P_{\text{HS}(0-)}] \frac{V_{\text{HS}}}{RT} \quad (\text{B-2})$$

where C_{L} is the concentration of liquid adsorbent (moles/L) and the remaining symbols were defined in Appendix A. The first term on the left side in Eq. (B-2) is the number of moles of SO_2 in the gas phase at equilibrium; the second term is the number of moles of SO_2 in the liquid adsorbent at equilibrium (rearrange Eq. (B-1)); and the right side of Eq. (B-2) is the number of moles of SO_2 initially (see Eq. (A-3)).

Eq. (B-2) may be rearranged to yield

$$H = \frac{[V_{\text{HS}} + V_{\text{SC}} - V_{\text{L}}] P_{\text{SO}_2(\text{f})}^2 - [C_{\text{L}} V_{\text{L}} RT - y^{\circ} (P_{\text{HS}(0)} - P_{\text{HS}(0-)})] P_{\text{SO}_2(\text{f})}}{[V_{\text{HS}} + V_{\text{SC}} - V_{\text{L}}] P_{\text{SO}_2} - y^{\circ} [P_{\text{HS}(0)} - P_{\text{HS}(0-)}] V_{\text{HS}}} \quad (\text{B-3})$$

Each term on the right side of this equation is known during an experiment.

Because H is defined in terms of mole fraction liquid, comparing absorption into different liquids can be difficult. Hence, we define H^* :

$$H^* = \frac{\text{volume (STP) of SO}_2 \text{ absorbed}}{\text{volume of liquid absorbent}} \quad (\text{B-4})$$

$$= \frac{(\text{moles SO}_2 \text{ in liquid}) 22410}{V_{\text{L}}} \quad (\text{B-5})$$

where V_{L} is the liquid volume in cm^3 . We may substitute the second term of Eq. (B-2) into Eq. (B-5) and rearrange:

$$H^* = \frac{22410 C_{\text{L}} P_{\text{SO}_2(\text{f})}}{H - P_{\text{SO}_2(\text{f})}} \quad (\text{B-6})$$

Hence, knowing H, we can calculate H^* .

Appendix C

EQUILIBRIUM CONSTANT FROM BREAKTHROUGH CURVES

EQUILIBRIUM CONSTANT FROM BREAKTHROUGH CURVES

Consider the reaction



where A is in the gas phase and B is a compound in the liquid phase that complexes with A to form C, also in the liquid phase. When A at concentration C_0 is fed to a bubbler containing B, the concentration of A leaving the bubbler will be reduced initially. As B becomes saturated with A, this exit concentration of A will increase with time. This concentration change of A over time is called the breakthrough curve. A typical curve was shown in Figure 2-16 for NO being absorbed by aqueous Fe(II)-EDTA. From such data, we can readily calculate the solubility of A in the liquid as well as the equilibrium constant K for the reaction listed in Eq. (C-1).

To obtain the solubility, we first write a mass balance:

$$\begin{aligned} \text{amount of solute} &= \text{amount of solute in} - \text{amount of solute out} \\ \text{accumulated in liquid} & \\ &= QC_0t_s - Q \int_0^{t_s} C \, dt \end{aligned} \quad (C-2)$$

where Q is the total gas flow rate, C_0 is the inlet concentration of A, and t_s is the time at which the outlet and inlet concentration of A are the same. Dividing by the liquid volume V yields

$$C_s = \frac{QC_0}{V} t_s - \frac{Q}{V} \int_0^{t_s} C \, dt \quad (C-3)$$

where C_s is the total solubility of A in the liquid. Thus the area between the breakthrough curve and a horizontal line at C_0 (i.e., the area above the breakthrough curve) is proportional to the solubility as implied by Eq. (C-3).

From these data, we can also compute the equilibrium constant. First, however, we write the reaction in the form



where A(l) is assumed to be in equilibrium with A(g). This equilibrium is often written as a Henry's law partition coefficient:

$$A(l) = H A(g) \quad (C-5)$$

Thus, we may write the equilibrium constant for the reaction listed in Eq. (C-4) as

$$K = \frac{[C]}{[A(l)][B]} = \frac{[C]}{H[A(g)][B]} \quad (C-6)$$

By stoichiometry, we have

$$[C] = [B]_0 - [B] = C_s - [A(l)] \quad (C-7)$$

where $[B]_0$ is the concentration of B initially and C_s is given by Eq. (C-3). Thus we obtain

$$K = \frac{C_s - H[A(g)]}{H[A(g)]\{[B]_0 - C_s + H[A(g)]\}} \quad (C-8)$$

All quantities on the right side of this expression are now known and we may readily calculate K.

Appendix D

**EQUATIONS USED FOR OVERALL MASS TRANSFER
COEFFICIENT CALCULATIONS**

EQUATIONS USED FOR OVERALL MASS TRANSFER COEFFICIENT CALCULATIONS

MASS TRANSFER COEFFICIENT

In the Task 4 experiments with hollow fiber contactors, the mass transfer coefficient was defined as

$$K_{OLM} = (V_L C_L^{OUT}) / (A \Delta C_{LM})$$

where

K_{OLM} = Overall mass transfer coefficient, cm/s

V_L = Liquid flow rate, cm³/s

A = Area of transfer based on outside diameter of fiber, cm²

C_L^{OUT} = Concentration of CO₂ in the liquid outlet, moles/cm³

ΔC_{LM} = Logarithmic mean concentration difference, mole/cm³
= $[(C_G^{IN} - C_L^{OUT}) - C_G^{OUT}] / \ln [(C_G^{IN} - C_L^{OUT}) / C_G^{OUT}]$

C_G^{IN}, C_G^{OUT} = Liquid phase concentration of CO₂ in equilibrium with feed gas at inlet and outlet, respectively, mole/cm³

The values of C_G^{IN} and C_G^{OUT} are calculated by the equations

$$C_G^{IN} = P_G^{IN} * H$$

$$C_G^{OUT} = P_G^{OUT} * H$$

where C_G^{IN}, C_G^{OUT} = Liquid phase concentration of CO₂ in equilibrium with the feed gas at the inlet and the outlet, respectively, mole/cm³

P_G^{IN}, P_G^{OUT} = Gas inlet and outlet pressures, respectively, atm

H = Henry's law constant, mole/cm³ atm

PROCEDURE TO DETERMINE THE VALUE OF H

Carbon dioxide solubility in water at different temperatures (in the units of atm/mole fraction in liquid) are available in Geankoplis, C. J. (1972) *Mass Transport Phenomena* (Ohio State University Bookstores, Columbus, Ohio). The following correlation is developed from those data:

$$h = [0.07245 + 0.00295 t + 0.00003 t^2] \times 10^4$$

where h = Henry's law constant, atm/mole fraction in liquid
 t = temperature, °C

For a given temperature, h is calculated from the above equation and converted to the units of mole/cm³ atm using the following expression

$$H = 1 / (MW_{H_2O} / \rho_{H_2O} * h)$$

where H = Henry's law constant, mole/cm³ atm
 MW_{H_2O} = molecular weight of water, g/mole
 ρ_{H_2O} = density of water, g/cm³

Appendix E

CALCULATION OF MINIMUM LIQUID FLOW RATE

CALCULATION OF MINIMUM LIQUID FLOW RATE

Fe^{II}(edta) is known to complex with NO according to the liquid-phase reaction



whose equilibrium constant, K, is given by

$$K = \frac{[\text{Fe}^{\text{II}}(\text{edta})(\text{NO})^{2-}(\text{l})]}{[\text{NO}(\text{l})][\text{Fe}^{\text{II}}(\text{edta})^{2-}(\text{l})]} \quad (\text{E-2})$$

All species in the two equations above are assumed to be dissolved in an aqueous solution. From these relations, we can obtain the maximum gas phase NO concentration that can be absorbed by a scrubbing solution. To do so, we first assume that a linear isotherm exists between NO dissolved in the liquid phase and NO in the gas phase:

$$[\text{NO}(\text{l})] = \alpha[\text{NO}(\text{g})] \quad (\text{E-3})$$

Next we note that the total NO in the liquid phase is that complexed plus that uncomplexed:

$$[\text{NO}(\text{l})]_{\text{total}} = [\text{Fe}^{\text{II}}(\text{edta})(\text{NO})^{2-}(\text{l})] + [\text{NO}(\text{l})] \quad (\text{E-4})$$

and the amount of Fe^{II}(edta) initially in the liquid phase is that complexed plus that uncomplexed:

$$[\text{Fe}^{\text{II}}(\text{edta})^{2-}(\text{l})]_{\text{initial}} = [\text{Fe}^{\text{II}}(\text{edta})(\text{NO})^{2-}(\text{l})] + [\text{Fe}^{\text{II}}(\text{edta})^{2-}(\text{l})] \quad (\text{E-5})$$

Substituting Eqs. (E-3), (E-4), and (E-5) into Eq. (E-2) and rearranging yields

$$[\text{NO}(\text{l})]_{\text{total}} = \frac{\alpha[\text{NO}(\text{g})] \{1 + K\alpha[\text{NO}(\text{g})] + K[\text{Fe}^{\text{II}}(\text{edta})^{2-}(\text{l})]_{\text{initial}}\}}{1 + K\alpha[\text{NO}(\text{g})][\text{Fe}^{\text{II}}(\text{edta})^{2-}(\text{l})]_{\text{initial}}} \quad (\text{E-6})$$

Thus, knowing the initial concentration of Fe^{II}(edta) in the liquid phase and the concentration of NO in the gas phase, we can compute the total NO concentration absorbed by the liquid phase at equilibrium. This is essentially the liquid's sorption capacity.

Now imagine that we treat a flue gas having a concentration of $[\text{NO}(\text{g})]$ with a scrubbing liquid having a sorption capacity of $[\text{NO}(\text{l})]_{\text{total}}$. A quick calculation shows that

$$\frac{\text{Liquid flow rate}}{\text{Gas flow rate}} = \frac{10^{-6}}{22.4} \frac{[\text{NO}(\text{g})]}{[\text{NO}(\text{l})]_{\text{total}}} \quad (\text{E-7})$$

where the liquid flow rate is in L/min, the gas flow rate is in L(STP)/min, $[\text{NO}(\text{g})]$ is in ppm, and $[\text{NO}(\text{l})]_{\text{total}}$ is in mole/L. This ratio represents the minimum liquid flow rate necessary to treat a given gas flow rate; it may be combined with Eq. (E-6) to yield

$$\frac{\text{Liquid flow rate; L/min}}{\text{Gas flow rate; L(STP)/min}} = \frac{10^{-6}}{22.4} \frac{1 + K\alpha[\text{NO}(\text{g})][\text{Fe}^{\text{II}}(\text{edta})^{2-}(\text{l})]_{\text{initial}}}{\alpha\{1 + K\alpha[\text{NO}(\text{g})] + K[\text{Fe}^{\text{II}}(\text{edta})^{2-}(\text{l})]_{\text{initial}}\}} \quad (\text{E-8})$$

Appendix F

SOP FOR SYNTHESIS OF d-DMA[2,2'-BIS(N-METHYL-N-PHENYL)ETHYL ETHER)

SRI STANDARD OPERATING PROCEDURE

SOP No: 340.3064

Laboratory: Chem. Eng. Development Center

Page 1 of 9

Supersedes: NA (Original)

Effective:

Subject: Pilot Sclae Synthesis of 2,2'-bis (N-methyl-N-phenyl)ethyl ether

A. PURPOSE

This procedure describes the techniques and approach to be used in synthesizing pilot scale quantities (approximately 10 L) of 2,2'-bis(N-methyl-N-phenyl) ethyl ether (d-DMA).

B. BACKGROUND

d-DMA has been developed as an SO₂ absorbing chemical for use in flue gas purification operations. As of yet, d-DMA has only been tested in small laboratory applications. Samples for these tests were supplied from small scale synthesis. Larger quantities are needed to test the effect of the d-DMA in a hollow fiber contactor. d-DMA has been successfully synthesized at the 100 g lab scale. The next step will be to synthesize a 10-20 L pilot scale batch of d-DMA.

C. HEALTH AND SAFETY

All personnel involved in utilizing this procedure should observe standard laboratory safety procedures. All personnel involved should wear protective equipment, including; safety glasses or goggles, polymer gloves, chemical resistant boots, and a chemically resistant suit. Since the process being used involves harmful chemicals, the operation should be performed in a hood. The following is a list of potential hazards that may be encountered during the operation of the process. steps on how to handle these hazards will be outlined in Section G.

- Highly reactive materials
- Toxic liquids
- Flammable liquids (flash point < 95°F)
- Flammable gases
- High and low pressure hazards
- Unattended operation
- Skin burns
- Power failure
- Cooling water failure
- Spills

APPROVALS

Preparers:

Paul Stearns_____
Date

Management Approval:

Org 340 Director, R. Thomas Podoll._____
Date

Health and Safety Approval:

Health and Safety_____
Date

Subject: Pilot Scale Synthesis of 2,2'-bis(N-methyl-N-phenyl)ethyl ether

D. TRAINING

All personnel involved in handling chemicals, equipment and instruments should have a general education in either chemistry or chemical engineering and should have attended at least one laboratory safety class from SRI's Health and Safety Department. All personnel must have received training for the specific equipment and instruments required by the procedures. This training should be recorded in the record of staff training in the group's training files.

E. MATERIALS AND METHOD

- E.1 Nash vacuum pump with dry ice trap operated according to SOP 360.822 and SOP 360.823 respectively
- E.2 100 L round glass reactor operated according to SOP 340.827 and cleaned according to SOP 340.829.
 - E.2.1 Overhead stirrer with air control and cooling water
 - E.2.2 Heating mantle and power control
 - E.2.3 Thermocouple probe and meter
 - E.2.4 Condenser
 - E.2.5 2 L addition funnel
 - E.2.6 4" reaction vessel head with three 24/40 necks
- E.3 12 L glass reactor for product distillation.
 - E.3.1 Claisen adaptor
 - E.3.2 Condenser
 - E.3.3 Receiving flask
 - E.3.4 Heating mantle
 - E.3.5 Capillary tube inlet
 - E.3.6 120 V Powerstat
- E.4 240 V Powerstat
- E.5 Gas supply (nitrogen and/or argon)

Subject: Pilot Scale Synthesis of 2,2'-bis(N-methyl-N-phenyl)ethyl ether

- E.6 Balance capable of measuring weights up to 25 kg within 1%.
- E.7 Chemical cylinders and transfer line
- E.8 Vacuum regulator
- E.9 Condenser cooling system (Portable Chiller operated according to SOP 340.820).
- E.10 Supplied air breathing apparatus operated according to SOP 340.839
- E.11 20 L glass carboys (cleaned according to SOP 360.830) in plastic containers for liquid collection and transfer
- E.12 Filtration system including buchner funnel, filter paper (Whatman number 5 or 6), and vacuum collection flask
- E.13 Alcoholic KOH bath prepared according to SOP 360.832
- E.14 pH meter
- E.15 Air scrubbing system operated according to SOP 360.801
- E.16 Chemicals
 - E.16.1 Tetrahydrofuran (THF) in 18 L Kilo Lab cylinders
 - E.16.2 10M Butyllithium in hexanes in 18 L Kilo Lab cylinder
 - E.16.3 n-Methyl Aniline
 - E.16.4 Bis-Chloroethyl Ether
 - E.16.5 Sodium Chloride
 - E.16.6 Anhydrous Magnesium Sulfate
 - E.16.7 Trichloroethylene
 - E.16.8 Milli-Q water
 - E.16.9 1 N HCl
- E.17 Chemical resistant boots
- E.18 Portable shield
- E.19 Chemical resistant suit

Subject: Pilot Scale Synthesis of 2,2'-bis(N-methyl-N-phenyl)ethyl ether

F. APPARATUS - SETUP

- F.1 Move the 100 L round reaction vessel to bay 2 cell. Set the reaction vessel into a heating mantle and secure it to a scaffolding rack. Make necessary adjustment to ensure that the rack and vessel are flat. The reactor has four necks. Secure the stirring mechanism through the center neck. Secure the condenser and 2 L addition funnel to the two small side ports. Secure the four inch reaction vessel head to the large side port. Through two of the necks on the head connect argon purge and thermocouple. Plug the third neck with a stopper until it is used for vacuum transfer. Shut the bottom valve on the reactor.
- F.2 Connect the condenser to the portable chiller. Connect cooling water and air to overhead stirrer. Check for leaks in both. Connect condenser liquid discharge to receiving vessel using teflon tubing. With the stirring controller turned off, turn on low pressure air supply to overhead stirrer.

G. PROCEDURES

G.1 Calibration

- G.1.1 When used, vacuum gauges should be calibrated prior to use according to SOP 340.3017.
- G.1.2 The thermocouple has been pre-calibrated by the manufacturer.
- G.1.3 The pH meter should be calibrated against pH 4 and pH 7 buffers before use.

G.2 Liquid transfer from Kilo Lab cylinders

- G.2.1 Tetrahydrofuran and butyllithium are supplied from the manufacturer in 18 L Kilo Lab cylinders. Transfer the liquid into the addition funnel using methods outlined in Aldrich Technical Bulletin AL-149 (Attachment I.1). An argon blanket must be maintained in the reaction vessel and addition funnel.
- G.2.2 Before using the chemical cylinders, ground the cylinder to a water line using jumper cables or grounding straps.

G.3 Reaction procedure

- G.3.1 Complete start up checklist (Attachment I.2).

Subject: Pilot Scale Synthesis of 2,2'-bis(N-methyl-N-phenyl)ethyl ether

- G.3.2 Purge the vessel with dry argon by setting the argon rate at 10 L/min for 15 minutes. Continue a slow purge of argon (1 L/min) flowing until otherwise specified.
- G.3.3 **DON THE SELF CONTAINED BREATHING APPARATUS, PROTECTIVE CHEMICAL BOOTS AND PROTECTIVE SUIT.**
- G.3.4 Attach THF cylinder to addition funnel using the Aldrich liquid transfer line.
- G.3.5 Add 10.2 L n-methyl aniline to the reactor by vacuum transfer through the 24/40 neck of the reactor head. The n-methyl aniline comes in 3 kg containers (3.03 L) transfer all the contents from three of the containers into the reactor (9.1 L). Add the final 1.1 L by weighing the container during the addition. The weight difference should be 1.1 Kg. Begin stirring slowly.
- G.3.6 Transfer 45 L THF according to instructions outlined in G.2 to the reaction vessel through the addition funnel. For the first 36 L (two 18 L cylinders), open the stopcock on the 2 L addition funnel and allow the THF to flow directly into the reactor. For the last 9 L, fill the funnel and transfer into the reactor in 2 L increments.
- G.3.7 Disconnect transfer line from THF cylinder and attach it to the butyllithium cylinder according to procedure cited in G.2.
- G.3.8 Add 9.4 L 10 M butyllithium slowly through addition funnel. Allow the reaction to slowly reflux during addition to drive heat away by vaporization/condensation. Since the addition funnel has a capacity of only 2 L, the addition must be accomplished by filling the addition funnel four separate times completely. For the last addition, add only 1.4 L to the addition funnel.
- G.3.9 Disconnect transfer line from the butyllithium cylinder, being careful to follow procedures outlined in G.2 to prevent possibility of fire. Reconnect to THF cylinder.
- G.3.10 Rinse the addition funnel out with THF by filling it completely one time. Drain the funnel.
- G.3.11 Allow mixture to stir for 1 hour at reflux to ensure complete reaction.
- G.3.12 Remove Kilo Lab transfer line from the addition funnel.

Subject: Pilot Scale Synthesis of 2,2'-bis(N-methyl-N-phenyl)ethyl ether

- G.3.13 Add 5.5 L bis-chloroethyl ether slowly through addition funnel. Additions should be performed in 50 ml increments every minute for approximately 2 hours. The addition funnel will need to be filled completely two times (2 L each). Transfer the bis-chloroethyl ether first into a separatory funnel. Place the full separatory funnel on top of the addition funnel and drain the contents into the distillation funnel until the liquid is at the desired level. The third addition through the funnel will be 1.5 L. The temperature in the reactor should be kept between 55° C and the reflux temperature (68-70° C). Since the reaction is exothermic, external heating will probably not be needed.
- G.3.14 Heat to a slow boil and allow to reflux for 2 hours.
- G.3.15 Quench the reaction by adding approximately 1 L methanol slowly through the reflux condenser and allow the mixture to reflux an additional 30 minutes.
- G.3.16 Discontinue argon purge.
- G.3.17 Distill off approximately 50 L of the solvents at reflux until a thick liquid remains. Dispose of distillate in a 55 gallon drum labelled for chlorinated solvent waste.
- G.3.18 Allow to cool to room temperature.
- G.4 Extraction and purification
- G.4.1 SUPPLIED AIR, CHEMICAL RESISTANT BOOTS, AND CHEMICAL RESISTANT SUIT MUST BE WORN DURING THE EXTRACTION AND PURIFICATION PROCESS.
- G.4.2 Add 16 L trichloroethylene by adding eight 2 L increments (each bottle holds 2 L) using vacuum transfer. Stir.
- G.4.3 Acidify 32 L Milli-Q water by adding 1 N HCl until the pH is at 4.0.
- G.4.4 Add 32 L Milli-Q water wash using vacuum transfer. This will involve adding one full 20 L carboy of water followed by 12 L from a pre-calibrated jug. Agitate vigorously until well mixed.
- G.4.5 Drain the organic phase from the reactor into clean 20 L glass carboys.
- G.4.6 Drain the remaining aqueous phase from the reactor into 20 L glass carboys. Cap the carboys with aluminum foil. Dispose of the aqueous phase into a 55 gallon drum labelled for aqueous waste.

Subject: Pilot Scale Synthesis of 2,2'-bis(N-methyl-N-phenyl)ethyl ether

- G.4.7 Transfer organic contents back into the reactor using vacuum transfer and repeat steps G.4.3 through G.4.5.
- G.4.8 Again transfer organic contents back into reactor using vacuum transfer. This time, wash with 32 L saturated NaCl solution (brine). Add the brine in the same manner that the water was added (G.4.3). If the brine phase and the organic phase do not separate quickly, add 2 L trichloroethylene and agitate moderately. Stop agitation to see if separation occurs. Repeat until separation occurs.
- G.4.9 Drain organic contents from the reactor into 20 L glass carboys and add 500 g anhydrous magnesium sulfate to each full 20 L carboy. For the partially full carboy, adjust the amount of magnesium sulfate accordingly.
- G.4.10 Let stand for 1/2 hour, mixing occasionally with a glass rod.
- G.4.11 Vacuum filter the carboy contents into a 20 L vacuum flask using a buchner funnel with Whatman #5 or 6 filter paper.
- G.4.12 Drain the brine phase from the reactor and dispose of it as aqueous waste.
- G.4.13 Transfer filtrate into the 100 L reactor to vacuum distill off most of the remaining solvent. Use the maximum vacuum attainable but do not heat liquid above 90° C. Discard the distillate into a drum labelled for chlorinated solvent.
- G.4.14 Let the liquid cool.
- G.4.15 Attach duo seal vacuum pump to 12 L reactor.
- G.4.16 Vacuum transfer contents of the 100 L reactor into the 12 L reactor.
- G.4.17 Vacuum distill the impurities from the product. Use the maximum vacuum attainable in the 12 L reactor and temperatures up to 175° C. Distillation is complete when the distillate is pale yellow and the product is dark orange/brown.
- G.4.18 After distillation is complete, transfer the product to dry, clean 2 L solvent bottles. Label the bottles appropriately. Dispose of the distillate into the 55 gallon drum labelled for chlorinated solvent waste.
- G.5 Safety procedures and issues

Subject: Pilot Scale Synthesis of 2,2'-bis(N-methyl-N-phenyl)ethyl ether

- G.5.1 Butyllithium is highly reactive with water and combusts spontaneously when in contact with water or humid air. Butyllithium **must** be transferred using the chemical transfer line under an inert atmosphere.
- G.5.2 THF is hygroscopic and hazardous. It must be transferred using the chemical transfer line under an inert atmosphere.
- G.5.1 When two reactive materials are to be combined, one must be added slowly using the addition funnel, while temperature is carefully monitored.
- G.5.3 Flammable liquids should be kept away from spark or ignition sources.
- G.5.4 Flammable gases (specifically butane) released as a byproduct of the primary reaction in small quantities can be vented to the hood.
- G.5.5 High pressure cylinders must be secured at all times. If a regulator is not attached to the cylinder, the cylinder should be capped. While performing vacuum operations, a portable shield should be placed between the operator and the equipment under vacuum.
- G.5.6 Caution should be taken when operating the heating mantle in order to prevent burns.
- G.5.7 Store the butyllithium cylinder in an explosion-proof fridge.
- G.5.8 Chemical resistant boots and suit, air supplied respirator, and gloves should be worn at all times while handling chemicals.
- G.6 Emergency procedures
 - G.6.1 In the event of power failure, disconnect all power sources, leave the cell, and close the door.
 - G.6.2 If the condenser cooling fluid supply fails, remove heat sources from the reaction vessel until the supply is replenished.
 - G.6.3 In the event of a small chemical spill consult the MSDS and take necessary measures to rectify the situation. In the event of a large chemical spill that jeopardizes the safety of personnel, leave the cell immediately and call extension 7777 for emergency response.
 - G.6.4 In the event of failure in the cooling water supply to the stirrer bearing, discontinue stirring until supply can be replenished.

SRI STANDARD OPERATING PROCEDURE SOP No: 340.3064

Laboratory: Chem. Eng. Development Center **Page 9 of 9**

Supersedes: NA (Original) **Effective:**

Subject: Pilot Scale Synthesis of 2,2'-bis(N-methyl-N-phenyl)ethyl ether

G.6.5 If, during the reaction sequence, water is seen leaking into the reactor, leave the cell immediately and shut down water supply from the outside. Leaking water can react violently with butyllithium.

G.6.6 Should the breathing air supply fail, leave cell immediately and remove face mask.

G.6.7 In the event of fire, leave the cell immediately and call 7777 for emergency assistance.

G.7 Shut down

G.7.1 Shut down power to heating mantle.

G.7.2 Turn off cooling fluid flow to the condenser.

G.7.3 Turn off cooling water to mixer bearing.

G.7.4 Shut down air supply to overhead stirrer.

G.7.5 Clean the glassware as outlined in SOP's 360.829 and 360.830. Glassware containing residual chemicals should first be rinsed with an appropriate solvent. Chemicals and solvents should be disposed of into properly labeled barrels.

H. MAINTENANCE

H.1 Perform maintenance as required in the operating manual for the air pump. Enter all maintenance operations in the equipment log.

H.2 Check the glassware, overhead stirrer, and heating mantle periodically for wear or damage. Take the necessary steps to rectify the problem in the event one is discovered.

I. ATTACHMENT

I.1 Aldrich Chemical Bulletin AL-149

I.2 Start up checklist